Metabolomics and biochemical evaluation of skeletal muscle from *Ndufs4* knockout mice

K Terburgh



orcid.org 0000-0001-5700-6890

Dissertation submitted in partial fulfilment of the requirements for the degree *Masters of Science in Biochemistry* at the North-West University

Supervisor: Prof R Louw
Co-supervisor: Dr JZ Lindeque

Graduation May 2019
23475684


NOT TO US,
Lord
BUT TO YOU BE THE
glory
PSALM 115:1

ACKNOWLEDGEMENTS

First, I would like to acknowledge and thank my supervisor, **Prof Roan Louw**, for his guidance, wisdom, extraordinary support and enthusiasm. I could not have asked for a better mentor. Second, my co-supervisor, **Dr Zander Lindeque**, for his invaluable assistance and guidance.

Furthermore, I would like to thank the following individuals whose contributions made this study possible:

- **Prof Francois van der Westhuizen**, for his role in the acquisition of funding and the animal model, as well as his constant motivation and interest in the study.
- **Dr Shayne Mason**, for his valued assistance and guidance regarding NMR spectroscopy and the publications resulting from the study.
- **Wessel Horak**, for his vital guidance and training regarding the metabolomics analyses. His patience and willingness to help are much appreciated.
- **Peet Jansen van Rensburg** and **Dr Leonie Venter**, for their support and advice regarding the LC-MS/MS work.
- **Michelle Mereis**, for her assistance and organisation regarding the breeding- and genotyping strategy of the animals used in this study.
- **Kobus Venter** and **Antoinette Fick** from the PCDDP (NWU), for their assistance regarding the breeding, housing and euthanasia of the animals used in this study.
- **Mari van Reenen**, for her advice and assistance regarding the statistics performed in this study.
- **Valerie Viljoen**, for the language editing of the dissertation.
- **Janeé, Carien, Liesel**, **Hayley, Maryke**, all the **Biochemistry Anonymous** girls and everyone at the **Mitochondria Research Laboratory (NWU)**. Your extraordinary emotional support, understanding and fellowship are greatly appreciated.

I would also like to thank my great big family, with special gratitude towards my parents, **Drikus** and **Theresa**, as well as my sister and brother-in-law, **Leandri** and **Trevor**, for their interest in my work, unwavering emotional support, love and motivation.

Above all, I thank my **Lord and Saviour** for His unfathomable love, grace and guidance. He has given me much more than I could ever deserve.

ABSTRACT

The dysfunction of mitochondrial complex I (CI) impedes the most efficient mechanism feeding electrons into the respiratory chain (RC) — a system that, together with ATP synthase (CV), is responsible for the majority of cellular energy production via oxidative phosphorylation (OXPHOS). Although CI deficiency is the most common defect in mitochondrial energy metabolism, it is among the most complex, multifactorial, poorly understood disorders that currently lack an effective treatment. One of the most promising tools used to gain insight into this form of mitochondrial disease (MD), is the whole-body *Ndufs4* knockout (*Ndufs4*$^{-/-}$) mouse model. Although the neurological phenotype of these animals has been widely studied, the effect of CI deficiency on *Ndufs4*$^{-/-}$ skeletal muscle metabolism remains elusive. The lack of research on this tissue is largely owed to the view that these animals do not display strong muscle involvement. However, neuromuscular involvement is a hallmark feature of MD and considering skeletal muscle's high energetic demand, metabolic activity, and integration with the nervous system, this tissue needs to be investigated.

The aim of this study was, therefore, to combine hypothesis-generating metabolic profiling and biochemical strategies to gain insight into the energy metabolism of both glycolytic (white quadriceps) and oxidative (soleus) skeletal muscles from *Ndufs4*$^{-/-}$ mice. Profiling methods that utilise various high-content analytical platforms were employed in order to generate a broad metabolic phenotype of CI deficient muscles. This multi-platform metabolomics approach comprised of targeted liquid chromatography-tandem mass spectrometry (LC-MS/MS), untargeted gas chromatography time-of-flight mass spectrometry (GC-TOF-MS) and proton nuclear magnetic resonance (^{1}H-NMR) spectroscopy. However, extensive multi-platform metabolomics of mouse tissues presents a challenge due to the limited-quantity samples obtained — especially in the case of NMR spectroscopy, which is inherently insensitive. Therefore, one of the chief objectives of the study was to develop a ^{1}H-NMR method that enables the analysis of small-quantity biological samples.

In the first part of the study, we present a novel miniaturised ^{1}H-NMR method utilising 2 mm NMR tubes, which enables metabolic profiling on a tenth of the sample quantity required by a well-established standard operating protocol (SOP). We demonstrate the miniaturised method's acceptability regarding precision (CV < 15%), relative accuracy (80–120 %), linearity ($R^2 > 0.95$) and statistical equivalence ($p < 0.05$) to the SOP when analysing spiked synthetic urine as well as mouse muscle extracts. In addition, we exhibit the novel method's advantages for large-scale metabolomics when; i) adequate sample quantities are available by analysing increasingly concentrated versions (up to 10×) of samples to expand metabolome coverage; or ii) sample

quantities are limited by performing a pilot metabolomics study on minute *Ndufs4*$^{-/-}$ (n = 3) and wild-type (WT; n = 3) solei, which identified five metabolites (previously linked to MD) strongly discriminating the two genotypes.

In the second part of the study, we investigate the effects of CI deficiency in *Ndufs4*$^{-/-}$ skeletal muscles. Through multi-platform metabolic profiling of *Ndufs4*$^{-/-}$ (n = 19), and WT (n = 20) white quadriceps and soleus muscles, we provide the first empirical evidence of adaptive responses to CI dysfunction involving non-classical pathways that fuel the ubiquinone (Q)-cycle. By restoring the electron flux to CIII via the Q-cycle, these adaptive mechanisms could maintain adequate oxidative ATP production, despite CI deficiency — providing a possible explanation for the lack of muscle involvement in the *Ndufs4*$^{-/-}$ phenotype. We report a respective 48 and 34 discriminatory metabolites between *Ndufs4*$^{-/-}$, and WT white quadriceps and soleus muscles, among which the most prominent alterations indicate the involvement of the glycerol-3-phosphate shuttle, the electron transfer flavoprotein system, respiratory chain CII, and the proline cycle in fuelling the Q-cycle. Enzyme (CI-CIV and CS) activity assays confirmed severely reduced (80 %) CI activity in both *Ndufs4*$^{-/-}$ (n = 12) muscle types, compared to WTs (n = 10), along with moderate reductions in CS (12 %) and CIII (18 %) activities in *Ndufs4*$^{-/-}$ solei. When comparing muscle fibre types, glycolytic fibres seemed to be more vulnerable to CI deficiency, as greater disturbances in metabolic profiles were evident, along with much lower residual CI activity (4.58 ± 1.67 nmol/min/mg) compared to oxidative fibres (14.74 ± 6.67 nmol/min/mg).

Taken together, this study contributes to the natural science field in two ways. Firstly, through our novel miniaturised ^{1}H-NMR method, we provide a cost-effective alternative solution for the current restrictions of NMR spectroscopy in the analysis of limited-quantity biological samples. Traditionally, cryoprobe technology is required for such studies; however, we show that a typical NMR spectrometer with a standard probe head can be used to analyse small sample quantities with adequate analytical efficiency. Secondly, through discover-phase multi-platform metabolic profiling, we provide novel mechanistic insight into CI deficiency — thereby highlighting the value of metabolomics in MD research. We report skeletal muscle-specific changes in several metabolic pathways that result from whole-body mitochondrial dysfunction, which upon further investigation could provide novel targets for therapeutic intervention in CI deficiency and potentially lead to the development of new treatment strategies.

Keywords: Complex I deficiency • *Ndufs4* knockout mice • Skeletal muscle • Metabolomics • Ubiquinone-cycle • Nuclear magnetic resonance (NMR) spectroscopy ·

TABLE OF CONTENTS

ACKNOWLEDGEMENTS ii
ABSTRACT iii
TABLE OF CONTENTS v
LIST OF TABLES xii
LIST OF FIGURES xiii
LIST OF EQUATIONS xv
LIST OF REACTIONS xv
LIST OF SYMBOLS, UNITS, ABBREVIATIONS & LATIN TERMS xvi

CHAPTER 1 INTRODUCTION 1

1.1 Background, research rationale and problem statement 2
1.2 Aim and objectives of the study 3
1.2.1 Aim 3
1.2.2 Specific objectives 3
1.3 Structure of the dissertation 4
1.4 Outcomes of the study 5
1.4.1 Published peer-reviewed article I (Chapter 4, Annexure C) 5
1.4.2 Published peer-reviewed article II (Chapter 5, Annexure D) 5
1.4.3 Oral presentation 6
1.5 Ethical considerations 6
1.6 Financial support 6
1.7 Author contributions 6
1.8 References 8

CHAPTER 2 LITERATURE STUDY 9

2.1 Introduction 10
2.2 The mitochondrion 10
2.2.1 Mitochondrial structure, organisation and heterogeneity 10
2.2.2 Mitochondrial function 11
2.2.3 Mitochondrial genome 11
2.3 The oxidative phosphorylation (OXPHOS) system 12
2.3.1 Structure and organisation of the OXPHOS system 12
2.3.2 Function of the OXPHOS system 14
2.3.2.1 Electron entry into and transport through the respiratory chain 14
2.3.2.2 The proton circuit across the inner mitochondrial membrane 15
2.3.3 NADH shuttles and non-classical pathways feeding into the respiratory chain ... 15

2.4 Complex I (CI) of the OXPHOS system 16
2.4.1 CI structure 16
2.4.2 CI function 17
2.4.2.1 CI central subunits 17
2.4.2.2 CI accessory subunits 18
2.4.3 CI biogenesis and assembly 18
2.4.4 NDUFS4 accessory subunit of CI 19
2.5 Mitochondrial disease 20
2.5.1 An introduction to mitochondrial disease 20
2.5.2 Prevalence, genetics and clinical phenotype 21
2.5.3 Pathophysiology 23
2.5.3.1 Introduction 23
2.5.3.2 Alterations in cellular bioenergetics and signalling pathways 23
2.5.3.3 Metabolic adaptions 25
2.6 CI deficiency and Leigh syndrome 27
2.7 The *Ndufs4* knockout mouse model for human CI deficiency 28
2.7.1 Development 28
2.7.2 Clinical phenotype 29
2.7.3 Respiratory chain enzyme abundance and activity 30
2.7.4 ATP homeostasis and oxygen consumption 31
2.7.5 Metabolic alterations 31
2.7.6 Recent advances and limitations of research on *Ndufs4* knockout mouse models 33
2.8 Skeletal muscle 34
2.8.1 Myofibre structure 34
2.8.2 Myofibre type heterogeneity 35
2.8.3 Mitochondrial content and metabolic profile 36
2.9 Metabolomics 36
2.10 Experimental design 37
2.11 References 39

CHAPTER 3 MATERIALS AND METHODS 49

3.1 Introduction 50
3.2 Animals and sampling 50
3.2.1 Animal care and breeding 50
3.2.2 Animal identification and numbering 51
3.2.3 Sample size and animal groups 51
3.2.4 Euthanasia and humane endpoints 52
3.2.5 Tissue sampling and hind-limb muscle dissection 52

3.3 Confirming the *Ndufs4* genotypes 54
3.3.1 Chemicals…… 54
3.3.2 Instrumentation and software packages 55
3.3.3 Methods…….. 55
3.3.3.1 Isolation and quantification of genomic DNA……..55
3.3.3.2 PCR amplification of DNA……..56
3.3.3.3 Agarose gel electrophoresis characterisation of DNA……....56
3.4 Respiratory chain enzyme activity assays 57
3.4.1 Chemicals…… 57
3.4.2 Instrumentation and software packages 57
3.4.3 Methods……. 58
3.4.3.1 Buffer solution preparation……58
3.4.3.2 Sample preparation……58
3.4.3.2.1 Isolation of mitochondrial fractions 58
3.4.3.2.2 Total protein content determination 58
3.4.3.3 Kinetic spectrophotometric enzyme assays……...59
3.4.3.3.1 Citrate synthase enzyme activity assay 60
3.4.3.3.2 Complex I enzyme activity assay 61
3.4.3.3.3 Complex II enzyme activity assay 61
3.4.3.3.4 Complex III enzyme activity assay 62
3.4.3.3.5 Complex IV enzyme activity assay 63
3.4.4 Data analysis…….. 63
3.5 Multi-platform metabolic profiling..... 64
3.5.1 Chemicals……..... 64
3.5.2 Instrumentation and software packages 66
3.5.3 Methods…….. ..... ….67
3.5.3.1 Internal standard preparation……...67
3.5.3.2 Metabolite extraction from muscle……...68
3.5.3.3 Quality control samples……69
3.5.3.4 Sample preparation……...69
3.5.3.4.1 Miniaturised ^{1}H-NMR spectroscopy sample preparation.... 70
3.5.3.4.2 GC-TOF-MS sample derivatisation 70
3.5.3.4.3 LC-MS/MS sample derivatisation 71
3.5.3.5 Metabolic profiling analyses……....*72*
3.5.3.5.1 Miniaturised ^{1}H-NMR spectroscopy 72
3.5.3.5.2 GC-TOF-MS..... 72
3.5.3.5.3 LC-MS/MS 73
3.5.4 Bioinformatics…….. 76

3.5.4.1 Data extraction……76
3.5.4.2 Data preprocessing……77
3.5.4.3 Data pretreatment……78
3.5.4.4 Statistical analysis……79
3.6 References 81

CHAPTER 4 MINIATURISED ^{1}H-NMR METHOD FOR ANALYSING LIMITED-QUANTITY SAMPLES APPLIED TO A MOUSE MODEL OF LEIGH SYNDROME 84

4.1 Introduction 85
4.2 Materials and methods 86
4.2.1 Spiked synthetic urine 86
4.2.2 Animals and sampling 87
4.2.3 Metabolite extraction 87
4.2.4 ^{1}H-NMR sample preparation 88
4.2.4.1 NMR buffer solution……88
4.2.4.2 Established standard operating protocol……88
4.2.4.3 Miniaturised ^{1}H-NMR protocol……88
4.2.5 ^{1}H-NMR spectroscopy……89
4.2.6 Statistics……89
4.3 Results and discussion 90
4.3.1 Establishing method equivalency 90
4.3.1.1 Precision……91
4.3.1.2 Relative accuracy……91
4.3.1.3 Linearity……92
4.3.1.4 Statistical equivalence testing……92
4.3.2 Exploring the miniaturised ^{1}H-NMR method 95
4.3.2.1 Method comparability……95
4.3.2.2 Quantitative linearity……95
4.3.2.3 Metabolome coverage……95
4.3.2.4 Sample carry-over……96
4.3.3 Pilot metabolomics application on limited-quantity samples 96
4.4 Conclusion 99
4.5 Supplementary information 100
4.6 References 109

CHAPTER 5 METABOLOMICS OF *NDUFS4*$^{-/-}$ SKELETAL MUSCLE: ADAPTIVE MECHANISMS CONVERGE AT THE UBIQUINONE-CYCLE 111

5.1 Introduction 112

5.2 Materials and methods 113

5.2.1 Animals and sampling…….. 113

5.2.2 Enzyme assays…….. 114

5.2.3 Metabolic profiling…….. 114

5.2.3.1 Extract preparation and derivatisation……..114

5.2.4 Data processing……..... 115

5.2.4.1 Enzyme assays……...115

5.2.4.2 Metabolic profiling……115

5.2.5 Statistical analyses……115

5.2.5.1 Enzyme assays……115

5.2.5.2 Metabolic profiling……115

5.3 Results and discussion 116

5.3.1 Respiratory chain enzyme activities in *Ndufs4*$^{-/-}$ muscles of different fibre type composition……..... 116

5.3.2 Statistical significance and discriminative power of *Ndufs4*$^{-/-}$ metabolic profiles 118

5.3.3 Common metabolic alterations in *Ndufs4*$^{-/-}$ skeletal muscles of different fibre type composition……..……119

5.3.3.1 Glycolysis, triglyceride catabolism and the glycerol-3-phosphate (GP) shuttle……...121

5.3.3.2 β-oxidation, amino acid catabolism and the electron transfer flavoprotein (ETF/ETF-QO) system……122

5.3.3.3 One-carbon metabolism, the methylation cycle and the transsulfuration pathway……123

5.3.3.4 The Krebs cycle and mitochondrial complex II (succinate dehydrogenase)……...124

5.3.3.5 Proline metabolism and the proline cycle……...125

5.3.4 Fibre type-specific metabolic alterations in *Ndusf4*$^{-/-}$ skeletal muscles..... 125

5.4 Conclusions 126

5.5 Supplementary information 127

5.5.1 Enzyme assays……..128

5.5.1.1 Mitochondrial isolation……128

5.5.1.2 CI enzyme assay……....128

5.5.1.3 CII enzyme assay……....129

5.5.1.4 CIII enzyme assay……..…129

5.5.1.5 CIV enzyme assay……...129

5.5.2 Metabolic profiling……....130

5.5.2.1 Metabolite extraction……..130
5.5.2.2 Quality control samples……..131
5.5.2.3 ^{1}H-NMR sample preparation and analysis……..131
5.5.2.4 LC-MS/MS sample preparation and analysis……..132
5.5.2.5 GC-TOF-MS sample preparation and analysis……..133
5.6 References 139

CHAPTER 6 SUMMARY AND CONCLUSIONS 142

6.1 Introduction 143
6.2 Summary of the findings from this study 143
6.2.1 Phase I: sample collection — Annexure A 143
6.2.2 Phase II: biochemical evaluation — Chapter 5 and Annexure B 144
6.2.3 Phase III: metabolic profiling — Chapter 4, Chapter 5 and Annexure B 145
6.3 Strengths and limitations of the study 147
6.3.1 Animals and sampling……..147
6.3.1.1 Strengths……..147
6.3.1.2 Limitations……..147
6.3.2 Multi-platform metabolomics approach 148
6.3.2.1 Strengths……..148
6.3.2.2 Limitations……..148
6.3.3 Metabolomics data and bioinformatics 148
6.3.3.1 Strengths……..148
6.3.3.2 Limitations……..149
6.4 Future prospects 150
6.4.1 Applying the novel miniaturised ^{1}H-NMR method 150
6.4.2 Investigating the adaptive pathways identified 150
6.5 References 151

ANNEXURE A: ANIMAL INFORMATION 153

A.1 Introduction 154
A.2 Genotypic characterisation of *Ndufs4* mice 154
A.3 References 158

ANNEXURE B: METHOD STANDARDISATION FOR MOUSE MUSCLES 159

B.1 Standardising the spectrophotometric enzyme assays 160
B.1.1 Introduction…… 160

B.1.2 Standardising the protein assay (BCA method)..... 160
B.1.3 Standardising the citrate synthase assay..... 161
B.1.4. Standardising the respiratory chain enzyme assays 162
B.2 Standardising the metabolic profiling methods..... 164
B.2.1 Introduction..... 164
B.2.2 Repeatability and intermediate precision studies 164
B.2.3 Data quality..... 165
B.2.4 Bioinformatics approaches..... 169
B.3 References..... 176

ANNEXURE C: PUBLISHED PEER-REVIEWED ARTICLE I 177

ANNEXURE D: PUBLISHED PEER-REVIEWED ARTICLE II 190

ANNEXURE E: METABOLOMICS AUTHOR GUIDELINES 200

ANNEXURE F: BBA — MOLECULAR BASIS OF DISEASE AUTHOR GUIDELINES 213

LIST OF TABLES

Table 3-1: Animals and sample sizes used for the study 52

Table 3-2: Information on PCR primers used to genotype *Ndufs4* mice..... 54

Table 3-3: Conditions for kinetic spectrophotometric enzyme assays 60

Table 3-4: Mass internal standard mixture analysed on various platforms 68

Table 3-5: MRM parameters for metabolites and internal standard isotopes monitored..... 74

Table 4-1: Measure of precision and accuracy 92

Table 4-2: Test of equivalence 93

Table 4-3: Chemical information and shifts for Figure 4.3 — representative ^{1}H-NMR spectra from the miniaturised method on muscle tissue. 100

Table 5-1: Mitochondrial respiratory chain enzyme activities in skeletal muscles from WT and *Ndufs4*$^{-/-}$ mice 117

Table 5-2: Volume extracts and mass internal standard mixture analysed on various platforms 131

Table 5-3: List of 48 significant discriminatory metabolites between *Ndufs4*$^{-/-}$ and WT white quadriceps muscles 135

Table 5-4: List of 34 significant discriminatory metabolites between *Ndufs4*$^{-/-}$ and WT soleus muscles..... 137

Table A-1: Animals used for biochemical evaluation..... 156

Table A-2: Animals used for metabolic profiling 157

Table B-1: GC-TOF-MS intra- and inter-batch CV-values for the quadriceps and soleus..... 166

Table B-2: LC-MS/MS intra- and inter-batch CV-values for the quadriceps and soleus 166

Table B-3: ^{1}H-NMR spectroscopy intra- and inter-batch CV-values for the quadriceps..... 166

Table B-4: Effect of different normalisation methods on important metabolites for the white quadriceps 171

Table B-5: Effect of different normalisation methods on important metabolites for the soleus 172

Table B-6: List of important metabolites for white quadriceps and soleus muscles determined using the XERp method..... 174

LIST OF FIGURES

Figure 2-1: Schematic representation of the mitochondrion 11

Figure 2-2: Overview of the structure and function of the OXPHOS system 13

Figure 2-3: Structure of the (porcine) respirasome 14

Figure 2-4: Overview of the structure and function of mammalian complex I. 17

Figure 2-5: The heterogeneity of mitochondrial disease manifestations..... 22

Figure 2-6: Deletion of *Ndufs4* exon two from the germline via Cre-loxP recombination..... 29

Figure 2-7: Structure of a single skeletal muscle cell or myofibre 35

Figure 2-8: Schematic representation of the experimental strategy 38

Figure 3-1: Front view depiction of the mouse ear numbering system 51

Figure 3-2: Anatomical location of the collected mouse hind-limb skeletal muscles..... 53

Figure 3-3: Bioinformatics workflow from raw spectral data to important metabolites. 76

Figure 3-4: Levels of metabolite identification..... 80

Figure 4-1: Experimental design and workflow 90

Figure 4-2: Test of equivalence 94

Figure 4-3: Representative ^{1}H-NMR spectra from the miniaturised method on muscle tissue 97

Figure 4-4: Application of the miniaturised ^{1}H-NMR method in a pilot metabolomics study of *Ndufs4*$^{-/-}$ mice 98

Figure 4-5: Linearity graphs for nine selected metabolites, all with R^2 values ≥ 0.99.. 108

Figure 5-1: Univariate analyses indicating the practical significance of important skeletal muscle metabolites 118

Figure 5-2: Multivariate analyses indicating the discriminative power of important skeletal muscle metabolites 119

Figure 5-3: Venn diagram of important metabolites discriminating *Ndufs4*$^{-/-}$ and WT groups in skeletal muscles 120

Figure 5-4: Common metabolic alterations in *Ndufs4*$^{-/-}$ skeletal muscles 120

Figure 5-5: Experimental workflow 127

Figure 5-6: Enzyme assays workflow 128

Figure 5-7: Metabolic profiling workflow 130

Figure A-1: Agarose gel electrophoretogram depicting PCR genotyping results obtained from mouse tailsnip-DNA 155

Figure B-1: BCA assay linearity for mitochondria-enriched 700 ×g supernatants of mouse skeletal muscle homogenates 161

Figure B-2: CS assay linearity for mitochondria-enriched 700 ×g supernatants of mouse skeletal muscle homogenates 162

Figure B-3: Respiratory chain enzyme assay linearity for mitochondria-enriched 700 ×g supernatants of mouse skeletal muscle homogenates 163

Figure B-4: Performance of the various metabolic profiling methods 167

Figure B-5: Sequential total signal scatter plot of various metabolic profiling methods..... 168

Figure B-6: Multivariate analyses indicating the clustering of groups after important metabolite selection..... 169

Figure B-7: The effect of different normalisation methods on the total signal scatter plots for individual metabolites..... 170

LIST OF EQUATIONS

Equation 3-1: Protein concentration (µg/µL) 59
Equation 3-2: Rotenone sensitive CI v_0 64
Equation 3-3: Enzyme activity per mg protein (µmol/min/mg) 64
Equation 3-4: Fisher ratio 77
Equation 3-5: Generalised logarithm transformation 79
Equation 3-6: Mean centering 79
Equation 3-7: Effect size D-value 79
Equation B-1: Percentage coefficient of variance 164

LIST OF REACTIONS

Reaction 2-1: Q-cycle 14
Reaction 2-2: Malate-aspartate shuttle 16
Reaction 2-3: Glycerol-3-phosphate shuttle 16
Reaction 3-1: CS-dependent CoA-SH formation 60
Reaction 3-2: CoA-SH-dependent TNB formation 60
Reaction 3-3: CI-dependent decylubiquinone reduction 62
Reaction 3-4: CII-dependent decylubiquinone reduction 62
Reaction 3-5: Decylubiquinol-dependent DCIP reduction 62
Reaction 3-6: CIII-dependent cytochrome c reduction 63
Reaction 3-7: CIV-dependent cytochrome c oxidation 63
Reaction 3-8: Oximation 71
Reaction 3-9: Silylation 71
Reaction 3-10: Butylation of amino acids 72
Reaction 3-11: Butylation of acylcarnitines 72

LIST OF SYMBOLS, UNITS, ABBREVIATIONS & LATIN TERMS

Symbols	
&	And
*	Asterisk
-/-	Homozygous knockout genotype; both alleles of interest are absent from the specific gene locus
~	Approximately
+/-	Heterozygous knockout genotype; one allele of interest is absent from the specific gene locus, while the other is present
+/+	Homozygous wild-type genotype; both alleles of interest are present at the specific gene locus
<	Less-than
>	Greater-than
±	Plus-minus
×	Times
↑	Increase
↓	Decrease
©	Copyright
®	Registered
♀	Female
♂	Male
I	One (Roman numeral)
II	Two (Roman numeral)
III	Three (Roman numeral)
IV	Four (Roman numeral)
Ø	Diameter
™	Trademark
V	Five (Roman numeral)
α	Alpha
β	Beta
Δ	Delta
ΔpH_m	Mitochondrial pH gradient
Δpmf	Proton motive force
$\Delta\psi_m$	Mitochondrial membrane potential
ε	Molar extinction coefficient
λ	Wavelength
v	Reaction velocity

Units	
%	Percentage
×g	Relative centrifugal force
°	Degrees
°C	Degrees Celsius
Abs	Absorbance
amu	Atomic mass unit

cm	Centimetres
eV	Electron volt
g	Gram
h	Hours
Hz	Hertz
kb	Kilobase
kDa	Kilodaltons
L	Litres
M	Molarity; moles solute per litre of solvent
m/z	Mass-to-charge ratio
mAbs	Milliabsorbance
mg	Milligram
MHz	Megahertz
min	Minutes
mL	Millilitre
mm	Millimetre
mM	Millimolar
mol	Mole
mV	Millivolt
N	Normality; molar concentration divided by an equivalence factor
ng	Nanogram
nm	Nanometre
nmol	Nanomole
pH	Potential of hydrogen; the negative of the base 10 logarithm of the H^+ molar concentration
ppm	Parts per million
psi	Pound-force per square inch; unit of pressure
sec	Seconds
V	Volt
v/v	Volume of solute per volume of solvent
w/v	Weight of solute per volume of solvent
µg	Microgram
µL	Microlitre
µM	Micromolar

Abbreviations

^{1}H-NMR	Proton nuclear magnetic resonance
1-Mhis	1-Methylhistidine
2-AA	2-Aminoadipate
2-Mhis	2-Methylhistidine
3’	3-prime end; 3-prime hydroxyl group of the polynucleotide chain
^{31}P-NMR	Phosphorus-31 NMR
3-HB	3-Hydroxybutyric acid
3-PBA	3-phenylbutyric acid
5’	5-prime end; 5-prime phosphate group of the polynucleotide chain
5’ to 3’	Polynucleotide directionality; from the 5-prime end to the 3-prime end of the polynucleotide chain

5-MTHF	5-Methyltetrahydrofolate
ACN	Acetonitrile
ADP	Adenosine diphosphate
AIDS	Acquired immune deficiency syndrome
Ala	Alanine
AM	*Ante meridiem* (Latin): before noon
AMDIS	Automated Mass Spectral Deconvolution and Identification System
AMP	Adenosine 5′-monophosphate
Arg	Arginine
Asn	Asparagine
Asp	Aspartate
Asp-NAT	Aspartate N-acetyltransferase
ATF	Activating transcription factors
ATP	Adenosine triphosphate
ATPase	Adenosine triphosphatase
AVMA	American Veterinary Medical Association
BAIBA	β-aminoisobutyrate
BBA	*Biochimica et Biophysica Acta* (Latin): Journal of Biochemistry and Biophysics
BCA	Bicinchoninic acid
BCAA	Branched-chain amino acid
bp	Base pairs
BSA	Bovine serum albumin
BSTFA	O-bis(trimethylsilyl)trifluoro acetamide
C0-carnitine	Carnitine
C12-carnitine	Dodecanoyl-carnitine
C14-carnitine	Myristoyl-carnitine
C16-carnitine	Palmitoyl-carnitine
C18-carnitine	Stearoyl-carnitine
C2-carnitine	Acetyl-carnitine
C3-carnitine	Propionyl-carnitine
C4-carnitine	Butanoyl-carnitine
C5-carnitine	Isovaleryl-carnitine
C6-carnitine	Hexanoyl-carnitine
C8-carnitine	Octanoyl-carnitine
Ca^{2+}	Calcium(II) ion
cAMP	Cyclic adenosine monophosphate
Car	Carnitine; C0-carnitine
Cat. #	Catalogue number
CH_3OH	Methanol
$CHCl_3$	Chloroform
Chol	Choline
CI	Complex I; NADH:ubiquinone oxidoreductase; EC 1.6.5.3 or confidence interval (depending on the context)
CII	Complex II; succinate:ubiquinone oxidoreductase; EC 1.3.5.1
CIII	Complex III; ubiquinol:ferricytochrome c oxidoreductase; EC 1.10.2.2
Cit	Citrulline

CIV	Complex IV; ferrocytochrome-c:oxygen oxidoreductase; EC 1.9.3.1
CO_2	Carbon dioxide
CoA	Coenzyme A
CPEO	Chronic progressive external ophthalmoplegia
CS	Citrate synthase
Cu	Copper
Cu^+	Copper(I) ion
Cu^{2+}	Copper(II) ion
$CuSO_4$	Copper(II) sulphate
CV	Complex V; ATP synthase; EC 3.6.1.3. or coefficient of variance (depending on the context)
CV %	Percentage coefficient of variance
Cys	Cysteine
Cyt c	Oxidised cytochrome c
Cyt c H_2	Reduced cytochrome c
D_2O	Deuterium oxide
DCIP	2,6-dichloroindophenol
$DCIPH_2$	Reduced 2,6-dichloroindophenol
DDM	n-Dodecyl-β-D-maltoside
DHAP	Dihydroxyacetone phosphate
DMG	*N, N*-dimethylglycine
DMPA	*N, N*-dimethyl-L-phenylalanine
DMSO	Dimethyl sulfoxide
DNA	Deoxyribonucleic acid
dNTP	Deoxyribonucleotide triphosphate
dQ	Decylubiquinone
dQH_2	Decylubiquinol
DTNB	2,2'-Dinitro-5,5'-dithiobenzoic acid
D-value	Effect size value of practical significance
e^-	Electron
e.g.	*Exempli gratia* (Latin): for example
EC number	Enzyme commission number
EDTA	Ethylenediaminetetraacetic acid
EGTA	ethylene glycol-bis(β-aminoethyl ether)-*N,N,N′,N′*-tetraacetic acid
EI	Electron impact
ESI	Electrospray ionisation
EtBr	Ethidium bromide
etc.	*Etcetera* (Latin): indicates that further, similar items are included
ETF	Electron transfer flavoprotein
ETF-QO	Electron transfer flavoprotein-ubiquinone oxidoreductase
FAD	Oxidised flavin adenine dinucleotide
$FADH_2$	Reduced flavin adenine dinucleotide
FASBMB	Federation of African Societies of Biochemistry and Molecular Biology
FDA	Food and Drug Administration
FDR	False discovery rate
Fe^{2+}	Iron(II) ion
Fe^{3+}	Iron(III) ion

Fe-S	Iron-sulfur
FGF-21	Fibroblast growth factor 21
FMN	Oxidised flavin mononucleotide
$FMNH_2$	Reduced flavin mononucleotide
F-ratio	Fisher ratio
GAA	Guanidineacetic acid
GC-TOF-MS	Gas chromatography time-of-flight mass spectrometry
GDF-15	Growth differentiation factor-15
Gln	Glutamine
Glu	Glutamate
Gly	Glycine
GP	Glycerol-3-phosphate
GPDH	Glycerol-3-phosphate dehydrogenase
GSH	Reduced glutathione
GSSG	Oxidised glutathione; glutathione disulfide
H^+	Hydrogen ion; proton
H0	Null hypothesis
H_2O	Water
H_2O_2	Hydrogen peroxide
HCl	Hydrogen chloride
Hcys	Homocysteine
HEPES	2-[4-(2-hydroxyethyl)piperazin-1-yl]ethanesulfonic acid
HK	Hexokinase
HMDB	Human Metabolome Database
HPLC	High-performance liquid chromatography
Hpro	Hydroxyproline
ID	Identification number
IMM	Inner mitochondrial membrane
IMS	Intermembrane space
IS	Internal standard
K^+	Potassium ion
KCl	Potassium chloride
KH_2PO_4	Potassium phosphate monobasic
KOH	Potassium hydroxide
KPi	Potassium phosphate
KSS	Kearns-Sayre syndrome
Lac	Lactate
LC-MS/MS	Liquid chromatography-tandem mass spectrometry
LDH	Lactate dehydrogenase
LHON	Leber’s hereditary optic neuropathy
LOQ	Limit of quantification
loxP	Locus of X(cross)-over in P1
LS	Leigh syndrome
Lys	Lysine
MD	Mitochondrial disease
ME	Maine
MELAS	Mitochondrial encephalopathy, lactic acidosis, and stroke-like episodes

MERRF	Mitochondrial encephalopathy with ragged red fibres
Met	Methionine
m-FDH	Mitochondrial flavoprotein dehydrogenase
MHC	Myosin heavy chain
MILS	Maternally inherited Leigh syndrome
MRM	Multiple reaction monitoring
mRNA	Messenger ribonucleic acid
MSI	Metabolomics standards initiative
MSTUS	Mass spectrum total useful signal
mtDNA	Mitochondrial DNA
mTORC1	Mammalian target of rapamycin complex 1; mechanistic target of rapamycin complex 1
n	Number of; amount
N module	NADH binding module
N/A	Not applicable or not available (depending on context)
Na^+	Sodium ion
NAA	*N*-acetylaspartate
NaCl	Sodium chloride
NAD	Nicotinamide adenine dinucleotide
NAD^+	Oxidised nicotinamide adenine dinucleotide
NADH	Reduced nicotinamide adenine dinucleotide
$NADP^+$	Oxidised nicotinamide adenine dinucleotide phosphate
NADPH	Reduced nicotinamide adenine dinucleotide phosphate
NAG	*N*-Acetylglutamate
NaN_3	Sodium azide
NARP	Neuropathy, ataxia, and retinitis pigmentosa
ND	NADH dehydrogenase subunit
nDNA	Nuclear DNA
NDUF	NADH:ubiquinone oxidoreductase (core) subunit
NDUFAF	NADH:ubiquinone oxidoreductase complex assembly factor
NDUFS4	NADH dehydrogenase (ubiquinone) iron-sulfur protein 4; NADH:ubiquinone oxidoreductase subunit S4
Ndufs4	NADH dehydrogenase (ubiquinone) iron-sulfur protein 4 gene; NADH:ubiquinone oxidoreductase subunit S4 gene
Ndufs4$^{-/-}$ mouse	Ndufs4 knockout mouse
NIST	National Institute of Standards and Technology
NMR	Nuclear magnetic resonance
NOESY	Nuclear overhauser effect spectroscopy
NRF	National Research Foundation of South Africa
NWU	North-West University
O_2	Oxygen
$O_2^{\bullet -}$	Superoxide anion radical
OAA	Oxaloacetate
OMIM	Online Mendelian Inheritance in Man
OMM	Outer mitochondrial membrane
Orn	Ornithine
OXPHOS	Oxidative phosphorylation

P	Postnatal day
P module	Proton pumping module
P-5-C	Pyrroline-5-carboxylate
PCA	Principal component analysis
PCDDP	Preclinical Drug Development Platform
pCO_2	Partial pressure of carbon dioxide
PCR	Polymerase chain reaction
P_D module	Distal proton pumping module
PDH	Pyruvate dehydrogenase
pGlu	Pyroglutamate
Phe	Phenylalanine
P_i	Inorganic phosphate
Pip	Pipecolate
Polg	DNA polymerase gamma gene
P_P module	Proximal proton pumping module
Pro	Proline
ProDH	Proline dehydrogenase
PSST	NADH:ubiquinone oxidoreductase core subunit S7 or NDUFS7
PTFE	Polytetrafluoroethylene
p-value	Probability value; the probability of making a Type I error
PYCR	Pyrroline-5-carboxylate reductase
Q	Ubiquinone; oxidised coenzyme Q
Q module	Ubiquinone binding module
QC	Quality control
QH_2	Ubiquinol; reduced coenzyme Q
R^2	Coefficient of determination; indicated the linearity data
RC	Respiratory chain
Redox	Reduction-oxidation
RNA	Ribonucleic acid
ROS	Reactive oxygen species
rpm	Revolutions per minute
rRNA	Ribosomal ribonucleic acid
RSA	Republic of South Africa
RT	Retention time
S/N	Signal-to-noise ratio
SAH	*S*-adenosylhomocysteine
SAM	*S*-adenosylmethionine
Sar	Sarcosine
SASBMB	South African Society for Biochemistry and Molecular Biology
SAVC	South African Veterinary Council
SC	Supercomplex
SD	Standard deviation
SDH	Succinate dehydrogenase
Ser	Serine
SHC	Src Homology 2 Domain Containing
SOL	Soleus
SOP	Standard operating procedure

SPF	Specific pathogen-free
Surine	Synthetic urine
Tau	Taurine
TGFβ	Transforming growth factor-β
THFA	Tetrahydrofolate
Thr	Threonine
TIA	Technology Innovation Agency
T_m	Melting temperature
TMCS	Trimethylchlorosilane
TMG	Trimethylglycine
TMS	Trimethylsilyl
TNB	2-nitro-5-thiobenzoic acid
TOST	Two one-sided test
tRNA	Transfer ribonucleic acid
$Trx(SH)_2$	Reduced thioredoxin
Trx(SS)	Oxidised thioredoxin
Tryp	Tryptophan
TSP	Trimethylsilyl-2,2,3,3-tetradeuteropropionic acid
TXI	Triple-resonance inverse
TYKY	NADH:ubiquinone oxidoreductase core subunit S8 or NDUFS8
USA	United States of America
UV	Ultraviolet
v	Version; relating to software
VIP	Variable important in projection
VUmc	Vrije Universiteit (VU) university medical center
WQ	White quadriceps
WT	Wild-type; genetically unaltered sample (specific to this study)
XERp	Variable selection for binary classification based error rate p-values using an extension of ERp that accounts for zero
β-Ala	Beta-alanine

Latin terms	
Ad libitum	According to pleasure; feeding habits are the choice of the animal as food is constantly available
De novo	Anew; from the beginning
Drosophila	A genus of small fruit flies
Homo sapiens	A species of primate to which modern humans belong
In utero	In the uterus; before birth
In vitro	In the glass; a process outside of a living organism
In vivo	In life; a process within a living organism
Mus musculus	A species of rodent; commonly known as a house mouse
Post-mortem	After death
Yarrowia lipolytica	Aerobic yeast

CHAPTER 1

Introduction

1.1 Background, research rationale and problem statement

Mitochondrial diseases (MDs) are amongst the most severe and prevalent groups of inborn disorders featuring genetic-, biochemical- and clinical heterogeneity, diagnostic difficulties, and currently — incurability. As a consequence of the extreme heterogeneity, fundamental MD mechanisms remain poorly grasped, which ultimately impedes the development of effective treatments. The dysfunction of complex I (CI) of the oxidative phosphorylation (OXPHOS) system is the most common form of MD and most often presents as Leigh syndrome — a severe childhood-onset neurometabolic disorder affecting approximately 1 in 40 000 new-borns (Darin *et al.*, 2001; Lake *et al.*, 2015; OMIM, 2017). Animal studies are vital to improve our understanding of underlying, complex MD processes. At present, one of the most reliable animal models of MD includes the whole-body *Ndufs4* knockout (*Ndufs4*$^{-/-}$) mouse, which presents with symptoms similar to human CI deficiency and develops a progressive Leigh-like phenotype.

Current research on *Ndufs4*$^{-/-}$ mice is focused on understanding their progressive neuropathology — as the disease primarily, and most severely, manifests in the motor centres of the brain (Quintana, 2010; Quintana *et al.*, 2012; Sterky *et al.*, 2012). Contrastingly, the *Ndufs4*$^{-/-}$ phenotype is widely considered to lack muscle involvement and consequently, little information is available on the skeletal muscle-specific consequences of the knockout. However, the muscular- and nervous systems are highly integrated, function interdependently and represent the two tissues most frequently affected by MD. Thus, the contribution of the muscular system to disease pathology cannot be ruled out, especially considering the possibility that faster progressing neurological phenotypes, with greater severity, might mask others. This notion was confirmed by a recent study reporting similar symptoms (including locomotor impairment and early mortality) between skeletal muscle-specific and whole-body *Ndufs4* knockout *Drosophila* (Foriel *et al.*, 2018). Taken together with the imperative role of the muscular system in systemic health and responses to disease states, as well as the regulation of whole-body metabolism, it is important to elucidate the downstream effects of the *Ndufs4* knockout on skeletal muscle metabolism.

A powerful investigative tool with which to achieve this, is the application of large-scale metabolomics. Metabolites serve as reporters of cellular activity, are the closest to the tissue phenotype, and are therefore prospective contributors to the novel pathological and mechanistic understanding of CI deficiency in tissues. To the best of our knowledge, metabolomics studies on *Ndufs4*$^{-/-}$ skeletal muscle have not been performed yet.

1.2 Aim and objectives of the study

1.2.1 Aim

The aim of the study is to investigate the *in vivo* effect of a *Ndufs4* knockout on skeletal muscles with different fibre type composition (i.e. white quadriceps femoris and soleus muscles) from *Ndufs4*$^{-/-}$ mice by combining biochemical strategies and multi-platform metabolomics.

1.2.2 Specific objectives

The objectives formulated to achieve the above-mentioned aim, were divided into three phases referred to as the sample collection-, biochemical evaluation- and metabolic profiling phases.

First, the *objectives* of the *sample collection phase* of this study include:

1.1 Interbreeding, genotyping and selecting mice for the study.

1.2 Animal euthanasia, tissue collection and storage.

1.3 *Post-mortem* genotype verification via standardised polymerase chain reaction.

Second, the *objectives* of the *biochemical evaluation phase* of this study include:

2.1 Standardising spectrophotometric enzyme activity assays for respiratory chain CI-CIV in mouse skeletal muscles.

2.2 Evaluating CI-CIV enzyme activity in *Ndufs4*$^{-/-}$ and wild-type skeletal muscles.

2.3 Data processing and statistical analysis.

Third, the *objectives* of the *metabolic profiling phase* of this study include:

3.1 Developing and standardising a miniaturised nuclear magnetic resonance spectroscopy (^{1}H-NMR) method for the analysis of limited-quantity biological samples and mouse skeletal muscles.

3.2 Standardising a liquid chromatography-tandem mass spectrometry (LC-MS/MS) method for the targeted analysis of amino acids and acylcarnitines in mouse skeletal muscles.

3.3 Standardising a gas chromatography time-of-flight mass spectrometry (GC-TOF-MS) method for the untargeted analysis of metabolites in mouse skeletal muscles.

3.4. Multi-platform (^{1}H-NMR, LC-MS/MS, and GC-TOF-MS) metabolic profiling of *Ndufs4*$^{-/-}$ and wild-type skeletal muscles.

3.5. Data preprocessing and pretreatment.

3.6. Statistical analysis and discriminatory metabolite discovery.

3.7. Pathway analysis and biological interpretation.

1.3 Structure of the dissertation

This dissertation is presented in chapter format, as required by the North-West University (NWU). The research presented in this dissertation is organised into six chapters, which includes two peer-reviewed publications.

Chapter 1 provides the rationale behind the research, the problem statement as well as the aim and objectives of the study. Furthermore, the structure of the dissertation along with the outcomes of the research, ethical considerations and funding is discussed. The chapter closes with signed statements from all of the co-authors, declaring their individual roles in the study.

Chapter 2 consists of a detailed literature study on the mitochondrion, the OXPHOS system, CI of the OXPHOS system and its NDUFS4 subunit, mitochondrial disease with focus on CI deficiency and Leigh syndrome, as well as the *Ndufs4* knockout mouse model and skeletal myofibres.

Chapter 3 provides detailed information regarding the materials used and methods employed in the study. The materials section presents the chemicals, instrumentation and software packages used, while the methods section includes analytical protocols, quality control measures, data analyses and statistical analyses performed.

Chapter 4 contains the first peer-reviewed paper resulting from the study, published in *Metabolomics* (Mason *et al.*, 2018). The paper describes a novel miniaturised ^{1}H-NMR method developed for the analysis of limited-quantity biological samples. The main focus of the paper is proving method equivalency between a well-established standard operating protocol (SOP) and the newly developed method. In addition, the miniaturised ^{1}H-NMR method's applicability is demonstrated in a pilot metabolomics study using minute soleus muscle tissue from *Ndufs4*$^{-/-}$ mice.

Chapter 5 contains the second peer-reviewed paper resulting from the study, published in *Biochimica et Biophysica Acta (BBA) — Molecular Basis of Disease* (Terburgh *et al.*, 2019). The paper provides fibre type-specific enzymatic and metabolic data from *Ndufs4*$^{-/-}$ skeletal muscles along with a detailed discussion of the hypothesised adaptive mechanisms taking place in CI deficient skeletal muscles.

Chapter 6 offers a summary of the research along with concluding remarks, strengths and limitations of the study, as well as future research prospects arising from the study.

Annexures: the dissertation concludes with Annexures A, B, C, D, E and F, consisting of; A) additional information on the animals used in the study; B) information regarding the

standardisation of the methods employed and the quality of the data obtained from this study; C-D) the two published peer-reviewed articles; and E-F) the instructions to authors for *Metabolomics* and *BBA — Molecular Basis of Disease*, as required by the NWU to be included in the dissertation.

1.4 Outcomes of the study

This study contributes to the field of natural science and mitochondrial disease research in the form of two peer-reviewed articles and an oral presentation at an international conference.

1.4.1 Published peer-reviewed article I (Chapter 4, Annexure C)

Mason, S.W., Terburgh, K. & Louw, R. 2018. Miniaturized ^{1}H-NMR method for analyzing limited-quantity samples applied to a mouse model of Leigh disease. *Metabolomics*, 14:1-12.

The article (https://doi.org/10.1007/s11306-018-1372-6) was published in the journal: *Metabolomics (*https://link.springer.com/journal/11306*),* which has an impact factor of 3.511 (2017). The journal publishes a broad scope of current research regarding the development of technology platforms for metabolomics. Author guidelines (Annexure E) can be accessed at: https://www.springer.com/life+sciences/biochemistry+%26+biophysics/journal/11306?detailsPage=pltci_1709154

1.4.2 Published peer-reviewed article II (Chapter 5, Annexure D)

Terburgh, K., Lindeque, J.Z., Mason, S.W., van der Westhuizen, F.H. & Louw, R. 2019. Metabolomics of *Ndufs4*$^{-/-}$ skeletal muscle: adaptive mechanisms converge at the ubiquinone-cycle. *Biochimica et Biophysica Acta — Molecular Basis of Disease*, 1865(1):98-106.

The article (https://doi.org/10.1016/j.bbadis.2018.10.034) was published in the journal: *BBA — Molecular Basis of Disease* (https://www.journals.elsevier.com/bba-molecular-basis-of-disease) with an impact factor of 5.108 (2017). The journal publishes research on disease processes and models of human disease, with focus on underlying pathological mechanisms contributing to disease understanding and/or treatment. Author guidelines are given in Annexure F or can be accessed at: https://www.elsevier.com/journals/bba-molecular-basis-of-disease/0925-4439?generatepdf=true

1.4.3 Oral presentation

Terburgh, K., Lindeque, J.Z., Mason, S.W, van der Westhuizen, F.H. & Louw, R. 2018, 8-11 July. *Ndufs4*$^{-/-}$ skeletal muscle reveals fibre type-specific bioenergetic and metabolic disturbances. Oral presentation at the SASBMB-FASBMB 2018 Conference, North-West, Potchefstroom, South Africa.

1.5 Ethical considerations

The AnimCare animal research ethics committee of the North-West University approved this study in 2016 (NWU-00378-16-A5) along with the animal protocols used here. All animals were maintained and all procedures performed in accordance with the code of ethics in research, training and testing of drugs in South Africa and complied with national legislation.

1.6 Financial support

This work was supported by the National Research Foundation of South Africa (NRF, Grant No. 92736 and 111247), the Technological Innovation Agency of the Department of Science and Technology of South Africa (TIA, Grant No. Metabol. 01), and the North-West University (NWU). Opinions expressed and conclusions arrived at, are those of the authors and are not necessarily to be attributed to the NRF, TIA or NWU.

1.7 Author contributions

Paper I presented in Chapter 4: Both Shayne Mason and Karin Terburgh were involved in analytical work, data analysis and manuscript writing. Roan Louw was involved in data analysis, manuscript writing and supervision. The authors declare equal contributions to the writing of the manuscript.

Paper II presented in Chapter 5: Karin Terburgh was involved in the design of the study, sub-study ethics application, sample collection, analytical work, data analysis, graphical images and manuscript writing. Shayne Mason was involved in NMR analytical work, NMR data analysis and manuscript editing. Francois van der Westhuizen was involved in the acquisition of funding, ethical approval and animal models, as well as manuscript editing. Zander Lindeque was involved in the design of the study, metabolic data analysis, manuscript editing and supervision. Roan Louw was involved in the acquisition of funding and ethical approval, the design of the study, enzyme assay analytical work, enzymatic- and metabolic data analysis, manuscript editing and supervision.

All authors signed the declaration on this page:

As a co-author, I hereby give consent that the mentioned articles may be used for the MSc dissertation of Karin Terburgh. I declare that my role in the study, as indicated above, is an accurate representation of my contribution.

Signature: _____
Prof R. Louw

Signature: _____
Prof F.H. van der Westhuizen

Signature: _____
Dr J.Z. Lindeque

Signature: _____
Dr S.W. Mason

Signature: _____
Ms K. Terburgh

1.8 References

Darin, N., Oldfors, A., Moslemi, A., Holme, E. & Tulinius, M. 2001. The incidence of mitochondrial encephalomyopathies in childhood: clinical features and morphological, biochemical, and DNA abnormalities. *Annals of Neurology*, 49(3):377-383.

Foriel, S., Beyrath, J., Eidhof, I., Rodenburg, R.J., Schenck, A. & Smeitink, J.A.M. 2018. Feeding difficulties, a key feature of the *Drosophila* NDUFS4 mitochondrial disease model. *Disease Models & Mechanisms*, 11:10.

Lake, N.J., Bird, M.J., Isohanni, P. & Paetau, A. 2015. Leigh syndrome: neuropathology and pathogenesis. *Journal of Neuropathology and Experimental Neurology*, 74(6):482-492.

Mason, S.W., Terburgh, K. & Louw, R. 2018. Miniaturized ^{1}H-NMR method for analyzing limited-quantity samples applied to a mouse model of Leigh disease. *Metabolomics*, 14:1-12.

OMIM (Online Mendelian Inheritance in Man). 2017. Leigh syndrome; LS. https://www.omim.org/entry/256000?search=256000&highlight=256000 Date of access: 10 Mar. 2017.

Quintana, A., Kruse,S.E., Kapurb, R.P, Sanz, E. & Palmiter, R.D. 2010. Complex I deficiency due to loss of Ndufs4 in the brain results in progressive encephalopathy resembling Leigh syndrome. *Proceedings of the National Academy of Sciences*, 107(24):10996-11001.

Quintana, A., Morgan, P.G., Kruse, S.E., Palmiter, R.D. & Sedensky, M.M. 2012. Altered anesthetic sensitivity of mice lacking Ndufs4, a subunit of mitochondrial complex I. *Public Library of Science One*, 7(8):e42904.

Sterky, F.H., Hoffman, A.F., Milenkovic, D., Bao, B., Paganelli, A., Edgar, D., Wibom, R., Lupica, C.R., Olson, L. & Larsson, N.G. 2012. Altered dopamine metabolism and increased vulnerability to MPTP in mice with partial deficiency of mitochondrial complex I in dopamine neurons. *Human Molecular Genetics*, 21(5):1078-1089.

Terburgh, K., Lindeque, J.Z., Mason, S.W., van der Westhuizen, F.H. & Louw, R. 2019. Metabolomics of *Ndufs4*$^{-/-}$ skeletal muscle: adaptive mechanisms converge at the ubiquinone-cycle. *Biochimica et Biophysica Acta — Molecular Basis of Disease*, 1865(1):98-106.

CHAPTER 2

Literature study

2.1 Introduction

This chapter provides a detailed outline of the literature relevant to this dissertation. Altogether, the provided information equips the reader with a basic background of the study and its key concepts. The chapter begins with a broad review of the mitochondrion, which gradually tapers down to the mitochondrial oxidative phosphorylation system, its first enzyme complex (CI), and the NDUFS4 subunit of CI. Thereafter, the focus is shifted towards mitochondrial dysfunction and the diseases that arise as a consequence thereof. Initially, general information is given on mitochondrial disease characteristics and pathophysiology, after which the chapter narrows in on the main focus of the study — CI dysfunction, NDUFS4 deficiency and Leigh syndrome. Next, a comprehensive overview of the whole-body *Ndufs4* knockout mouse model of CI deficiency is given, with the focus shifting towards tissue-specific investigations of the model, and finally, skeletal muscle tissue. The chapter then closes with a description of the experimental design of the study.

2.2 The mitochondrion

2.2.1 Mitochondrial structure, organisation and heterogeneity

The mitochondrial architecture comprises a (generally) reticular organelle encapsulated by a distinctive double membrane, creating four sub-compartments: a fairly permeable outer membrane (OMM), a protein-dense inter-membrane space (IMS), an impermeable inner membrane (IMM), and a protein-dense matrix. The latter houses numerous anabolic and catabolic enzymes, including those involved in the Krebs cycle and β-oxidation, as well as the mitochondrion's own genome. The IMM protrudes into the matrix through the formation of several invaginations (cristae) and houses the five enzyme complexes (complex I–V) of the oxidative phosphorylation (OXPHOS) system (Mannella, 2006; Shokolenko & Alexeyev, 2015; Prasai, 2017). Nucleated eukaryotic cells contain numerous (~ 800 to 2 500) mitochondria ubiquitously, however, the morphology, size, subcellular localisation, and number of mitochondria is remarkably heterogeneous within different cell types (Koopman *et al.*, 2005; Nunnari & Suomalainen, 2012; Vasava & Mashiyava, 2016; Prasai, 2017) and in some cases, even within a single cell e.g. myocytes (Schiaffino & Reggiani, 2011). Due to constant processes of fission and fusion as well as movement through the cytoskeleton, the mitochondrial structure is not fixed, but highly dynamic in nature (Ni *et al.*, 2015). In addition, a cell's mitochondrial volume is generally regulated to match its bioenergetic demand (Prasai, 2017), leaving energy-expensive tissues (e.g. brain, skeletal muscle, heart, liver and kidneys) with a much higher mitochondrial abundance than other tissues (Koopman *et al.*, 2005; Greaves *et al.*, 2012; Nunnari & Suomalainen, 2012; Vasava & Mashiyava, 2016).

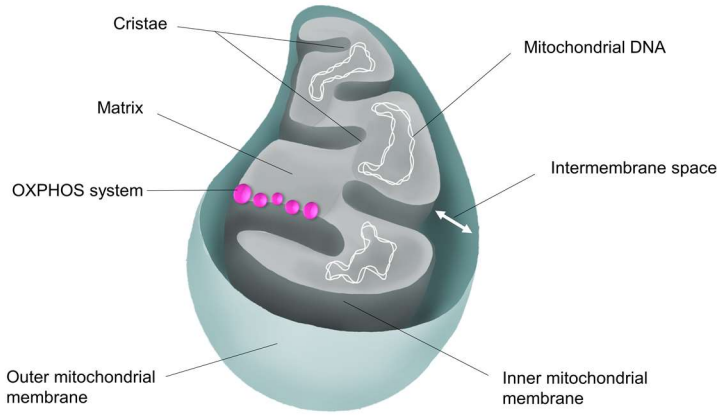


Figure 2-1: Schematic representation of the mitochondrion. The mitochondrion is a double-membraned organelle, housing the five enzyme complexes of the oxidative phosphorylation (OXPHOS) system (indicated by pink spheres) in the inner mitochondrial membrane cristae, as well as multiple copies of its own circular genome in the mitochondrial matrix.

2.2.2 Mitochondrial function

Mitochondria play a vital role in a myriad of processes involved in cellular bioenergetics, metabolic cell signalling and metabolism. As the primary source of cellular adenosine triphosphate (ATP) synthesis via the process of OXPHOS, mitochondria are vital for maintaining normal energy homeostasis and play an essential role in the adaptive responses to pathological conditions that cause stress to energy metabolism. Mitochondria function as signalling organelles, constantly communicating with the nucleus and other subcellular compartments in order to monitor and regulate the cell's energetic and metabolic status. This is achieved through the mitochondrial modulation of various cell-signalling pathways, such as: intracellular calcium signalling; reactive oxygen species (ROS) production and release; the initiation of apoptosis and necrosis; cellular stress responses; as well as innate immune responses and the maintenance of the cellular redox status ($NADH/NAD^+$ ratio). Furthermore, mitochondria have major anabolic and catabolic functions, and are central to the regulation of glucose-, amino acid-, lipid-, sulfur- and metal-metabolism as well as the production of heat (Greaves *et al.*, 2012; Nunnari & Suomalainen, 2012; Calmettes *et al.*, 2013; Acin-Perez & Enriquez, 2014; Shaughnessy *et al.*, 2014; Cherry & Piantadosi, 2015; Prasai, 2017; Suomalainen & Battersby, 2017; Rahman & Rahman, 2018).

2.2.3 Mitochondrial genome

Mitochondria function and are regulated by ~ 1 500 proteins encoded by two genomes — the nuclear and mitochondrial genome (Calvo *et al.*, 2016). In contrast to nuclear DNA (nDNA), mitochondrial DNA (mtDNA) is a multi-copy, circular, double-stranded DNA molecule (Chinnery & Hudson, 2013; Lagouge & Larsson, 2013; Grady *et al.*, 2014) thought to exist in clusters,

called nucleoids, tethered to the IMM (Carling *et al.*, 2011). mtDNA is strictly maternally inherited, contains no introns, and ranges in size from 16.3 kilobase pairs (kb) in the mouse to 16.6 kb in humans (Carling *et al.*, 2011; Greaves *et al.*, 2012; St. John, 2014). Furthermore, mtDNA has one major-noncoding region (1.1 kb), the D-loop, which is the site of interaction for the nuclear-encoded transcription and replication factors that initiate and drive mitochondrial transcription and replication (Greaves *et al.*, 2012; St. John, 2014). mtDNA contains 37 genes, necessary for mitochondrial function, that encode for: 13 essential structural genes of the OXPHOS system (Figure 2-2: seven, one, three and two subunits of complexes I, III, IV and V, respectively), and 24 ribonucleic acid (RNA) components of the mitochondrial translational apparatus (22 transfer RNAs and two ribosomal RNAs), necessary for protein synthesis (Greaves *et al.*, 2012; Grady *et al.*, 2014; St. John, 2014; Shokolenko & Alexeyev, 2015). Notably, mitochondria are only partially autonomous as the entire OXPHOS complex II and all other mitochondrial proteins — including those responsible for mtDNA replication, repair, transcription and translation — are encoded by the nuclear genome and require mitochondrial import (Chinnery & Hudson, 2013; Shokolenko & Alexeyev, 2015; Calvo *et al.*, 2016). Several hundred to thousands of mtDNA copies are found within a single cell, with this number varying greatly in different cell types, depending on the tissue's energy demand (Greaves *et al.*, 2012; St. John, 2014). High-energy demanding cells require large quantities of ATP to undertake their complex functions and, therefore, maintain high numbers of mtDNA copies to enable sufficient ATP generation through OXPHOS (Dickinson *et al.*, 2012; St. John, 2014).

2.3 The oxidative phosphorylation (OXPHOS) system

2.3.1 Structure and organisation of the OXPHOS system

As mentioned in 2.2.1, the IMM houses the five enzyme complexes (CI–CV)[1] of the OXPHOS system, of which the first four as well as two mobile electron carriers, ubiquinone (Q) and cytochrome c (cyt c), form the respiratory chain (RC). Although the complexes of the RC have long been viewed as individual entities in the IMM (random collision model), as depicted in Figure 2-2, it is now well recognised that individual complexes associate with each other to form higher order macromolecular assemblies, called supercomplexes (SC). However, whether the RC complexes exist solely as supercomplexes (solid state model) or may exist as both supercomplexes and individual entities (plasticity model), is still debated (Boekema & Braun,

[1] Complex I: NADH:ubiquinone oxidoreductase, EC 1.6.5.3; complex II: succinate:ubiquinone oxidoreductase, EC1.3.5.1; complex III: ubiquinol:ferricytochrome *c* oxidoreductase, EC 1.10.2.2; complex IV: ferrocytochrome-*c*:oxygen oxidoreductase, EC 1.9.3.1; and complex V: ATP phosphohydrolase, EC 3.6.1.3.

2007; Chaban *et al.*, 2014; Milenkovic *et al.*, 2017; Lobo-Jarne & Ugalde, 2018). SCs of varying stoichiometry have been identified in mammalian mitochondria, including assemblies of CI, CIII dimers and CIV or oligomers thereof ($CI/CIII_2/CIV_{1-4}$); CI and CIII dimers ($CI/CIII_2$); as well as assemblies of CIII dimers and CIV or dimers thereof ($CIII_2/CIV_{1-2}$.). The fraction of mammalian RC structures localised in the two largest SCs ($CI/CIII_2/CIV_{1-4}$ and $CI/CIII_2$) have been estimated to be ~ 90 % of CI, ~ 40-50 % of CIII and ~ 20-30 % of CIV; while only ~ 5–10 % of the enzymes are found in $CIII_2/CIV_{1-2}$ (Milenkovic *et al.*, 2017; Lobo-Jarne & Ugalde, 2018). The most abundant SC ($CI/CIII_2/CIV_{1-4}$) in eukaryotes containing CI, is called the respirasome (Figure 2-3), as it comprises all the components required for electron transfer from NADH to molecular oxygen. Several studies have underscored the important role of the respirasome in the proper assembly and stability of CI, as the absence of the SC (due to the primary lack of $CIII_2$, CIV or cyt c) was shown to result in reverse electron transport from ubiquinol (QH_2) to CI — triggering local ROS generation, CI instability, degradation and loss. Contrastingly, the loss of CI generally does not seem to cause severe defects in other RC enzymes. Nevertheless, the functional role of RC organisation into SCs remains unclear with current theories, including: the stabilisation of enzyme complexes (especially CI), the catalytic enhancement of the electron flux through substrate channelling, and the modulation and decrease of ROS production (Boekema & Braun, 2007; Chaban *et al.*, 2014; Milenkovic *et al.*, 2017; Lobo-Jarne & Ugalde, 2018).

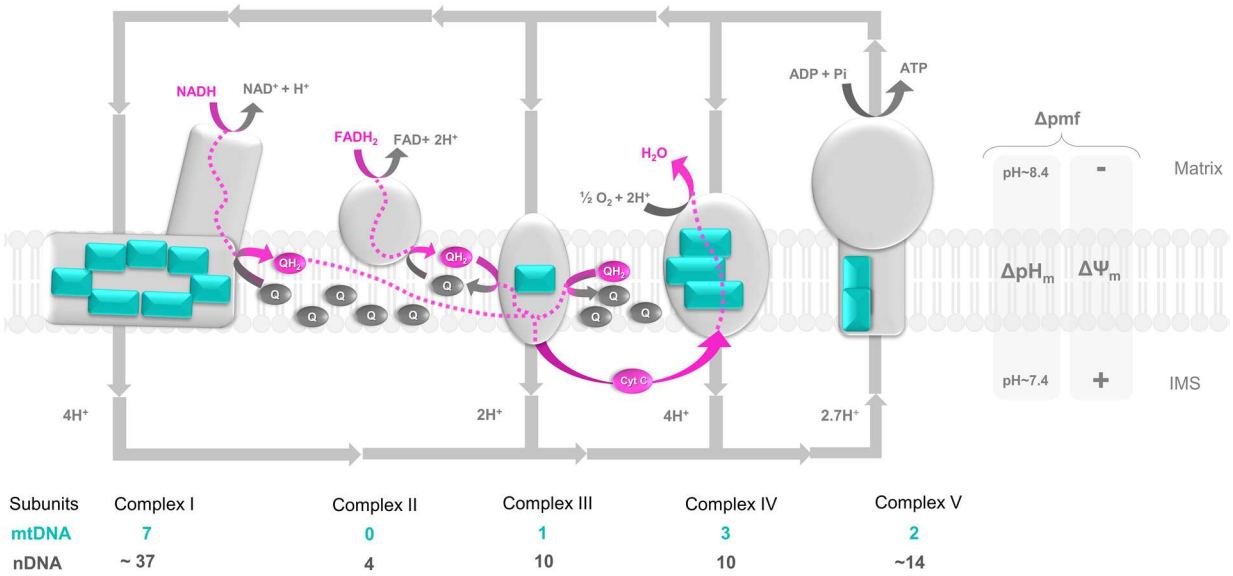


Figure 2-2: Overview of the structure and function of the OXPHOS system. The subunits of the OXPHOS enzyme complexes (I-V) are encoded by both mitochondrial- and nuclear DNA, with the number of subunits encoded by each genome indicated in blue and grey respectively. Electron flow (in pink) through the respiratory chain (CI-CIV) to molecular oxygen is coupled to proton (H^+) translocation (light grey arrows) from the matrix to the intermembrane space (IMS) creating a proton motive force (Δpmf) across the IMM comprising a pH gradient (ΔpH_m) and a mitochondrial membrane potential ($\Delta\Psi_m$) which drives ATP synthesis via CV. *Abbreviations: ADP, adenosine diphosphate; ATP, adenosine triphosphate; Cyt c, cytochrome c; $FADH_2$, flavine adenine dinucleotide; H_2O, water; mtDNA, mitochondrial DNA; NADH:reduced nicotinamide adenine dinucleotide; nDNA, nuclear DNA; O_2, oxygen; Pi, inorganic phosphate; Q, ubiquinone; QH_2, ubiquinol.*

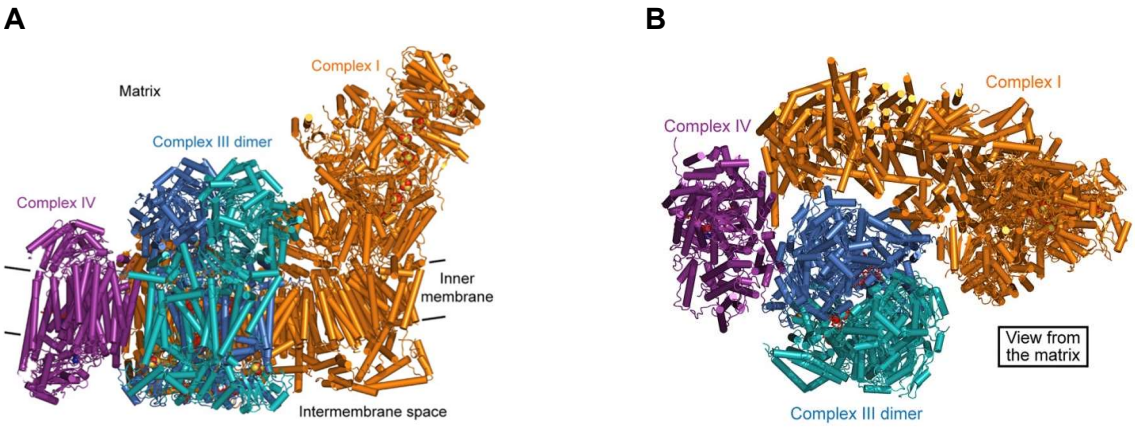


Figure 2-3: Structure of the (porcine) respirasome. The arrangement of CI (orange), the CIII dimer (the monomers are shown in blue and cyan), and CIV (magenta) in the largest respiratory chain supercomplex, called the respirasome. The respirasome viewed **A:** along the membrane plane and **B:** from the matrix. *Reprinted from Milenkovic et al. (2017), Copyright (2017), with permission from Elsevier*.

2.3.2 The function of the OXPHOS system

2.3.2.1 Electron entry into and transport through the respiratory chain

Electrons enter the RC from reducing equivalents (NADH and $FADH_2$) produced by the catabolism of carbohydrates, fatty- or amino acids and are transferred through the RC to the molecular acceptor, oxygen, to produce water. Classical sites of electron entry into the RC is at CI, through the oxidation of NADH, and at CII (succinate dehydrogenase), through the oxidation of succinate. Both complexes reduce ubiquinone (Q) to ubiquinol (QH_2), which exists as a common pool dissolved in the mitochondrial lipid bilayer that exchanges freely between RC complexes (Quinlan *et al.*, 2011; Blaza *et al.*, 2014). In addition to CI and CII, several other enzymes (discussed in Section 2.3.3) also provide electrons to the RC at the Q pool (McDonald *et al.*, 2018). Once reduced by CI or Q-linked dehydrogenases, QH_2 is ultimately oxidised by CIII via the ubiquinone-cycle. The Q-cycle refers to the overall process during which CIII oxidises one QH_2 molecule from the membrane pool, reduces two cytochrome c (cyt c) molecules, and extrudes the equivalent of two positive charges via proton translocation out of the matrix with each complete turnover (Reaction 2-1). Each cycle consists of a two-step reaction, during which two QH_2 molecules are oxidised in the Qo site of CIII (cytosolic side); two electrons are transferred to cyt c; one Q molecule is reduced sequentially to form QH_2 in the Qi site of CIII (matrix side); and two protons vanish from the matrix, while four protons appear in the cytosol (Quinlan *et al.*, 2011). Finally, electron transport concludes with reduced cyt c transferring the electrons to CIV, which in turn reduces oxygen to produce water.

Reaction 2-1: Q-cycle	$QH_2 + 2$ cyt c (Fe^{3+}) $+ 2\ H^+_{(matrix)} \rightarrow Q + 2$ cyt c (Fe^{2+}) $+ 4\ H^+_{(IMS)}$

2.3.2.2 The proton circuit across the inner mitochondrial membrane

As a consequence of electron transport through the RC, the three proton-translocating complexes (CI, CIII and CIV), along with complex V (CV, F_1F_0-ATP synthase) create a proton circuit across the IMM, which is vital to mitochondrial bioenergetics. As electrons pass through each complex, the consequent drop in redox potential is coupled to the transfer of protons (H^+) out of the matrix to the IMS — thus generating a proton electrochemical potential gradient across the IMM, comprising a pH gradient (ΔpH_m = ~ 0.8 pH units/50 mV; matrix: basic) and a mitochondrial membrane potential[2] ($\Delta\Psi_m$ = ~ 120–180 mV; matrix: negative) (Logan *et al.*, 2016). Together, this transmembrane potential provides a matrix-directed proton-motive force[3] (Δpmf in mV) and proton flux across the IMM back into the matrix via CV, which drives ATP synthesis from ADP and P_i. In parallel, protons also endogenously leak from mitochondria — a process that controls the magnitude of the Δpmf and completes the proton circuit in the absence of ATP production. Total proton extrusion from the matrix differs based on the electron donor, with electron pairs from NADH and Q-linked dehydrogenases leading to a proton-pumping stoichiometry of ten protons per electron pair (10 $H^+/2e^-$) and six protons per electron pair (6 $H^+/2e^-$), respectively (Brand & Nicholls, 2011).

2.3.3 NADH shuttles and non-classical pathways feeding into the respiratory chain

In addition to matrix-derived NADH and $FADH_2$, cytosolic reducing equivalents may also enter the RC through several metabolite shuttles[4], such as the malate-aspartate shuttle (Reaction 2-2), which transfers cytosolic-derived electrons to the RC at CI via NADH through the interconversion of oxaloacetate and malate in the cytosol and matrix; and the glycerol-3-phosphate (GP) shuttle (Reaction 2-3), which transfers cytosolic-derived electrons to the RC via $FADH_2$ at the Q pool through the interconversions of dihydroxyacetone phosphate (DHAP) and GP in the cytosol and IMS. These shuttles are mainly active when the cytosolic NADH/NAD^+ ratio is higher than that of the mitochondria, since they serve as redox exchange mechanisms, replenishing cytosolic NAD^+ (Dawson, 1979; Garrett & Grisham, 2013; McDonald *et al.*, 2018). In addition to the mitochondrial GP dehydrogenase enzyme of the GP shuttle, several other enzymes also donate electrons to the RC at the Q pool. Some examples include: the electron transfer flavoprotein (ETF) dehydrogenase of the ETF/ETF-QO system, which accepts electrons

---

[2] $\Delta\psi_m$ refers to the concentration of ions (electrical potential) on opposite sides of the IMM (matrix = negatively charged; cytoplasm = positively charged).

[3] Protonmotive force (Δpmf) is formally defined as the transmembrane potential divided by Faraday's constant: $\Delta pmf = \Delta\psi_m - 59\ \Delta pH_m$ (Logan *et al.*, 2016).

[4] Due to the impermeability of the IMM, NADH and NAD^+ cannot freely exchange between the cytosol and mitochondrial matrix, therefore, metabolite shuttles are required to transfer these molecules between the two compartments.

from acyl-CoA's derived from fatty acid oxidation, branched-chain amino acid- and lysine catabolism, as well as dimethylglycine and sarcosine catabolism (Watmough & Frerman, 2010; Mailloux *et al.*, 2016; McDonald *et al.*, 2018); proline dehydrogenase, which obtains electrons from the catabolism of proline (McDonald *et al.*, 2018); sulfide-ubiquinone oxidoreductase, which obtains electrons from amino acid-derived sulfides (Bouillaud & Blachier, 2011); and dihydro-orotate dehydrogenase which accepts electrons from pyrimidine synthesis (Fang *et al.*, 2013).

Reaction 2-2: Malate-aspartate shuttle	Oxaloacetate + NADH $_{(cytosol)}$ → Malate + NAD^+ $_{(cytosol)}$ Malate transported to matrix Malate + NAD^+ $_{(Matrix)}$ → Oxaloacetate + NADH $_{(matrix)}$
Reaction 2-3: Glycerol-3-phosphate shuttle	DHAP + NADH $_{(cytosol)}$ → GP + NAD^+ $_{(cytosol)}$ GP transported to IMS GP + FAD $_{(IMS)}$ → DHAP + $FADH_2$ $_{(IMS)}$

2.4 Complex I (CI) of the OXPHOS system

2.4.1 CI structure

Complex I (CI, NADH:ubiquinone oxidoreductase, EC 1.6.5.3) is the first enzyme in the mitochondrial RC, and its architecture is among the largest and most intricate of membrane enzyme complexes. As depicted in Figure 2-4 A, the enzyme has an overall L-shaped structure with two multi-heteromeric arms, separated by an angle of ~ 120°. The hydrophilic matrix arm protrudes into the mitochondrial matrix, while the hydrophobic membrane arm is embedded in the IMM. The entire holo-CI is an assembly of 45 (44 unique), protein subunits with a molecular mass of ~ 980 kDa. The enzyme is composed of 14 central subunits (displayed in colour in Figure 2-4 A), constituting the catalytic core of the enzyme, which executes the bioenergetic core functions of CI. Among the central subunits, those forming the matrix arm (n = 7; 75-kDa, 51-kDa, 24-kDa, 49-kDa, 30-kDa, PSST and TYKY) are nuclear-encoded, while those constituting the membrane arm (n = 7; ND1, ND2, ND3, ND4L, ND6, ND4 and ND5) are mitochondrial-encoded. The remaining 31 (30 unique) nuclear-encoded polypeptides of the enzyme are called accessory subunits (depicted in grey in Figure 2-4 A), as they encase the catalytic core of the enzyme. The central subunits of CI are further organised into three modules, based on their function. The distal and proximal halves of the matrix arm contain the NADH oxidation (N) and ubiquinone reduction (Q) modules, respectively, which are involved in the electron transfer activity of CI. The proton pumping (P) module, which is involved in the proton translocation activity of CI, is found in the membrane arm with the distal and proximal

halves of the arm containing the proximal pump (P_P) module, and the distal pump (P_D) module, respectively (Sazanov, 2015; Zickermann *et al.*, 2015; Fiedorczuk *et al.*, 2016; Hirst & Roessler, 2016).

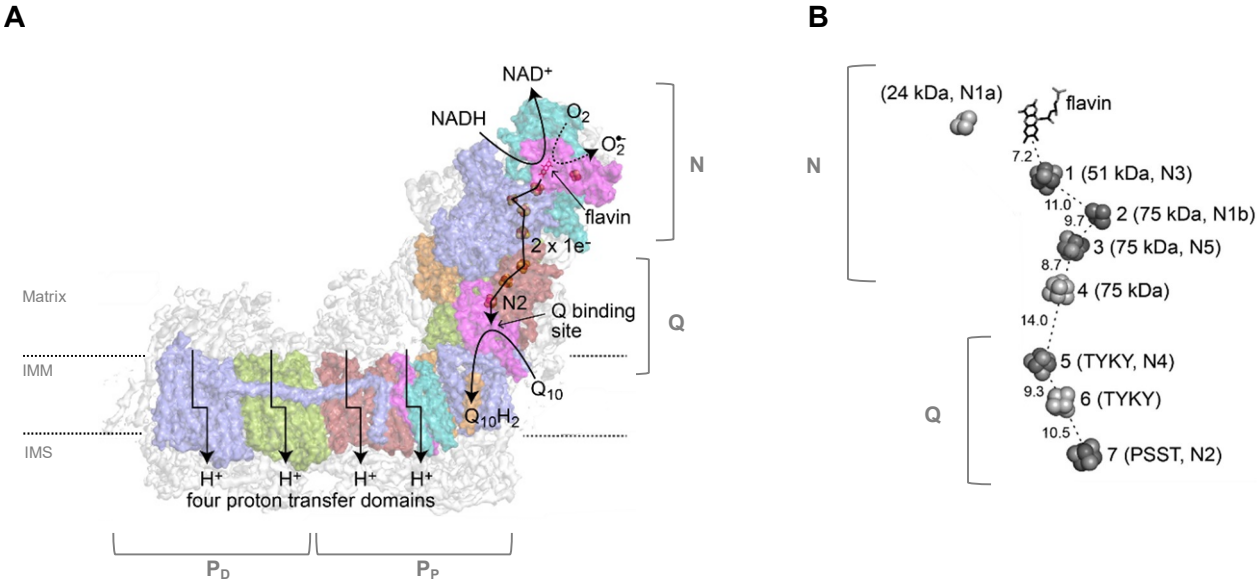


Figure 2-4: Overview of the structure and function of mammalian complex I. A: CryoEM density for the complete CI enzyme with accessory subunits (n = 31) depicted in grey and central subunits (n = 14) shown in colour. N module: blue, 75-kDa; cyan, 51-kDa; pink, 24-kDa. Q module: green, 49-kDa; orange, 30-kDa; pink, PSST; red, TYKY. P_D module: blue, ND5; green, ND4. P_P module: red, ND2; pink, ND4L; cyan, ND6; orange, ND3; blue, ND1. NADH is oxidised by a flavin mononucleotide in the N module, then electrons are passed along a chain of iron–sulfur clusters (ending in cluster N2) to reduce bound ubiquinone. Four protons are transferred from the matrix to the intermembrane space (IMS) for each NADH oxidised. **B:** Structure of the iron-sulfur cluster chain in the matrix arm. Clusters are labelled according to their position in the chain, with their corresponding subunits shown in brackets. *Adapted and reprinted from Hirst and Roessler (2016), https://doi.org/10.1016/j.bbabio.2015.12.009, as permitted by the Creative Commons Attribution License (CC BY).*

2.4.2 CI function

2.4.2.1 CI central subunits

CI is the primary entry point of electrons into the RC in the form of NADH (Bakker *et al.*, 2000; Papa *et al.*, 2010; Sazanov, 2015) and produces up to 40 % of the Δpmf required for mitochondrial ATP synthesis (Hunte *et al.*, 2010; Hoefs *et al.*, 2012). The bioenergetic core functions of CI (depicted in Figure 2-4) involve three main redox reactions in the matrix arm [NADH oxidation, iron-sulfur (Fe-S) cluster electron transfer, and ubiquinone reduction], which release energy that is transmitted to the membrane arm, allowing proton translocation from the matrix to the IMS. First, an NADH molecule binds to CI at specific redox centres located in the NDUFV1 subunit of the N module and donates two electrons to the primary electron acceptor, flavin mononucleotide (FMN) — reducing it to $FMNH_2$. Second, electrons are transferred from $FMNH_2$ to the 4Fe-4S cluster of PSST (cluster N2) in the Q module via a chain of seven Fe-S

clusters running through the matrix arm (Figure 2-4 B). Third, electrons from cluster N2 are transferred to Q — reducing it to QH_2, which then donates its electrons to CIII. Finally, the energy transduction by the above-mentioned redox reactions is utilised to transfer matrix-derived protons across the IMM at a suggested proton pump stoichiometry of four protons to two electrons ($4H^+/2e^-$) via four putative proton channels (three antiporter-like domains and the other ND subunits) located in the P module. The exact mechanism of proton pumping is still debated. One of the most recent hypotheses — the two-state stabilisation-charge mechanism — provides a putative link between electron- and proton transfer in CI. In this model, CI is hypothesised to switch between two states: the E state, in which electrons are transferred through CI and Q can be reduced by cluster N2, and the P state, in which Q travels away from CI. The conformational change from E to P state is postulated to be driven by the stabilisation of negatively charged quinone intermediates, thereby transmitting energy from the matrix arm to the membrane arm to drive proton pumping (Zickermann *et al.*, 2015). However, it is still questioned whether N2 oxidation, Q binding, Q reduction, or QH_2 dissociation is coupled to proton translocation and whether the reaction proceeds by a single-stroke or double-stroke mechanism (Hirst & Roessler, 2016).

2.4.2.2 CI accessory subunits

In order to function efficiently, CI must be successfully assembled into a stable holoenzyme and maintained via the continuous exchange of old, damaged subunits for new ones (Papa *et al.*, 2010; Mimaki *et al.*, 2012; Sánchez-Caballero *et al.*, 2016). Although the exact function of the various accessory subunits of CI is not well known, their importance to the assembly, structural stability, and regulation of the holoenzyme's function is becoming increasingly clear (Friedrich & Bottcher, 2004; Hoefs *et al.*, 2012; Sazanov, 2015; Stroud *et al.*, 2016). In addition, these subunits have also been implicated in the assembly of supercomplexes, reducing ROS production and protecting the enzyme against the damaging effects of ROS (Friedrich & Bottcher, 2004; Hoefs *et al.*, 2012; Sazanov, 2015; Stroud *et al.*, 2016).

2.4.3 CI biogenesis and assembly

CI biogenesis initiates with the mitochondrial and nuclear transcription of CI subunits and assembly factors, followed by the mitochondrial and cytosolic translation thereof. The majority of these proteins are synthesised in the cytosol and need to be imported into the mitochondrion where they are then sorted into the different mitochondrial sub-compartments for CI assembly, depending on their localisation in the holoenzyme. CI assembly comprises the sequential and coordinated association of the various central and accessory subunits as well as cofactors of CI to form the mature holoenzyme. For the assembly process to proceed effectively, several

nuclear DNA-encoded assembly factors (14 currently identified) are required, which assist in the assembly of CI (mainly membrane arm assembly) without forming part of the final structure (Sánchez-Caballero *et al.*, 2016; Stroud *et al.*, 2016; Guerrero-Castillo *et al.*, 2017). Although the mechanisms of CI assembly are not yet fully elucidated, the modular assembly model describes the current understanding of the process. CI assembly starts with the independent formation of five assembly intermediates (N, Q/P_P-a, P_P-b, P_D-a, and P_D-b) corresponding to the functional modules of the enzyme. The process continues with the association of these five assembly intermediates — first, the preassembled submodules interact to form the P_P-b/P_D-a subassembly, which then interacts with the Q/P_P-a and the P_D-b intermediates to form the Q/P subassembly. In the final steps, the preassembled N module is added to the Q module of the Q/P subassembly and the assembly factors are removed to produce the mature CI holoenzyme (Sánchez-Caballero *et al.*, 2016; Kahlhöfer *et al.*, 2017). As mentioned in Section 2.3.1, the majority of mature mammalian CI is found in supercomplexes with $CIII_2$ or $CIII_2$ + CIV_{1-4}. It is still debated whether supercomplex assembly takes place through the direct association of fully-assembled RC complexes or through the association of partially-assembled RC complexes and submodules to a CI-scaffold that lacks the N module, which is incorporated at the latest assembly stage (Mimaki *et al.*, 2012; Stroud *et al.*, 2016; Guerrero-Castillo *et al.*, 2017; Lobo-Jarne & Ugalde, 2018)

2.4.4 NDUFS4 accessory subunit of CI

One of the accessory subunits of CI, NADH dehydrogenase (ubiquinone) iron-sulfur protein 4 or NDUFS4 has been shown to be particularly essential for holo-CI assembly, stability and activity (Scacco *et al.*, 2003; Papa *et al.*, 2010; Quintana, 2010; Calvaruso *et al.*, 2012; Andrews *et al.*, 2013; Alam *et al.*, 2015; Kahlhöfer *et al.*, 2017; Lamont *et al.*, 2017). The nuclear *Ndufs4* gene — encoding 175 amino acids of the NDUFS4 protein — is localised on chromosome 5 in humans (gene ID: 4724) and chromosome 13 in mice (gene ID: 17993) (Papa, 2002; Kruse *et al.*, 2008; NCBI, 2017a; NCBI, 2017b). Once translated in the cytosol, the precursor NDUFS4 protein contains a canonical RVSTK sequence within its carboxyl terminus, which enables the reversible phosphorylation thereof. Posttranslational modification [phosphorylation by cyclic adenosine monophosphate (cAMP)-dependent protein kinase] of precursor NDUFS4 is required to enable its import into the mitochondrion, the subsequent maturation of the protein, and incorporation into CI. NDUFS4's posttranslational modification seems to play an important role in the regulation of CI activity (Scacco *et al.*, 2003; Papa *et al.*, 2010), with increased protein kinase-mediated NDUFS4 phosphorylation linked to increased CI activity (Papa, 2002; Valsecchi *et al.*, 2013). Mature NDUFS4 is ubiquitously expressed, non-enzymatic, 18 kDa in size and seems to be added to CI during the final stages of biogenesis and/or supercomplex

assembly (Calvaruso *et al.*, 2012; Kahlhöfer *et al.*, 2017). Bovine and ovine orthologues of NDUFS4 have been modelled to be attached to the central 75-kDa subunit of the N module; contacting three central subunits of the Q module (Fiedorczuk *et al.*, 2016; Zhu *et al.*, 2016). In agreement, the knockout of the NDUFS4 orthologue in aerobic yeast (*Yarrowia lipolytica*) disrupted several Fe-S clusters (N1b, N3 and N4) spanning the matrix arm of CI and resulted in the destabilisation of CI, reduction of CI activity and increased ROS release (Kahlhöfer *et al.*, 2017). Taken together, the importance of the NDUFS4 accessory subunit of CI is evident; even though the subunit's exact function is still unclear.

2.5 Mitochondrial disease

2.5.1 An introduction to mitochondrial disease

The collective term, mitochondrial disease (MD), refers to a heterogeneous group of genetic disorders affecting OXPHOS and mitochondrial function, which results in a clinically heterogeneous spectrum of phenotypes (Chinnery & Hudson, 2013; Gorman *et al.*, 2016; Niyazov *et al.*, 2016; Craven *et al.*, 2017; Keshavan & Rahman, 2018). Despite being the most common group of inherited metabolic disorders, MDs and their underlying pathogenic mechanisms are poorly understood. The reason for this is the extremely complex and heterogeneous nature of these disorders — genetically, biochemically and clinically. Consequently, both the diagnosis and treatment of MD present a severe challenge. MD can be categorised into primary and secondary MD, according to the cause thereof. Primary MD results from pathogenic mutations encoding the subunits or assembly factors of the OXPHOS system, as well as mutations affecting pathways that influence OXPHOS system biogenesis — such as RC cofactor biosynthesis; mtDNA replication, transcription and translation; mitochondrial biogenesis, etc. (Nouws *et al.*, 2012; Koopman *et al.*, 2016; Ghezzi & Zeviani, 2018; Keshavan & Rahman, 2018). Contrastingly, secondary MD results from either genetic causes not related to OXPHOS system biogenesis or function, or non-genetic causes such as environmental factors. The development of secondary MD has been observed in conjunction with many common (hereditary) non-communicable diseases such as cancer, diabetes mellitus, neurodegenerative diseases (e.g. Alzheimer's disease and Parkinson's disease), cardiovascular- and kidney disease, as well as acquired immune deficiency syndrome (AIDS) (Taylor & Turnbull, 2005; Koopman *et al.*, 2016; Niyazov *et al.*, 2016). In this dissertation, the term MD refers to primary mitochondrial disease.

2.5.2 Prevalence, genetics and clinical phenotype

MD has an estimated collective prevalence of 1 in 4 300 to 1 in 5 000, with many cases still mis- or undiagnosed (Thorburn, 2004; Gorman *et al.*, 2015; Keshavan & Rahman, 2018), and specific MDs more common in certain populations with genetic founder mutations and high consanguinity[5] (Gorman *et al.*, 2016; Craven *et al.*, 2017; Suomalainen & Battersby, 2017). Due to the dual genetic control of mitochondrial function, MDs can originate from mutations in nuclear or mitochondrial encoded genes and can follow different inheritance patterns — sporadic, maternal, autosomal recessive, autosomal dominant, X linked or *de novo* occurrence during embryogenesis. Hence, disease-causing mutations can be present in all cells of the embryo or can be tissue-specific; resulting in multisystemic or single tissue phenotypes (Gorman *et al.*, 2016; Craven *et al.*, 2017; Suomalainen & Battersby, 2017). Pathogenic mutations have been identified in more than 350 genes, of both mitochondrial and nuclear origin, with the majority of MD cases resulting from nDNA mutations (Gorman *et al.*, 2015; Alston *et al.*, 2017; Rahman & Rahman, 2018). Most nDNA mutations are inherited as autosomal recessive traits with a small number of autosomal dominant and X-linked dominant (XLD) defects reported (Niyazov *et al.*, 2016; Alston *et al.*, 2017; Keshavan & Rahman, 2018). Contrastingly, mtDNA mutations are primarily maternally inherited or sporadic with patients being homoplasmic[6] or heteroplasmic[7] for the mutation. In the (more common) case of heteroplasmy, a cell's proportion of mutant to wild-type mtDNA is important in disease manifestation as the level of mtDNA mutation (or heteroplasmy) must exceed a critical threshold[8] before biochemical consequences are detected — this phenomenon is called the biochemical threshold effect. Heteroplasmy levels can fluctuate over time in either direction (higher or lower) with fast-dividing tissues (e.g. blood) often showing decreases in mutation levels and non-dividing tissues (post-mitotic e.g. muscle), often showing highly increased mutation levels over time (Gorman *et al.*, 2016; Craven *et al.*, 2017; Suomalainen & Battersby, 2017).

In light of the above-mentioned genetic heterogeneity of MD, it is not surprising that patients present with a remarkably wide spectrum of clinical symptoms (depicted in Figure 2-5) in almost

---

[5] Consanguinity, or inbreeding, denotes a reproductive relationship between two closely related individuals. The degree of kinship between individuals defines the proportion of genes shared between them, therefore, the offspring of consanguineous couples are at higher risk for autosomal recessive disorders due to their increased probability for homozygosity by descent (Koellner *et al.*, 2018).

[6] Homoplasmy refers to an individual cell containing a pathogenic mtDNA mutation in all copies of the genome.

[7] Heteroplamy refers to an individual cell containing a mixture of mutated and wild-type mtDNA copies.

[8] The threshold level is typically considered to be 60-80% mutant mtDNA, but is dependent on the particular mtDNA mutation, organ and individual (Craven *et al.*, 2017).

any organ, differing in age of onset (neonatal-, infantile-, childhood-, or adult-onset) and severity (mild, severe, or fatal). Infantile- and childhood-onset MDs are generally the most severe, with nDNA mutations accounting for the majority (~ 75 %) of cases. While mtDNA mutations mainly cause adult-onset MD, very high levels of mtDNA heteroplasmy also account for childhood-onset MD (Gorman *et al.*, 2015; Niyazov *et al.*, 2016; Alston *et al.*, 2017). As OXPHOS is required to supply energy to essentially any cell[9], MD can affect any organ and is often multisystemic — with high metabolic demand post-mitotic tissues (e.g. muscle, heart, brain, liver, kidneys and eyes) being most commonly affected (Breuer *et al.*, 2013; Ghezzi & Zeviani, 2018; Keshavan & Rahman, 2018). MD patients often present with clinical features that can be organised into a few syndromes[10], however, most often, patients cannot be distinctly categorised. Common, nonspecific clinical features of MD include hypotonia, fatigue, exercise intolerance, generalised weakness, failure to thrive, dysautonomia[11], vomiting, seizures, and encephalopathy[12] (Gorman *et al.*, 2016; Suomalainen & Battersby, 2017).

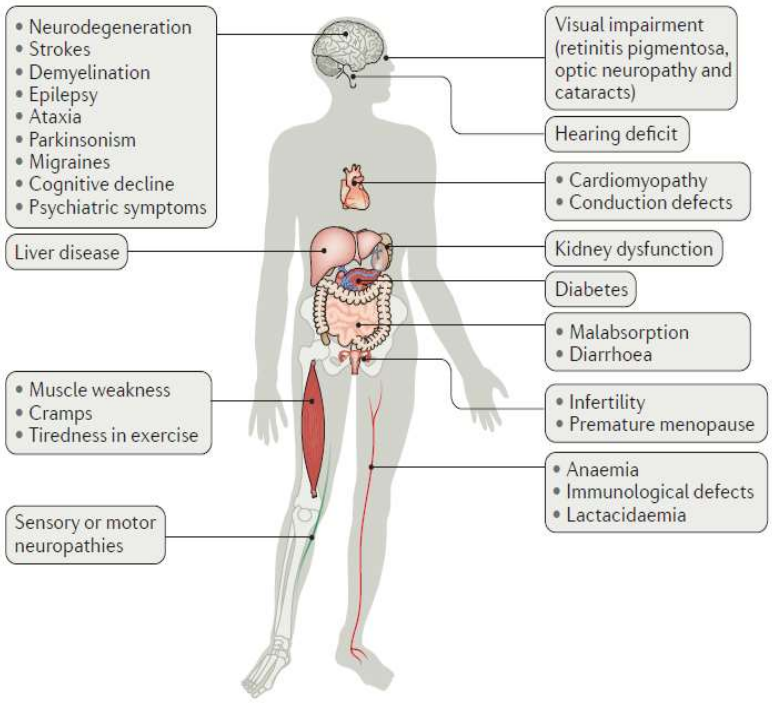


Figure 2-5: The heterogeneity of mitochondrial disease manifestations. Mitochondrial diseases are typically progressive disorders, which can manifest in almost any organ (including multiple organs), differing in age of onset (neonatal-, infantile-, childhood-, or adult-onset) and severity (mild, severe, or fatal). *Reprinted by permission from Springer Nature Customer Service Centre GmbH: Springer Nature, Nature Reviews — Molecular Cell Biology, Suomalainen and Battersby (2017), Copyright (2017)*.

[9] Except red blood cells, which do not have mitochondria.
[10] Some examples include LHON, MILS, NARP, MELAS, MERRF, CPEO, KSS, Leigh syndrome, Alpers-Huttenlocher syndrome and Pearson's syndrome (Gorman *et al.*, 2016; Niyazov *et al.*, 2016).
[11] A broad term for disorders affecting the functioning of the autonomic nervous system.
[12] A broad term for disorders affecting the brain structure or function.

2.5.3 Pathophysiology

2.5.3.1 Introduction

Although pathogenic mutations resulting in MDs typically cause OXPHOS defects, the pathophysiology is extremely complex and cannot be accounted for by aberrant ATP homeostasis (ATP/ADP ratio, decreased) alone. Accumulating evidence supports the notion that mitochondrial stress responses (triggered by the molecular defect) rather than the OXPHOS defect itself, are the main culprits in MD pathology (Suomalainen & Battersby, 2017; Rahman & Rahman, 2018). In addition to ATP production capacity, MD also affects several molecules that form part of the cell's bioenergetic-sensing pathways — these molecules constantly monitor the cell's developmental- and physiological state and participate in the cross-talk between the mitochondrial- and nuclear genomes. Mito-nuclear cross-talk forms a central part of the cell's adaptive response programme, which enables the altered expression of nuclear genes to reprogram mitochondrial- and cellular function along with metabolism as needed (Quirós *et al.*, 2016). Indeed, another poorly understood consequence of MD is the remodelling of biosynthetic and possibly whole-organism metabolism (Suomalainen & Battersby, 2017). Ultimately, the efficacy of adaptive responses to MD determine whether cellular homeostasis can be restored (Rossignol *et al.*, 2003; Zieliński *et al.*, 2016) — therefore putative contributors to tissue-specific MD phenotypes currently include cell type-specific availability of molecules (e.g. dNTPs, cofactors, or metabolites) required for such adaptive responses (Gorman *et al.*, 2016; Zieliński *et al.*, 2016; Suomalainen & Battersby, 2017). In this section, some of the most prominent cell biological consequences of MD will be discussed.

2.5.3.2 Alterations in cellular bioenergetics and signalling pathways

Mitochondria fine-tune nutrient- and retrograde[13] signalling through several factors, many of which seem to be affected by MD — such as the mitochondrial membrane potential, calcium (Ca^{2+}) fluxes across the mitochondrial membrane, mitochondrial ROS (mtROS) as well as mitochondrial bioenergetic (AMP/ATP) and redox [$NAD(P)^+$/NAD(P)H] ratios (Suomalainen & Battersby, 2017; Rahman & Rahman, 2018). A decrease in $\Delta\psi_m$ (less negative) has been reported in MD and although impaired OXPHOS may affect $\Delta\psi_m$, the exact mechanisms thereof remain elusive (Distelmaier *et al.*, 2009; Koopman *et al.*, 2010). As the dominant component of the mitochondrion's transmembrane potential[14], $\Delta\psi_m$ is central to the organelle's various

[13] Mito-nuclear crosstalk consists primarily of retrograde and anterograde signalling, respectively referring to mitochondrion-to-nucleus and nucleus-to-mitochondrion communication.

[14] Consists of two components measured across the IMM: $\Delta\psi_m$ and ΔpH, with the latter contributing to ~ 15 % of the total transmembrane potential (Logan *et al.*, 2016)

functions, metabolism and health (Brand & Nicholls, 2011; Logan *et al.*, 2016; Zorova *et al.*, 2018). The chief function of $\Delta\psi_m$ is to drive ATP synthesis by OXPHOS (discussed in Section 2.3.2). Therefore, $\Delta\psi_m$ serves as a sensitive indicator of cellular energetics as its magnitude is determined by the balance between its generation (by RC proton pumps) and its consumption (by ATP synthesis). Additionally, $\Delta\psi_m$ plays a key role in mitochondrial quality control and homeostasis, the assembly of mitochondrial transport systems, as well as the mitochondrial transport of proteins (e.g. ATP/ADP exchange) and ions such as Ca^{2+}, Na^+, and K^+ (Alder & Theg, 2003; Koopman *et al.*, 2010; Zorova *et al.*, 2018). OXPHOS dysfunction and the resulting loss of $\Delta\psi_m$ (as well as hormonal- or nutrient-stimulation) can, therefore, also alter intracellular Ca^{2+} signalling and homeostasis, which has been reported to be disrupted in MD (Brini *et al.*, 1999; Visch *et al.*, 2006; Voets *et al.*, 2012). Ca^{2+} signalling, in turn, plays an important role in several vital cellular processes such as the initiation of stress responses, the regulation of ATP homeostasis, muscle contraction and cell proliferation (Willems *et al.*, 2009; Quirós *et al.*, 2016).

Increased mtROS[15] and modified mtROS signalling are also often implicated in MD and considered to be one of the key initiators of MD pathology. Although OXPHOS defects are expected to result in excessive mtROS production and oxidative damage of macromolecules (e.g. DNA, cellular lipids and proteins), recent research indicates that mtROS may rather contribute to pathology by adjusting cellular activities and fate through signalling pathways, than by causing oxidative damage (Suomalainen & Battersby, 2017). Known sources of mtROS include RC complexes I, II and III, mitochondrial GPDH, ETF-QO, proline dehydrogenase, pyruvate dehydrogenase, α-ketoglutarate dehydrogenase and isoform p66Shc of the SHC-transforming protein 1 (Reinecke *et al.*, 2009; Koopman *et al.*, 2013; McDonald *et al.*, 2018). At physiological concentrations, mROS appears to be vital to cell signalling, the modulation of gene expression and redox homeostasis (Reinecke *et al.*, 2009; Rahman & Rahman, 2018). A disruption in redox homeostasis (most commonly increased $NADH/NAD^+$ ratios) is often linked to MD-related metabolic disturbances (Kelso *et al.*, 2001; Smeitink *et al.*, 2004; Koopman *et al.*, 2010; Bilan & Belousov, 2016; Esterhuizen *et al.*, 2017) and could also affect cellular function on a genomic and proteomic level (Bilan & Belousov, 2016). The general cellular redox status consists of an intricate, controlled redox network, which sustains cellular oxidant- and antioxidant production as well as reductive biosynthesis (Lindeque *et al.*, 2010; Bilan & Belousov, 2016). In addition to pyridine nucleotide [$NAD(P)H/NAD(P)^+$] redox couples, other redox systems include flavin adenine dinucleotide ($FADH_2/FAD^+$), glutathione (2GSH/GSSG),

[15] ROS are formed by the monoelectron reduction of O_2. $O_2^{-}\bullet$ is the primary form of mtROS, but H_2O_2 is the only species that can cross the IMM. Apart from mitochondria, the cell produces ROS from several other sources (Koopman *et al.*, 2013; Suomalainen & Battersby, 2017).

and thioredoxin [$Trx(SH)_2$/Trx(SS)]. Some of these redox couples act as possible rate-limiting cofactors for numerous enzymes [e.g. NAD(P)H/$NAD(P)^+$ and $FADH_2$/FAD^+], while others are involved in the initiation or execution of antioxidant defences that clear excessive ROS [e.g. NAD(P)H/$NAD(P)^+$, 2GSH/GSSG and $Trx(SH)_2$/Trx(SS)] (Schafer & Buettner, 2003; Circu *et al.*, 2011; Sena & Chandel, 2012).

2.5.3.3 Metabolic adaptions

Considering the complex, interlinked nature of metabolic networks; studying the effect of MDs on cellular metabolism is one of the most challenging tasks (Zieliński *et al.*, 2016). The use of transcriptomics, proteomics and metabolomics to investigate metabolic adaptions in MDs, have led to the identification of numerous disease biomarkers[16] — however, such biomarkers are often not MD-specific, have limited sensitivity and specificity, and the mechanisms regulating these metabolic alterations are difficult to elucidate (Reinecke *et al.*, 2009; van der Lee *et al.*, 2015; Gorman *et al.*, 2016; Reznik *et al.*, 2016; Esterhuizen *et al.*, 2017). Transcriptomics[17] has identified elevated levels of two cytokines — fibroblast growth factor 21 (FGF-21) and growth differentiation factor 15 (GDF-15) — which serve as good serum biomarkers of MD (Tyynismaa *et al.*, 2010; Suomalainen *et al.*, 2011; Fujita *et al.*, 2015; Rahman & Rahman, 2018). FGF-21 is considered to be a cytokine of the fasting response, while GDF-15 is part of the transforming growth factor-β (TGFβ) family, and although both cytokines are not exclusive to mitochondrial dysfunction[18], they are currently among the most specific biomarkers of MD (Suomalainen & Battersby, 2017). These biomarkers have been linked to several MD-related metabolic alterations (increased catabolism of fatty acids and amino acids) with which they share a bioenergetics-sensing induction pathway (Esterhuizen *et al.*, 2017). Additionally, ATF transcription factors have also been identified as putative mediators between MD and metabolism; which integrate nutrient availability with ATP production and biosynthesis pathways via the mTORC1 pathway (Suomalainen & Battersby, 2017). Furthermore, proteomics[19] has implicated several metabolic alterations in MD, such as increased glycolytic enzymes, increased protein acetylation, decreased oxidoreductases and variably altered ribonucleoprotein levels (Sahebekhtiari *et al.*, 2016; Rahman & Rahman, 2018).

---

[16] Typical MD biomarkers include lactate, pyruvate, creatine kinase, alanine, thymidine and deoxyuridine, acylcarnitines and organic acids (Gorman *et al.*, 2016).

[17] Performed on a mouse model with mutations in the Twinkle helicase and patient-derived transmitochondrial cybrids bearing the m.3243A→G mtDNA mutation, associated with MELAS syndrome.

[18] FGF-21 levels are also increased in a wide range of metabolic disorders, e.g. diabetes mellitus, obesity and metabolic syndrome, while levels of GDF-15 are also increased in cardiac failure, renal insufficiency and prostate cancer (Gorman *et al.*, 2016).

[19] Performed on the liver of a mouse model of ethylmalonic encephalopathy.

To date, the application of global metabolomics in MD is uncommon (Zieliński *et al.*, 2016), with most metabolomics studies done on cell and animal models of MD and few large-scale metabolomics datasets available for human MD (Reinecke *et al.*, 2009; Rahman & Rahman, 2018). Furthermore, making comparisons between the metabolomics of human patients and different disease models of MD is complicated by variations in specific genetic defects and -backgrounds, the parameters investigated, as well as the protocols used (Reinecke *et al.*, 2009; Rahman & Rahman, 2018). This is evident in a recent review by Esterhuizen *et al.* (2017), as the authors report quite a few inconsistencies between the metabolome of MD patients and animal models. However, from their review, it is clear that several metabolic pathways are consistently affected by MD. Some of the most prominent metabolic alterations are ascribed to the altered cellular redox state ($NADH/NAD^+$ and/or $FAD/FADH_2$ ratio) and the apparent intimate link between MD, nutrient-sensing pathways and the one-carbon cycle (Esterhuizen *et al.*, 2017; Suomalainen & Battersby, 2017). Common metabolic alterations include: an increased glycolytic flux towards lactate production, with elevations in pyruvate, lactate and alanine serving as classic biomarkers of MD; increased levels of ketone bodies (acetoacetate and 3-hydroxybutyric acid), perturbed lysine and branched-chain amino acid catabolism, alterations in the Krebs cycle, urea cycle, fatty acid-, nucleotide- and one-carbon metabolism, as well as the folate cycle, methylation cycle and the transsulfuration pathway (Esterhuizen *et al.*, 2017). Many of these pathways provide metabolites and cofactors central to cellular anabolic biosynthetic pathways, thereby contributing to e.g. cellular dNTP metabolism, glutathione biosynthesis, methylation reactions and phospholipid synthesis (Suomalainen & Battersby, 2017).

Regarding the analysis and interpretation of experimental omics-data, new computational systems biology methods have proven to be of great value. To model the metabolic consequences of MD on overall metabolism, Zieliński *et al.* (2016) simulated known features of RC disorders through the inhibition of CI-CIV to varying degrees and identified several metabolic alterations predicted by the model to take place in the human cardiomyocyte metabolism. From their simulations, the authors concluded that in the case of more common forms of OXPHOS deficiency (CI and CII defects) there are more adaptive pathways, able to better maintain ATP production, while the opposite is true for the scarcer forms (CIII and CIV defects) of the disease. Furthermore, they putatively link tissue-specific substrate availabilities and efficacy of compensatory pathways to the differential severity of mitochondrial defects observed in different tissues (Zieliński *et al.*, 2016).

2.6 CI deficiency and Leigh syndrome

Isolated CI deficiency (OMIM 252010) accounts for the majority (30 %) of primary MD cases, with an estimated prevalence of 1 in 10 000 live births (Smeitink *et al.*, 2001; Hoefs *et al.*, 2012; Rodenburg, 2016; Ghezzi & Zeviani, 2018). As is the case with all types of MD, CI deficiency is characterised by genetic and clinical heterogeneity. Pathogenic mutations have been identified in all seven mtDNA-encoded CI subunits, 20 of the 38 nDNA-encoded CI subunits (seven core- and 13 accessory subunits), and 9 CI assembly factors. Despite extreme heterogeneity, the majority (70 % to 80 %) of cases are caused by nDNA mutations with patients developing symptoms during the first year of life and displaying rapid disease progression with a fatal outcome in early childhood. The nuclear *Ndufs4* gene is considered a mutational hotspot in CI deficiency, with over 13 different pathogenic mutations currently identified (Budde *et al.*, 2000; Papa, 2002; Bris *et al.*, 2017; Lamont *et al.*, 2017). The majority of these mutations are considered loss of function alleles and include missense-, nonsense-, splicing-, frameshift- and point mutations, as well as a multi-exon deletion (Bris *et al.*, 2017; Kahlhöfer *et al.*, 2017; Lamont *et al.*, 2017). Patients with *Ndufs4* mutations present with symptoms of Leigh(-like[20]) syndrome (LS) — a disorder accounting for approximately 80 % of CI-deficient patients (Smeitink *et al.*, 2004; Fassone & Rahman, 2012; Hoefs *et al.*, 2012; Breuer *et al.*, 2013; Rodenburg, 2016). LS or subacute necrotising encephalopathy (OMIM 256000) is caused by approximately 100 different genetic defects (Rahman & Rahman, 2018); of which *Ndufs4* mutations account for some of the more severe autosomal recessive forms of the disease (Kalman, 2006; Jain *et al.*, 2016). Being one of the most common neurometabolic diseases, LS affects approximately 1 in 40 000 new-borns (Darin *et al.*, 2001; Lake *et al.*, 2015; OMIM, 2017). Although rare adult-onset cases have been reported, LS typically presents in early infancy (Assouline *et al.*, 2012; Hoefs *et al.*, 2012), with the most characteristic features including a neurodegenerative phenotype, mitochondrial dysfunction and symmetrical bilateral necrotic lesions in different regions of the central nervous system (primarily the brainstem or basal ganglia). *Ndufs4* mutations often result in a wide spectrum of symptoms, however clinical hallmarks of *Ndufs4* mutations have been proposed to include early-onset, failure to thrive, developmental delay, muscular hypotonia and depressed tendon reflexes, nystagmus[21], feeding difficulties, respiratory anomalies, psychomotor regression, neonatal cardiomyopathy, seizures

[20] When clinical features strongly resemble Leigh syndrome, but do not fulfil key diagnostic criteria the term "Leigh-like syndrome" is used. Examples include: normal blood and CSF lactate levels, atypical/normal neuroimaging, atypical neuropathology and/or incomplete evaluation (Rahman & Thorburn, 2015).

[21] A condition of (involuntary) abnormal eye movement.

and hepatomegaly[22], with death occurring in infancy or early childhood due to cardio-respiratory failure. Paediatric patients normally have uneventful births, however, occasional observations of intrauterine growth retardation, premature birth and vomiting have been reported (Assouline *et al.*, 2012; Lamont *et al.*, 2017).

2.7 The *Ndufs4* knockout mouse model for human CI deficiency

Considering the genetic complexity of Leigh syndrome, the neurological involvement, difficulty of diagnosis, and short lifespan of most patients — it is essential to use animal models to study disease progression and pathology. Currently, one of the most reliable and best characterised models of CI deficiency, is the whole-body *Ndufs4* knockout (*Ndufs4*$^{-/-}$) mouse, which presents with symptoms similar to human CI deficiency at around postnatal day (P) 35 and develops a progressive Leigh-like phenotype leading to early death (P50-60) (Kruse *et al.*, 2008; Breuer *et al.*, 2013). In this section, the development, phenotype and current knowledge on *Ndufs4* deficiency, obtained from the mouse model, will be discussed.

2.7.1 Development

The *Ndufs4* knockout mouse model (B6.129S4-*Ndufs4*$^{tm1.1Rpa}$/J) can be obtained from Jackson Laboratories (JAX; ME, USA), as heterozygous carrier (*Ndufs4*$^{+/-}$) mice on a mixed 129/Sv:C57Bl/6 genetic background, with Dr Richard Palmiter (University of Washington) acting as the donating investigator. *Ndufs4*$^{+/-}$ mice contain a mutant allele of the *Ndufs4* gene (gene ID: 17993) from which the second exon was deleted via standard gene targeting techniques. In short, exon two of the *Ndufs4* gene was flanked with loxP sites, deleted from the germline via Cre-loxP recombination (Figure 2-6), and the resulting line was backcrossed for more than 20 generations to C57BL6/J. This excision of *Ndufs4* exon two produces a frameshift mutation that precludes the synthesis of the mature NDUFS4 protein — as exon two encodes the end of a mitochondrial targeting sequence and the first 17 amino acids of the mature protein. *Ndufs4*$^{+/-}$ mice must then be interbred to produce homozygous knockout (*Ndufs4*$^{-/-}$) and wild-type (*Ndufs4*$^{+/+}$) mice, of which the former contains a whole-body knockout of the NDUFS4 protein (Kruse *et al.*, 2008; JAX, 2017).

[22] Abnormal enlargement of the liver.

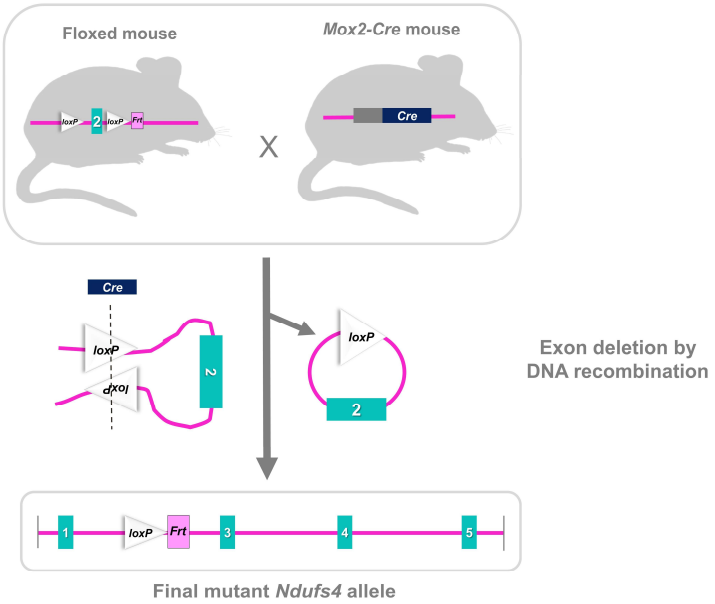


Figure 2-6: Deletion of *Ndufs4* exon two from the germline via Cre-loxP recombination. Floxed mice possess the correctly targeted mutant allele which contains two LoxP sites (indicated by white triangles) flanking *Ndufs4* exon two, and one frt site (pink square) left over after the removal of the positive selectable marker. By crossing the floxed mice with mice expressing *Mox2-Cre*, exon two is deleted from the *Ndufs4* allele via DNA recombination.

2.7.2 Clinical phenotype

Initially, the phenotype and general behaviour of *Ndufs4*$^{-/-}$ pups appear similar to their heterozygous (*Ndufs4*$^{+/-}$) and wild-type (*Ndufs4*$^{+/+}$) littermates regarding locomotor activity during day and night, grooming, feeding, response to novel objects and socialising (Kruse *et al.*, 2008). The first phenotypic difference is seen at ~ P12 with *Ndufs4*$^{-/-}$ pups appearing smaller than *Ndufs4*$^{+/-}$ and *Ndufs4*$^{+/+}$ littermates (Manjeri, 2017). Next, *Ndufs4*$^{-/-}$ pups display transient alopecia (hair loss) with severe hair loss evident at ~ P16, but peaking at P20–24 (Kruse *et al.*, 2008; Jin *et al.*, 2014). The whole-body *Ndufs4* knockout causes macrophage activation and systemic inflammation which manifests as alopecia with the majority of *Ndufs4*$^{-/-}$ pups and some (~ 4 %) of *Ndufs4*$^{+/-}$ pups developing hair loss (Jin *et al.*, 2014). Regarding the skeletal phenotype, *Ndufs4*$^{-/-}$ pups display an intrinsic defect in osteoclastogenesis, leading to a decreased bone resorption and an increased bone mass (Jin *et al.*, 2014). Furthermore, *Ndufs4*$^{-/-}$ pups are blind with cataracts occasionally appearing in one or both eyes as early as P20. At ~ P30 *Ndufs4*$^{-/-}$ mice become lethargic, reach their maximum body weight (~ 15 g), and their body temperature decreases (~ 2 ºC; after P30).

After P30 (P26-37), *Ndufs4*$^{-/-}$ mice display normal total oxygen consumption, CO_2 clearance and food consumption during both day and night as well as during fasting. However, these parameters were only measured over three consecutive days in metabolic chambers (Kruse *et al.*, 2008) and with recent literature highlighting feeding difficulties as an often overlooked key

feature in *Ndufs4*$^{-/-}$ models (Foriel *et al.*, 2018), eventual feeding difficulties cannot be excluded. *Ndufs4*$^{-/-}$ mice recover from alopecia after weaning (P35), during the next hair-growth cycle (Kruse *et al.*, 2008; Jin *et al.*, 2014). However, at ~ P35 the onset of an encephalomyopathic phenotype becomes evident. *Ndufs4*$^{-/-}$ mice develop rapid hearing loss, deterioration of motor ability, and severe ataxia — with some mice being unable to open their eyes or experiencing seizures. *Ndufs4*$^{-/-}$ mice also show a profound decrease in body fat compared to controls (Johnson *et al.*, 2013). Between P35 and P50, *Ndufs4*$^{-/-}$ mice stop gaining weight and start to display weight loss, display worsened ataxia, cease grooming, and die between P50-60 from a fatal necrotising encephalomyopathy (Kruse *et al.*, 2008; Johnson *et al.*, 2013; Jin *et al.*, 2014).

2.7.3 Respiratory chain enzyme abundance and activity

As an accessory subunit of the N module, NDUFS4 is essential to CI assembly and stability (discussed in Section 2.4.4). CI assembly studies in NDUFS4 deficient patient fibroblasts demonstrated that the NDUFS4 subunit is inserted in the complex at a late stage of the assembly process (Ugalde *et al.*, 2004) and revealed that the absence of NDUFS4 leads to CI assembly defects, resulting in the formation of a partially assembled CI subcomplex, lacking the N module (~ 830 kDa) (Scacco *et al.*, 2003; Ugalde *et al.*, 2004; Breuer *et al.*, 2013). Similar to patients, the whole-body *Ndufs4* knockout results, in the absence of intact CI in mouse tissues (Calvaruso *et al.*, 2012) with two partially assembled CI subcomplexes observed in *Ndufs4*$^{-/-}$ muscle, brain, heart and kidney, which correspond to a subassembly of the CI Q and P modules (830 kDa), and a CI N module subassembly (200kDa) (Calvaruso *et al.*, 2012). Despite the absence of holo-CI, NDUFS4 deficient patient fibroblasts retain residual CI activity (ranging from 15 %-75 % of control values), which positively correlates with the amount of subcomplex present (Valsecchi *et al.*, 2010). In accordance, CI enzyme activity is significantly, but variably reduced in mouse *Ndufs4*$^{-/-}$ energy-demanding tissues, compared to controls with residual CI activity present in heart, skeletal muscle, brain, kidney, pancreas, liver and lung at a respective 44 %, 29 %, 26 %, 25 %, 17 %, 19 % and 9 % (Calvaruso *et al.*, 2012).

Additionally, the CI assembly defect seems to influence CIII assembly, as reduced CIII activity was observed in some NDUFS4 deficient patient fibroblasts (Budde *et al.*, 2000; Ugalde *et al.*, 2004; Breuer *et al.*, 2013) and tissues from *Ndufs4*$^{-/-}$ mice (Kruse *et al.*, 2008; de Haas *et al.*, 2017). This observation links with a possible explanation for the presence of residual CI activity in the absence of holo-CI, which came from the study of *Ndufs4*$^{-/-}$ skeletal muscle. In this tissue, the two CI subassemblies were shown to be stabilised by associating with CIII, producing an unstable but functional supercomplex that retains CI enzymatic activity (Calvaruso *et al.*, 2012). Regarding CII activity, *Ndufs4*$^{-/-}$ oxidative skeletal muscles show slightly increased succinate dehydrogenase staining, with CII driven O_2 consumption also often slightly higher than controls

(Kruse *et al.*, 2008). However, literature reports on RC enzyme activities in *Ndufs4*$^{-/-}$ mice are quite diverse, with multiple studies reporting variations in CII-CIV activity (Kruse *et al.*, 2008; Calvaruso *et al.*, 2012; Valsecchi *et al.*, 2012; Alam *et al.*, 2015; de Haas *et al.*, 2017).

2.7.4 ATP homeostasis and oxygen consumption

Since NDUFS4 deficiency directly affects OXPHOS, the resulting CI deficiency may result in impaired oxidative ATP production and a consequent disruption of the cellular ATP/ADP ratio (Reinecke *et al.*, 2009; Rodenburg, 2016). However, NDUFS4 deficient cells seem to effectively maintain ATP homeostasis. Resting *Ndufs4*$^{-/-}$ immortalised embryonic fibroblasts display no detectable alterations in total cellular ATP content and free cytosolic ATP concentration (Valsecchi *et al.*, 2012), while *Ndufs4*$^{-/-}$ (P30) muscle displays normal resting ATPase (equivalent to ATP demand), phosphorylation capacity and maximal rate of mitochondrial ATP production determined by *in vivo* ^{31}P-NMR spectroscopy of ATP turnover reactions during ischemia-reperfusion. After ischemia-reperfusion, *Ndufs4*$^{-/-}$ muscle had ATP levels at the low end of the normal range, but phosphocreatine, creatine and inorganic phosphate levels were all normal (Kruse *et al.*, 2008). *Ndufs4*$^{-/-}$ (P35) skeletal muscle mitochondria also display normal maximal pyruvate oxidation and ATP production as determined by mathematical modelling and flux measurements (Alam *et al.*, 2015). Furthermore, NDUFS4 deficiency also does not drastically alter the rate of O_2 consumption, with no detectable alterations in normal resting O_2 consumption in *Ndufs4*$^{-/-}$ mice[23] (Kruse *et al.*, 2008), and moderately reduced maximal and routine O_2 consumption in *Ndufs4*$^{-/-}$ immortalised embryonic fibroblasts (Valsecchi *et al.*, 2012). The recently proposed hypocapnic hypothesis argues against energy deprivation as the mechanism of Leigh syndrome and proposes that the main detrimental factor is hypocapnia (decrease in pCO_2) and respiratory alkalosis (increase in pH) due to hyperventilation — permanent or in response to stress (Pronicka, 2017). In agreement, chronic hypoxia (*Ndufs4*$^{-/-}$ mice breathing 11 % vs 55 % O_2) was shown to markedly improve survival, body weight, body temperature, behaviour, neuropathology, and disease biomarkers in *Ndufs4*$^{-/-}$ mice — linking the involvement of aberrant oxygen metabolism, signalling or toxicity in MD pathogenesis (Jain *et al.*, 2016).

2.7.5 Metabolic alterations

Elucidating the downstream metabolic effects of NDUFS4 deficiency has proven to be difficult. Although lactic acidosis is one of the most common metabolic alterations in humans with MD (including patients with Leigh syndrome), patients with *Ndufs4* mutations do not usually display

[23] Determined by *in vivo* optical spectroscopy of haemoglobin and myoglobin saturation levels.

lactic acidosis (Rahman *et al.*, 1996; Loeffen *et al.*, 2000; Finsterer, 2008). In agreement, serum lactate levels are normal in young (P18) and only slightly elevated in older (> P40) *Ndufs4*$^{-/-}$ mice (Kruse *et al.*, 2008). Contrastingly, *Ndufs4*$^{-/-}$ whole-brain (P30) metabolomics revealed a significant accumulation of lactate along with pyruvate, glycolytic intermediates and oxidative stress markers; as well as a decrease in free amino acids, free fatty acids, nucleotides and their catabolic products, together with γ-aminobutyric acid and dopamine (Johnson *et al.*, 2013). Although a major upregulation of the glycolytic pathway was considered a common metabolic consequence of the *Ndufs4* knockout, normal protein levels of hexokinase (HK) I, HK-II and phosphorylated pyruvate dehydrogenase found in mitochondrial fractions from *Ndufs4*$^{-/-}$ immortalised embryonic fibroblasts (Valsecchi *et al.*, 2012), as well as normal blood glucose levels (Kruse *et al.*, 2008), seem to argue against a ubiquitous upregulation of glycolysis. Furthermore, NDUFS4 deficiency was linked to increased protein succination in the voltage-dependent anion channels 1 and 2[24] in *Ndufs4*$^{-/-}$ brainstem vestibular nuclei (the most affected region in the *Ndufs4*$^{-/-}$ brain), which was ascribed to the accumulation of NADH and subsequently, fumarate. However, this was not seen in *Ndufs4*$^{-/-}$ skeletal muscle, which the authors linked to the apparent lack of muscle pathology in the mouse model (Piroli *et al.*, 2016). In a similar whole-body *Ndufs4* knockout (*Ndufs4*$^{fky/fky}$) mouse model[25] (~ P40), blood metabolomics suggested an overall inhibition of mitochondrial fatty acid β-oxidation (increased hydroxy-acylcarnitine levels) due to NADH accumulation; however, oil red O staining of *Ndufs4*$^{fky/fky}$ quadriceps failed to detect lipid accumulation, which lead the authors to conclude that NDUFS4 deficiency does not cause a gross defect in fatty acid oxidation, but rather alters ratios of fatty acyl species (Leong *et al.*, 2012). Using flux measurements and mathematical modelling to predict changes in the metabolism of *Ndufs4*$^{-/-}$ skeletal muscle mitochondria (P31-34), Alam *et al.* (2015) observed a bifurcation in the Krebs cycle, with an increase in flux (10-11 %) through reactions providing substrates to CII (α-ketoglutarate dehydrogenase, succinyl-CoA synthetase, CII and fumarase) and a slight decrease in the other (generally NAD^+ consuming) reactions, which mainly fuel CI (citrate synthase, aconitase, isocitrate dehydrogenase and malate dehydrogenase). Furthermore, compared to controls, *Ndufs4*$^{-/-}$ skeletal muscle mitochondria exhibit an altered isocitrate dehydrogenase flux, with a greater part of the flux diverted towards the Krebs cycle and less towards the α-ketoglutarate/malate antiporter mechanism (Alam *et al.*, 2015).

[24] Voltage-dependent anion channel isoforms play an important role in the exchange of ADP/ATP between the cytosol and the mitochondria (Piroli *et al.*, 2016).

[25] Also contains a whole-body knockout of the NDUFS4 protein, however the knockout was achieved via the insertion of transposable elements into the *Ndufs4* gene (Leong *et al.*, 2012).

2.7.6 Recent advances and limitations of research on *Ndufs4* knockout mouse models

In order to gain insight into tissue-specific consequences of CI dysfunction, several conditional *Ndufs4* knockout mice have been developed in addition to the whole-body knockout [reviewed by Torraco *et al.* (2015)]. This includes neuronal- and glial- (Quintana, 2010; Quintana *et al.*, 2012; Sterky *et al.*, 2012), cardiac- (Sterky *et al.*, 2012; Karamanlidis *et al.*, 2013), hematopoietic-, and hepatic- (Jin *et al.*, 2014) *Ndufs4* knockout mice. Using these animal models, it became clear that the origin of the disease phenotype was predominantly neurological and most severe in specific brain regions (Quintana, 2010; Quintana *et al.*, 2012; Sterky *et al.*, 2012). Consequently, the majority of research has focused on the neurological manifestations of the disease. While both brain and skeletal muscle are the most affected tissues in MD (Distelmaier *et al.*, 2009; Gorman *et al.*, 2016), limited information is available on skeletal muscle-specific consequences of the *Ndufs4* knockout. This is primarily due to the apparent lack of muscle involvement in the disease phenotype (Kruse *et al.*, 2008; Leong *et al.*, 2012; Piroli *et al.*, 2016). However, a recent study by Foriel *et al.* (2018) highlighted the involvement of skeletal muscle in *Ndufs4* knockout pathology, with similarities reported between the phenotypes of skeletal muscle-specific and whole-body *Ndufs4* knockout *Drosophila*, such as reduced lifespan, feeding difficulties, locomotor impairment and climbing defects. It is, therefore, imperative to understand the effects of a *Ndufs4* knockout on muscle metabolism, especially considering how the muscular system functions interdependently with the nervous system (Goody & Henry, 2018), is generally involved in MD (Distelmaier *et al.*, 2009; Gorman *et al.*, 2016), and how its mitochondrial function (and content) can influence whole-body metabolism and health (Wolfe, 2006; Russell *et al.*, 2014). Skeletal muscle not only facilitates breathing and locomotion, but also plays an essential role in various systemic, energy-demanding processes such as whole-body protein metabolism, glucose and fatty acid consumption, thermoregulation, immunity, as well as the maintenance of adequate bone strength and density (Wolfe, 2006; Schiaffino & Reggiani, 2011; Goody & Henry, 2018). As *Ndufs4*$^{-/-}$ mice display weight loss (Kruse *et al.*, 2008), a significant decrease in body fat (Johnson *et al.*, 2013), decreases in body temperature (Kruse *et al.*, 2008), as well as systemic inflammation and osteoporosis (Jin *et al.*, 2014), it can be hypothesised that aberrant skeletal muscle metabolism might also play an important role in *Ndufs4*$^{-/-}$ phenotypes. To the best of our knowledge, skeletal muscle metabolomics of whole-body *Ndufs4*$^{-/-}$ mice has not yet been done.

2.8 Skeletal muscle

2.8.1 Myofibre structure

Skeletal muscle (Figure 2-7) is a complex, striated tissue composed of heterogeneous bundles of cylindrical muscle cells called myofibres. Each individual myofibre is a multinucleate syncytium[26] that formed during development from the fusion of mononucleated myogenic precursor cells (MPCs) via the process of myogenesis. During myogenesis, the first muscle fibres form when myoblasts fuse into myotubes, followed by waves of additional fibre production by the fusion of myoblasts on the surfaces of myotubes. Finally, myotubes and secondary fibres mature into a single, cylindrical, multinucleate myofibre with skeletal muscle differentiation, completed around the time of birth (Partridge, 2002; Widmaier *et al.*, 2011; Bentzinger *et al.*, 2012). Preserving the nuclei from the original myoblasts is vital to the maintenance and function of these relatively large cells, as nuclei are spread out through the length of the myofibre, each participating in the regulation of gene expression and protein synthesis within its local domain (Widmaier *et al.*, 2011). Mature skeletal muscle is post-mitotic, as myofibres are in the G_0 phase and incapable of further division. However, mature skeletal muscle is capable of growth (hypertrophy) and regeneration from myogenic precursor cells (Partridge, 2002). The predominant source of these, is a population of undifferentiated stem cells, called satellite cells, located between the plasma- and basement membrane of each myofibre. When activated, these cells proliferate rapidly to produce myoblasts that fuse with pre-existing myofibres and with one another to replace part or all of any damaged myofibres (Partridge, 2002; Widmaier *et al.*, 2011; Bentzinger *et al.*, 2012). Each myofibre is composed of bundles of myofibrils containing actin and myosin filaments, which form the basic machinery necessary for muscle contraction. Most of the cytoplasm of a skeletal muscle cell is filled with myofibrils, each extending from one end of the cell to the other (Widmaier *et al.*, 2011). Myofibres contain two subpopulations of mitochondria that might exist as a continuous reticulum but differ according to their subcellular localisation, morphology and biochemical properties (Kirkwood *et al.*, 1986; Schiaffino & Reggiani, 2011). Subsarcolemmal (SS) mitochondria are located just underneath the sarcolemma (membrane surrounding myofibrils) and have a large, lamellar shape, while intermyofibrillar (IMF) mitochondria are smaller, more compact, and located between the myofibrils, in close proximity to the lateral sacks of the sarcoplasmic reticulum where calcium is released (Koves *et al.*, 2005; Schiaffino & Reggiani, 2011). These subpopulations of

[26] A single cell containing numerous nuclei; formed by the fusion of several precursor cells each contributing a single nucleus to the final cell.

mitochondria seem to be unique in different myofibre types; distinctly adapt in response to energy stress; and are differently affected by disease (Koves *et al.*, 2005).

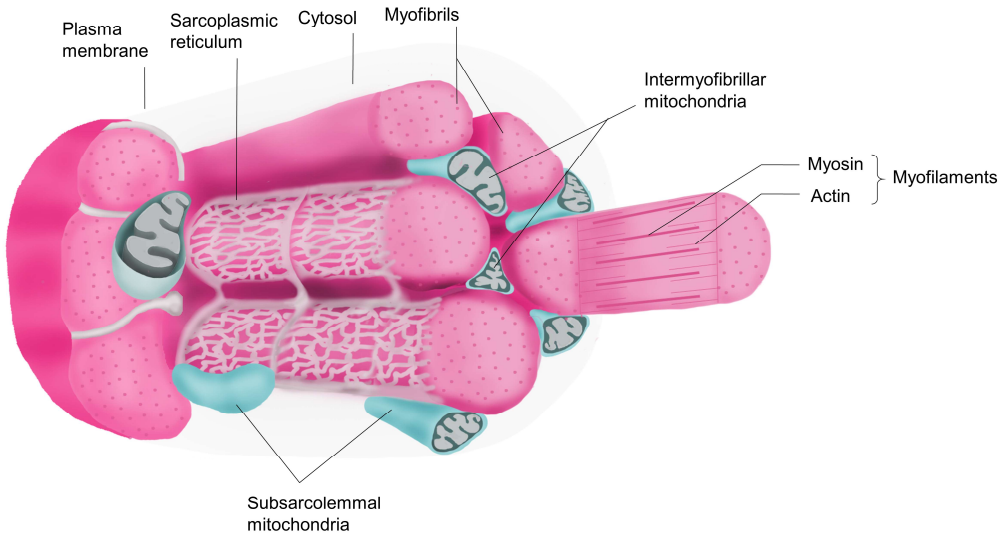


Figure 2-7: Structure of a single skeletal muscle cell or myofibre. Each myofibre is composed of myofibril bundles, containing myofilaments (actin and myosin). Myofibres contain two mitochondrial subpopulations: subsarcolemmal mitochondria, located just underneath the sarcolemma and intermyofibrillar mitochondria, located between the myofibrils.

2.8.2 Myofibre type heterogeneity

Different types of myofibres exist in order to meet different energetic demands. The main heterogeneity among myofibres relates to contractile (fast or slow shortening velocity) and metabolic (predominance of glycolytic or mitochondrial activities) properties. Myofibres are generally classified based on the myosin heavy chain (MHC) isoforms found therein: type I, type IIA, type IIX and type IIB (Guth & Samaha, 1969; Schiaffino & Reggiani, 1994; Zhang *et al.*, 2017). First, regarding contractile activity, these MHC isoforms split ATP at different maximal rates and thus have different maximal cross bridge-cycling rates and shortening velocities (Widmaier *et al.*, 2011). Among the four fibre types, one is slow-twitch (type I), while the other three are fast-twitch (type II) fibres. Second, regarding metabolic properties, type I fibres have the highest mitochondrial content as they are highly dependent on aerobic-oxidative metabolic pathways to produce ATP, favouring fatty acid oxidation (Schiaffino & Reggiani, 2011). Oppositely, type IIB fibres are poor in mitochondria, depending mainly on anaerobic glycogen and glucose catabolism for ATP production. Muscles primarily composed of type I myofibres (e.g. the soleus) display less fatigue and are ideally suited for slow, continuous contractions such as locomotion. Whereas muscles comprised of primarily type IIB fibres (e.g. superficial quadriceps femoris) are more susceptible to fatigue and contain attributes more amenable to rapid and sudden activity of shorter duration (Arany *et al.*, 2007; Arany, 2008; Tseng *et al.*,

2010). The remaining myofibre types (IIA and IIX) tend to be oxidative and rich in mitochondria whilst displaying intermediate biophysical properties (Arany, 2008). Furthermore, post-mitotic muscle fibres are highly flexible — adjusting their contractile and metabolic properties according to altered functional demands (Schiaffino & Reggiani, 2011; Zhang *et al.*, 2017).

2.8.3 Mitochondrial content and metabolic profile

Mitochondrial composition and metabolic strain differ between skeletal muscle fibre types. Oxidative fibres generally contain approximately two to three times more mitochondria than glycolytic fibres, each with a higher oxidative capacity — accordingly, the former expresses higher levels of enzymes and proteins involved in oxidative phosphorylation, while the latter has higher levels of enzymes and proteins involved in glycolysis. Compared to glycolytic fibres, oxidative fibres have a higher blood-, oxygen- and substrate supply (two-fold greater uptake of glucose and three-fold greater fatty acid transport), as well as higher oxygen-binding protein (myoglobin) content. Furthermore, oxidative fibres have a twofold higher lactate uptake, with the primary fate thereof being the conversion to pyruvate and acetyl-CoA; a greater abundance of amino acids in the free amino acid pool, with higher rates of protein turnover (protein synthesis and breakdown); and a higher abundance of intracellular lipid stores. Contrastingly, in glycolytic fibres, the primary fate of lactate is the release thereof into the bloodstream to enter the Cori cycle with the primary source of glucose being intracellular glycogen stores. Compared to oxidative fibres, glycolytic fibres have 16-30 % greater abundance of intracellular glycogen stores and higher rates of glucose turnover (glycolysis and glycogenolysis) as well as a higher resting ATP content (Glancy & Balaban, 2011; Schiaffino & Reggiani, 2011). The mouse soleus with its primarily oxidative fibre composition has been reported to express the closest molecular resemblance to several human skeletal muscles (Kho *et al.*, 2006), while reportedly, the respiratory capacity and control of the primarily glycolytic mouse quadriceps better represents human skeletal muscle mitochondrial function (Jacobs *et al.*, 2013). Therefore, these two skeletal muscles were selected for this study.

2.9 Metabolomics

Metabolomics presents a powerful tool with which to analyse the downstream effects of MD on a global scale — this includes the consequences of energy deficiency, oxidative stress and redox imbalance (Rahman & Rahman, 2018). The latest advances in the use of metabolites to understand disease, employ broad profiling methods that utilise high-content analytical chemistry to generate a metabolic phenotype. Generally, metabolic profiling aims to provide information on the changes in the relative concentrations of metabolites as a result of a certain biochemical state. These metabolic profiles ideally provide new insights into the biological

impact of disease states on cells, tissues, organs and whole organisms (Rainville *et al.*, 2014). Mass spectrometry-based metabolomics is the latest technology used to find biomarkers and drug targets for MD (Rahman & Rahman, 2018). However, no single analytical approach has the ability to analyse all the metabolites found in a biological sample, as they consist of different compound classes that differ in size and polarity over a wide concentration range (Rhee & Gerszten, 2012). Therefore, global metabolite profiling is currently achieved through multiplatform metabolomics i.e. the combination of various analytical platforms, such as nuclear magnetic resonance (NMR) spectroscopy and mass spectrometry (MS) coupled to a chromatographic separation platform [i.e., gas chromatography (GC)-MS or liquid chromatography (LC)-MS] (Rainville *et al.*, 2014).

2.10 Experimental design

This study consisted of three phases, namely: i) sample collection, ii) biochemical evaluation and iii) metabolomics investigation. These phases, and the overall experimental strategy of the study, are depicted in Figure 2-8. The first phase entailed interbreeding heterozygous *Ndufs4* knockout carrier mice (*Ndufs4*$^{+/-}$) and genotyping their litter in order to obtain and select male *Ndufs4*$^{-/-}$ and wild-type (WT) mice for the study. The selected animals (*Ndufs4*$^{-/-}$: n = 31 and WT: n = 30) were then euthanised between postnatal day (P) 45-50, via cervical dislocation, and their tissues (white quadriceps, soleus and tailsnips) were collected, snap frozen in liquid nitrogen, and stored at − 80ºC. Next, DNA was isolated from mouse tailsnips and used to confirm the genotype of each animal via standardised PCR. In parallel to the first phase, both the second and third phases of the study commenced with the development and/or standardisation of various methods for applicability on mouse white quadriceps and soleus muscles, using mice not selected for the study (WT or *Ndufs4*$^{+/-}$). Thereafter, the standardised methods were used to analyse the collected muscle tissues from *Ndufs4*$^{-/-}$ and WT mice on an enzymatic and metabolic level. RC enzyme (CI-IV) activity assays were performed on 700 ×g enriched mitochondrial fractions prepared from previously frozen white quadriceps and soleus tissues (*Ndufs4*$^{-/-}$: n = 12 and WT: n = 10) via differential centrifugation. The enzymatic data were then pretreated and processed (normalisation to protein content and glog transformation), statistically analysed (*t* test), and compared to that found in the literature as part of the characterisation of *Ndufs4*$^{-/-}$ skeletal muscle tissue. Multi-platform metabolomics (miniaturised ^{1}H-NMR spectroscopy, targeted LC-MS/MS and untargeted GC-TOF-MS) analyses were performed on monophasic tissue extracts prepared from previously frozen white quadriceps and soleus tissues (*Ndufs4*$^{-/-}$: n = 19 and WT: n = 20). Tissue extracts were divided into aliquots for each analytical platform [as well as quality control (QC) sample preparation], however, due to the limited quantity thereof, ^{1}H-NMR spectroscopy could not be performed on soleus samples.

QCs and samples were randomised and analysed in batches, and spectral data obtained from the analytical platforms were extracted into matrices. Data matrices were individually inspected (correct peak picking and alignment, batch effect and data integrity), pre-processed (data filtering, missing value imputation and normalisation), pretreated (mean centering and generalised logarithm transformation) and examined for outliers [principal component analysis (PCA) and heatmaps]. The data from each analytical platform were then statistically analysed (univariate- and multivariate analyses) and the findings were used to investigate metabolic pathways and biologically interpret the data in order to generate hypotheses on the underlying mechanisms involved in skeletal muscle's metabolic response to CI deficiency.

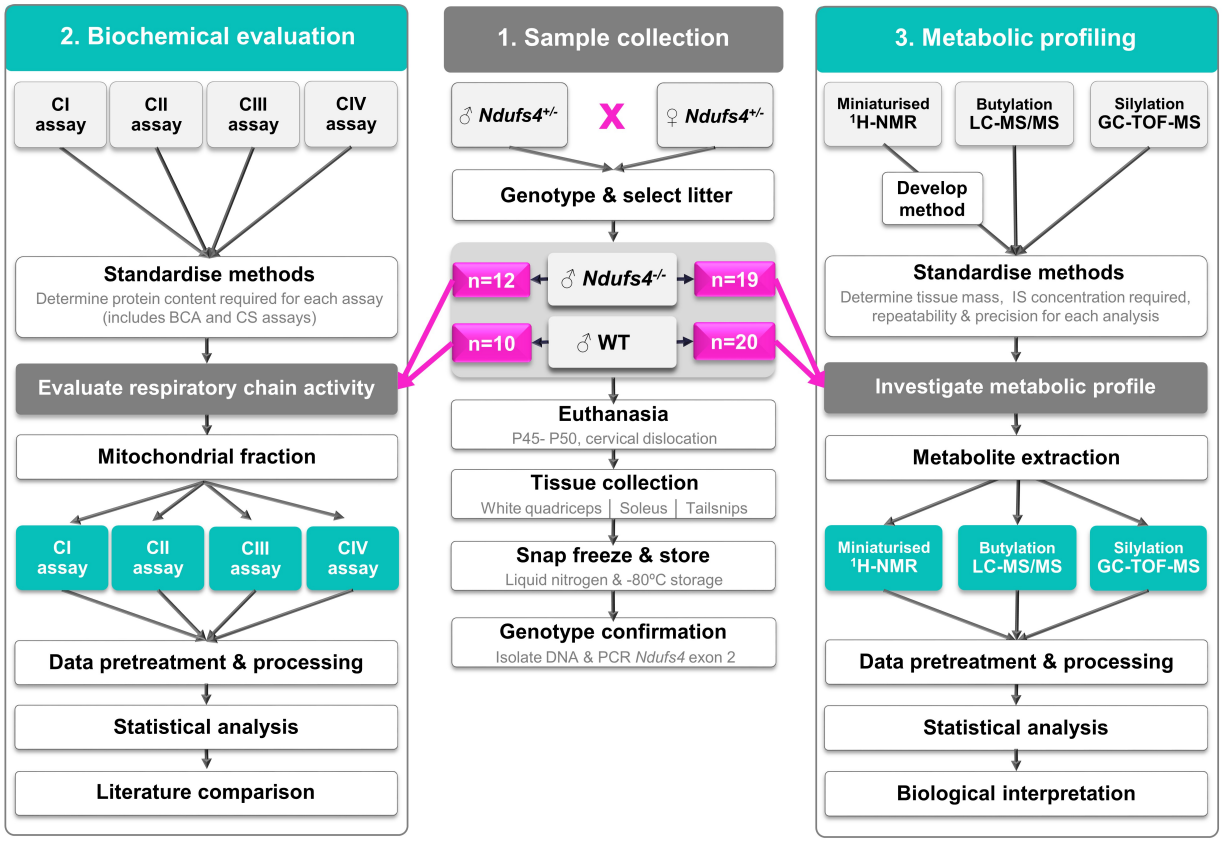


Figure 2-8: Schematic representation of the experimental strategy. The study is divided into three phases. **1.** Sample collection: consists of objectives 1.1 to 1.3, which aim to interbreed heterozygous carrier mice (*Ndufs4*$^{+/-}$) to obtain *Ndufs4*$^{-/-}$ and WT mice as well as collect and store their tissues for the study. **2.** Biochemical evaluation: comprises of objectives 2.1 to 2.3 and aims to standardise and employ methods to evaluate respiratory chain enzyme activity in 700 ×g enriched mitochondrial fractions prepared from white quadriceps and soleus skeletal muscles of *Ndufs4*$^{-/-}$ (n = 12) and WT (n = 10) mice. **3.** Metabolic profiling: consists of objectives 3.1 to 3.7, which aim to develop and/or standardise, and employ analytical methods with which to investigate the metabolic profile of white quadriceps and soleus skeletal muscles from *Ndufs4*$^{-/-}$ (n = 19) and WT (n = 20) mice. *Symbols: ♀, female; ♂, male. Abbreviations: ^{1}H-NMR, proton nuclear magnetic resonance; BCA, bicinchoninic acid; CS, citrate synthase; GC-TOF-MS, gas chromatography time-of-flight mass spectrometry; IS, internal standard; LC-MS/MS; liquid chromatography-tandem mass spectrometry; Ndufs4*$^{-/-}$*, homozygous Ndufs4 knockout mice; P, postnatal day; PCR, polymerase chain reaction, WT, wild-type.*

2.11 References

Acin-Perez, R. & Enriquez, J.A. 2014. The function of the respiratory supercomplexes: the plasticity model. *Biochimica et Biophysica Acta — Bioenergetics*, 1837(4):444-450.

Alam, M.T., Manjeri, G.R., Rodenburg, R.J., Smeitink, J.A.M., Notebaart, R.A., Huynen, M., Willems, P.H.G.M. & Koopman, W.J.H. 2015. Skeletal muscle mitochondria of NDUFS4$^{-/-}$ mice display normal maximal pyruvate oxidation and ATP production. *Biochimica et Biophysica Acta — Bioenergetics*, 1847(6-7):526-533.

Alder, N.N. & Theg, S.M. 2003. Energy use by biological protein transport pathways. *Trends in Biochemical Sciences*, 28(8):442-451.

Alston, C.L., Rocha, M.C., Lax, N.Z., Turnbull, D.M. & Taylor, R.W. 2017. The genetics and pathology of mitochondrial disease. *Journal of Pathology*, 241(2):236-250.

Andrews, B., Carroll, J., Ding, S., Fearnley, I.M. & Walker, J.E. 2013. Assembly factors for the membrane arm of human complex I. *Proceedings of the National Academy of Sciences*, 110(47):18934-18939.

Arany, Z. 2008. PGC-1 coactivators and skeletal muscle adaptations in health and disease. *Current Opinion in Genetics & Development*, 18(5):426-434.

Arany, Z., Lebrasseur, N., Morris, C., Smith, E., Yang, W., Ma, Y., Chin, S. & Spiegelman, B.M. 2007. The transcriptional coactivator PGC-1β drives the formation of oxidative type IIX fibers in skeletal muscle. *Cell Metabolism*, 5(1):35-46.

Assouline, Z., Jambou, M., Rio, M., Bole-Feysot, C., de Lonlay, P., Barnerias, C., Desguerre, I., Bonnemains, C., Guillermet, C., Steffann, J., Munnich, A., Bonnefont, J.P., Rötig, A. & Lebre, A.S. 2012. A constant and similar assembly defect of mitochondrial respiratory chain complex I allows rapid identification of NDUFS4 mutations in patients with Leigh syndrome. *Biochimica et Biophysica Acta — Molecular Basis of Disease*, 1822(6):1062-1069.

Bakker, B.M., Bro, C., Kotter, P., Luttik, M.A.H., van Dijken, J.P. & Pronk, J.T. 2000. The mitochondrial alcohol dehydrogenase Adh3p is involved in a redox shuttle in *Saccharomyces cerevisiae*. *Journal of Bacteriology*, 182(17):4730-4737.

Bentzinger, C.F., Wang, Y.X. & Rudnicki, M.A. 2012. Building muscle: molecular regulation of myogenesis. *Cold Spring Harbor Perspectives in Biology*, 4(2):a008342.

Bilan, D.S. & Belousov, V.V. 2016. Genetically encoded probes for NAD^+/NADH monitoring. *Free Radical Biology and Medicine*, 100:32-42.

Blaza, J.N., Serreli, R., Jones, A.J.Y., Mohammed, K. & Hirst, J. 2014. Kinetic evidence against partitioning of the ubiquinone pool and the catalytic relevance of respiratory-chain supercomplexes. *Proceedings of the National Academy of Sciences*, 111(44):15735-15740.

Boekema, E.J. & Braun, H.-P. 2007. Supramolecular structure of the mitochondrial oxidative phosphorylation system. *Journal of Biological Chemistry*, 282(1):1-4.

Bouillaud, F. & Blachier, F. 2011. Mitochondria and sulfide: a very old story of poisoning, feeding, and signaling? . *Antioxidants & Redox Signaling*, 15(2):379-391.

Brand, M.D. & Nicholls, D.G. 2011. Assessing mitochondrial dysfunction in cells. *Biochemical Journal*, 435(Pt2):297-312.

Breuer, M.E., Willems, P.H.G.M., Smeitink, J.A.M., Koopman, W.J.H. & Nooteboom, M. 2013. Cellular and animal models for mitochondrial complex I deficiency: a focus on the NDUFS4 subunit. *International Union of Biochemistry and Molecular Biology Life*, 65(3):202-208.

Brini, M., Pinton, P., King, M.P., Davidson, M., Schon, E.A. & Rizzuto, R. 1999. A calcium signaling defect in the pathogenesis of a mitochondrial DNA inherited oxidative phosphorylation deficiency. *Nature Medicine*, 5:951.

Bris, C., Rouaud, T., Desquiret-Dumas, V., Gueguen, N., Goudenege, D., Barth, M., Bonneau, D., Amati-Bonneau, P., Lenaers, G., Reynier, P., Lebre, A.-S. & Procaccio, V. 2017. Novel NDUFS4 gene mutation in an atypical late-onset mitochondrial form of multifocal dystonia. *Neurology — Genetics*, 3(6):e205.

Budde, S.M.S., van den Heuvel, L.P.W.J., Janssen, A.J., Smeets, R.J.P., Buskens, C.A.F., DeMeirleir, L., van Coster, R., Baethmann, M., Voit, T., Trijbels, J.M.F. & Smeitink, J.A.M. 2000. Combined enzymatic complex I and III deficiency associated with mutations in the nuclear encoded NDUFS4 gene. *Biochemical and Biophysical Research Communications*, 275(1):63-68.

Calmettes, G., John, S.A., Weiss, J.N. & Ribalet, B. 2013. Hexokinase–mitochondrial interactions regulate glucose metabolism differentially in adult and neonatal cardiac myocytes. *The Journal of General Physiology*, 142(4):425-436.

Calvaruso, M.A., Willems, P., van den Brand, M., Valsecchi, F., Kruse, S., Palmiter, R., Smeitink, J.A.M. & Nijtmans, L. 2012. Mitochondrial complex III stabilizes complex I in the absence of NDUFS4 to provide partial activity. *Human Molecular Genetics*, 21(1):115-120.

Calvo, S.E., Clauser, K.R. & Mootha, V.K. 2016. MitoCarta2.0: an updated inventory of mammalian mitochondrial proteins. *Nucleic Acids Research*, 44:D1251-1257.

Carling, P.J., Cree, L.M. & Chinnery, P.F. 2011. The implications of mitochondrial DNA copy number regulation during embryogenesis. *Mitochondrion*, 11(5):686-692.

Chaban, Y., Boekema, E.J. & Dudkina, N.V. 2014. Structures of mitochondrial oxidative phosphorylation supercomplexes and mechanisms for their stabilisation. *Biochimica et Biophysica Acta — Bioenergetics*, 1837(4):418-426.

Cherry, A.D. & Piantadosi, C.A. 2015. Regulation of mitochondrial biogenesis and its intersection with inflammatory responses. *Antioxidants & Redox Signaling*, 22(12):965-976.

Chinnery, P.F. & Hudson, G. 2013. Mitochondrial genetics. *British Medical Bulletin*, 106(1):135-159.

Circu, M.L., Maloney, R.E. & Aw, T.Y. 2011. Disruption of pyridine nucleotide redox status during oxidative challenge at normal and low-glucose states: implications for cellular adenosine triphosphate, mitochondrial respiratory activity, and reducing capacity in colon epithelial cells. *Antioxidants & Redox Signaling*, 14(11):2151-2162.

Craven, L., Alston, C.L., Taylor, R.W. & Turnbull, D.M. 2017. Recent advances in mitochondrial disease. *Annual Review of Genomics and Human Genetics*, 18(1):257-275.

Darin, N., Oldfors, A., Moslemi, A., Holme, E. & Tulinius, M. 2001. The incidence of mitochondrial encephalomyopathies in childhood: clinical features and morphological, biochemical, and DNA abnormalities. *Annals of Neurology*, 49(3):377-383.

Dawson, A.G. 1979. Oxidation of cytosolic NADH formed during aerobic metabolism in mammalian cells. *Trends in Biochemical Sciences*, 4(8):171-176.

de Haas, R., Das, D., Garanto, A., Renkema, H.G., Greupink, R., van den Broek, P., Pertijs, J., Collin, R.W.J., Willems, P., Beyrath, J., Heerschap, A., Russel, F.G. & Smeitink, J.A.M. 2017. Therapeutic effects of the mitochondrial ROS-redox modulator KH176 in a mammalian model of Leigh disease. *Scientific Reports*, 7(1):11733.

Dickinson, A., Yeung, K.Y. & John, J.C. 2012. The regulation of mitochondrial DNA copy number in glioblastoma cells. *Cell Death and Differentiation*, 20(12):1644-1653.

Distelmaier, F., Koopman, W.J.H., van den Heuvel, L.P., Rodenburg, R.J., Mayatepek, E., Willems, P.H.G.M. & Smeitink, J.A.M. 2009. Mitochondrial complex I deficiency: from organelle dysfunction to clinical disease. *Brain*, 132(4):833-842.

Esterhuizen, K., van der Westhuizen, F.H. & Louw, R. 2017. Metabolomics of mitochondrial disease. *Mitochondrion*, 35:97-110.

Fang, J., Uchiumi, T., Yagi, M., Matsumoto, S., Amamoto, R., Takazaki, S., Yamaza, H., Nonaka, K. & Kang, D. 2013. Dihydro-orotate dehydrogenase is physically associated with the respiratory complex and its loss leads to mitochondrial dysfunction. *Bioscience Reports*, 33(2):300021.

Fassone, E. & Rahman, S. 2012. Complex I deficiency: clinical features, biochemistry and molecular genetics. *Journal of Medical Genetics*, 49(9):578-590.

Fiedorczuk, K., Letts, J.A., Degliesposti, G., Kaszuba, K., Skehel, M. & Sazanov, L.A. 2016. Atomic structure of the entire mammalian mitochondrial complex I. *Nature*, 538(7625):406-410.

Finsterer, J. 2008. Leigh and Leigh-like syndrome in children and adults. *Pediatric Neurology*, 39(4):223-235.

Foriel, S., Beyrath, J., Eidhof, I., Rodenburg, R.J., Schenck, A. & Smeitink, J.A.M. 2018. Feeding difficulties, a key feature of the *Drosophila* NDUFS4 mitochondrial disease model. *Disease Models & Mechanisms*, 11:10.

Friedrich, T. & Bottcher, B. 2004. The gross structure of the respiratory complex I: a Lego system. *Biochimica et Biophysica Acta — Bioenergetics*, 1608(1):1-9.

Fujita, Y., Ito, M., Kojima, T., Yatsuga, S., Koga, Y. & Tanaka, M. 2015. GDF15 is a novel biomarker to evaluate efficacy of pyruvate therapy for mitochondrial diseases. *Mitochondrion*, 20:34-42.

Garrett, R.H. & Grisham, C.M. 2013. Biochemistry. 6th ed. Belmont, CA: Brooks/Cole.

Ghezzi, D. & Zeviani, M. 2018. Human diseases associated with defects in assembly of OXPHOS complexes. *Essays in Biochemistry*, 62(3):271-286.

Glancy, B. & Balaban, R.S. 2011. Protein composition and function of red and white skeletal muscle mitochondria. *American Journal of Physiology — Cell Physiology*, 300(6):C1280-C1290.

Goody, M.F. & Henry, C.A. 2018. A need for NAD^+ in muscle development, homeostasis, and aging. *Skeletal Muscle*, 8:14.

Gorman, G.S., Chinnery, P.F., DiMauro, S., Hirano, M., Koga, Y., McFarland, R., Suomalainen, A., Thorburn, D.R., Zeviani, M. & Turnbull, D.M. 2016. Mitochondrial diseases. *Nature Reviews — Disease Primers*, 2:16080.

Gorman, G.S., Schaefer, A.M., Ng, Y., Gomez, N., Blakely, E.L., Alston, C.L., Feeney, C., Horvath, R., Yu-Wai-Man, P., Chinnery, P.F., Taylor, R.W., Turnbull, D.M. & McFarland, R. 2015. Prevalence of nuclear and mitochondrial DNA mutations related to adult mitochondrial disease. *Annals of Neurology*, 77(5):753-759.

Grady, J.P., Murphy, J.L., Blakely, E.L., Haller, R.G., Taylor, R.W., Turnbull, D.M. & Tuppen, H.A.L. 2014. Accurate measurement of mitochondrial DNA deletion level and copy number differences in human skeletal muscle. *Public Library of Science One*, 9(12):1-15.

Greaves, L.C., Reeve, A.K., Taylor, R.W. & Turnbull, D.M. 2012. Mitochondrial DNA and disease. *Journal of Pathology*, 226(2):274-286.

Guerrero-Castillo, S., Baertling, F., Kownatzki, D., Wessels, H.J., Arnold, S., Brandt, U. & Nijtmans, L. 2017. The assembly pathway of mitochondrial respiratory chain complex I. *Cell Metabolism*, 25(1):128-139.

Guth, L. & Samaha, F.J. 1969. Qualitative differences between actomyosin ATPase of slow and fast mammalian muscle. *Experimental Neurology*, 25(1):138-152.

Hirst, J. & Roessler, M.M. 2016. Energy conversion, redox catalysis and generation of reactive oxygen species by respiratory complex I. *Biochimica et Biophysica Acta — Bioenergetics*, 1857(7):872-883.

Hoefs, S.J., Rodenburg, R.J., Smeitink, J.A.M. & van den Heuvel, L.P. 2012. Molecular base of biochemical complex I deficiency. *Mitochondrion*, 12(5):520-532.

Hunte, C., Zickermann, V. & Brandt, U. 2010. Functional modules and structural basis of conformational coupling in mitochondrial complex I. *Science*, 329(5990):448-451.

Jacobs, R.A., Díaz, V., Meinild, A.-K., Gassmann, M. & Lundby, C. 2013. The C57Bl/6 mouse serves as a suitable model of human skeletal muscle mitochondrial function. *Experimental Physiology*, 98(4):908-921.

Jain, I.H., Zazzeron, L., Goli, R., Alexa, K., Schatzman-Bone, S., Dhillon, H., Goldberger, O., Peng, J., Shalem, O., Sanjana, N.E., Zhang, F., Goessling, W., Zapol, W.M. & Mootha, V.K. 2016. Hypoxia as a therapy for mitochondrial disease. *Science*, 352(6281):54-61.

JAX (Jackson Laboratory). 2017. Mouse strain datasheet — 027058. https://www.jax.org/strain/027058 Date of access: 10 Mar. 2017.

Jin, Z., Wei, W., Yang, M., Du, Y. & Wan, Y. 2014. Mitochondrial complex I activity suppresses inflammation and enhances bone resorption by shifting macrophage-osteoclast polarization. *Cell Metabolism*, 20(3):483-498.

Johnson, S.C., Yanos, M.E., Kayser, E.-B., Quintana, A., Sangesland, M., Castanza, A., Uhde, L., Hui, J., Wall, V.Z., Gagnidze, A., Oh, K., Wasko, B.M., Ramos, F.J., Palmiter, R.D., Rabinovitch, P.S., Morgan, P.G., Sedensky, M.M. & Kaeberlein, M. 2013. mTOR inhibition alleviates mitochondrial disease in a mouse model of Leigh syndrome. *Science*, 342(6165):1524.

Kahlhöfer, F., Kmita, K., Wittig, I., Zwicker, K. & Zickermann, V. 2017. Accessory subunit NUYM (NDUFS4) is required for stability of the electron input module and activity of mitochondrial complex I. *Biochimica et Biophysica Acta — Bioenergetics*, 1858(2):175-181.

Kalman, B. 2006. Role of mitochondria in multiple sclerosis. *Current Neurology and Neuroscience Reports*, 6(3):244-252.

Karamanlidis, G., Lee, C.F., Garcia-Menendez, L., Kolwicz Jr., S.C., Suthammarak, W., Gong, G., Sedensky, M.M., Morgan, P.G., Wang, W. & Tian, R. 2013. Mitochondrial complex I deficiency increases protein acetylation and accelerates heart failure. *Cell Metabolism*, 18(2):239-250.

Kelso, G.F., Porteous, C.M., Coulter, C.V., Hughes, G., Porteous, W.K., Ledgerwood, E.C., Smith, R.A. & Murphy, M.P. 2001. Selective targeting of a redox-active ubiquinone to mitochondria within cells: antioxidant and antiapoptotic properties. *Journal of Biological Chemistry*, 276(7):4588-4596.

Keshavan, N. & Rahman, S. 2018. Natural history of mitochondrial disorders: a systematic review. *Essays in Biochemistry*, 62(3):423-442.

Kho, A.T., Kang, P.B., Kohane, I.S. & Kunkel, L.M. 2006. Transcriptome-scale similarities between mouse and human skeletal muscles with normal and myopathic phenotypes. *BioMed Central — Musculoskeletal Disorders*, 7(1):1-9.

Kirkwood, S.P., Munn, E.A. & Brooks, G.A. 1986. Mitochondrial reticulum in limb skeletal muscle. *American Journal of Physiology — Cell Physiology*, 251(3):C395-C402.

Koellner, C.M., Mensink, K.A. & Highsmith, W.E. 2018. Basic concepts in human molecular genetics. *(In* Coleman, W.B. & Tsongalis, G.J., *eds*. Molecular Pathology. 2nd ed. San Diego, CA: Academic Press. p. 99-120).

Koopman, W.J., Verkaart, S., Visch, H.J., van der Westhuizen, F.H., Murphy, M.P., van den Heuvel, L.W., Smeitink, J.A.M. & Willems, P.H.G.M. 2005. Inhibition of complex I of the electron transport chain causes $O_2^{-\cdot}$ mediated mitochondrial outgrowth. *American Journal of Physiology — Cell Physiology*, 288(6):C1440-C1450.

Koopman, W.J.H., Beyrath, J., Fung, C.W., Koene, S., Rodenburg, R.J., Willems, P.H.G.M. & Smeitink, J.A.M. 2016. Mitochondrial disorders in children: toward development of small-molecule treatment strategies. *European Molecular Biology Organization Molecular Medicine*, 8(4):311-327.

Koopman, W.J.H., Distelmaier, F., Smeitink, J.A.M. & Willems, P.H.G.M. 2013. OXPHOS mutations and neurodegeneration. *European Molecular Biology Organization Journal*, 32(1):9-29.

Koopman, W.J.H., Nijtmans, L.G.J., Dieteren, C.E.J., Roestenberg, P., Valsecchi, F., Smeitink, J.A.M., & Willems, P.H.G.M.. 2010. Mammalian mitochondrial complex I: biogenesis regulation and reactive oxygen species generation. *Antioxidants & Redox Signaling*, 12(12):1431-1470.

Koves, T.R., Noland, R.C., Bates, A.L., Henes, S.T., Muoio, D.M. & Cortright, R.N. 2005. Subsarcolemmal and intermyofibrillar mitochondria play distinct roles in regulating skeletal muscle fatty acid metabolism. *American Journal of Physiology — Cell Physiology*, 288(5):C1074-C1082.

Kruse, S.E., Watt, W.C., Marcinek, D.J., Kapur, R.P., Schenkman, K.A. & Palmiter, R.D. 2008. Mice with mitochondrial complex I deficiency develop a fatal encephalomyopathy. *Cell Metabolism*, 7(4):312-320.

Lagouge, M. & Larsson, N.G. 2013. The role of mitochondrial DNA mutations and free radicals in disease and ageing. *Journal of Internal Medicine*, 273(6):529-543.

Lake, N.J., Bird, M.J., Isohanni, P. & Paetau, A. 2015. Leigh syndrome: neuropathology and pathogenesis. *Journal of Neuropathology and Experimental Neurology*, 74(6):482-492.

Lamont, R.E., Beaulieu, C.L., Bernier, F.P., Sparkes, R., Innes, A.M., Jackel-Cram, C., Ober, C., Parboosingh, J.S. & Lemire, E.G. 2017. A novel NDUFS4 frameshift mutation causes Leigh disease in the Hutterite population. *American Journal of Medical Genetics Part A*, 173(3):596-600.

Leong, D.W., Komen, J.C., Hewitt, C.A., Arnaud, E., McKenzie, M., Phipson, B., Bahlo, M., Laskowski, A., Kinkel, S.A., Davey, G.M., Heath, W.R., Voss, A.K., Zahedi, R.P., Pitt, J.J., Chrast, R., Sickmann, A., Ryan, M.T., Smyth, G.K., Thorburn, D.R. & Scott, H.S. 2012. Proteomic and metabolomic analyses of mitochondrial complex I-deficient mouse model generated by spontaneous B2 short interspersed nuclear element (SINE) insertion into NADH dehydrogenase (ubiquinone) Fe-S protein 4 (Ndufs4) gene. *Journal of Biological Chemistry*, 287(24):20652-20663.

Lindeque, J.Z., Levanets, O., Louw, R. & van der Westhuizen, F.H. 2010. The involvement of metallothioneins in mitochondrial function and disease. *Current Protein and Peptide Science*, 11(4):292-309.

Lobo-Jarne, T. & Ugalde, C. 2018. Respiratory chain supercomplexes: structures, function and biogenesis. *Seminars in Cell & Developmental Biology*, 76:179-190.

Loeffen, J.L.C.M., Smeitink, J.A.M., Trijbels, J.M.F., Janssen, A.J.M., Triepels, R.H., Sengers, R.C.A. & van den Heuvel, L.P. 2000. Isolated complex I deficiency in children: clinical, biochemical and genetic aspects. *Human Mutation*, 15(2):123-134.

Logan, A., Pell, V.R., Shaffer, K.J., Evans, C., Stanley, N.J., Robb, E.L., Prime, T.A., Chouchani, E.T., Cochemé, H.M., Fearnley, I.M., Vidoni, S., James, A.M., Porteous, C.M., Partridge, L., Krieg, T., Smith, R.A.J. & Murphy, M.P. 2016. Assessing the mitochondrial membrane potential in cells and *in vivo* using targeted click chemistry and mass spectrometry. *Cell Metabolism*, 23(2):379-385.

Mailloux, R.J., Young, A., Chalker, J., Gardiner, D., O'Brien, M., Slade, L. & Brosnan, J.T. 2016. Choline and dimethylglycine produce superoxide/hydrogen peroxide from the electron transport chain in liver mitochondria. *Federation of European Biochemical Societies Letters*, 590 (23):4318-4328.

Manjeri, G.R. 2017. Characterization of the Ndufs4$^{-/-}$ model to evaluate a novel therapeutic strategy towards mitochondrial dysfunction. Nijmegen: RU. (Thesis — PhD).

Mannella, C.A. 2006. Structure and dynamics of the mitochondrial inner membrane cristae. *Biochimica et Biophysica Acta — Molecular Cell Research*, 1763(5-6):542-548.

McDonald, A.E., Pichaud, N. & Darveau, C.A. 2018. "Alternative" fuels contributing to mitochondrial electron transport: importance of non-classical pathways in the diversity of animal metabolism. *Comparative Biochemistry and Physiology Part B: Biochemistry and Molecular Biology*, 224:185-194.

Milenkovic, D., Blaza, J.N., Larsson, N.-G. & Hirst, J. 2017. The enigma of the respiratory chain supercomplex. *Cell Metabolism*, 25(4):765-776.

Mimaki, M., Wang, X., McKenzie, M., Thorburn, D.R. & Ryan, M.T. 2012. Understanding mitochondrial complex I assembly in health and disease. *Biochimica et Biophysica Acta — Bioenergetics*, 1817(6):851-862.

NCBI (National Center for Biotechnology Information). 2017a. Ndufs4 NADH dehydrogenase (ubiquinone) Fe-S protein 4 [*Mus musculus* (house mouse)]. https://www.ncbi.nlm.nih.gov/gene/?term=17993 Date of access: 10 Mar. 2017.

NCBI (National Center for Biotechnology Information). 2017b. NDUFS4 NADH:ubiquinone oxidoreductase subunit S4 [*Homo sapiens* (human)]. https://www.ncbi.nlm.nih.gov/gene/4724 Date of access: 10 Mar. 2017.

Ni, H., Williams, J.A. & Ding, W. 2015. Mitochondrial dynamics and mitochondrial quality control. *Redox Biology*, 4:6-13.

Niyazov, D.M., Kahler, S.G. & Frye, R.E. 2016. Primary mitochondrial disease and secondary mitochondrial dysfunction: importance of distinction for diagnosis and treatment. *Molecular Syndromology*, 7(3):122-137.

Nouws, J., Nijtmans, L.G.J., Smeitink, J.A. & Vogel, R.O. 2012. Assembly factors as a new class of disease genes for mitochondrial complex I deficiency: cause, pathology and treatment options. *Brain*, 135(1):12-22.

Nunnari, J. & Suomalainen, A. 2012. Mitochondria: in sickness and in health. *Cell*, 148(6):1145-1159.

OMIM (Online Mendelian Inheritance in Man). 2017. Leigh syndrome; LS. https://www.omim.org/entry/256000?search=256000&highlight=256000 Date of access: 10 Mar. 2017.

Papa, S. 2002. The NDUFS4 nuclear gene of complex I of mitochondria and the cAMP cascade. *Biochimica et Biophysica Acta — Bioenergetics*, 1555(1-3):147-153.

Papa, S., Scacco, S., De Rasmo, D., Signorile, A., Papa, F., Panelli, D., Nicastro, A., Scaringi, R., Santeramo, A., Roca, E., Trentadue, R. & Larizza, M. 2010. cAMP-dependent protein kinase regulates post-translational processing and expression of complex I subunits in mammalian cells. *Biochimica et Biophysica Acta — Bioenergetics*, 1797(6):649-658.

Partridge, T.A. 2002. Cells that participate in regeneration of skeletal muscle. *Gene Therapy*, 9:752.

Piroli, G.G., Manuel, A.M., Clapper, A.C., Walla, M.D., Baatz, J.E., Palmiter, R.D., Quintana, A. & Frizzell, N. 2016. Succination is Increased on select proteins in the brainstem of the NADH dehydrogenase (ubiquinone) Fe-S protein 4 (Ndufs4) knockout mouse, a model of Leigh syndrome. *Molecular & Cellular Proteomics*, 15(2):445-461.

Prasai, K. 2017. Regulation of mitochondrial structure and function by protein import: a current review. *Pathophysiology*, 24(3):107-122.

Pronicka, E. 2017. Hypocapnic hypothesis of Leigh disease. *Medical Hypotheses*, 101:23-27.

Quinlan, C.L., Treberg, J.R. & Brand, M.D. 2011. Mechanisms of mitochondrial free radical production and their relationship to the aging process. *(In* Masoro, E.J. & Austad, S.N., *eds*. Handbook of the biology of aging. 7th ed. San Diego, CA: Academic Press. p. 47-61).

Quintana, A., Kruse,S.E., Kapurb, R.P, Sanz, E. & Palmiter, R.D. 2010. Complex I deficiency due to loss of Ndufs4 in the brain results in progressive encephalopathy resembling Leigh syndrome. *Proceedings of the National Academy of Sciences*, 107(24):10996-11001.

Quintana, A., Morgan, P.G., Kruse, S.E., Palmiter, R.D. & Sedensky, M.M. 2012. Altered anesthetic sensitivity of mice lacking Ndufs4, a subunit of mitochondrial complex I. *Public Library of Science One*, 7(8):e42904.

Quirós, P.M., Mottis, A. & Auwerx, J. 2016. Mitonuclear communication in homeostasis and stress. *Nature Reviews — Molecular Cell Biology*, 17:213.

Rahman, J. & Rahman, S. 2018. Mitochondrial medicine in the omics era. *The Lancet*, 391(10139):2560-2574.

Rahman, S., Blok, R.B., Dahl, H.H., Danks, D.M., Kirby, D.M., Chow, C.W., Quintana, A. & Frizzell, N. 1996. Leigh syndrome: clinical features and biochemical and DNA abnormalities. *Annals of Neurology*, 39(3):343-351.

Rahman, S. & Thorburn, D. 2015. Nuclear gene-encoded Leigh syndrome overview. (*In* Adam, M.P., Ardinger, H.H., Pagon, R.A., Wallace, S.E., Bean, L.J.H., Stephens, K. & Amemiya, A., *eds.* GeneReviews® [Internet]. Seattle, WA: University of Washington. p. 1-34).

Rainville, P.D., Theodoridis, G., Plumb, R.S. & Wilson, I.D. 2014. Advances in liquid chromatography coupled to mass spectrometry for metabolic phenotyping. *Trends in Analytical Chemistry*, 61:181-191.

Reinecke, F., Smeitink, J.A.M. & van der Westhuizen, F.H. 2009. OXPHOS gene expression and control in mitochondrial disorders. *Biochimica et Biophysica Acta — Molecular Basis of Disease*, 1792(12):1113-1121.

Reznik, E., Miller, M., Senbabaoglu, Y., Riaz, N., Lee, W. & Sander, C. 2016. Mitochondrial DNA copy number variation across human cancers. *eLife*, 5:e10769.

Rhee, E.P. & Gerszten, R.E. 2012. Metabolomics and cardiovascular biomarker discovery. *Clinical Chemistry*, 58(1):139-147.

Rodenburg, R.J. 2016. Mitochondrial complex I-linked disease. *Biochimica et Biophysica Acta — Bioenergetics*, 1857(7):938-945.

Rossignol, R., Faustin, B., Rocher, C., Malgat, M., Mazat, J. & Letellier, T. 2003. Mitochondrial threshold effects. *Biochemical Journal*, 370(Pt 3):751-762.

Russell, A.P., Foletta, V.C., Snow, R.J. & Wadley, G.D. 2014. Skeletal muscle mitochondria: a major player in exercise, health and disease. *Biochimica et Biophysica Acta — General Subjects*, 1840(4):1276-1284.

Sahebekhtiari, N., Thomsen, M., Sloth, J., Stenbroen, V., Zeviani, M., Gregersen, N., Viscomi, C. & Palmfeldt, J. 2016. Quantitative proteomics suggests metabolic reprogramming during ETHE1 deficiency. *Proteomics*, 16:1166-1176.

Sánchez-Caballero, L., Guerrero-Castillo, S. & Nijtmans, L. 2016. Unraveling the complexity of mitochondrial complex I assembly: a dynamic process. *Biochimica et Biophysica Acta — Bioenergetics*, 1857(7):980-990.

Sazanov, L.A. 2015. A giant molecular proton pump: structure and mechanism of respiratory complex I. *Nature Reviews — Molecular Cell Biology*, 16(6):375-388.

Scacco, S., Petruzzella, V., Budde, S., Vergari, R., Tamborra, R., Panelli, D., van den Heuvel, L.P., Smeitink, J.A.M. & Papa, S. 2003. Pathological mutations of the human NDUFS4 gene of the 18-kDa (AQDQ) subunit of complex I affect the expression of the protein and the assembly and function of the complex. *Journal of Biological Chemistry*, 278(45):44161-44167.

Schafer, F.Q. & Buettner, G.R. 2003. Redox state and redox environment in biology. *(In* Torres, M. & Forman, H.J., *eds*. Signal transduction by reactive oxygen and nitrogen species: pathways and chemical principles. Dordrecht, HL: Springer. p. 1-14).

Schiaffino, S. & Reggiani, C. 1994. Myosin isoforms in mammalian skeletal muscle. *Journal of Applied Physiology*, 77(2):493-501.

Schiaffino, S. & Reggiani, C. 2011. Fiber types in mammalian skeletal muscles. *Physiological Reviews*, 91(4):1447-1531.

Sena, L.A. & Chandel, N.S. 2012. Physiological roles of mitochondrial reactive oxygen species. *Molecular Cell*, 48:158-167.

Shaughnessy, D.T., McAllister, K., Worth, L., Haugen, A.C., Meyer, J.N., Domann, F.E., van Houten, B., Mostoslavsky, R., Bultman, S.J., Baccarelli, A.A., Begley, T.J., Sobol, R.W., Hirschey, M.D., Ideker, T., Santos, J.H., Copeland, W.C., Tice, R.R. & Balshaw, D.M. 2014. Mitochondria, energetics, epigenetics, and cellular responses to stress. *Environmental Health Perspectives*, 122(12):1271-1278.

Shokolenko, I.N. & Alexeyev, M.F. 2015. Mitochondrial DNA: a disposable genome? *Biochimica et Biophysica Acta*, 1852(9):1805-1809.

Smeitink, J.A.M., Sengers, R., Trijbels, F. & van den Heuvel, L.W.P.J. 2001. Human NADH:ubiquinone oxidoreductase. *Journal of Bioenergetics and Biomembranes*, 33(3):259-266.

Smeitink, J.A.M., van den Heuvel, L.W.P.J., Koopman, W.J.H., Nijtmans, L.G.J., Ugalde, C. & Willems, P.H.G.M. 2004. Cell biological consequences of mitochondrial NADH:ubiquinone oxidoreductase deficiency. *Current Neurovascular Research*, 1(1):29-40.

St. John, J. 2014. The control of mtDNA replication during differentiation and development. *Biochimica et Biophysica Acta*, 1840(4):1345-1354.

Sterky, F.H., Hoffman, A.F., Milenkovic, D., Bao, B., Paganelli, A., Edgar, D., Wibom, R., Lupica, C.R., Olson, L. & Larsson, N.G. 2012. Altered dopamine metabolism and increased vulnerability to MPTP in mice with partial deficiency of mitochondrial complex I in dopamine neurons. *Human Molecular Genetics*, 21(5):1078-1089.

Stroud, D.A., Surgenor, E.E., Formosa, L.E., Reljic, B., Frazier, A.E., Dibley, M.G., Osellame, L.D., Stait, T., Beilharz, T.H., Thorburn, D.R., Salim, A. & Ryan, M.T. 2016. Accessory subunits are integral for assembly and function of human mitochondrial complex I. *Nature*, 538(7623):123-126.

Suomalainen, A. & Battersby, B.J. 2017. Mitochondrial diseases: the contribution of organelle stress responses to pathology. *Nature Reviews — Molecular Cell Biology*, 19(2):77-92.

Suomalainen, A., Elo, J.M., Pietiläinen, K.H., Hakonen, A.H., Sevastianova, K., Korpela, M., Isohanni, P., Marjavaara, S.K., Tyni, T., Kiuru-Enari, S., Pihko, H., Darin, N., Õunap, K., Kluijtmans, L.A.J., Paetau, A., Buzkova, J., Bindoff, L.A., Annunen-Rasila, J., Uusimaa, J., Rissanen, A., Yki-Järvinen, H., Hirano, M., Tulinius, M., Smeitink, J.A.M. & Tyynismaa, H. 2011. FGF-21 as a biomarker for muscle-manifesting mitochondrial respiratory chain deficiencies: a diagnostic study. *The Lancet Neurology*, 10(9):806-818.

Taylor, R.W. & Turnbull, D.M. 2005. Mitochondrial DNA mutations in human disease. *Nature Reviews — Genetics*, 6(5):389-402.

Thorburn, D.R. 2004. Mitochondrial disorders: prevalence, myths and advances. *Jourrnal of Inherited Metabolic Disease*, 27(3):349-362.

Torraco, A., Peralta, S., Iommarini, L. & Diaz, F. 2015. Mitochondrial diseases part I: mouse models of OXPHOS deficiencies caused by defects on respiratory complex subunits or assembly factors. *Mitochondrion*:76-91.

Tseng, Y.-H., Cypess, A.M. & Kahn, C.R. 2010. Cellular bioenergetics as a target for obesity therapy. *Nature Reviews — Drug Discovery*, 9(6):465-482.

Tyynismaa, H., Carroll, C.J., Raimundo, N., Ahola-Erkkilä, S., Wenz, T., Ruhanen, H., Guse, K., Hemminki, A., Peltola-Mjøsund, K.E., Tulkki, V., Orešič, M., Moraes, C.T., Pietiläinen, K., Hovatta, I. & Suomalainen, A. 2010. Mitochondrial myopathy induces a starvation-like response. *Human Molecular Genetics*, 19(20):3948-3958.

Ugalde, C., Janssen, R.J.R.J., van den Heuvel, L.P., Smeitink, J.A.M. & Nijtmans, L.G.J. 2004. Differences in assembly or stability of complex I and other mitochondrial OXPHOS complexes in inherited complex I deficiency. *Human Molecular Genetics*, 13(6):659-667.

Valsecchi, F., Koopman, W.J.H., Manjeri, G.R., Rodenburg, R.J., Smeitink, J.A.M. & Willems, P.H.G.M. 2010. Complex I disorders: Causes, mechanisms, and development of treatment strategies at the cellular level. *Developmental Disabilities Research Reviews*, 16(2):175-182.

Valsecchi, F., Monge, C., Forkink, M., de Groof, A.J.C., Benard, G., Rossignol, R., Swarts, H.G., van Emst-de Vries, S.E., Rodenburg, R.J., Calvaruso, M.A., Nijtmans, L.G.J., Heeman, B., Roestenberg, P., Wieringa, B., Smeitink, J.A.M., Koopman, W.J.H. & Willems, P.H.G.M. 2012. Metabolic consequences of NDUFS4 gene deletion in immortalized mouse embryonic fibroblasts. *Biochimica et Biophysica Acta — Bioenergetics*, 1817(10):1925-1936.

Valsecchi, F., Ramos-Espiritu, L.S., Buck, J., Levin, L.R. & Manfredi, G. 2013. cAMP and mitochondria. *Physiology*, 28(3):199-209.

van der Lee, R., Szklarczyk, R., Smeitink, J.A.M., Smeets, H.J., Huynen, M.A. & Vogel, R. 2015. Transcriptome analysis of complex I-deficient patients reveals distinct expression programs for subunits and assembly factors of the oxidative phosphorylation system. *BioMed Central — Genomics*, 16:691.

Vasava, A.A. & Mashiyava, P.H. 2016. Electron transport chain: role in reactive oxygen species production and aging. *Scholars Journal of Agriculture and Veterinary Sciences*, 3(5):378-388.

Visch, H.J., Koopman, W.J.H., Leusink, A., van Emst-de Vries, S.E., van den Heuvel, L.W.P.J., Willems, P.H.G.M. & Smeitink, J.A.M. 2006. Decreased agonist-stimulated mitochondrial ATP production caused by a pathological reduction in endoplasmic reticulum calcium content in human complex I deficiency. *Biochimica et Biophysica Acta — Molecular Basis of Disease*, 1762(1):115-123.

Voets, A.M., Huigsloot, M., Lindsey, P.J., Leenders, A.M., Koopman, W.J.H., Willems, P.H.G.M., Rodenburg, R.J., Smeitink, J.A.M. & Smeets, H.J.M. 2012. Transcriptional changes in OXPHOS complex I deficiency are related to anti-oxidant pathways and could explain the disturbed calcium homeostasis. *Biochimica et Biophysica Acta — Molecular Basis of Disease*, 1822(7):1161-1168.

Watmough, N.J. & Frerman, F.E. 2010. The electron transfer flavoprotein: ubiquinone oxidoreductases. *Biochimica et Biophysica Acta — Bioenergetics*, 1797(12):1910-1916.

Widmaier, E.P., Raff, H. & Strang, K.T. 2011. Vander's human physiology : the mechanisms of body function. 12th ed. Boston, MA: McGraw-Hill.

Willems, P.H.G.M., Smeitink, J.A.M. & Koopman, W.J.H. 2009. Mitochondrial dynamics in human NADH:ubiquinone oxidoreductase deficiency. *International Journal of Biochemistry & Cell Biology*, 41(10):1773-1782.

Wolfe, R.R. 2006. The underappreciated role of muscle in health and disease. *American Journal of Clinical Nutrition*, 84(3):475-482.

Zhang, L., Zhou, Y., Wu, W., Hou, L., Chen, H., Zuo, B., Xiong, Y. & Yang, J. 2017. Skeletal muscle-specific overexpression of PGC-1α induces fiber-type conversion through enhanced mitochondrial respiration and fatty acid oxidation in mice and pigs. *International Journal of Biological Sciences*, 13(9):1152-1162.

Zhu, J., Vinothkumar, K.R. & Hirst, J. 2016. Structure of mammalian respiratory complex I. *Nature*, 536:354-358

Zickermann, V., Wirth, C., Nasiri, H., Siegmund, K., Schwalbe, H., Hunte, C. & Brandt, U. 2015. Mechanistic insight from the crystal structure of mitochondrial complex I. *Science*, 347(6217):44-49.

Zieliński, Ł.P., Smith, A.C., Smith, A.G. & Robinson, A.J. 2016. Metabolic flexibility of mitochondrial respiratory chain disorders predicted by computer modelling. *Mitochondrion*, 31:45-55.

Zorova, L.D., Popkov, V.A., Plotnikov, E.Y., Silachev, D.N., Pevzner, I.B., Jankauskas, S.S., Babenko, V.A., Zorov, S.D., Balakireva, A.V., Juhaszova, M., Sollott, S.J. & Zorov, D.B. 2018. Mitochondrial membrane potential. *Analytical Biochemistry*, 552:50-59.

CHAPTER 3

Materials and methods

3.1 Introduction

This chapter provides detailed information regarding the materials (chemicals, instrumentation and software packages) used as well as the methods employed in this study. The chapter is divided into four main sections. First, the various aspects of animal care, handling and sample collection are discussed. Second, information on the polymerase chain reaction (PCR)-based process of genotype confirmation is given. Third, the different spectrophotometric assays (BCA, CS, CI, CII, CIII and CIV) utilised to evaluate respiratory chain (RC) enzyme activity is discussed, along with the methods used to analyse the enzymatic data. Fourth, the chapter concludes with a detailed discussion of the different analytical methods utilised to perform multi-platform metabolic profiling (^{1}H-NMR spectroscopy, GC-TOF-MS, and LC-MS/MS), as well as the bioinformatics of the metabolic data.

3.2 Animals and sampling

3.2.1 Animal care and breeding

Male knockout *(Ndufs4$^{-/-}$)* mice (B6.129S4-*Ndufs4$^{tm1.1Rpa}$*/J) along with age- and sex-matched controls (*Ndufs4$^{+/+}$*) were used in this study. Due to the known differences in hormone cycles, tissue-specific metabolism and, consequently, metabolic profiles between sexes (Wells *et al.*, 2016; Ruoppolo *et al.*, 2018), only one sex-group was used in order to minimise sex-related metabolic variation. It has become increasingly clear, especially in the case of metabolomics studies, that combining both sexes into a single group is not optimal — rather comparing sex-specific metabolic responses to disease is required. However, this was beyond the scope of our study. In order to avoid unneccecary complications due to estrous cycles, males were the selected sex-group. The genotypes of the mice were confirmed by PCR on tailsnip-derived DNA. As *Ndufs4$^{-/-}$* mice themselves are unable to breed[27], the animals were born from heterozygous (*Ndufs4$^{+/-}$)* crosses at the expected Mendelian ratio (Kruse *et al.*, 2008). The two original *Ndufs4$^{+/-}$* breeding trios (consisting of one male and two female *Ndufs4$^{+/-}$* mice) were obtained from Jackson Laboratory (JAX; ME, USA, stock #027058) in 2015 after acquiring import permits (Department of Agriculture, RSA). The animals were bred and housed at the specific pathogen-free (SPF) unit of the Vivarium (SAVC reg. #FR15/13458) of the Pre-Clinical Drug Development Platform (PCDDP; NWU, RSA). From the original trios, more breeding colonies were set up and monitored by a research animal technician at the Vivarium of the PCDDP. The animals were housed in polysulphone type II long, individually ventilated cages (396 x 215 x 172 mm) held under temperature- (22 ± 1°C), humidity- (55 ± 10 %) and light-

[27] *Ndufs4$^{-/-}$* mice are considered infertile and typically die before reaching sexual maturity (JAX, 2017).

controlled (12:12 hour light/dark cycle) conditions with standard laboratory chow (Laboratory animal food: Rodent Breeder, Cat. #RM1845, LabChef, Nutritionhub) and water provided *ad libitum*.

3.2.2 Animal identification and numbering

Wean age (P21-23) mice were visually identified using an ear numbering system that allows numbering from 1 to 99. Using this technique, each animal was assigned a distinctive identification number (ID) via notches or holes punched into the ears, with specific positions representing specific digits (Figure 3-1). Furthermore, records were kept on each animal's date of birth and parental lineage using unique litter numbers (1a to 1z, 2a to 2z, etc.).

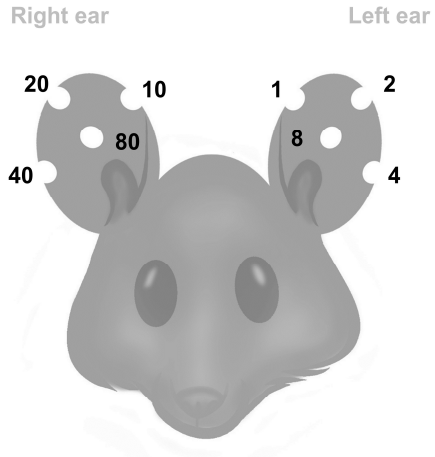


Figure 3-1: Front view depiction of the mouse ear numbering system. Holes or notches in the right and left ear respectively represent digits in the tens and ones position of the mouse ID number. The sum of the digits on the right ear (ranging from 10 to 90) and left ear (ranging from 1 to 9) represents the mouse ID number. For instance, mouse number 33 is indicated by a 10 and a 20 on the right ear, as well as a 1 and a 2 hole in the left ear.

3.2.3 Sample size and animal groups

Table 3-1 summarises the sample sizes used for each analysis. Replicate sampling and analyses are imperative for providing a strong statistical basis for data evaluation and interpretation. Therefore, after considering the scientific objectives and practical limitations of each analysis, the minimum required animal numbers were determined, in collaboration with Statistical Consultation Services (Faculty of Natural and Agricultural Sciences, NWU, RSA). The required number of animal per group were determined to be approximately n = 10 for the enzyme assays and n = 20 for the metabolomics analyses. However, the used sample sizes slightly deviated from these numbers, depending on animal availability. A total of 61 mice were used in this study. For spectrophotometric enzyme assays, 22 mice [*Ndufs4*$^{-/-}$ (n = 12) and WT (n = 10)] were used, while 39 mice [*Ndufs4*$^{-/-}$ (n = 19) and WT (n = 20)] were used for the metabolomics investigation.

Table 3-1: Animals and sample sizes used for the study

Mouse Strain	Age range (days)	Sex	Analyses	Genotype	Quantity
Ndufs4 (PUK 9)	45-50	Male	Enzyme assays	WT	10
				Ndufs4$^{-/-}$	12
			Metabolomics analyses	WT	20
				Ndufs4$^{-/-}$	19

3.2.4 Euthanasia and humane endpoints

The mice used in this study were euthanised between postnatal day (P) 45-50, as significant central nervous system symptoms are only apparent at this age (Kayser *et al.*, 2016). Euthanasia was done via cervical dislocation as described by the AVMA (2013) in order to avoid adverse effects of anaesthesia (Quintana *et al.*, 2012; Roelofs *et al.*, 2014). The animals were euthanised by a research animal technician (PCDDP, NWU, RSA) after a 12 hour fasting period at the same time of day (8:00 to 9:00 AM) in order to reduce inter-animal physiological variation due to differences in nocturnal feeding habits and stages of the circadian cycle, respectively (Deprez *et al.*, 2002; Griffin & Nicholls, 2006). Throughout the study, animal pain and distress were monitored using a humane endpoint score sheet (SOP_Viv_Anim 27: Determining pain and distress in lab rodents) in order to establish whether any mice needed to be considered for euthanasia (score of 10 to 14) or be euthanised immediately (score of 15 to 20). Furthermore, any mice that were not included in this study (heterozygous mice not used for breeding and female mice) were euthanised at P30 — since all mice were already genotyped by that age and *Ndufs4*$^{-/-}$ mice start to develop the mitochondrial disease phenotype after P30. In both humane endpoint cases mentioned, euthanasia was conducted via anaesthetic overdose (SOP_Viv_Anim 1: Euthanasia of rodents, procedure 12.3). These humane endpoint aspects were enacted upon by a research animal technician (PCDDP) overseeing the breeding of the mice.

3.2.5 Tissue sampling and hind-limb muscle dissection

After euthanasia, various tissues including the tailsnips and skeletal muscles, from both hind-limbs of the mice, were rapidly excised. Figure 3-2 indicates the anatomical location of the two hind-limb muscles used in this study. The quadriceps femoris, which is positioned on the anterior portion of the proximal femur, was removed first. This was done by first removing the adipose pad over the quadriceps origin point, after which the tendon that is attached to the patella was cut. Thereafter, the aponeurosis between the bone and the quadriceps was cut to release the muscle from the bone. Finally, the tendon at the origin point on the femur was cut to

release the quadriceps muscle. Following muscle excision, the two visible red muscle portions (lying near the lateral edge of each of the two lobes of the quadriceps) were removed and the white muscle portion of the quadriceps was placed in a collection tube. Next, the soleus, which is located in the superficial posterior compartment of the hind-limb running from the knee to the heel, was removed. First, the Achilles tendon was exposed by peeling the skin overlying the tendon towards the paw of the mouse. Thereafter, the tendon was clamped underneath the heel, cut from the bone and peeled towards the body of the mouse. With the gastrocnemius muscle pulled backwards, the soleus is visible as a flat, deep red muscle lying on the back of the gastrocnemius. The proximal tendon of the soleus was then cut and the soleus was pulled from the gastrocnemius until it only remained attached by the distal tendon. The soleus was then carefully separated from its tendon and placed in a collection tube.

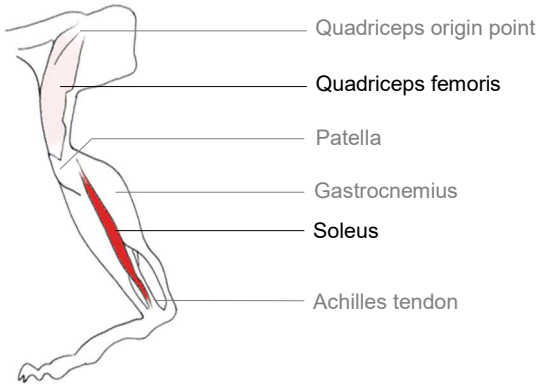


Figure 3-2: Anatomical location of the collected mouse hind-limb skeletal muscles. The quadriceps and soleus muscles are respectively located on the anterior portion of the proximal femur and the superficial posterior compartment of the hind-limb. The quadriceps is generally whiter in colour as it is largely composed of glycolytic fibres, while the soleus is redder due to its primarily oxidative fibre composition.

As mice of the correct genotype became available, their tissues were collected as described above and snap-frozen in liquid nitrogen to “quench” metabolic activity. Due to the comparatively rapid turnover of metabolites, the processes of sampling and quenching need to be as swift as possible in order to preserve (avoid alterations in) metabolite concentrations (Deprez *et al.*, 2002; Erban *et al.*, 2007; Villas-Boas *et al.*, 2007). The time from euthanasia to liquid nitrogen snap-freezing remained under 15 minutes for all muscle samples (Annexure A). After quenching, samples were stored at − 80 °C to temporarily prevent residual enzyme activity and metabolic degradation. All samples were clearly marked (ID number, litter number, genotype, sex, tissue type and date of collection) and record was kept as the samples were obtained.

3.3 Confirming the *Ndufs4* genotypes

The standard PCR genotyping technique described by Valsecchi *et al.* (2010) was used to distinguish the different genotypes of the *Ndufs4* (PUK 9) mouse strain. All breeding pairs and litters were initially genotyped by M. Mereis (MSc. Biochemistry) as part of the breeding- and animal selection program. Thereafter, the same method was employed on the tailsnips (collected *post-mortem*) of mice selected and euthanised for this study, in order to confirm that tissues of the correct genotype were collected. The reader is referred to Annexure A for an example of the obtained electrophoretograms and a discussion of the genotyping results.

3.3.1 Chemicals

For the isolation of genomic DNA from tailsnips, the ZR Genomic DNA™-Tissue MiniPrep Kit (Cat. #D3050, Inqaba Biotech™) was used. This DNA isolation kit contains: proteinase K and storage buffer, 2× digestion buffer, genomic lysis buffer, DNA pre-wash buffer, g-DNA wash buffer, DNA elution buffer, Zymo-Spin™ IIC columns and collection tubes (full contents/composition of buffers are undisclosed).

For the PCR amplification of *Ndufs4* DNA, the Phire™ Tissue Direct PCR Master Mix Kit (Cat. #F-170L; Thermo Fisher Scientific) was used together with specific forward (*Ndufs4* 1060, Cat. #S32E6, Inqaba Biotec™) and reverse (*Ndufs4* Rev, Cat. #S3424, Inqaba Biotec™) primers designed for the *Ndufs4* gene. The PCR Master Mix Kit contains: 2× Phire™ Tissue Direct PCR Master Mix with loading dye, dilution buffer, DNA release additive and nuclease-free water (full contents are undisclosed). Table 3-2 provides additional information on the forward and reverse primers used during genotyping, which includes the sequences in 5' to 3' notation, melting temperature (T_m) and length of each primer.

Table 3-2: Information on PCR primers used to genotype *Ndufs4* mice

Primer	Primer sequence (5' – 3')	T_m (ºC)	Length (bases)
Ndufs4 1060 (Forward)	AGCCTGTTCTCATACCTCGG	62.45	20
Ndufs4 Rev (Reverse)	TTGTGCTTACAGGTTCAAAGTGA	59.2	23

For agarose gel electrophoresis visualisation of the amplified DNA bands, the following was used: agarose (Cat. #8100; CONDA pronadisa), ethidium bromide nucleic acid stain (EtBr; Cat. #46065, Sigma-Aldrich®), 10× Bionic™ Buffer (Cat. #B6185, Sigma-Aldrich®), nuclease-free PCR grade water (H_2O; Cat. #129114, Qiagen), GeneRuler™ 100 bp DNA ladder (Cat. #SM0241, Thermo Fisher Scientific), as well as 6× DNA loading dye (Cat. #SM0242, Thermo Fisher Scientific).

3.3.2 Instrumentation and software packages

Instrumentation used during DNA isolation and quantification include: the Heraeus™ Multifuge™ X3 centrifuge (Thermo Fisher Scientific), vortex mixer (VELP® Scientifica), ABH 2 dry block heater (FMH-instruments, Labotec), and NanoDrop® ND1000 spectrophotometer (NanoDrop® Technologies, Thermo Fisher Scientific) and Operating Software (v 3.8.1). Instrumentation used during the PCR amplification and electrophoretic characterisation of DNA include the: T100™ Thermal Cycler (Bio-Rad), Sub-Cell® GT Cell Horizontal electrophoresis apparatus (Bio-Rad) and ChemiDoc™ MP system (Bio-Rad) with Image Lab (v 5.2.1) software.

3.3.3 Methods

3.3.3.1 Isolation and quantification of genomic DNA

Genomic DNA was isolated from tailsnips according to the standard protocol for solid tissue using the ZR Genomic DNA™-Tissue MiniPrep Kit. Each sample (~ 25 mg) was sliced up and placed into a collection tube. Pre-lysis was achieved by incubating the samples at 55 °C (1-3 hour) in a mixture of 2× digestion buffer (95 µL), nuclease-free H_2O (95 µL), and proteinase K (10 µL). Thereafter, lysis[28] was achieved by the addition of genomic lysis buffer (700 µL) and samples were centrifuged (10,000 ×g, 1 minute) to remove insoluble debris. Supernatants were then transferred to spin column-collection tube assemblies and centrifuged (10 000 ×g, 1 minute) to bind[29] DNA to the silica column while separating it from the flow-through. Next, DNA was purified by removing contaminants (e.g. chaotropic salts) via two separate wash-steps, using DNA pre-wash buffer (200 µL) and g-DNA wash buffer (400 µL) respectively, followed by centrifugation (10,000 ×g, 1 minute). Finally, spin columns were transferred to sterile microcentrifuge tubes and DNA was eluted by incubating (room temperature, 2-5 minutes) the columns in pre-heated (60-70 °C) DNA elution buffer (200 µL), followed by centrifugation (16 000 ×g, 30 seconds).

Subsequently, DNA quantification was done as described in Meissner-Roloff (2009). First, DNA samples were completely resuspended by gently vortexing, after which the NanoDrop® ND1000 spectrophotometer was used to determine the concentration of the DNA at a wavelength of 260 nm. In addition, DNA purity was assessed by determining the ratio of DNA absorbance to a measurement of protein absorbance at 280 nm (A_{260}/A_{280}), with an A_{260}/A_{280} ratio of ~ 1.8,

[28] Lysis is required to break up cells and nuclei to free DNA.

[29] DNA binding to the silica column is enabled by buffer-components such as chaotrophic salts and alcohol, which disrupt nucleic acid-water interactions and allow DNA precipitation and separation from the aqueous phase.

indicating acceptable DNA purification. Thereafter, the eluted DNA samples were stored at − 20 ºC for further use.

3.3.3.2 PCR amplification of DNA

Conventional PCR amplification was used to differentiate the three mouse genotypes [homozygous wild-types (*Ndufs4*$^{+/+}$), homozygous knockouts (*Ndufs4*$^{-/-}$) and heterozygous carrier mice (*Ndufs4*$^{+/-}$)] based on the length of a section spanning the site of Cre-loxP excision in the mutant *Ndufs4* alleles. Amplification was achieved using primers corresponding to the introns flanking *Ndufs4* exon two, as given in Table 3-2. In addition to the isolated genomic DNA samples (25 ng/µL), three control samples corresponding to a *Ndufs4*$^{+/+}$, *Ndufs4*$^{-/-}$ and *Ndufs4*$^{+/-}$ genotype were also amplified. All PCR amplifications were done in a final reaction volume of 10 µL, containing: 1× Phire™ Tissue Direct PCR Master Mix[30], 0.5 µM *Ndufs4* forward and reverse primers, nuclease-free H_2O and 25 ng DNA. The DNA samples were amplified according to the following PCR cycle conditions: i) initial incubation at 98 °C (5 minutes) to ensure total DNA denaturation and Phire™ Hot Start II DNA polymerase activation; ii) 34 cycles of incubation at: 98 °C (5 seconds), 57.3 °C (5 seconds) for primer annealing, and 72 °C (20 seconds) for DNA extension; and iii) incubation at 72 °C (1 minute) to ensure amplicon completion.

3.3.3.3 Agarose gel electrophoresis characterisation of DNA

To identify the amplified PCR fragments in each sample, electrophoresis was performed using a 1 % (w/v) agarose gel containing EtBr (0.5 µg/mL) as a nucleic acid stain in 1× Bionic™ Buffer. To each gel, 10 µL of diluted (30 %, v/v) PCR products[31] and 100 bp DNA Ladder (containing a 2:1:3 ratio of DNA ladder : 6× DNA loading dye : nuclease-free H_2O) were loaded, respectively. Thereafter, the gel was run at 40 V (15 minutes) followed by 70 V (~ 1.5 hours) to separate amplicons[32]. Next, the gel was photographed under ultraviolet (UV) light, thereby visualising the amplicons and their sizes. The genotypes were then identified based upon fragment length as the amplicons of *Ndufs4*$^{+/+}$, *Ndufs4*$^{-/-}$ and *Ndufs4*$^{+/-}$ DNA, respectively, display bands corresponding to two intact *Ndufs4* allele segments (1229 bp), two shortened allele segments without the second *Ndufs4* exon (429 bp), as well as one allele with (1229 bp) and without (429 bp) the second *Ndufs4* exon.

---

[30] The Phire™ Tissue Direct PCR Master Mix employs a Phire™ Hot Start II DNA polymerase, which has a higher degree of specificity allowing for greater distinction among genotypes.

[31] Contains loading dye from the Phire™ Tissue Direct PCR Master Mix.

[32] Separation is achieved due to differences in amplicon size i.e. differential cathode-to-anode migration rates.

3.4 Respiratory chain enzyme activity assays

3.4.1 Chemicals

The following reagents from Sigma-Aldrich® were used during mitochondrial isolation: sucrose (Cat. #S7903), ethylene glycol-bis(2-aminoethylether)-*N,N,N′,N′*-tetra-acetic acid (EGTA; Cat. #E4378), D-mannitol (Cat. #M9546), 2-[4-(2-hydroxyethyl)piperazin-1-yl] ethanesulfonic acid (HEPES; Cat. #H3375) and potassium hydroxide (KOH; Cat. #P5958).

For determination of protein content, the following reagents from Sigma-Aldrich® were used: bicinchoninic acid kit for protein determination (Cat. #BCA1), bicinchoninic acid solution (BCA; Cat. #B9643), copper (II) sulfate solution ($CuSO_4 \cdot 5H_2O$; Cat. #C2284) and bovine serum albumin (BSA; Cat. #P0914).

For the citrate synthase (CS) assay, the following reagents from Sigma-Aldrich® were used: 2,2'-dinitro-5,5'-dithiobenzoic acid (DTNB; Cat. #D8130), oxaloacetate (OAA; Cat. #O4126), acetyl-CoA lithium salt (Cat. #A218) and Triton™X-100 (Cat. #T9284).

For the respiratory chain enzyme activity assays the following reagents from Sigma-Aldrich® were used: BSA (Cat. #P0914), decylubiquinone (dQ; Cat. #D7911), 2,6-dichloroindophenol sodium salt hydrate (DCIP; Cat. #D1878), rotenone (Cat. #R8875), dimethyl sulfoxide (DMSO; Cat. #D2650), antimycin A (Cat. #A8674), succinate (Cat. #S7903), cytochrome c (Cat. #C7752), n-dodecyl-β-D-maltoside (DDM; Cat. #D4641), and sodium ascorbate (Cat. #A4034); together with potassium dihydrogen phosphate (KH_2PO_4; Cat. #60218), dipotassium phosphate (K_2HPO_4; Cat. #60353), and EDTA.K (Cat. #O3660) purchased from Fluka™, as well as reduced nicotinamide adenine dinucleotide disodium salt (NADH; Cat. #10 107 735 001) and adenosine triphosphate disodium salt (ATP; Cat. #10 519 979 001) purchased from Roche Diagnostics, along with Tween® 20 (Cat. #822184) purchased from Merck Chemicals, Sodium azide (NaN_3; Cat. #S2002) purchased from BDH, and Milli-Q® prepared water[33].

3.4.2 Instrumentation and software packages

The following instruments were utilised: 10 mL Glass/Teflon® Tight Fitting Potter-Elvehjem Homogeniser (Glas-Col), Heraeus™ Multifuge™ X3 centrifuge (Thermo Fisher Scientific), ABH 2 dry block heater, (FMH-instruments, Labotec), Synergy™ HT Multi-detection microplate reader (Biotek® Instruments), and Gen5™ Data Analysis software (v 1.11.5).

[33] Water that has been purified using the Milli-Q® system from Millipore™ (Billerica, MA).

3.4.3 Methods

3.4.3.1 Buffer solution preparation

A 0.5 M potassium phosphate buffer (KPi-buffer) was prepared to contain 95 mM KH_2PO_4 and 405 mM K_2HPO_4, with pH 7.4. This buffer was used throughout the RC assays and, when indicated, was further diluted with Milli-Q® water.

3.4.3.2 Sample preparation

Sample preparation for kinetic enzyme analyses involved preparing enriched mitochondrial fractions via differential centrifugation and spectrophotometrically, determining their protein content as described below.

3.4.3.2.1 Isolation of mitochondrial fractions

The following steps were performed at 4 °C, where possible, to minimise the activation of destructive phospholipases and proteases (Palmer & Bonner, 2007). Frozen white quadriceps (n = 22) and soleus (n = 22) muscles were thawed on ice, placed on a pre-chilled metal table and minced (~ 2 minutes) using two single edge razor blades. Next, the minced tissue was weighed (white quadriceps: 148.05 ± 25.5 mg and soleus: 9.59 ± 3.0 mg), transferred to a chilled (4 °C) glass homogeniser tube and suspended in ice-cold Zheng buffer (white quadriceps: 10 %, w/v and soleus: 2 %, w/v). Zheng buffer (pH 7.2) for tissue homogenate preparation consisted of 210 mM mannitol, 70 mM sucrose, 5 mM HEPES and 0.1 mM EGTA. The pH of the buffer was set to 7.2 using KOH. The tissue mixture was then homogenised (~ 15 passes; 164 rpm) using a Glass/Teflon® tissue grinder assembly, with the pestle attached to a motor-driven tissue homogeniser. Next, the homogenate was transferred to a new microcentrifuge tube (2 mL, Eppendorf®) and centrifuged at 700 ×g (4 °C, 10 minutes) to pellet nuclei and cell debris. The supernatant was gently transferred to a new centrifuge tube and stored (− 80 °C). Thereafter, the supernatants were freeze-thawed twice in liquid nitrogen and water in order to disrupt the mitochondrial membranes.

3.4.3.2.2 Total protein content determination

A prerequisite to obtaining comparable enzyme activity results is normalisation to tissue mass (i.e. µg protein). Therefore, the total protein content of the 700 ×g supernatants was quantified using the bicinchoninic acid (BCA) assay [described by Smith *et al.* (1985)] as standardised at the Mitochondria Research Laboratory (NWU). The BCA assay involves two distinct reactions that include the reduction of cupric ions (Cu^{2+}) to cuprous ions (Cu^{+}) by peptide bonds via the biuret reaction and the concomitant secondary detection of Cu^{+} ions via its chelation with two BCA molecules to produce a purple complex, with a strong absorbance maximum at 562 nm.

Therefore, the measured absorbance is directly proportional to the protein content of the sample (Smith *et al.*, 1985). The BCA assay was performed according to the kit manufacturer's instructions in a 96-well UV microtiter plate with a final reaction volume of 200 µL per well. First, duplicate reactions of a bovine serum albumin (BSA) protein standard dilution series (0 µg to 20 µg) were plated in increments of 4 µg. Next, 700 ×g supernatants (10 µL of 1:5 diluted quadriceps or undiluted soleus supernatant) were plated in triplicate and topped up to a final volume of 20 µL with Milli-Q® H_2O. To initiate the reaction, 200 µL BCA reagent (1:50 ratio of $CuSO_4$•$5H_2O$: BCA) was added to each well and the plate was incubated (37 °C, 30 minutes). Thereafter, the absorbance was measured at 562 nm and the protein content (µg) per well was determined from the BSA standard curve ($R^2 > 0.99$) via least mean squares linear regression. Finally, the protein concentration (Cp) in µg/µL was calculated (as shown in Equation 3-1) from the protein content (M_p) via division by the effective sample volume (V_{Ef}) used. The effective sample volume is determined by correcting the sample volume added per well (V_s) for the dilution factor.

Equation 3-1: Protein concentration (µg/µL)

$$Cp = \frac{M_p\,(\mu g)}{V_{Ef}\,(\mu L)} = \frac{M_p\,(\mu g)}{V_s\,/dilution factor\,(\mu L)}$$

$M_p =$ mass protein, $V_{Ef} =$ effective sample volume, $V_s =$ sample volume added per well

3.4.3.3 Kinetic spectrophotometric enzyme assays

The activities of respiratory chain enzymes (CI-CIV) and citrate synthase (CS), were measured in freeze-thawed 700 ×g supernatants of white quadriceps and soleus muscle homogenates. Enzyme activities were quantified via kinetic spectrophotometric assays, during which the absorbance of a single coloured analyte (product or substrate of a two-step coupled redox reaction catalysed by the enzyme) is repeatedly measured over time and used to calculate the initial (pseudo-first-order) reaction velocity (v_0 in mAbs/min). Analyses were performed according to standard operating procedures (SOPs), standardised at the Mitochondria Research Laboratory (NWU), and are based on previously described methods (Shepherd & Garland, 1969; Rahman *et al.*, 1996; Janssen *et al.*, 2007; Luo *et al.*, 2008; Rodenburg, 2011; Smuts *et al.*, 2013). As the aforementioned SOPs were standardised using human muscle, the required sample volumes for mouse muscle homogenates needed to be established for each assay. Detailed information regarding the standardisation of the spectrophotometric assays, for applicability on mouse muscles, can be found in Annexure B. Table 3-3 provides a summary of the conditions for each spectrophotometric assay discussed below.

Table 3-3: Conditions for kinetic spectrophotometric enzyme assays

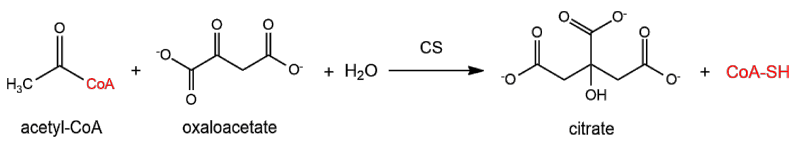
Conditions	CS	CI	CII	CIII	CIV
λ (nm)	412	600	600	550	550
ε[34] (Abs/mM)	7465	12712	12712	4180	4180
Substrates	Acetyl-CoA Oxaloacetate DNTB	NADH dQ DCIP	Succinate dQ DCIP	dQH_2 Cyt c	O_2 Cyt c H_2
Products	TNB	$DCIPH_2$	$DCIPH_2$	Cyt c H_2	Cyt c
Detergent	Triton™X-100			Tween® 20	DDM
Specific inhibitor		Rotenone			

λ =wavelength, ε= molar extinction coefficient for 200 µL reactions. Highlighted in blue are the compounds that absorb light at the λ indicated.

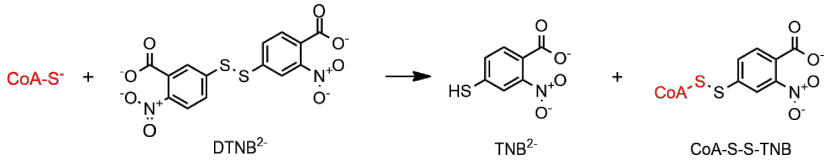
3.4.3.3.1 Citrate synthase enzyme activity assay

CS is commonly used as a quantitative mitochondrial marker, therefore, the activity of this mitochondrial matrix enzyme was measured and quantified as an indicator of mitochondrial mass/content. The assay involves two coupled reactions, which include the CS catalysed production of free CoA-SH from the condensation of oxaloacetate (OAA) with acetyl-coenzyme A (acetyl-CoA) (Reaction 3-1), and the secondary detection of CoA-SH sulfhydryl groups via reaction with DNTB (2,2'-dinitro-5,5'-dithiobenzoic acid) yielding the yellow-coloured product, TNB (2-nitro-5-thiobenzoic acid) (Reaction 3-2) with an absorbance maximum at 412 nm. The assay was performed at 30 °C with triplicate reactions for each sample in a 96-well UV microtiter plate with a final reaction volume of 200 µL per well. The reaction entailed 140 µL of CS master mixture consisting of 60 µM acetyl-CoA, 0.1 mM DTNB, 0.04 % (v/v), Triton™X-100, and 700 ×g supernatant (14 µL of 1:2.5 diluted quadriceps or 15 µL of 1:3 diluted soleus supernatant). After a 10 minute incubation (30 °C) period, 5 mM oxaloacetate (50 µL; preheated to 33 °C) was used to initiate the reaction, and the formation of the coloured product (TNB) was kinetically measured at 412 nm in 1 minute intervals for 5 minutes.

Reaction 3-1: CS-dependent CoA-SH formation



Reaction 3-2: CoA-SH-dependent TNB formation



Yellow (A_{max}=412 nm)

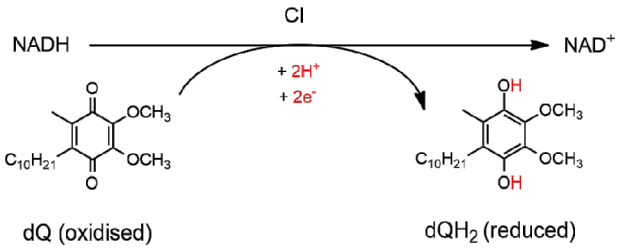
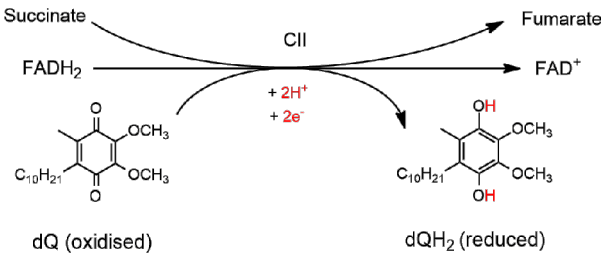
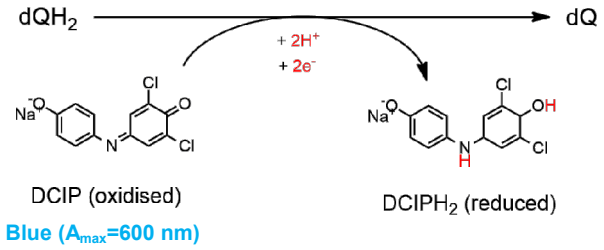
[34] The ε used for each assay was previously determined for a 200 µL reaction by a standard series of the measured substrate in the assay conditions.

3.4.3.3.2 Complex I enzyme activity assay

The CI assay comprises a two-step coupled reaction, which includes the CI catalysed transfer of electrons from NADH to an artificial electron carrier, decylubiquinone (dQ) (Reaction 3-3), and the subsequent transfer of electrons from dQH_2 to the blue-coloured redox dye, 2, 6-dichloroindophenol (DCIP; with an absorbance maximum at 600 nm), which becomes colourless upon its reduction to $DCIPH_2$ (Reaction 3-5). Normally, the electrons carried by decylubiquinol (dQH_2) are accepted by CIII, therefore, antimycin A is added to the reaction mixture, which inhibits the binding of dQH_2 to the QI binding site of CIII. Furthermore, in order to evaluate any nonspecific NADH dehydrogenase activity, the CI assay is performed in the presence, and absence, of rotenone, which inhibits the transfer of electrons from iron-sulfur centres in CI to dQ. The assay was performed at 30 °C with triplicate reactions for each sample in a 96-well UV microtiter plate with a final reaction volume of 200 µL per well. The reaction consisted of 120 µL of CI master mixture containing 50 mM KPi-buffer, 1 µM antimycin A, 70 µM dQ in DMSO, 60 µM DCIP, 0.35 % (w/v) BSA, and 700 ×g supernatant (10 µL of 9:1 diluted quadriceps or undiluted soleus supernatant). Each sample was analysed in the presence of 2.5 µM DMSO (v_1) and 2.5 µM rotenone (v_2), respectively (50 µL). After a 10 minute incubation (30 °C) period, 0.2 mM NADH (20 µL; preheated to 33 °C) was used to initiate the reaction, and the reduction of the coloured substrate (DCIP) to colourless was kinetically measured at 600 nm in 1 minute intervals for 5 minutes.

3.4.3.3.3 Complex II enzyme activity assay

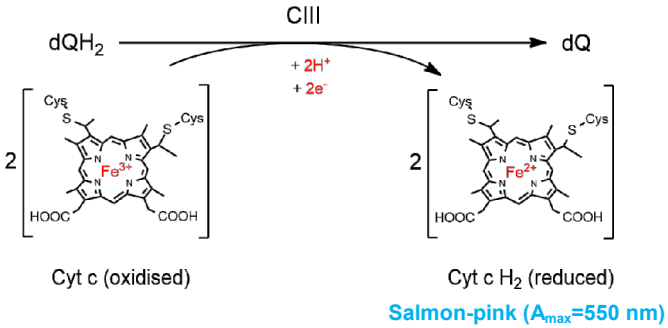
Similar to the CI assay, the CII assay comprises two coupled redox reactions, involving the CII-catalysed transfer of electrons from succinate (Reaction 3-4) via dQ to the final electron acceptor, DCIP, of which the reduction is followed at 600 nm (Reaction 3-5). In order to measure CII specific activity, two inhibitors are added to the reaction: rotenone, which inhibits the transfer of electrons from CI to dQ and antimycin A, which inhibits CIII from accepting electrons from dQH_2. The assay was performed at 30 °C with duplicate reactions for each sample in a 96-well UV microtiter plate, with a final reaction volume of 200 µL per well. The reaction contained 162 µL of CII master mixture consisting of 50 mM KPi-buffer, 1 µM antimycin A, 2.5 µM rotenone, 50 µM dQ in DMSO, 80 µM DCIP, 0.2 mM ATP, 0.08 % (w/v) EDTA, 0.10 % (w/v) BSA and 700 ×g supernatant (8 µL of undiluted quadriceps or soleus supernatant). After a 10 minute incubation (30 °C) period, 10 mM succinate (30 µL; preheated to 33 °C) was used to initiate the reaction, and the reduction of the coloured substrate (DCIP) to colourless was kinetically measured at 600 nm in 1 minute intervals for 5 minutes.

Reaction 3-3: CI-dependent decylubiquinone reduction	
Reaction 3-4: CII-dependent decylubiquinone reduction	
Reaction 3-5: Decylubiquinol-dependent DCIP reduction	

3.4.3.3.4 Complex III enzyme activity assay

The CIII assay involves a two-step redox reaction (Reaction 3-6) during which CIII catalyses the oxidation of dQH_2 to dQ, and transfers the electrons to cytochrome c (cyt c; appears dark orange-red), which upon its reduction to cyt c H_2, becomes light salmon-pink coloured with an absorbance maximum at 550 nm. The assay was performed at 30 °C with duplicate reactions for each sample in a 96-well UV microtiter plate with a final reaction volume of 200 µL per well. The reaction mixture consisted of 125 µL cyt c (83.3 µM) and 700 ×g supernatant (10 µL of a 1:9 dilution of quadriceps or soleus supernatant). After a 10 minute incubation (30 °C) period, the reaction was initiated by the addition of 65 µL of CIII master mixture, consisting of 250 mM KPi buffer, 20 mM NaN_3, 0.05 %, (w/v) BSA, 0.25 % (v/v), Tween® 20 and 0.25 mM dQH_2. The reduction (increase in absorbance) of the coloured substrate (cyt c) was kinetically measured at 550 nm in 1 minute intervals for 5 minutes.

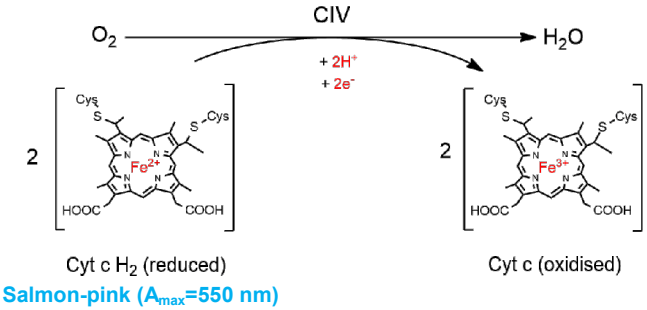
Reaction 3-6: CIII-dependent cytochrome c reduction



3.4.3.3.5 Complex IV enzyme activity assay

The CIV assay involves a two-step redox reaction (Reaction 3-7) during which CIV catalyses the transfer of electrons from the light salmon-pink coloured cyt c H_2 (reduced cyt c; with an absorbance maximum at 550 nm) to dioxygen molecules, yielding the dark orange-red oxidised form of cyt c. The assay was performed at 30 °C with duplicate reactions for each sample in a 96-well UV microtiter plate, with a final reaction volume of 200 µL per well. The reaction mixture consisted of 42.5 µL or 45 µL (depending on the tissue type analysed) of 50 mM Kpi buffer and 700 ×g supernatant (7.5 µL of a 1:9 dilution of quadriceps and 5 µL of a 1:9 dilution of soleus supernatant), thus totalling 50 µL. After a 10 minute incubation (30 °C) period, the reaction was initiated by the addition of 150 µL of CIV master mixture, consisting of 50 mM Kpi buffer, 0.5 mM DDM and 25 µM cyt c H_2. The oxidation (decrease in absorbance) of the coloured substrate (cyt c H_2) was kinetically measured at 550 nm in 1 minute intervals for 5 minutes.

Reaction 3-7: CIV-dependent cytochrome c oxidation



3.4.4 Data analysis

Data analysis followed similarly for each of the kinetic enzyme assays. First, the initial reaction velocity (v_0 in mAbs/min) of the assays was determined via linear rate calculations over 3 minutes (first 4 readings) using the Gen5™ Data Analysis Software (v 1.11.5) and slope linearity (R^2 > 0.99) was examined. In the case of the rotenone-sensitive CI activity assay, v_0 was calculated as the difference between the v_0 measurements obtained in the absence (v_1) and presence (v_2) of rotenone (Equation 3-2). Second, the enzyme activity was calculated according to Equation 3-3 in Excel 2013 (Microsoft), as micromoles of substrate

reduced/oxidised per minute and normalised to protein content. The calculation involves using the average velocity values ($\overline{v_0}$) of the replicate wells and the molar extinction coefficient (ε_λ) of the substrate/product, measured at a specific wavelength (λ) (as summarised in Table 3-3). Finally, the data were pretreated [generalised logarithm (glog) transformation] in MetaboAnalyst 3.0 (Xia *et al.*, 2015). Univariate statistical analysis was done using the Student's *t* test. Differences between *Ndufs4*$^{-/-}$ and WT enzyme activities were regarded as statistically significant with a *t* test p-value of < 0.05.

Equation 3-2: Rotenone sensitive CI v_0	$CI\ v_0 = \overline{v_1} - \overline{v_2}$
Equation 3-3: Enzyme activity per mg protein (µmol/min/mg)	$activity/\ mg = \left(\frac{\overline{v_0}}{\varepsilon_\lambda} \times V_R\right) \Big/ \frac{V_{Ef}}{C_p}$ $= \left(\frac{\overline{v_0}\ (mAbs/min)}{\varepsilon\ (mAbs/mM)} \times 0.2\ mL\right) \Big/ \left(\frac{V_{Ef}\ (\mu L)}{C_p\ (\mu g/\mu L)} \times 10^{-3}\right)$

$\overline{v_0}$= mean velocity, ε = molar extinction coefficient, V_R = reaction volume, V_{Ef} = effective sample volume (volume added divided by dilution factor), C_p = sample protein concentration

3.5 Multi-platform metabolic profiling

3.5.1 Chemicals

The following reagents were used during metabolite extraction: methanol (CH_3OH; Honeywell, Burdick & Jackson, HPLC grade, Cat. #2304), water (H_2O; Honeywell, Burdick & Jackson, HPLC grade, Cat. #BJ365CS), chloroform ($CHCl_3$; Honeywell, Burdick & Jackson, HPLC grade, Cat. #0494). The internal standards used were: *N, N*-dimethyl-L-phenylalanine (DMPA; 99 %, Sigma-Aldrich®, Cat. #273910) and 3-phenylbutyric acid (3-PBA; Sigma-Aldrich®, 98 %, Cat. #116807).

For NMR analysis the following reagents were used throughout sample preparation: water (H_2O, Honeywell, Burdick & Jackson, HPLC grade, Cat. #BJ365CS), potassium phosphate monobasic anhydrous (KH_2PO_4; Sigma-Aldrich®, ≥ 99.5 %, Cat. #229806), deuterium oxide (D_2O; Merck, 99.9 % for NMR spectroscopy MagniSolv™, Cat. #435767), 3-(Trimethylsilyl) propionic acid (TSP; Merck, D_4 sodium salt deuteration degree minimum 98 % for NMR spectroscopy MagniSolv™, Cat. #269913), sodium azide (NaN_3; Sigma-Aldrich®, ≥ 99.5 %, Cat. #S2002) and potassium hydroxide (KOH; Sigma-Aldrich®, Cat. #P1767).

To prepare spiked synthetic urine the following reagents were used: synthetic urine (Surine; Industrial Analytical, Cat. # N/A), sodium-L-lactate (Sigma-Aldrich®, 98 %, Cat. # L7022), L-alanine (Sigma-Aldrich®, ≥ 98 %, Cat. # A7627), taurine (Fluka Chemicals, > 99 %, Cat. # N/A), glycine (Sigma-Aldrich®, ≥ 99 %, Cat. # G7126), creatine hydrate (Sigma-Aldrich®,

99 %, Cat. # C3630), 5-adenosine monophosphate disodium salt (AMP; Sigma-Aldrich®, ≥ 99 %, Cat. # 1930), guanidineacetic acid (Sigma-Aldrich®, 99 %, Cat. # G11608), 3-hydroxybutyric acid sodium salt (3-HB; BDH biochemical, Cat. # N/A), (±)-carnitine hydrochloride (Sigma-Aldrich®, ≥ 98 %, Cat. # C9500) and choline chloride (Sigma-Aldrich®, ≥ 98 %, Cat. # C1879).

For LC-MS/MS analysis the following reagents were used throughout sample preparation: acetyl chloride (Fluka analytical, ≥99 %, Cat. #00990), 1-butanol (Sigma-Aldrich®, 99.8 %, Cat. #281549), acetonitrile (ACN; Honeywell, Burdick & Jackson, >99 % for HPLC, gas chromatography and spectrophotometry, Cat. #BJ015CS), formic acid (Sigma-Aldrich®, 98 %, for mass spectrometry, Cat. #06440) and water (H_2O; Honeywell, Burdick & Jackson, HPLC grade, Cat. #BJ365CS).

An isotope mixture was prepared to aid in analyte identification (and quantification), which consisted of the following amino acids and derivative isotopes purchased from Cambridge Isotope Laboratories: L-lysine-4,4,5,5_d_4·2HCl (96-98 %, Cat. #DLM-2640), L-arginine_4,4,5,5-d_4·HCl (93 %, Cat. #DLM-6038), L-isoleucine_d_{10} (98 %, Cat. #DLM-141-0.1.), L-asparagine_C^{13}4-N^{15}2 : H_2O (Cat. #CNLM-3819-H), L-glutamine_C^{13}5-N^{15}2 (Cat. #CNLM-1275-H), L-citrulline_4,4,5,5-d_4 (93 %, Cat. #DLM-6039) as well as L-valine_d_8 (99 %, Cat. #E161P), and L-phenylalanine_ring_d_5 (98 %, Cat. #E151P) purchased from Euriso-top. The following acyl-carnitine isotopes[35], obtained from VUmc, were also included in the mixture: L-carnitine_methyl-d_3·HCl, octanoyl-L-carnitine_8,8,8-d_3·HCl, dodecanoyl-L-carnitine_10,10,10-d_3·HCl, and stearoyl-L-carnitine_18,18,18-d_3·HCl.

An in-house quality control standard mixture was prepared consisting of the following reagents purchased from Sigma-Aldrich®: L-ornithine hydrochloride (99 %, Cat. #O830-5), 3-methyl-L-histidine (Cat. #M9005), 1-methyl-L-histidine (≥ 98 %, Cat. #67520), glycine (≥ 99 %, Cat. #G7126), L-sarcosine (98 %, Cat. #S-9881), *N,N*-dimethylglycine (≥ 99 %, Cat. #D1156), *trans*-4-hydroxy-L-proline (≥ 99 %, Cat. #41875), γ-aminobutyric acid (GABA; (≥ 99 %, Cat. #A5835), L-proline (≥ 99 %, Cat. #P0380), L-pipecolic acid (99 %, Cat. #P2519), L-homocysteine (≥ 98 %, Cat. #H6010), DL-isoleucine (99 %, Cat. #298689), L-leucine (≥ 98 %, Cat. #L8000), L-pyroglutamic acid (99 %, Cat. #F-3634), L-glutamic acid (≥ 98 %, Cat. #G-8415), L-2-aminoadipic acid (≥ 98 %, Cat. #A7275), isothreonine (Cat. #H6515), L-valine (≥ 98 %, Cat. #V0500), *N*-acetylaspartic acid (NAA; ≥ 99.0 %, Cat. #00920), *N*-acetyl-L-glutamic acid (NAG; 99 %, Cat. #855642), L-carnitine hydrochloride (C0; ≥ 98 %, Cat. #C0283), acetyl-L-

[35] No Cat. # available as the isotopes were obtained from Dr Brink at the VU medical center.

carnitine hydrochloride (C2; 99 %, Cat. #360929), propionyl-L-carnitine (C3; ≥ 97 %, Cat. #42602), butyryl-L-carnitine (C4; ≥ 97 %, Cat. #42623), isovalerylcarnitine (C5; ≥ 97 %, Cat. #51371), hexanoyl-L-carnitine (C6; ≥ 97 %, Cat. #07439), octanoyl-L-carnitine (C8; ≥ 97 %, Cat. #50892), decanoyl-L-carnitine (C10; ≥ 97 %, Cat. #50637), dodecanoyl-L-carnitine (C12; ≥ 97 %, Cat. #39953), myristoyl-L-carnitine (C14; ≥ 97 %, Cat. #61367), palmitoyl-L-carnitine (C16; ≥ 97.0 %, Cat. #61251), stearoyl-L-carnitine (C18; ≥ 97 %, Cat. #61229), and the following reagents from Fluka: taurine (≥ 99 %, Cat. #86330), L-histidine (≥ 99 %, Cat. #53320), L-lysine (≥ 98%, Cat. #62840), L-arginine (≥ 99 %, Cat. #11010), L-asparagine anhydrous (≥ 99 %, Cat. #11150), L-serine (≥ 99 %, Cat. #84960), L-glutamine (≥ 99 %, Cat. #49419), L-threonine (≥ 98 %, Cat. #89180), L-alanine (≥ 99 %, Cat. #5130), trimethylgycine anhydrous (≥ 98 %, Cat. #61962), creatine monohydrate (≥ 99 %, Cat. #27900), DL-beta-aminoisobutyric acid (BAIBA; ≥ 98 %, Cat. #8290), L-citrulline (≥ 99 %, Cat. #27510), L-cystine (≥ 99 %, Cat. #30200), L-cysteine (≥ 99 %, Cat. #30090), L-cystathionine (≥ 98 %, Cat. #30055), L-methionine (≥ 99 %, Cat. #64320), L-tyrosine (≥ 99 %, Cat. #93830), L-phenylalanine (≥ 99 %, Cat. #78020), L-aspartic acid (≥ 99 %, Cat. #11190), as well as beta-alanine (BDH biochemical, ≥ 99 %, Cat. #37009),

For GC-TOF-MS analysis the following reagents were used throughout sample preparation: acetonitrile (ACN; Honeywell, Burdick & Jackson, > 99 % for HPLC, gas chromatography and spectrophotometry, Cat. #BJ015CS), hexane (Sigma-Aldrich®, ≥ 99 %, Cat. #296090), methoxyamine hydrochloride (Aldrich, 98 %, Cat. #226904), O-bis(trimethylsilyl) trifluoroacetamide (BSTFA; Supelco, 98 %, Cat. #33027), trimethylchlorosilane (TMCS; Fluka analytical, 98 %, Cat. #92360), pyridine anhydrous (Sigma-Aldrich®, 99.8 %, Cat. #270970) and water (H_2O, Honeywell, Burdick & Jackson, HPLC grade, Cat. #BJ365CS).

3.5.2 Instrumentation and software packages

The following instruments were utilised during sample preparation: mixer mill MM 400 (Retsch®), 3 mm Ø tungsten carbide beads (Qiagen, Cat. #69997), 5 mm Ø stainless steel beads (Qiagen, Cat. #69989), Heraeus™ Multifuge™ X3 centrifuge (Thermo Fisher Scientific), and Dri-Block® heater and sample concentrators from Techne®.

The NMR system consisted of a 500 MHz Bruker Avance™ III HD NMR spectrometer equipped with a 5 mm triple-resonance inverse (TXI) [^{1}H,^{15}N, ^{13}C] probe head and x, y, z gradient coils with the inner coil of the TXI optimised for ^{1}H observation. The eVol® NMR digital syringe equipped with a 100 µL syringe and a 180-mm-long bevel-tipped needle was used for the miniaturised ^{1}H-NMR method. The Bruker Topspin (v 3.1) and Bruker AMIX (v 3.9.12) software

were used for spectral processing and metabolite identification, respectively while the Bruker pH 7.0 and in-house spectral libraries were used to confirm metabolite identities.

The GC-TOF-MS system consisted of an Agilent© 7890A series gas chromatograph with Agilent© 7693 autosampler coupled to a LECO Pegasus HT time-of-flight mass analyser with an electron impact (EI) ionisation source. The LECO Corporation ChromaTOF® software (v 4.5x) was used for data acquisition and extraction. This included automatic baseline removal via the "spanning" tracking method (offset of 1; just above the noise) and auto smoothing, with the software's Statistical Compare feature used to align peaks. Spectral matching was done using the NIST11 commercial library and an in-house mass spectral library in order to identify important analytes.

The LC-MS/MS system consisted of an Agilent© 1200 series LC front end with binary pump coupled to an Agilent© 6410 series triple quadrupole mass analyser with electrospray ionisation (ESI) source operated in positive ionisation mode. The system is equipped with a vacuum degasser as well as thermostatted autosampler and column compartments. The Agilent© MassHunter Workstation Software (v B02.01; Data acquisition for 6400 Series Triple Quadrupole) and MassHunter Optimiser software (v B02.01) were used for data acquisition in the multiple reaction monitoring (MRM) configuration setting for maximum sensitivity, while data extraction was done using the Agilent© MassHunter Workstation software (v B06.00; Qualitative Analysis and Quantitative Analysis).

3.5.3 Methods

The metabolic profiling methods, described hereafter, were all standardised for applicability to mouse white quadriceps and soleus muscles. For more information on the standardisation process, refer to Annexure B, Section B.2.2

3.5.3.1 Internal standard preparation

A known quantity of internal standard (IS) mixture was added to each biological sample at the onset of metabolome extraction to account for biases (Type A) that arise during the metabolite extraction process. The IS mixture contained compounds naturally absent in mouse muscle tissue that could be detected reliably on all three analytical platforms. *N, N*-dimethyl-L-phenylalanine (DMPA) and 3-phenylbutyric acid (3-PBA) were selected as internal standards for LC-MS/MS and GC-TOF-MS, respectively, due to their repeatable derivatisation, favourable elution time and consistent detection, while DMPA also acted as a repeatable IS for ^{1}H-NMR analysis. The use of DMPA as an IS for multiple metabolomics platforms was first described by van Aardt *et al.* (2016), while 3-PBA is a commonly used IS for GC-MS analyses. Due to the

limited soleus sample quantity, different liquid/liquid extraction ratios were used for the two muscles. Consequently, separate IS mixtures were prepared for the soleus (SOL) and white quadriceps (WQ) muscles. To SOL muscles, 19.25 µL IS mixture (26 ppm DMPA and 32 ppm 3-PBA) was added per mg tissue, while to WQ muscles, 1.25 µL IS mixture (370 ppm DMPA and 463 ppm 3-PBA) was added per mg tissue. The concentrations (ppm) of internal standards in the mixture were calculated to allow the analysis of 50 ng DMPA in NMR samples, 25 ng DMPA in LC samples, and 25 ng 3-PBA in GC samples (see Table 3-4). Stock solutions for DMPA and 3-PBA (10 000 ppm) were prepared in methanol/water (50:50, v/v), while the final internal standard mixtures were prepared in water.

In addition, a stable isotope internal standard mixture (2.5 ppm) was added to LC-M/MS samples (WQ: 50 µL; SOL: 25 µL) before derivatisation in order to account for some of the biases (Type B) that arise due to differential derivatisation and ionisation. The isotope mixture contained various amino acid (valine_d_8, isoleucine_d_{10}, phenylalanine_d_5, lysine_d_4, glutamine_$C^{13}5$-$N^{15}2$, asparagine_$C^{13}4$-$N^{15}2$, arginine_d_4 and citrulline_d_4) as well as acylcarnitine (free carnitine_d_3, octanoylcarnitine_d_3, dodecanoylcarnitine_d_3 and octadecanoylcarnitine_d_3) isotopes in water, prepared from 500 ppm isotope stock solutions in methanol.

Table 3-4: Mass internal standard mixture analysed on various platforms

Analytical platform	Tissue type	Extract volume (µL)	Final sample volume (µL)	Injection volume (µL)	Mass IS analysed (ng)
^{1}H-NMR	WQ	70	70	N/A	50
LC-MS/MS	WQ	50	100	1	25
	SOL	50	25	2.5	25
GC-TOF-MS	WQ	40	100	1	25
	SOL	200	50	1	25

For each platform, the table displays the initial muscle extract aliquot used (column 3), the final volume of each prepared sample (column 4), the sample volume injected on-column for chromatographic platforms (column 5), and the resulting mass IS in the analysed sample volume (column 6). For chromatographic platforms, the on-column IS mass was calculated from the final IS concentration in the sample and the injection volume. *Abbreviations: IS, internal standard; N/A, not applicable; SOL, soleus; WQ, white quadriceps.*

3.5.3.2 Metabolite extraction from muscle

A modified monophasic Bligh–Dyer extraction method (Gullberg *et al.*, 2004), using a solvent ratio of 3:1:1 (methanol:water:chloroform) was employed. This adjusted solvent ratio at neutral pH allows for the repeatable and time-efficient extraction of both hydrophilic and lipophilic compounds in a single phase. Prior to the extraction, frozen muscle samples were placed on a pre-chilled metal table (4 °C), rinsed with physiological saline solution to remove unwanted

external components, such as hair, and minced (~ 2 minutes) using two scalpel blades. The minced tissue was then transferred to a Safe-Lock microcentrifuge tube (Eppendorf®) and weighed for pre-analysis normalisation. As soleus muscles (~ 5 mg) were much smaller than white quadriceps muscles (~ 80 mg), the extraction solvent volumes used for SOL samples were ten-fold greater than those used for the WQ, in order to obtain a sufficient sample volume. Taking into account that approximately 75 % to 80 % of the wet muscle samples consist of water (i.e. 0.75 to 0.8 µL/mg tissue), cold methanol (WQ: 6 µL/mg tissue; SOL: 60 µL/mg tissue) and water (WQ: 1.25 µL/mg tissue; SOL: 19.25 µL/mg tissue), containing internal standard solution (Section 3.5.3.1), were added to the tissue-containing tubes. Subsequently, tungsten carbide and stainless steel beads (~ 7:1 (w/w), WQ: 5 mm Ø; SOL: 3 mm Ø) were added to the tubes and the tissues were pulverised in a vibration mill for 2 minutes at 30 Hz. Next, after the addition of chloroform (WQ: 2 µL/mg tissue; SOL: 20 µL/mg tissue), homogenates were thoroughly vortexed (1 minute) and incubated on ice (10 minutes). Samples were then centrifuged at 20 000 ×g (10 minutes; 4 °C) and the supernatants transferred to new tubes.

3.5.3.3 Quality control samples

For each platform, quality control (QC) samples were included into randomised sample batches, containing *Ndufs4*$^{-/-}$ and WT samples, in order to monitor metabolomics data integrity. QC samples were prepared for each muscle type, respectively, by pooling equal amounts of the *Ndufs4*$^{-/-}$ and WT sample extracts. The QC samples were then aliquoted, stored (− 80 °C) and prepared for each analytical platform in the same manner as the other samples. Together, the two tissue types were analysed over four days on a single platform[36] — with samples and QCs of a single tissue type analysed in two batches over two days. For LC-MS/MS and GC-TOF-MS analyses, QC samples were analysed in the beginning, after every 5 samples, and at the end of each batch. For ^{1}H-NMR analyses, QC samples were analysed at the beginning, middle and end of each batch. In addition, for LC-MS/MS, an in-house standard mixture (consisting of all metabolites analysed) as well as a QC sample spiked with this standard mixture, was analysed at the end of each batch.

3.5.3.4 Sample preparation

After metabolite extraction and QC sample preparation, each sample was aliquoted (volumes indicated in Table 3-4) for separate analyses, evaporated under a stream of cold nitrogen gas and stored (− 80 °C). Due to the limited sample quantity, NMR analysis could not be performed on soleus muscles. Randomised sample batches containing quality control samples were then

[36] Except for ^{1}H-NMR spectroscopy.

prepared freshly on the day of analysis. This section provides information on the above-mentioned sample preparations done for each analytical platform. In short, ^{1}H-NMR sample preparation included removing organic solvents that would cause ^{1}H-NMR signal interference, while sample preparation for chromatographic techniques included derivatisation. For GC-TOF-MS, derivatisation is used to increase thermal stability and volatility, while LC-MS/MS derivatisation is required to enable the simultaneous measurement of compounds containing different functional groups with diverse ionisation properties. Furthermore, derivatisation not only aids in obtaining more reproducible chromatographic results (by improving peak shape and separation) but also assists in compound identification via existing spectral libraries (Halket *et al.*, 2005; Dunn *et al.*, 2013).

3.5.3.4.1 Miniaturised ^{1}H-NMR spectroscopy sample preparation

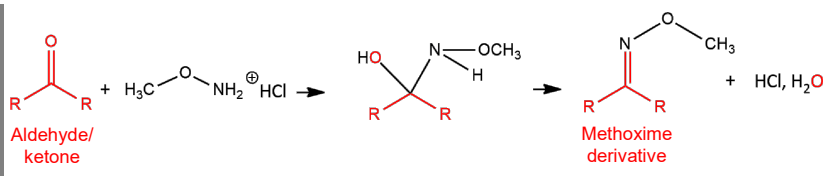
For ^{1}H-NMR spectroscopy, WQ muscle extracts (70 µL) were transferred to glass vials (2 mL, Agilent©) and evaporated under a stream of nitrogen gas at 37 °C. On the day of analysis, each dried extract was resuspended in sterile, filtered water (70 µL) to achieve single signal suppression (NOSEY pre-saturation) and centrifuged at 12 000 ×g (5 minutes, 25 °C) to remove macromolecules and other particulates. A buffer solution (pH 7.4) was prepared as described by Dona *et al.* (2014), containing 1.5 M KH_2PO_4 dissolved in D_2O, together with 100 ppm trimethylsilyl-2,2,3,3-tetradeuteropropionic acid (TSP) as chemical shift standard and 13 ppm NaN_3. Using an eVol® NMR digital syringe, the sample ultra-filtrate (54 µL), together with 10 % buffer solution (6 µL), was aspirated and the total volume (60 µL) was purged into a 2 mm NMR tube (outside Ø 2.0 mm, inside Ø 1.6 mm, length 100 mm). The sample was then mixed once inside the 2 mm NMR tube to ensure homogeneity by aspirating and purging the entire volume. Thereafter, a wash sequence was used to clean the syringe before the next sample was prepared: (1) aspirate 100 µL distilled water, (2) purge 100 µL (waste), (3) aspirate 100 µL distilled water, (4) purge 100 µL (waste), (5) aspirate 100 µL distilled water, (6) purge 100 µL (waste). Next, the NMR tubes were assembled using the Bruker MATCH system, which is an adapter with a gripper to hold the 2 mm NMR tube, inserted into a 10 mm spinner. Finally, each NMR MATCH assembly was loaded onto a SampleXpress autosampler for NMR analysis.

3.5.3.4.2 GC-TOF-MS sample derivatisation

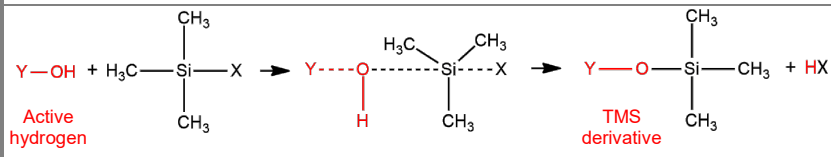
For GC-TOF-MS, muscle extracts (WQ: 40 µL; SOL: 200 µL) were transferred to glass vials (WQ: 2 mL, Agilent©; SOL: 1.1 mL microvial, Separations) and evaporated under a stream of nitrogen gas at 37 °C. On the day of analysis, derivatisation was achieved via a two-step reaction, which includes oximation and silylation. Oximation adds methoxyamine groups to aldehyde and ketone functional groups with the formation methoxime derivatives (Reaction 3-8), thereby preventing the formation of multiple peaks per single compound, while silylation adds

trimethylsilyl (TMS) groups to any functional groups containing active hydrogens (e.g. -COOH, -OH, -NH, and -SH), with the resulting formation of TMS-ethers, -esters, -amines or -sulphides (Reaction 3-9). Derivatisation reagents were prepared freshly on the day of the analysis. To oximate the samples, methoxyamine hydrochloride (20 mg/mL in pyridine, WQ: 50 µL; SOL: 25 µL) was added and the samples were vortex mixed (1 minute) to dissolve the dried compounds. The samples were then incubated at 60 ºC for 1 hour. Thereafter, the samples were silylated by adding BSTFA (WQ: 50 µL; SOL: 25 µL) containing 1 % (v/v) TMCS (catalyst for silylation reaction) and incubated at 60ºC for 1 hour. For the quadriceps samples, the final volume (100 µL) was then transferred to 250 µL pulled point glass inserts. Due to the small volumes used during derivatisation, soleus samples (50 µL) were derivatised in microvials designed to maximise recovery for small sample volumes, therefore, sample transfer to inserts was not necessary. Finally, each vial was loaded onto an Agilent© 7693 autosampler for GC-TOF-MS analysis.

Reaction 3-8: Oximation



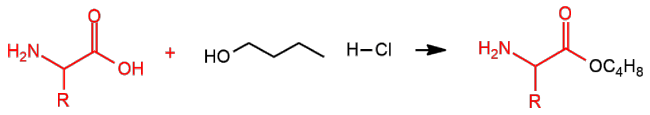
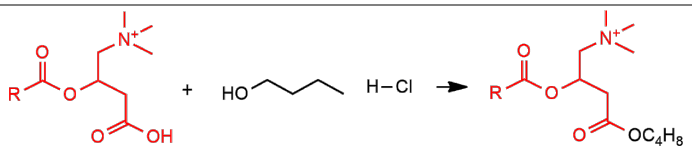
Reaction 3-9: Silylation



3.5.3.4.3 LC-MS/MS sample derivatisation

For LC-MS/MS, muscle extracts (50 µL) were transferred to glass vials (WQ: 2 mL, Agilent©; SOL: 250 µL insert with polymer feet, Separations) together with 2.5 ppm (WQ: 100 µL; SOL: 50 µL) of internal standard isotope mixture (Section 3.5.3.1) and evaporated under a stream of nitrogen gas at 37 °C. On the day of analysis, derivatisation was achieved via butylation, during which active hydrogens on COOH functional groups are replaced with a butyl (-C_4H_8) group, resulting in the formation of butyl esters of amino acids (Reaction 3-10) and acyl-carnitines (Reaction 3-11). To derivatise the samples, butanolic hydrochloric acid [4:1 (v/v) *N*-butanol:acetyl chloride] was added (WQ: 300 µL; SOL: 200 µL) and the samples were incubated at 50 °C for 1 hour. Thereafter, the butylated samples were evaporated to dryness under a stream of nitrogen gas at 37 °C. Finally, the dried residue was reconstituted in a final volume of water:acetonitrile (50:50, v/v) containing 0.1 % formic acid (WQ: 100 µL; SOL: 25 µL). The samples were thoroughly vortex mixed to dissolve the dried compounds in the final volume. In the case of quadriceps samples, the final volume was transferred to 250 µL pulled point glass inserts. Due to the small volumes used during derivatisation, soleus samples were derivatised in

inserts to maximise recovery for small sample volumes, therefore, sample transfer to an insert was not necessary. Finally, each vial was loaded onto an Agilent© 1200 series autosampler for LC-MS/MS analysis.

Reaction 3-10: Butylation of amino acids	 Amino acid
Reaction 3-11: Butylation of acylcarnitines	 Acylcarnitine

3.5.3.5 Metabolic profiling analyses

3.5.3.5.1 Miniaturised ^{1}H-NMR spectroscopy

^{1}H-NMR spectroscopy was performed according to the miniaturised method we developed, as described in Chapter 4. Samples were measured at 500 MHz in 2 mm NMR MATCH tubes, with the 5 mm triple-resonance inverse (TXI) probe head, optimised for ^{1}H observation. The sample temperature was maintained at a constant 300 K. ^{1}H spectra were acquired as 128 transients in 32K data points with a spectral width of 6000 Hz (12.0 ppm). The H_2O resonance at 4.70 ppm was suppressed using the pulse sequence program NOESY-presat, which presaturates the H_2O resonance by single-frequency irradiation during a relaxation delay of 4 seconds, with a 90° excitation pulse of 10 µs. The acquisition time and receiver gain were set for 2.7 seconds and 64, respectively. The number of dummy scans (n = 4) and scans (n = 128) yielded a run time of 15 minutes and 45 seconds per sample. Each sample was automatically shimmed on the deuterium signal, locked, probe tuned and matched, and pulse calibrated. NMR analysis and processing were performed using Bruker Topspin (v 3.5), and further processing conducted using Bruker AMIX (v 3.9.14).

3.5.3.5.2 GC-TOF-MS

The GC-TOF-MS protocol described by Lindeque *et al.* (2013) was slightly modified for this study. Chromatographic separation was done with an Rxi®-5Sil MS capillary column (Restek, 28.6 m x 250 µm x 0.25 µm). The derivatised samples (1 µL for both muscle types) were injected with the injector operating in splitless mode (purge hold 30 seconds) and the inlet temperature set to hold at 250 °C throughout the entire run. A split/splitless single taper deactivated FocusLiner® with glass wool (Phenomenex, outside Ø 6.3 mm, inside Ø 4.0 mm, length 78.5 mm) was used. The initial GC oven temperature was held at 70 ˚C for 1 minute.

Thereafter the oven temperature was increased by 7 °C/min until 120 °C, then 10 °C/min until 230 °C and finally 13 °C/min until 300 °C where the temperature was held for 1 minute before cooling to 70 °C in a total run time of ~ 25.53 minutes. Helium was used as carrier gas, with a pressure-programmed constant flow rate of 1.5 mL/min. Throughout the entire run, the transferline and ion source temperatures were held at 225 °C and 200 °C, respectively. Mass spectrometry was operated in electron impact (EI) ionisation (- 70 V) mode, which enabled the fragmentation of all eluting compounds. After an acquisition (solvent) delay of 250 seconds, data were acquired at a rate of 20 spectra/second using a mass-to-charge (m/z) ratio scan range of 50–950 amu. Peaks with 5 apexing masses were detected using an expected peak width of 3 seconds and a signal-to-noise (S/N) ratio of > 20.

3.5.3.5.3 LC-MS/MS

LC-MS/MS was performed as described by Mels *et al.* (2011) with slight modifications. For separation, a C18 Zorbax SB-Aq reverse phase column (Agilent©, 2.1mm x 150 mm x 3.5 µm) was used. The column was kept at 30 °C during the entire run. One µL and 2.5 µL of sample were injected, respectively, for the WQ and SOL samples. A mobile phase gradient was used to enhance metabolite separation. The chromatographic gradient started at 95 % solvent A (water with 0.1 % formic acid) with a flow of 0.3 mL/min and maintained for 1 minute before the gradient was increased to 20 % solvent B (acetonitrile with 0.1 % formic acid), over a period of 2 minutes. The gradient was then kept constant for 3 minutes, after which it was increased linearly to 100 % solvent B at 13 minutes. Over this period, the flow was linearly increased to 0.35 mL/min at 13.1 minutes. After maintaining these conditions for 5 minutes, the gradient was decreased to 5 % solvent B at 18.5 minutes and kept constant for 1.5 minutes. A post-run of 10 minutes was allowed to ensure equilibration of the column to give a total run time of 30 minutes (20 minute gradient and 10 minute post-run) per sample. Mass spectrometry was operated in multiple reaction monitoring (MRM) mode, with the MRM parameters of target amino acids, -derivatives, acylcarnitines, and isotopes indicated in Table 3-5. The electrospray ionisation (ESI) source gas (nitrogen) temperature was kept at 300 °C, with a flow rate of 7.5 L/min. Nebuliser pressure was kept at 30 psi and the capillary voltage at 3500 V.

Table 3-5: MRM parameters for metabolites and internal standard isotopes monitored.

Metabolite name	~ RT (min)	Transition		Dwell time (sec)	Fragmentor voltage (V)	Collision energy (eV)
		Precursor ion (m/z)	Product ion (m/z)			
AMINO ACIDS AND DERIVATIVES						
1-Methylhistidine	1.8	226.4	124.2	45	120	15
2-Aminoadipic acid	12.7	274.2	98.1	45	113	24
3-Methyl Histidine	1.7	226.4	96.2	45	130	25
Alanine	4.0	146.1	44.2	45	80	15
Arginine	1.9	231.2	70.1	45	103	40
Arginine__ 4,4,5,5__d_4	2.0	235.2	74.2	45	108	32
Asparagine	2.6	189.1	144.1	45	89	8
Asparagine__$C^{13}4$ __$N^{15}2$	2.6	195.2	148.1	45	89	8
Aspartic acid	12.3	246.2	144.1	45	98	12
Beta-Alanine	3.7	146.2	72.1	45	90	10
Beta-Aminoisobutyric acid	6.6	160.1	86.1	45	100	10
Citrulline	4.6	232.2	70.1	45	89	32
Citrulline__4,4,5,5__d_4	4.6	236.2	74.1	45	108	28
Creatine	6.6	188.1	90.1	45	104	16
Cystathionine	8.5	335.2	190.1	45	127	16
Cystine	8.4	353	130	45	118	16
Dimethylglycine	3.8	160.3	58.2	45	90	20
Gamma-Aminobutyric acid	6.1	160.1	87.1	45	79	8
Glutamic acid	12.5	260.2	84.1	45	89	24
Glutamine	3.4	203.1	84.1	45	89	20
Glutamine__$C^{13}5$__$N^{15}2$	3.2	210.2	89.1	45	89	20
Glycine	2.6	132.1	76.1	45	65	4
Histidine	1.6	212.1	110.1	45	89	16
Homocysteine	10.6	192	90	45	161	12
4-Hydroxyproline	4.0	188.1	68.1	45	120	35
Isoleucine__d_{10}	10.6	198.2	96.2	45	108	12
Leucine_Isoleucine	10.8	188.2	86.2	45	89	8
Lysine	1.7	203.2	84.1	45	89	20
Lysine__4,4,5,5__d_4	1.6	207.2	88.2	45	118	16
Methionine	9.1	206.1	104.1	45	94	8
N,N-Dimethylphenylalanine	12.5	250.1	148.1	45	103	20
N-Acetylaspartate	14.1	288.2	144.1	45	98	16
N-Acetylglutamate	14.2	302.2	186.1	45	113	12
Ornithine	1.5	189.2	70.2	45	74	20
Phenylalanine	11.9	222.2	120.1	45	108	16
Phenylalanine__ring__d_5	11.8	227.2	125.1	45	108	16
Pipecolic acid	7.9	186.1	84.1	45	108	16
Proline	6.5	172.1	70.2	45	94	20
Pyroglutamic acid	11.5	186.1	84.1	45	108	16
Sarcosine	2.8	146.1	44.2	45	80	15
Serine	2.7	162.1	60.1	45	94	12

Table 3-5 (continued)

Metabolite name	~ RT (min)	Transition		Dwell time (sec)	Fragmentor voltage (V)	Collision energy (eV)
		Precursor ion (m/z)	Product ion (m/z)			
AMINO ACIDS AND DERIVATIVES						
Taurine	1.4	126	107.9	45	93	10
Threonine	3.7	176.1	74.1	45	94	12
Trimethylglycine	5.4	174.2	58.2	45	130	45
Tryptophan	12.4	261.2	244.1	45	94	8
Tyrosine	9.5	238.2	136.1	45	94	12
Valine	8.7	174.2	72.2	45	89	12
Valine__d_8	8.5	182.2	80.2	45	103	12
ACYLCARNITINES						
Acetyl-carnitine (C2)	9.1	260.2	85.1	45	122	24
Butyryl-carnitine (C4)	12.4	288.2	85.1	45	110	20
Carnitine (C0)	6.3	218.2	103	45	132	16
Carnitine__d_3	6.3	221.2	103.1	45	127	16
Decanoyl-carnitine (C10)	14.4	372.3	85.1	45	125	28
Dodecanoyl-carnitine (C12)	14.6	400.3	85.1	45	155	28
Dodecanoyl-carnitine__d_3	14.6	403.4	85.1	45	155	28
Hexanoyl-carnitine (C6)	13.3	316.2	85.1	45	137	24
Isovaleryl-carnitine (C5)	12.8	302.2	85.1	45	105	24
Myristoyl-carnitine (C14)	15.0	428.4	85.1	45	150	28
Octanoyl-carnitine (C8)	13.8	344.3	85.1	45	115	28
Octanoyl-carnitine__d_3	13.8	347.3	85.1	45	136	24
Palmitoyl-carnitine (C16)	15.3	456.4	85.1	45	160	36
Propionyl-carnitine (C3)	11.2	274.2	85.1	45	127	20
Stearoyl-carnitine (C18)	15.7	484	85.1	45	155	36
Stearoyl-carnitine__d_3	15.7	487.5	85.1	45	160	36

Abbreviations: ~ RT, approximate retention time.

3.5.4 Bioinformatics

In this section, the bioinformatics workflow, as summarised in Figure 3-3, is reported. The reader is referred to Annexure B for an overview of other approaches investigated.

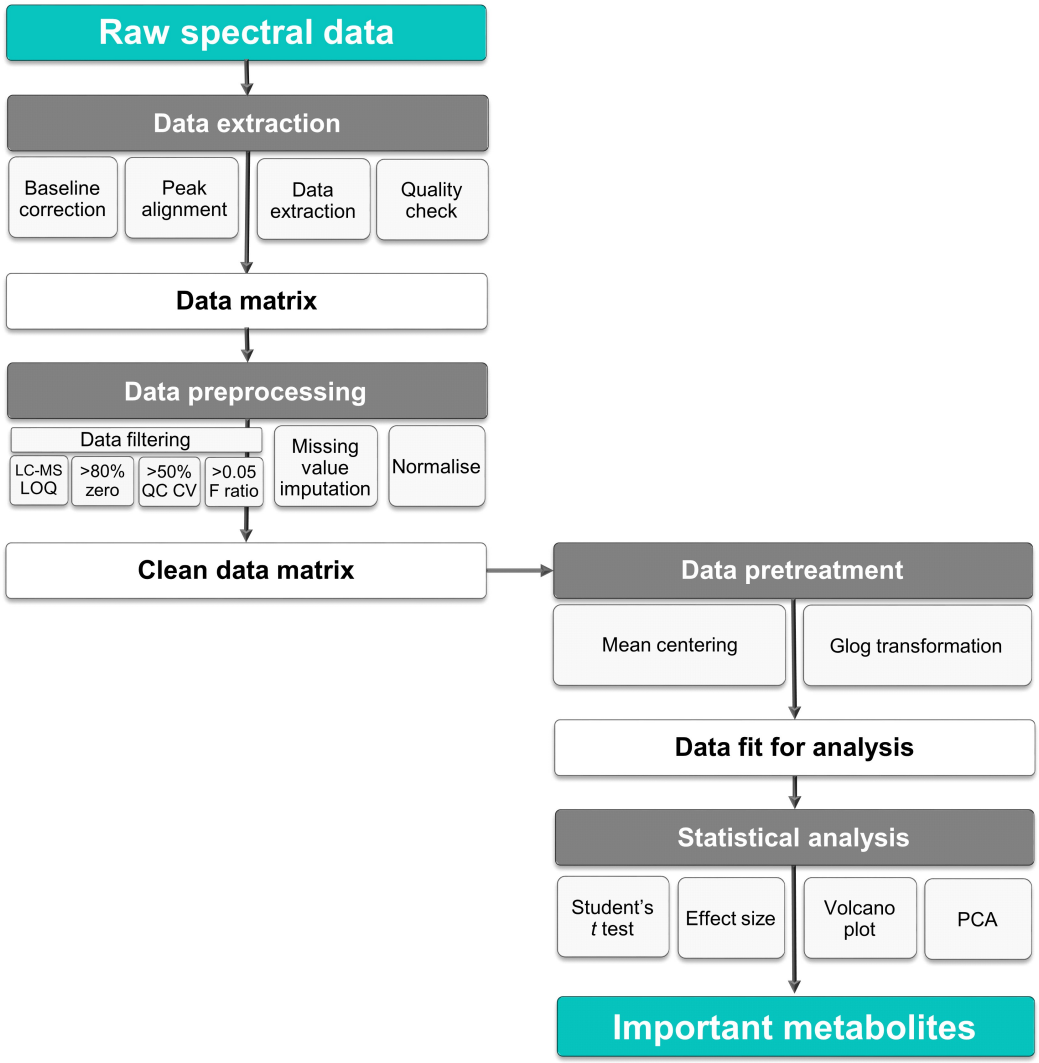


Figure 3-3: Bioinformatics workflow from raw spectral data to important metabolites. Spectral data obtained from each analytical platform underwent automatic baseline correction and peak alignment, after which the data were extracted into a matrix and manually quality checked (correct peak picking and alignment, batch effect and data integrity). Next, the data matrices were individually pre-processed (data filtering, missing value imputation and normalisation) as well as pretreated (mean centering and glog transformation) to obtain data fit for analysis. Finally, statistical analyses (Student's *t* test, effect size calculations, volcano plots and PCA) was used to obtain and inspect important metabolites discriminating between *Ndufs4*$^{-/-}$ and WT groups. *Abbreviations: F ratio, Fisher ratio; Glog, generalised logarithm; LOQ, limit of quantification; PCA, principal component analysis; QC CV, quality control sample coefficient of variance.*

3.5.4.1 Data extraction

After metabolomics analyses were performed, the raw spectral data from each platform were automatically baseline corrected, aligned and extracted into matrices using the instrument software. Thereafter, the data matrices were individually inspected to ensure good data quality

(results presented in Annexure B). This included: i) manual data inspection with regards to correct peak picking and alignment; ii) visual inspection of multivariate data clustering (including QC samples) via principal component analysis (PCA) to identify any biases in the data due to intra- or inter-batch effects; and univariate inspection of iii) metabolite intra- and inter-batch coefficient of variance (CV) distributions, as well as iv) scatter plots of relative intensity vs run order for both individual samples and metabolites. Altogether, the data proved to be of good quality, with no obvious batch effects visible.

3.5.4.2 Data preprocessing

Data preprocessing was applied in order to generate a "clean" data matrix in the form of normalised peak areas that reflect the relative intensities of metabolites in the sample. These steps were performed in Excel 2013 (Microsoft) and included, data filtering, missing value imputation and normalisation. No batch corrections were applied, due to the absence of significant batch effects (see Annexure B).

Firstly, data filtering was done in order to identify and remove variables in the dataset that were unreliable, unstable and unlikely to be of use. For targeted LC-MS/MS data, a peak intensity filter was applied to remove features with areas below the limit of quantification (LOQ cut-off of area < 1000). Thereafter, the following filters were applied to all datasets. First, a missing value (or 80 % zero) filter was applied to remove features that were not detected in 80 % of both[37] *Ndufs4*$^{-/-}$ and WT group samples. Second, a QC variance filter was applied to remove features from the dataset with a CV-value above 50 % in the QC samples. These features were regarded as unreliable due to their high variance among QC samples, as these are identical samples, prepared and analysed throughout the experiment. QC samples were normalised to internal standards (as described later in this section) prior to QC-CV filtering. Third, a Fisher ratio noise filter (Pierce *et al.*, 2006) was applied to remove the noisy components in the feature domain. The Fisher (F) ratio was determined according to Equation 3-4 and represents a type of "signal-to-noise ratio" as it is defined as the ratio of the variance (Var) between classes, to the variance within classes. Features with an F ratio of < 0.05 were removed from the dataset.

Equation 3-4: Fisher ratio

$$F\ ratio = \frac{\left(\bar{x}_{\mathrm{WT}} - \bar{x}_{\mathrm{Ndufs4}^{-/-}}\right)^2}{Var_{WT} + Var_{\mathrm{Ndufs4}^{-/-}}}$$

$\bar{x}$ = average peak area of a specific metabolite, Var= variance of a specific metabolite peak area

[37] If a feature was not detected in ≥ 80 % of one group, but detected in ≥ 80% of the other group, the feature was kept in the dataset.

Next, missing value imputation was done, which aims to form a complete dataset, as too many missing data points cause difficulties for downstream analyses[38]. Missing value imputation was done by replacing all empty data points with a small value (half of the minimum positive value in the original data), assumed to be the detection limit. Of course, the limitation of this method lies in the assumption that all missing values are caused by low abundance metabolites.

Lastly, sample normalisation to internal standards was done in order to adjust for differences among samples and improve sample comparability. For LC-MS/MS data, peak areas were normalised to two types of internal standards. The first (DMPA) was added at the beginning of sample work-up (during liquid-liquid extraction, indicative of mg tissue used), which compensated for most technical variation (sample extraction, derivatisation, and analytical errors). The second (a mixture of various stable isotopes) was added to muscle extracts before derivatisation, which compensates for variation due to derivatisation and analytical errors (e.g. ionisation/sensitivity). If available, metabolites were normalised to their own isotopes; otherwise, normalisation was done to an isotope with a similar retention time to which the metabolite strongly correlated. Correlations between metabolite and isotope peak areas were performed using Statistica (Dell software, v 13.0). Thus for LC-MS/MS, features were first normalised to the stable isotopes used, then to DMPA. For both ^{1}H-NMR and GC-TOF-MS data, peak areas were normalised to only one internal standard, which was added at the beginning of sample work-up (DMPA and 3-PBA, respectively).

3.5.4.3 Data pretreatment

The data were pretreated in order to convert the clean data to a more desirable scale, suitable for parametric statistical analyses. Data pretreatment was done in MetaboAnalyst (Xia *et al.*, 2015) and involved data transformation and data-centering techniques. First, generalised logarithm (glog) transformation was done (according to Equation 3-5) in order to correct for heteroscedasticity in the data, thereby obtaining a more normal data distribution. In addition, this transformation has a pseudo scaling effect as it reduces the difference between low and high abundance metabolites in the data (van den Berg *et al.*, 2006). Next, mean centering was done (according to Equation 3-6) to further reduce the offset between high and low abundant metabolites, as this technique converts metabolite concentrations to fluctuations around zero instead of around the mean of the metabolite concentrations — leaving only the relevant variation for analysis (van den Berg *et al.*, 2006). Finally, outlier detection was done using principal component analysis (PCA) and heatmaps.

[38] Glog transformation and multivariate statistical analyses as performed in MetaboAnalyst (Xia *et al.*, 2015) require full datasets, without missing values.

Equation 3-5: Generalised logarithm transformation	$glog\, x = \log_2 \frac{x + \sqrt{x^2 + 1^2}}{2}$
Equation 3-6: Mean centering	$x_{mean\ centered} = x - \bar{x}$

x = specific metabolite peak area, $\bar{x}$ = average of a specific metabolite peak area

3.5.4.4 Statistical analysis

In order to understand the full impact of data, it is essential to investigate both statistical significance and practical significance. Statistical significance examines whether findings are likely to be due to chance, whereas practical significance helps to understand the biological magnitude of the differences found (Sullivan & Feinn, 2012). Significantly discriminatory features between *Ndufs4*$^{-/-}$ and WT metabolic profiles were determined via univariate analyses. Statistically important differences (Student's *t* test p-values) were inspected at a 5 % and 10 % significance level, with false discovery rate (FDR)-adjusted p-values determined in MetaboAnalyst 3.0 (Xia *et al.*, 2015) using the Bonferroni-Holm approach (Holm, 1979; McLaughlin & Sainani, 2014). FDR adjustments are recommended in cases where multiple comparisons are made in order to compensate for the multiple testing problem[39] and reduce Type I errors (false positives). The effect size of each univariate comparison was determined in Excel 2013 (Microsoft) according to Equation 3-7 to ensure that only relevant metabolites that have a practical significance are identified (Ellis & Steyn, 2003). The cut-off threshold for practical significance was set at an effect size D-value of ≥ 0.5.

Equation 3-7: Effect size D-value	$\mathrm{D} = \frac{\overline{x}_{\mathrm{WT}} - \overline{x}_{\mathrm{Ndufs4}^{-/-}}}{\mathrm{SD}_{\mathrm{max}}}$

$\bar{x}$ = average of a specific metabolite peak area, $\mathrm{SD}_{\mathrm{max}}$= maximum standard deviation

After important feature identification, the datasets from all platforms were combined and visually investigated on a univariate- and multivariate level. Volcano plots were drawn in Excel 2013 (Microsoft) to visualise the statistical and practical significance of the various features. Thereafter, PCA was performed in MetaboAnalyst 3.0 (Xia *et al.*, 2015) on an autoscaled dataset — comprising only the important metabolites identified on each platform — to inspect the data clustering, covariance and discriminatory power. Finally, metabolite identities were assigned to important spectral features via spectral and retention time matching using commercial and in-house spectral libraries together with public databases. Metabolites were identified with high confidence, classified according to the levels depicted in Figure 3-4

[39] The chance of false positives increase with more comparisons made as a p-value of 0.05 implies that 5 % of *all tests* will result in false positives. Contrastingly, an FDR adjusted p-value of 0.05 implies that 5 % of *significant tests* will result in false positives.

(Schymanski *et al.*, 2014). Level one identification was achieved with both ^{1}H-NMR and LC-MS/MS operating in MRM mode, while level one to three identification was achieved with GC-TOF-MS.

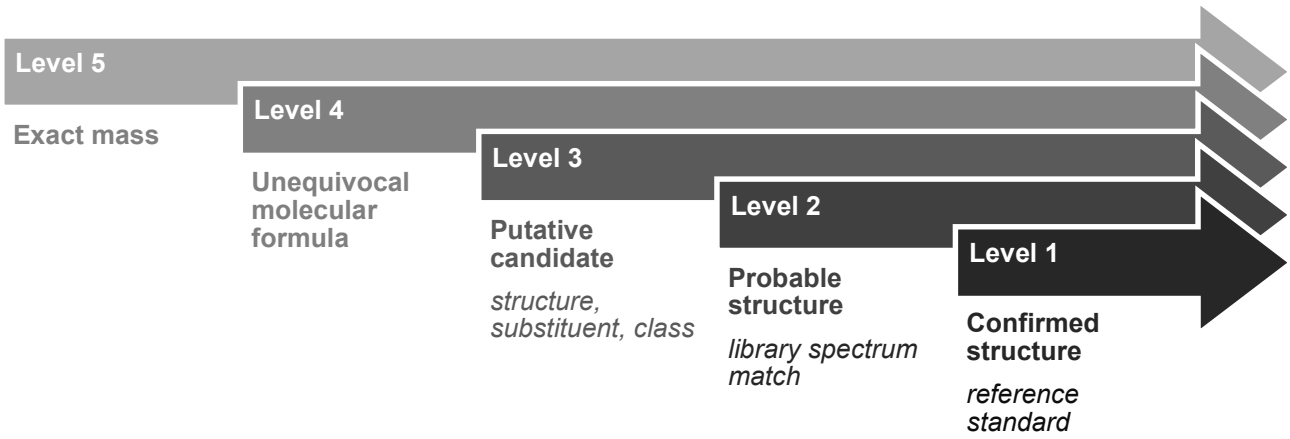


Figure 3-4: Levels of metabolite identification. As defined by Schymanski *et al.* (2014) the confidence with which metabolites are identified in metabolomics approaches can be divided into five levels: 1. confirmed structures, 2. probable structures, 3. putative candidates, 4. unequivocal molecular formula and 5. exact mass.

3.6 References

AVMA (American Veterinary Medical Association). 2013. *AVMA guidelines for the euthanasia of animals: 2013 edition*. https://www.avma.org/KB/Policies/Documents/euthanasia.pdf. Date of access: 12 Mar. 2017.

Deprez, S., Sweatman, B.C., Connor, S.C., Haselden, J.N. & Waterfield, C.J. 2002. Optimisation of collection, storage and preparation of rat plasma for ^{1}H NMR spectroscopic analysis in toxicology studies to determine inherent variation in biochemical profiles. *Journal of Pharmaceutical and Biomedical Analysis*, 30(4):1297-1310.

Dona, A.C., Jiménez, B., Schäfer, H., Humpfer, E., Spraul, M., Lewis, M.R., Pearce, J.T.M., Holmes, E., Lindon, J.C. & Nicholson, J.K. 2014. Precision high-throughput proton NMR Spectroscopy of human urine, serum, and plasma for large-scale metabolic phenotyping. *Analytical Chemistry*, 86(19):9887-9894.

Dunn, W.B., Erban, A., Weber, R.J.M., Creek, D.J., Brown, M., Breitling, R., R., Hankemeier, T., Goodacre, R., Neumann, S., Kopka, J. & Viant, M.R. 2013. Mass appeal: metabolite identification in mass spectrometry-focused untargeted metabolomics. *Metabolomics*, 9(1):44-66.

Ellis, S.M. & Steyn, H.S. 2003. Practical significance (effect sizes) versus or in combination with statistical significance (p-values). *Management Dynamics*, 12(4):51-53.

Erban, A., Schauer, N., Fernie, A.R. & Kopka, J. 2007. Nonsupervised construction and application of mass spectral and retention time index libraries from time-of-flight gas chromatography-mass spectrometry metabolite profiles. *(In* Weckwerth, W., *ed.* Metabolomics — Methods in Molecular Biology. Clifton, NJ: Humana Press. p. 19-38).

Griffin, J.L. & Nicholls, A.W. 2006. Metabolomics as a functional genomic tool for understanding lipid dysfunction in diabetes, obesity and related disorders. *Pharmacogenomics*, 7(7):1095-1107.

Gullberg, J., Jonsson, P., Nordström, A., Sjöström, M. & Moritz, T. 2004. Design of experiments: an efficient strategy to identify factors influencing extraction and derivatization of *Arabidopsis thaliana* samples in metabolomic studies with gas chromatography/mass spectrometry. *Analytical Biochemistry*, 331(2):283-295.

Halket, J.M., Waterman, D., Przyborowska, A.M., Patel, R.K.P., Fraser, P.D. & Bramley, P.M. 2005. Chemical derivatization and mass spectral libraries in metabolic profiling by GC/MS and LC/MS/MS. *Journal of Experimental Botany*, 56(410):219-243.

Holm, S. 1979. A simple sequentially rejective multiple test procedure. *Scandinavian Journal of Statistics*, 6(2):65-70.

Janssen, A.J.M., Trijbels, F.J.M., Sengers, R.C.A., Smeitink, J.A.M., van den Heuvel, L.P., Wintjes, L.T.M., Stoltenborg-Hogenkamp, B.J.M. & Rodenburg, R.J.T. 2007. Spectrophotometric assay for complex I of the respiratory chain in tissue samples and cultured fibroblasts. *Clinical Chemistry*, 53(4):729-734.

JAX (Jackson Laboratory). 2017. Mouse strain datasheet — 027058. https://www.jax.org/strain/027058 Date of access: 10 Mar. 2017.

Kayser, E.-B., Sedensky, M.M. & Morgan, P.G. 2016. Region-specific defects of respiratory capacities in the Ndufs4(KO) mouse brain. *Public Library of Science One*, 11(1):1-18.

Kruse, S.E., Watt, W.C., Marcinek, D.J., Kapur, R.P., Schenkman, K.A. & Palmiter, R.D. 2008. Mice with mitochondrial complex i deficiency develop a fatal encephalomyopathy. *Cell Metabolism*, 7(4):312-320.

Lindeque, J.Z., Hidalgo, J., Louw, R. & van der Westhuizen, F.H. 2013. Systemic and organ specific metabolic differences in metallothionein knockout mice when challenged with exercise. *Metabolomics*, 9(2):418-432.

Luo, C., Long, J. & Liu, J. 2008. An improved spectrophotometric method for a more specific and accurate assay of mitochondrial complex III activity. *Clinica Chimica Acta*, 395(1):38-41.

McLaughlin, M.J. & Sainani, K.L. 2014. Bonferroni, Holm, and Hochberg corrections: fun names, serious changes to p values. *Physical Medicine and Rehabilitation*, 6 (6):544-546.

Meissner-Roloff, M. 2009. The occurrence of mitochondrial DNA polymerase gamma gene mutations in mitochondrial deficiencies, in a selection of South African paediatric patients. Potchefstroom: NWU. (Disseration — MSc).

Mels, C.M.C., Jansen van Rensburg, P., van der Westhuizen, F.H., Pretorius, P.J. & Erasmus, E. 2011. Increased excretion of C4-carnitine species after a therapeutic acetylsalicylic acid dose: evidence for an inhibitory effect on short-chain fatty acid metabolism. *International Scholarly Research Network Pharmacology*:8.

Palmer, T. & Bonner, P.L. 2007. Enzymes: biochemistry, biotechnology, clinical chemistry. 2nd ed. Philadelphia, PA: Elsevier.

Pierce, K.M., Hoggard, J.C., Hope, J.L., Rainey, P.M., Hoofnagle, A.N., Jack, R.M., Wright, B.W. & Synovec, R.E. 2006. Fisher ratio method applied to third-order separation data to identify significant chemical components of metabolite extracts. *Analytical Chemistry*, 78(14):5068-5075.

Quintana, A., Morgan, P.G., Kruse, S.E., Palmiter, R.D. & Sedensky, M.M. 2012. Altered anesthetic sensitivity of mice lacking Ndufs4, a subunit of mitochondrial complex I. *Public Library of Science One*, 7(8):e42904.

Rahman, S., Blok, R.B., Dah, I.H.-H.M., Danks, D.M., Kirby, D.M., Chow, C.W., Christodoulou, J. & Thorburn, D.R. 1996. Leigh syndrome: clinical features and biochemical and DNA abnormalities. *Annals of Neurology*, 39(3):343-351.

Rodenburg, R.J.T. 2011. Biochemical diagnosis of mitochondrial disorders. *Journal of Inherited Metabolic Disease*, 34(2):283-292.

Roelofs, S., Manjeri, G., Willems, P., Scheffer, G., Smeitink, J.A.M. & Driessen, J. 2014. Isoflurane anesthetic hypersensitivity and progressive respiratory depression in a mouse model with isolated mitochondrial complex I deficiency. *Journal of Anesthesia*, 28(6):807-814.

Ruoppolo, M., Caterino, M., Albano, L., Pecce, R., Di Girolamo, M.G., Crisci, D., Costanzo, M., Milella, L., Franconi, F. & Campesi, I. 2018. Targeted metabolomic profiling in rat tissues reveals sex differences. *Scientific Reports*, 8(1):4663.

Schymanski, E.L., Jeon, J., Gulde, R., Fenner, K., Ruff, M., Singer, H.P. & Hollender, J. 2014. Identifying small molecules via high resolution mass spectrometry: communicating confidence. *Environmental Science & Technology*, 48(4):2097-2098.

Shepherd, D. & Garland, P.B. 1969. The kinetic properties of citrate synthase from rat liver mitochondria. *Biochemistry Journal*, 114(3):597-610.

Smith, P.K., Krohn, R.I., Hermanson, G.T., Mallia, A.K., Gartner, F.H., Provenzano, M.D., Fujimoto, E.K., Goeke, N.M., Olson, B.J. & Klenk, D.C. 1985. Measurement of protein using bicinchoninic acid. *Analytical Biochemistry*, 150(1):76-85.

Smuts, I., van der Westhuizen, F.H., Louw, R., Mienie, L.J., Engelke, U.F.H., Wevers, R.A. Mason, S.W., Koekemoer, G. & Reinecke, C.J. 2013. Disclosure of a putative biosignature for respiratory chain disorders through a metabolomics approach. *Metabolomics*, 9(2):379–391.

Sullivan, G.M. & Feinn, R. 2012. Using effect size — or why the p value is not enough. *Journal of Graduate Medical Education*, 4(3):279-282.

Valsecchi, F., Koopman, W.J.H., Manjeri, G.R., Rodenburg, R.J., Smeitink, J.A.M. & Willems, P.H.G.M. 2010. Complex I disorders: Causes, mechanisms, and development of treatment strategies at the cellular level. *Developmental Disabilities Research Reviews*, 16(2):175-182.

van Aardt, W.J., le Roux, J.M., Lindeque, J.Z., Mason, S.W. & Louw, R. 2016. The effect of temperature on the respiration and metabolism of the African burrowing scorpion (*Opistophthalmus latimanus*). *Comparative Biochemistry and Physiology Part D: Genomics and Proteomics*, 20:50-56.

van den Berg, R.A., Hoefsloot, H.C., Westerhuis, J.A., Smilde, A.K. & van der Werf, M.J. 2006. Centering, scaling, and transformations: improving the biological information content of metabolomics data. *BioMed Central — Genomics*, 7(1):142.

Villas-Boas, S.G., Nielsen, J., Smedsgaard, J., Hansen, M.A.E. & Roessner-Tunali, U. 2007. Metabolome analysis: an introduction. Hoboken, NJ: Wiley.

Wells, A., Barrington, W., Threadgill, D., Dearth, S., Campagna, S., Saxton, A. & Voy, B. 2016. Gene, sex and diet interact to control the tissue metabolome. *Federation of American Societies for Experimental Biology Journal*, 30(1_supplement):122-127.

Xia, J., Sinelnikov, I., Han, B. & Wishart, D.S. 2015. MetaboAnalyst 3.0 — making metabolomics more meaningful. *Nucleic Acids Research*, 43(W1):W251-W257.

CHAPTER 4

Miniaturised ^{1}H-NMR method for analysing limited-quantity samples applied to a mouse model of Leigh syndrome

This chapter was published in

Mason, S.W., Terburgh, K. & Louw, R. 2018. Miniaturized ^{1}H-NMR method for analyzing limited-quantity samples applied to a mouse model of Leigh disease. *Metabolomics*, 14:1-12.

4.1 Introduction

Nuclear magnetic resonance (NMR) spectroscopy is one of the most information-rich analytical techniques available (Lindon *et al.*, 2004). In contrast to its highly specific nature, however, NMR is inherently insensitive — a restriction that precludes its application when samples are very limited in quantity (Fratila & Velders, 2011). Here, limited-quantity samples are defined as < 20 mg of tissue. Increases in the sensitivity of NMR experiments have been achieved by improving upon the hardware, in particular by the use of miniaturised coils and greater field strength. In the late 1990s, the first examples of cryogenic NMR probe technology became available, and these high-sensitivity NMR probes have now become more readily available to investigators faced with small samples (Martin, 2005). All these developments in the analysis by NMR of small volumes and improvements in sensitivity have ultimately relied upon advances in technology and spectrometers. Often, however, it is not financially feasible to set up a dedicated NMR spectrometer for small-volume analyses. Compromise is achieved by developing new analytical methods.

In a 2014 study, Glaves *et al*. (2014) addressed the issue of limited-quantity samples from animal models in metabolomics studies. These authors developed a tube-in-tube system (2 mm NMR tube containing sample biofluid within a 5 mm NMR tube containing NMR standards) to analyse ~ 30 µL biofluids (probe not reported) in high-throughput, longitudinal, multimodal metabolomics studies of small animals. The compartmentalisation of sample and NMR standards in this tube-in-tube method, however, had the limitation of requiring chemical shift correction due to bulk magnetic susceptibility and ionic strength changes. Further improvements in the analytical method came from the Bruker company (Rheinstetten, Germany) and their development of the MATCH adaptor system, which consisted of a gripper that holds NMR tubes < 5 mm in diameter and can be loaded into a standard 5 mm probe. Indeed, as small as 3 mm NMR tubes have been used for analysis of various biofluids, but require ~ 200 µL of sample, for example (most recently): saliva [190 µL; Figueira *et al.* (2016)]; urine [250 µL; Cassiède *et al*. (2017)]; astrocyte–motor neuron co-cultures [250 µL; Madji Hounoum *et al*. (2017)]. Furthermore, these studies utilising 3 mm NMR tubes were all done using cryoprobes. In the study reported here, we specifically explored the uses of 2 mm NMR tubes, capable of holding a 60 µL sample, with the Bruker MATCH adaptor system on a room temperature probe.

The use of 2 mm NMR MATCH tubes itself is not novel, as it has been adopted elsewhere, for example in: biogeosciences (Schmitt-Kopplin *et al.*, 2012b); a drug metabolism study (Johansson *et al.*, 2009); and characterisation of meteorite material (Schmitt-Kopplin *et al.*, 2012a). These three studies reported using 2 mm NMR MATCH systems, although, also all relied upon cryoprobes, and none were used for murine models in metabolomics. In our case,

we report the first use of the 2 mm NMR MATCH system in the broad analysis of the metabolite profile in biofluids in the field of metabolomics, demonstrated first using spiked synthetic urine, followed by extracted muscle tissue samples from *Ndufs4*$^{-/-}$ (knockout) mice. Muscle tissues were chosen as they are among the most metabolically active and, consequently, the most affected by mitochondrial disorders such as Leigh syndrome (Li *et al.*, 2013). Comprehensive multi-platform metabolomics of tissues from mouse models remains a challenge due to the limited quantities of analyte obtained from mice. Multi-platform metabolomics of skeletal muscles with different fibre compositions is required to understand better the pathophysiological consequences of complex I deficiency in this tissue. Since the oxidative properties and unique subpopulations of muscle mitochondria depend on the muscle fibre composition (Koves *et al*., 2005), it is imperative to investigate both glycolytic and oxidative muscles. Glycolytic muscles, for example quadriceps, can be found in adequate quantities for metabolomics, whereas the primarily oxidative soleus is quite small (~ 4 mg in total in *Ndufs4*$^{-/-}$ mice). However, because complex I deficiency influences oxidative phosphorylation, it is imperative to investigate the muscle type most reliant on this pathway for energy production, which is the soleus muscles.

Here, we use a routine 500 MHz NMR setup with a 5 mm triple-resonance inverse (TXI) probe head in a biofluid analysis laboratory at room temperature and present a novel miniaturised method for limited-quantity samples (just 60 µL) that yields a result with equivalence to that of an established standard operating protocol (SOP) using a sample ten times greater. First, we tested the analytical parameters of this miniaturised method by using spiked synthetic urine. We show that there is acceptable equivalence between our miniaturised method and a well-established SOP, with the advantage of requiring ten times less sample. Next, using the more-abundant mouse quadriceps muscle, we further confirmed method equivalency and explored the analytical dynamics of the miniaturised method by concentrating samples up to ten times and demonstrating, qualitatively, increased identification of metabolites, with quantitative linearity. Finally, we concluded by applying this miniaturised method to the limited-quantity samples of minute soleus muscle from *Ndufs4*$^{-/-}$ mice in a pilot metabolomics study of Leigh syndrome

4.2 Materials and methods

4.2.1 Spiked synthetic urine

A biological matrix in the form of synthetic urine (surine) was used to spike with nine commercially available metabolites commonly found in muscle tissue, namely: lactic acid (Lac), alanine (Ala), taurine (Tau), glycine (Gly), adenosine 5′-monophosphate (AMP), guanidineacetic acid (GAA), 3-hydroxybutyric acid (3-HB), carnitine (Car) and choline (Chol). Using stock

solutions of each of the nine metabolites, prepared in surine, a combined stock concentration of 500 µM of each metabolite was created — designated high concentration. Thereafter, medium (250 µM) and low (50 µM) concentration spiked surine mixtures were prepared from the high concentration mixture by diluting 2× and 10× respectively with surine.

4.2.2 Animals and sampling

The AnimCare animal research ethics committee of North-West University approved (NWU-00378-16-A5) the animal protocols used here. All animals were maintained and all procedures performed in accordance with the code of ethics in research, training and testing of drugs in South Africa and complied with national legislation. *Ndufs4*$^{-/-}$ mice (B6.129S4-*Ndufs4*$^{tm1.1Rpa}$/J) along with age- and sex-matched controls (wild-type; WT) born from heterozygous crosses (Jackson Laboratories, ME, USA, JAX stock #027058) were used. Mice were held under controlled conditions of temperature (22 ± 1 °C), humidity (55 ± 10 %) and light (12:12 hour light/dark cycle) at the Vivarium (SAVC reg. no. FR15/13458) of the Pre-Clinical Drug Development Platform (PCDDP; NWU, RSA). The animals were fed a standard laboratory diet with food and water provided *ad libitum*. Mice were euthanised between P45–50 as significant central nervous system symptoms are only apparent at this age (Kayser *et al.*, 2016). After euthanasia via cervical dislocation, skeletal muscle tissues were rapidly dissected and snap-frozen in liquid nitrogen. Thereafter, tissues were stored at − 80 °C until extraction.

4.2.3 Metabolite extraction

A slightly modified monophasic Bligh–Dyer extraction method (Gullberg *et al.*, 2004) using a solvent ratio of 6:2:2 (methanol:water:chloroform) was employed. Because approximately 80 % of the wet tissue samples consists of water (i.e. 0.8 µL/mg tissue), cold methanol (6 µL/mg tissue), water (0.7 µL/mg tissue) and internal standard (DMPA) solution (0.5µL/mg tissue; 1840 ppm in water) were added to pre-minced and pre-weighed frozen muscle tissues. Subsequently, tungsten carbide and stainless steel beads [3 mm Ø and 5 mm Ø, respectively, ~ 7:1 (w/w), Qiagen] were added to the muscle tissues in Safe-Lock microcentrifuge tubes (Eppendorf®). Muscle tissues were pulverised in a vibration mill (MM 400, Retsch®) for 2 minutes at 30 Hz. After the addition of chloroform (2 µL/mg tissue), homogenates were thoroughly vortexed (1 minute) and incubated on ice (10 minutes). Samples were then centrifuged at 20,000 ×g (10 minutes; 4 °C) and the supernatant transferred to a new tube. Quadriceps skeletal muscle tissues were used to prepare extracts for further testing of method equivalency and exploration of the miniaturised method (Section 4.3.2). A minute muscle type (both soleus muscles) were used to prepare extracts for the application of the miniaturised method in a metabolomics pilot study (Section 4.3.3).

4.2.4 ^{1}H-NMR sample preparation

4.2.4.1 NMR buffer solution

Buffer solution (1.5 M KH_2PO_4) was prepared by dissolving 20.4 g of the reagent in 80 mL of D_2O. Then 100 mg of TSP and 13 mg of NaN_3 were dissolved in 6–10 mL of D_2O and added to the solution before mixing well. After adjusting the pH to 7.4 (by adding KOH pellets), the solution was transferred to a volumetric flask and the volume adjusted to 100 mL with D_2O (Dona *et al.*, 2014).

4.2.4.2 Established standard operating protocol

Of the muscle tissue extracts, 600 µL was transferred to a 2 mL screw-top glass vial (Agilent©) and dried under N_2 (g) at 37 °C. Solvent evaporation ensured the removal of organic solvents (methanol and chloroform) that would cause ^{1}H-NMR signal interference. Dried extracts were therefore resuspended in 600 µL sterile, filtered water to achieve single signal suppression (NOSEY pre-saturation). Sample preparation followed for both spiked surine (600 µL) and muscle tissues. Samples were centrifuged at 12 000 ×g at room temperature to remove particulates and other macromolecules. From this, 540 µL ultrafiltrate was collected and 60 µL NMR buffer solution added. Samples were then mixed in a vortex to ensure complete homogeneity and, finally, the entire volume transferred to 5 mm NMR tubes. Each tube was placed in a 5 mm spinner and loaded onto a SampleXpress autosampler for NMR analysis.

4.2.4.3 Miniaturised ^{1}H-NMR protocol

Of the muscle tissue extracts, 60 µL was transferred to a 2 mL screw-top glass vial (Agilent©) and dried under N_2 (g) at 37 °C. Each dried extract was resuspended in 60 µL sterile, filtered water. Apart from removing organic solvents, as described in Section 4.2.4.2, this resuspension step provides an opportunity to concentrate a sample (as described in Section 4.3.2.2). Sample preparation followed for both spiked surine (600 µL) and muscle tissues. Samples were centrifuged at 12 000 ×g at room temperature to remove particulates and other macromolecules. Each sample for the miniaturised method was prepared in a 2 mm NMR tube (outside Ø 2.0 mm, inside Ø 1.6 mm, length 100 mm) using the eVol® NMR digital syringe equipped with a 100 µL syringe and a 180 mm-long bevel-tipped needle. The programmed pipetting sequence of the eVol® NMR digital syringe was as follows: (1) aspirate 6 µL NMR buffer solution; (2) aspirate 54 µL sample— maintaining the 10:90 % ratio of D_2O:H_2O as per standard protocol; (3) purge 60 µL (this dispenses prepared sample into 2 mm NMR tube); (4) aspirate 60 µL; (5) purge 60 µL (mix sample once inside 2 mm NMR tube to ensure homogeneity); followed by a wash sequence: (6) aspirate 100 µL distilled water, (7) purge

100 µL (waste), (8) aspirate 100 µL distilled water, (9) purge 100 µL (waste), (10) aspirate 100 µL distilled water, (11) purge 100 µL (waste). For the miniaturised method the Bruker MATCH system was used—an adapter with a gripper to hold the 2 mm NMR tube, inserted into a 10 mm spinner. Each NMR MATCH assembly was loaded onto a SampleXpress autosampler for NMR analysis.

4.2.5 ^{1}H-NMR spectroscopy

Samples were measured at 500 MHz on a Bruker Avance III HD NMR spectrometer equipped with a 5 mm triple-resonance inverse (TXI) [^{1}H, ^{15}N, ^{13}C] probe head and x, y, z gradient coils. The inner coil of the TXI was optimised for ^{1}H observation, the focus of our study. ^{1}H spectra were acquired as 128 transients in 32K data points with a spectral width of 12 000 Hz (24.0 ppm) for the standard 600 µL method and 6 000 Hz (12.0 ppm) for the miniaturised 60 µL method. The sample temperature was maintained at a constant 300 K. The H_2O resonance at 4.70 ppm was suppressed using the pulse sequence program NOESY-presat, which presaturates the H_2O resonance by single-frequency irradiation during a relaxation delay of 4 seconds, with a 90° excitation pulse of 10 µs. The acquisition time and receiver gain were set for 2.7 seconds and 64, respectively. The number of dummy scans = 4 and number of scans = 128, yielding a run time of 15 minutes and 45 seconds per sample. These settings follow those given by established SOPs (Beckonert *et al.*, 2007; Dona *et al.*, 2014).

As in the traditional NMR protocol, each sample was automatically shimmed on the deuterium signal, locked, probe tuned and matched, and pulse calibrated. NMR analysis and processing were performed using Bruker Topspin (v 3.5), and further processing conducted using Bruker AMIX (v 3.9.14).

4.2.6 Statistics

Both untargeted and targeted metabolomics approaches were used to compare methods. For the untargeted data analysis, each NMR spectrum was quantified across 376 spectral bins of equal size — 0.02 ppm bins, excluding the water region of 4.0–6.0 ppm. For the targeted data analysis, nine clearly discernible, common metabolites were identified and quantified from the NMR spectra obtained for the quadriceps muscle tissue extract for both methods. The univariate analyses were performed in Excel 2013 (Microsoft), while the multivariate analyses were conducted using the online metabolomics suite MetaboAnalyst 3.0 (Xia *et al.*, 2015).

For the pilot study, the data were investigated with a targeted and untargeted approach. The data were normalised to the IS before an 80 % zero filter was applied. Thereafter, the data were log transformed and variables important in projection (VIPs) were selected using the Student's *t*

test ($p < 0.05$). Principal component analyses (PCA) score plots (MetaboAnalyst 3.0) were used to illustrate the natural separation in the data.

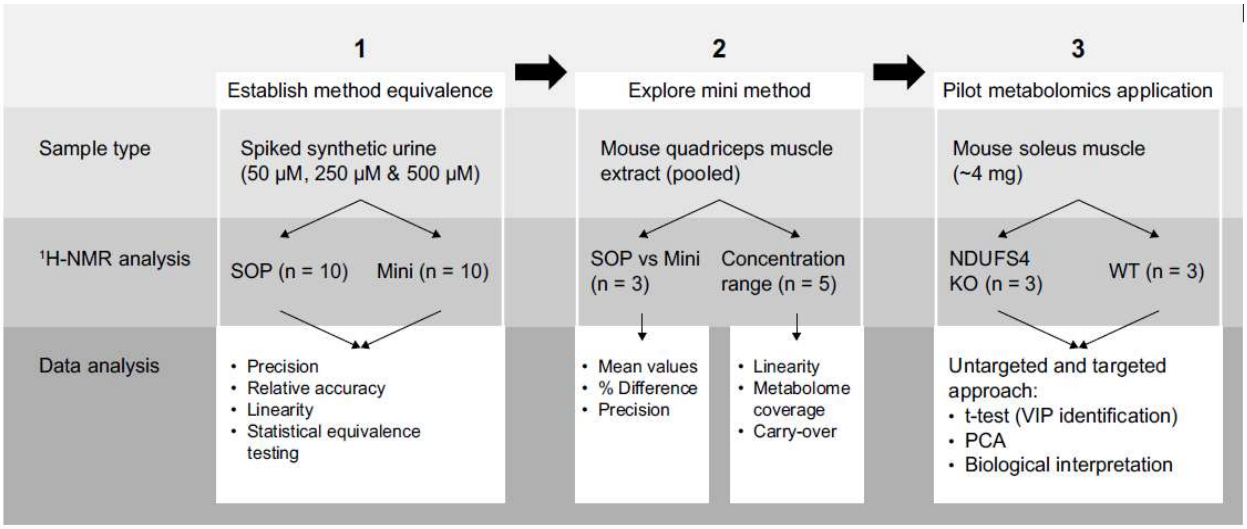


Figure 4-1: Experimental design and workflow

4.3 Results and discussion

The experimental workflow can be divided into three phases (illustrated in Figure 4-1). First, acceptable equivalence between the ^{1}H-NMR SOP and miniaturised method was established by analysing surine spiked with nine standards at low, medium, and high levels (n = 10). Second, pooled mouse muscle extract was used to further confirm this method equivalence (n = 3), as well as explore the capability of the miniaturised ^{1}H-NMR method. A concentration range (up to 10×) prepared from a pooled muscle extract in replicates of five was used to show quantitative linearity for nine metabolites, as well as the ability of the miniaturised method to effectively increase analytical sensitivity (i.e. metabolome coverage) through sample concentration. In addition, water blanks were analysed in between samples in order to show no carry-over when using the same eVol® syringe. Third, the applicability of the miniaturised ^{1}H-NMR method on the metabolomics of limited-quantity samples was demonstrated in a pilot study on the soleus muscle from a mouse model of Leigh syndrome.

4.3.1 Establishing method equivalency

The aim of method equivalency here was to prove that one method performs within an acceptable range of another for the intended application. Therefore, the acceptability of the miniaturised ^{1}H-NMR method as an alternative to the current SOP, when faced with limited sample quantities, was investigated. The samples used in the equivalency tests were chosen based on the desired application (i.e. metabolomics analysis of biological matrices) and therefore consisted of surine spiked with low (50 µM), medium (250 µM) and high (500 µM)

levels of standards. Ten replicate samples were prepared at each of the three concentrations, per method.

Hence, from the generated ^{1}H-NMR spectra, 30 data points were available for each method to test method equivalency. Again, due to the intended metabolomics application, the miniaturised method's acceptability was judged based upon: precision [coefficient of variance (CV) < 15 %], relative accuracy (80–120 %), linearity ($R^2 > 0.95$), and statistical equivalence ($p < 0.05$) to the SOP using the two one-sided test (TOST).

4.3.1.1 Precision

As a measure of precision, the CV was determined for each method at each concentration level (low, medium, and high). The results (Table 4-1) were weighed against predefined acceptable limits of variation. For samples spiked with low levels of standards (near the detection limit) a CV < 15% was considered acceptable while CVs < 10 and < 5 % were considered acceptable for the medium and high concentration levels, respectively. These precision cut-off values lie below the specified levels set out by the FDA for targeted studies: "the precision determined at each concentration level should not exceed 15 % of the CV except for the lower limit of quantification, where it should not exceed 20 % of the CV" (FDA, 2001), and far below the CV cut-off value of 50 % typically used in metabolomics studies (Dunn *et al.*, 2012). As expected, the SOP proved to be more precise than the miniaturised method, which despite having slightly higher variance still performed with excellent precision. For both methods, CVs fell well below the predefined limits in almost all cases (< 2 % in high and medium levels, and < 10 % in low levels). The only exceptions were seen with taurine and AMP. Taurine had a relatively high CV in both the SOP and miniaturised methods (clearly visible at low level). The higher CV observed for taurine is known, previously reported in quantitative ^{1}H-NMR analysis (Hohmann *et al.*, 2014) to have mean recovery rates ranged between 97.1 and 108.2 %, yielding an average value of 104.2 ± 4.9 %. For AMP, the SOP performed better than the miniaturised method (4.5 vs. 12.8 %) at the lowest level.

4.3.1.2 Relative accuracy

Relative recovery (Table 4-1) was used as a measure of accuracy at each concentration level. Recovery using the miniaturised method was compared to that of the SOP (where the average recovery of the SOP was taken as 100 %). A recovery range of 80–120 % was deemed acceptable as per bioanalytical method validation standards (Chan *et al.*, 2004). The miniaturised method performed well within these parameters for the medium and high concentrations. However, again, taurine, and to a small degree AMP, fell outside this acceptable recovery range at low concentrations.

Table 4-1: Measure of precision and accuracy

Standards CV % (recovery %)	Low		Medium		High	
	SOP	Mini	SOP	Mini	SOP	Mini
Lactic acid	5.1 (95–114)	5.5 (95–114)	0.3 (100–101)	1.1 (101–105)	0.3 (100–101)	1.1 (102–106)
Alanine	1.8 (98–105)	6.0 (89–108)	0.1 (100)	1.2 (100–104)	0.2 (100)	1.2 (101–105)
3-Hydroxybutyric acid	3.0 (93–103)	7.5 (91–118)	0.3 (100–100)	0.8 (101–103)	0.2 (100)	0.7 (102–104)
Choline	0.6 (99–101)	1.5 (96–100)	0.1 (100)	0.6 (98–99)	0.2 (100)	0.9 (98–102)
Carnitine	2.0 (98–106)	1.8 (101–106)	0.1 (100)	0.4 (102–103)	0.2 (100)	0.6 (103–104)
Taurine	15.0 (77–135)	16.0 (89–149)	1.7 (98–102)	4.1 (102–115)	0.7 (99–101)	2.2 (102–108)
Glycine	5.1 (91–113)	7.1 (85–113)	0.4 (100–101)	1.5 (99–104)	0.2 (100)	0.8 (102–104)
GAA	1.4 (99–104)	5.0 (90–108)	0.2 (100)	1.2 (99–102)	0.2 (100)	1.5 (99–104)
AMP	4.5 (90–105)	12.8 (79–122)	0.3 (99–100)	2.4 (97–104)	0.3 (99–100)	1.2 (101–106)

4.3.1.3 Linearity

Linear least squares regression was used to measure the correlation between the results obtained from the SOP and miniaturised method. For each standard the average (n = 10) concentration obtained using the SOP was plotted against that obtained from the miniaturised method across varying concentration levels (low, medium, and high). A coefficient of determination (R^2) larger than 0.95 was considered to describe a sufficiently linear relationship between the two methods. The results obtained were as follows: lactic acid ($y = 0.96x + 0.17$; $R^2 = 0.999$); alanine ($y = 0.96x + 2.43$; $R^2 = 0.999$); 3-HB ($y = 0.96x + 2.37$; $R^2 = 1.000$), choline ($y = 0.99x + 2.59$; $R^2 = 0.999$), carnitine ($y = 0.97x + 1.04$; $R^2 = 0.999$), taurine ($y = 0.97x - 10.65$; $R^2 = 0.9997$), glycine ($y = 0.97x + 2.23$; $R^2 = 1.000$), GAA ($y = 0.97x + 3{,}14$; $R^2 = 1.000$), and AMP ($y = 0.95x + 4.36$; $R^2 = 0.9998$). See Figure 4-5 for linearity graphs. Hence, linearity between the methods is evident for all nine metabolites with R^2 values ≥ 0.99. These results further confirm acceptable equivalency between the SOP and miniaturised method.

4.3.1.4 Statistical equivalence testing

Although commonly used in statistical hypothesis testing, the two-sample *t* test proves problematic when trying to establish equivalence. Since the aim of a *t* test is to determine whether a difference exists, the null hypothesis (H0: means are equivalent) is inappropriate for equivalence testing. As only an alternative hypothesis can be statistically proven, failure to reject H0 does not prove that equivalence truly exists (Chambers *et al.*, 2005). In the case of equivalency testing, incorrectly retaining a false H0 (Type II error: conclude equivalence) has more severe consequences than incorrectly rejecting a true H0 (Type I error: conclude

difference). Therefore the TOST approach was used as a statistical means to evaluate the equivalency between the two methods. TOST begins with an H0 that the two mean values are not equivalent. Next, TOST determines an upper and lower confidence interval (CI). Finally, TOST attempts to demonstrate that the mean values are equivalent within a practical, pre-set limit (designated as ± θ). Hence, TOST is conceptually opposite to the two-sample *t* test procedure. Unlike the two-sample *t* test, TOST appropriately penalises poor precision and/or small n values and places the burden on the analyst to prove that the datasets are equivalent (Limentani *et al.*, 2005).

Therefore TOST was used to evaluate the equivalence between the SOP and miniaturised method at each concentration level. For each standard, the difference between mean values (n = 10) along with the calculated 90 % CI was plotted (Figure 4-2). Margins were drawn at ± 5, ± 10, and ± 15 %, as per the precision cut-off CV-values. At low concentration levels the methods showed to be equivalent even within the ± 10 % margin for most of the standards (with lactic acid and taurine (not displayed) being the only exceptions). Similarly, at medium and high concentration levels the methods showed to be equivalent for all standards (except taurine) within the ± 5 % margin. When excluding taurine, the absolute percentage difference between mean values (Table 4-2) obtained from both methods was < 7 % at low levels, and < 5 % at medium and high levels. Table 4-2 also displays the p-values obtained from TOST when using the different preset equivalence margins for each concentration level. Thus acceptable equivalence between the methods was shown statistically ($p < 0.05$) at a 5 % significance level for all metabolites (except taurine) at each concentration level.

Table 4-2: Test of equivalence

Metabolites	SOP versus Mini						H0:difference
	Low θ = ± 15 %		Medium θ = ± 10 %		High θ = ± 5 %		
	|% D| between means	p-value	|% D| between means	p-value	|% D| between means	p-value	
Lactic acid	6.3	0.0010	2.9	< 0.0001	4.2	0.0190	Reject
Alanine	1.6	0.0001	1.9	< 0.0001	3.5	0.0012	Reject
3-Hydroxybutyric acid	0.5	0.0001	2.1	< 0.0001	3.4	< 0.0001	Reject
Choline	1.8	0.0001	2.1	< 0.0001	0.1	< 0.0001	Reject
Carnitine	3.6	< 0.0001	2.3	< 0.0001	3.4	< 0.0001	Reject
Taurine	21.4	0.7908	9.0	0.2527	4.5	0.2396	Accept
Glycine	0.1	< 0.0001	1.5	< 0.0001	2.6	< 0.0001	Reject
GAA	0.8	< 0.0001	0.7	< 0.0001	2.1	< 0.0001	Reject
AMP	1.9	0.0030	1.4	< 0.0001	4.1	0.0281	Reject

TOST (α = 0.05) approach to determine if the two methods are sufficiently equivalent in spiked synthetic urine (low, medium and high concentrations) at selected equivalence margins |% D| = absolute percentage difference between mean concentrations (n = 10) obtained with SOP and Mini method, θ = acceptable limit for equivalence

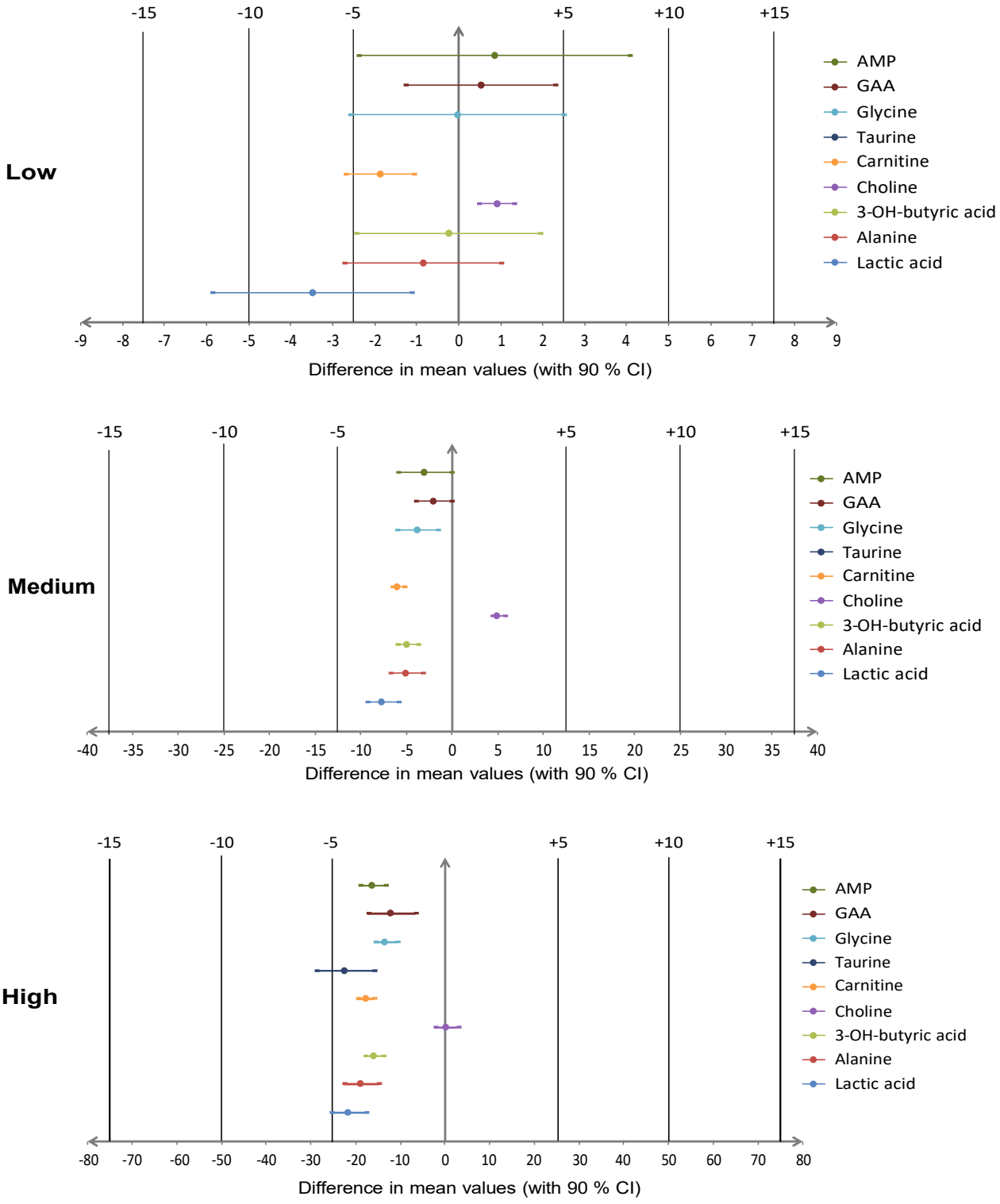


Figure 4-2: **Test of equivalence.** TOST (α = 0.05) comparing the two methods in spiked synthetic urine (at a low, medium, and high concentration).The graphs at each concentration level display the 90 % CI on the difference between the mean values (n = 10) obtained from the two methods for nine standards (from bottom to top: lactic acid, alanine, 3-hydroxybutyric acid, choline, carnitine, taurine, glycine, GAA, and adenosine 5′-monophosphate). Equivalence margins (±θ) for ± 5, ± 10 and ± 15 % difference between mean values are displayed. If |CI| < θ, reject H0 and conclude equivalence

4.3.2 Exploring the miniaturised ^{1}H-NMR method

After establishing the miniaturised ^{1}H-NMR method as an acceptable alternative for metabolomics studies using limited quantity samples, the miniaturised method's capabilities were further explored in a true biological matrix, namely, murine skeletal muscle extract.

4.3.2.1 Method comparability

In order to further confirm acceptable method equivalency, a pooled skeletal muscle extract was analysed using both the SOP and miniaturised ^{1}H-NMR methods in replicates of three. Nine clearly discernible targeted metabolites (same nine used for method equivalence testing in surine) were quantified from the ^{1}H-NMR spectra and used to further evaluate method equivalency. Firstly, the observed difference between the mean values obtained from each method were between 0.06 and 4.01 %. Secondly, comparing the precision of the two methods, as seen before, the SOP operated with higher precision than the miniaturised method in most cases [except for 3-HB (SOP: 8.32 % CV; Mini 4.82 % CV) and carnitine (SOP: 2.17 % CV; Mini 1.66 % CV)]. However, the CV-values for both methods were below 5 % (except for 3-HB in the SOP). Thus, the miniaturised protocol produced quantified data close to that of the current SOP, with acceptably equal precision.

4.3.2.2 Quantitative linearity

In order to validate whether the miniaturised ^{1}H-NMR protocol performed linearly with sample concentration, a muscle extract concentration range was analysed. Six different extract concentrations (1×, 2×, 4×, 6×, 8× and 10× concentrated) were prepared from a pooled muscle sample by transferring and drying [in N_2 (g) at 37 °C] various extract volumes (80, 160, 320, 480, 640 and 800 µL) in a glass vial and resuspending each in 80 µL of water. Five replicates of each concentration were analysed using the miniaturised protocol. A total of ten compounds, varying in composition and signal intensity, were identified from the NMR spectrum and their absolute concentrations determined. The linear relationship between instrument response and level of concentration for all nine metabolites (R^2 > 0.98) was clear: acetic acid (R^2 = 0.979); alanine (R^2 = 0.991); taurine (R^2 = 0.990); glycine (R^2 = 0.990); creatine (R^2 = 0.990); lactic acid (R^2 = 0.991); fumaric acid (R^2 = 0.991); AMP (R^2 = 0.989); carnitine (R^2 = 0.990); valine (R^2 = 0.986).

4.3.2.3 Metabolome coverage

In addition to analysing limited-quantity samples, another advantage of the miniaturised protocol is the possibility of concentrating samples to such an extent that essentially there is an increase in the analytical sensitivity, and consequently metabolome coverage. To illustrate this, ^{1}H-NMR

spectra of normal (1×) and concentrated (10×) muscle extracts were analysed and investigated in terms of metabolome coverage. Representative ^{1}H-NMR spectra, scaled relative to TSP, are given in Figure 4-3. The top spectrum represents a normal concentration extract (black spectrum), with windows A–F zoomed in 32×. The bottom spectrum shows the comparison between normal and 10× concentrated (blue spectrum) extracts, with windows A–F showing peaks that are either not clearly discernible or not detectable at all in the normal concentration. Qualitative inspection of Figure 4-3 shows that some of the identified metabolites not clearly discernible or detectable in the normal concentration are: 2-hydroxybutyric acid (0.90 t), 3-hydroxyisobutyric acid (1.07 d), proline (2.00 m), pyruvic acid (2.37 s), methylamine (2.61 s), aspartic acid (2.80 d, 2.83 d), NAD (6.04 d, 6.10 d, 8.18 s, 8.42 s), guanosine (5.92 d, 8.01 s), tyrosine (6.89 dd, 7.19 dd), nicotinamide (7.60 m, 8.72 dd, 8.94 d), hypoxanthine (8.19 s), and formic acid (8.46 s). Also present were at least 10 non-annotated peak assignments. Of interest, it was noted that some remaining methanol (3.36 s) from the extraction process, and ethanol (1.19 t, 3.64 q) from the cleaning of the instruments used during tissue sample collection and workup, were detected. These two alcohols were classified as exogenous.

4.3.2.4 Sample carry-over

An analytical question raised whilst examining the linearity of the miniaturised method was: Is there any potential carry-over from the same eVol® syringe being used during sample preparation? To test for carry-over, a clean water sample (blank) was drawn by the same eVol® syringe after the preparation of each muscle extract sample (concentrations: 1×, 2×, 4×, 6×, 8× and 10×). These blank samples were analysed as per experimental protocol and qualitatively there was no evidence of carry-over. Hence, the wash procedure (flushing the syringe with water three times) of the experimental method used was considered adequate

4.3.3 Pilot metabolomics application on limited-quantity samples

To further examine the applicability of the miniaturised ^{1}H-NMR protocol, we conducted a pilot metabolomics study using soleus muscle tissue (~ 4 mg) of wild-type (WT) and *Ndufs4*$^{-/-}$ mice. Metabolites were extracted as described earlier, with some adjustments. Owing to the limited sample quantity, the solvent ratio of 6:2:2 (methanol:water:chloroform) was multiplied by a factor of 10 for the soleus muscles. After drying, the tissue extracts were resuspended in water to obtain a final concentration of 0.05 mg tissue/µL. Although 0.1 mg tissue/µL is equal to that obtained from an unadjusted extraction (used earlier for quadriceps), this concentration could not be obtained for the soleus muscles due to the limited sample quantities. The samples were analysed using the miniaturised ^{1}H-NMR protocol and the data were investigated using an untargeted and targeted metabolomics approach.

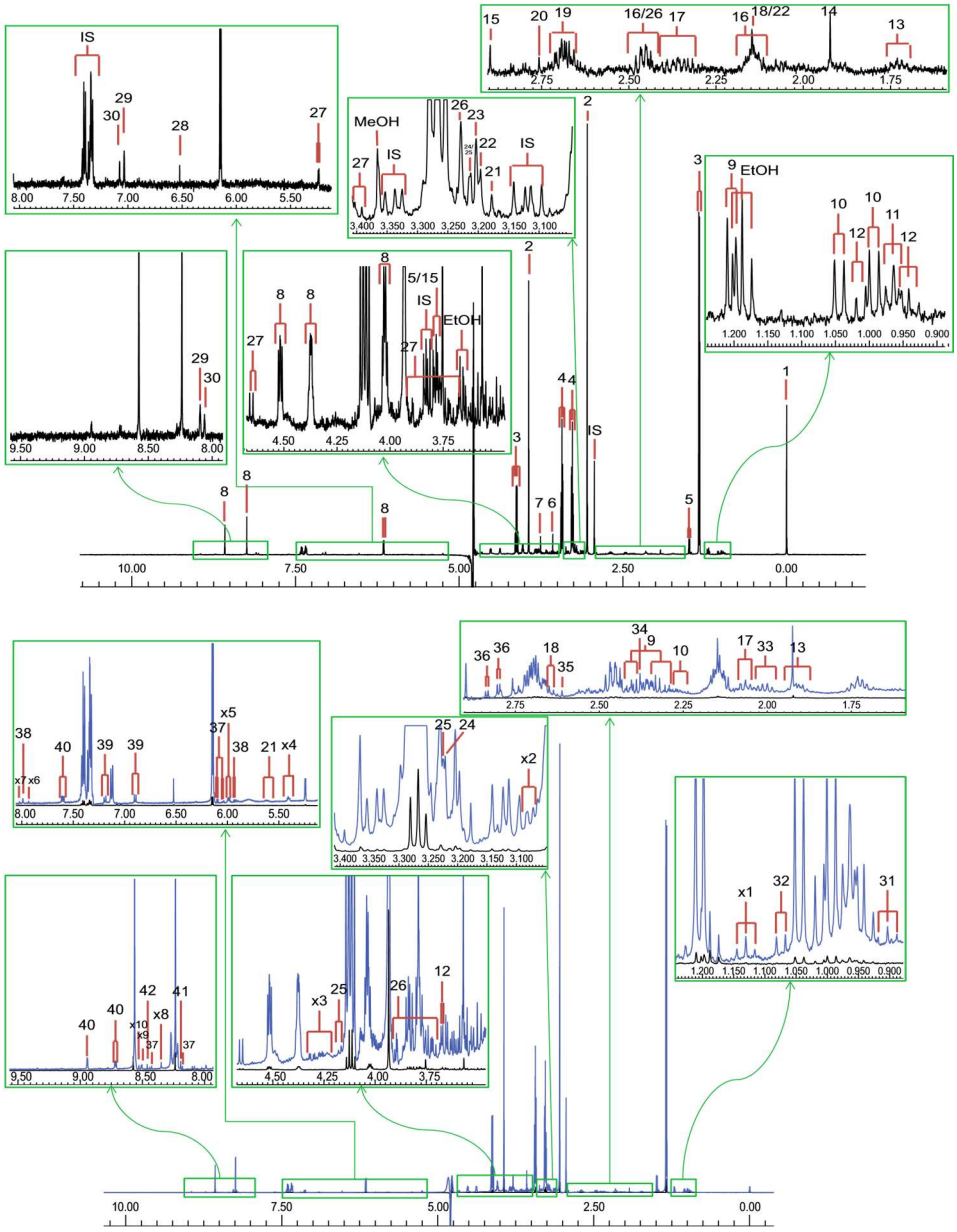


Figure 4-3: **Representative ^{1}H-NMR spectra from the miniaturised method on muscle tissue.** Scaled relative to TSP for (top) normal concentration (black spectrum), with windows A–F zoomed in 32×, and (bottom) 10× concentration (blue spectrum) compared to normal concentration, with windows A–F showing peaks that are either not clearly discernible or not detectable at all in normal concentration *[windows: A = 0.90–1.25 ppm, B = 1.60–2.82 ppm, C = 3.05–3.41 ppm, D = 3.55–4.65 ppm, E = 5.00–8.00 ppm, F = 8.00–9.50 ppm]. Peak assignments: 1 = TSP (0.00 s), 2 = creatine (3.04 s, 3.93 s), 3 = lactic acid (1.33 d, 4.12 q), 4 = taurine (3.26 t, 3.42 t), 5 = alanine (1.48 d, 3.78 q), 6 = glycine (3.57 s), 7 = guanidinoacetic acid (3.76 s), 8 = AMP (4.02 m, 4.37 m, 4.51 dd, 6.15 d, 8.23 s, 8.56 s), 9 = 3-hydroxybutyric acid (1.20 d, 2.36 AB), 10 = valine (0.99 d, 1.04 d), 11 = leucine (0.96 t), 12 = isoleucine (0.94 t, 1.01 d, 3.67 d), 13 = lysine (1.73 m, 1.91 m), 14 = acetic acid (1.92 s), 15 = trimethylamine (2.89 s), 16 = glutamine (2.14 m, 2.44 m, 3.77 t), 17 = glutamic acid (2.07 m, 2.36 m), 18 = methionine (2.14 s, 2.65 t), 19 = homocysteine (2.14 m, 2.69 m), 20 = sarcosine (2.75 s), 21 = dimethyl sulfone (3.17 s), 22 = acetylcarnitine (2.14 s, 3.19 s, 5.61 m), 23 = choline (3.20 s), 24 = acetylcholine (3.21 s), 25 = phosphocholine (3.21 s, 4.17 m), 26 = carnitine (3.22 s), 27 = glucose (3.40 m, 3.75 m, 4.63 d, 5.22 d), 28 = fumaric acid (6.52 s), 29 = histidine (7.03 s, 8.09 s), 30 = histamine (7.07 s, 8.06 s), 31 = 2-hydroxybutyric acid (0.90 t), 32 = 3-hydroxyisobutyric acid (1.07 d), 33 = proline (2.00 m), 34 = pyruvic acid (2.37 s), 35 = methylamine (2.61 s), 36 = aspartic acid (2.80 d, 2.83 d), 37 = NAD (6.04 d, 6.10 d, 8.18 s, 8.42 s), 38 = guanosine (5.92 d, 8.01 s), 39 = tyrosine (6.89 dd, 7.19 dd), 40 = nicotinamide (7.60 dd, 8.72 dd, 8.94 d), 41 = hypoxanthine (8.19 s), 42 = formic acid (8.46 s). IS = internal standard (N,N-dimethylphenylalanine (2.93 s, 3.12 dd, 3.34 dd, 7.37 m)), MeOH = methanol (3.36 s), EtOH = ethanol (1.19 t, 3.64 q), x1–x10 = unassigned].See Table 4-3 for additional chemical information on assigned peaks*

For the untargeted approach, each NMR spectrum was again quantified across 376 spectral bins of equal size — 0.02 ppm bins, excluding the water region 4.0–6.0 ppm. Statistical analyses (Student's *t* test) of the bins indicated that 14 bins differed significantly (VIPs) in the muscle samples. PCA score plots of the untargeted data (using only the VIPs) show a clear separation between the WT and KO groups (Figure 4-4 A).

For the targeted approach, ten clearly discernible metabolites were selected for quantification. Univariate statistical analysis (Student's *t* test) was used to identify variables that differed significantly ($p < 0.05$) between the WT and *Ndufs4*$^{-/-}$ groups. Five compounds differed significantly in the muscle samples: alanine, AMP, choline, fumaric acid and valine. The compounds detected as significant were used for PCA. Figure 4-4 B shows clear separation between the WT and *Ndufs4*$^{-/-}$ muscle samples. All of the metabolites identified as important have previously been linked to mitochondrial disease (Esterhuizen *et al.*, 2017). Understandably, one cannot draw definitive conclusions for a population from a sample size of only three. However, the preliminary findings of this pilot metabolomics study using the miniaturised ^{1}H-NMR protocol indicates information in line with the current knowledge of altered metabolism observed in mitochondrial disease.

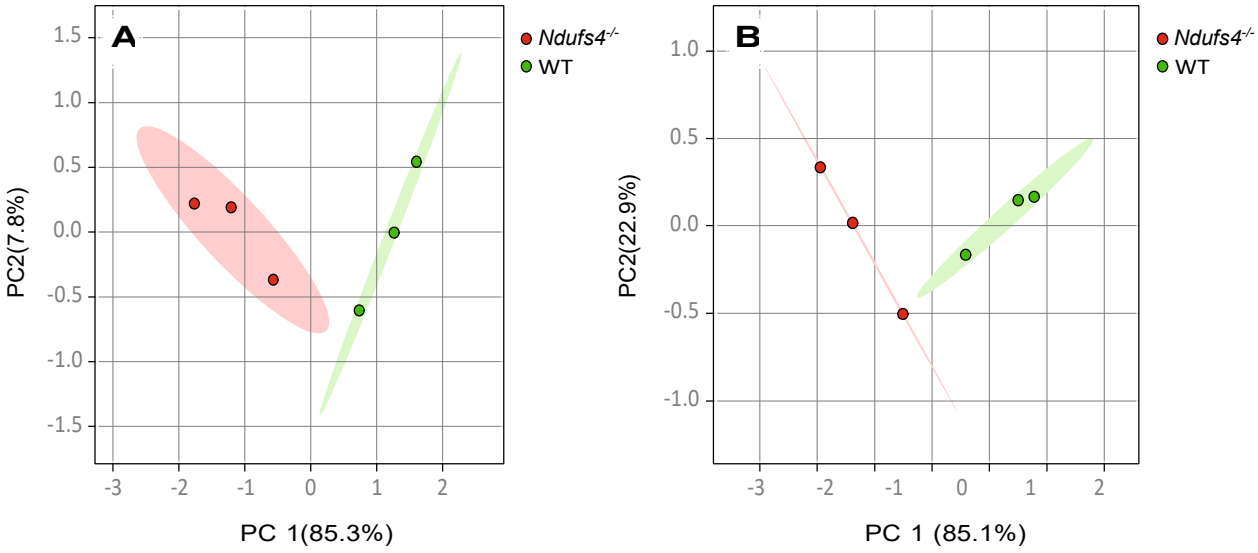


Figure 4-4: **Application of the miniaturised ^{1}H-NMR method in a pilot metabolomics study of *Ndufs4*$^{-/-}$ mice.** PCA score plots of extracts of soleus muscle from *Ndufs4*$^{-/-}$ and WT mice. **A:** Untargeted approach (using VIPs) for soleus muscles. **B:** Targeted approach (using VIPs) for soleus muscles. Ellipses indicate 90 % confidence.

4.4 Conclusion

We have presented a novel miniaturised ^{1}H-NMR protocol, which requires a sample volume of only 60 µL. This new method was compared with an established SOP, which requires a sample volume of at least 600 µL. Method equivalency was tested using spiked synthetic urine samples, as well as muscle tissue extracts from *Ndufs4*$^{-/-}$ mice. We demonstrated an acceptable equivalence between the two methods at a 95 % confidence level. Spectral data of equal quality from the two methods was obtained but with the new technique requiring only one-tenth of the sample of the other. We went further and analytically tested this miniaturised ^{1}H-NMR method by: (1) analysing samples up to 10× concentration, yielding qualitatively more identified metabolites (effectively addressing the sensitivity issues that attend NMR technology), with quantitative linearity ($R^2 > 0.98$), and (2) examining post-analysis blank samples to show no detectable carry-over from the miniaturised ^{1}H-NMR analytical method.

Finally, we applied the miniaturised method in a pilot metabolomics study using a very small tissue sample (as little as 4 mg), something that would not have been possible with an established SOP, which requires more sample, on a room temperature 5 mm NMR probe. In this pilot study, we were able to generate data that could separate the WT and knockout groups from *Ndufs4* mice, using both an untargeted and targeted approach. Furthermore, the metabolites detected as important with the targeted approach have all been linked to mitochondrial disease in previous studies, indicating important variables with biological relevance.

4.5 Supplementary information

Table 4-3: Chemical information and shifts for Figure 4.3 — representative ^{1}H-NMR spectra from the miniaturised method on muscle tissue.

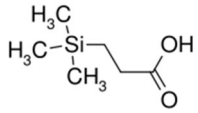
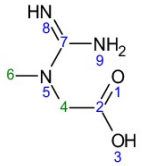
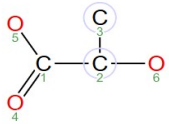
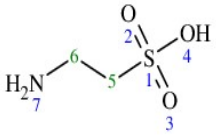
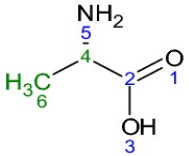
Peak assignment	Name	Chemical structure	HMDB ID	Chemical formula	δ (ppm), multiplicity (J coupling)	Chemical group	Atom(s)
1	TSP		N/A	$C_6H_{14}O_2Si$	0.00 s	$Si-(CH_3)_3$	
2	Creatine		HMDB0000064	$C_4H_9N_3O_2$	3.04 s	$N-CH_3$	6
					3.93 s	CH_2	4
3	Lactic acid		HMDB0000190	$C_3H_6O_3$	1.33 d (J = 6.9 Hz)	CH_3	3
					4.12 q (J = 6.9 Hz)	CH	2
4	Taurine		HMDB0000251	$C_2H_7NO_3S$	3.26 t (J = 6.5 Hz)	CH_2	5
					3.42 t (J = 6.7 Hz)	CH_2	6
5	Alanine		HMDB0000161	$C_3H_7NO_2$	1.48 d (J = 7.3 Hz)	CH_3	6
					3.78 q (ND)	CH	4

Table 4-3 (continued)

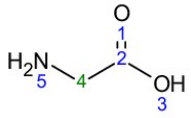
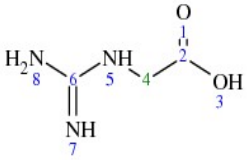
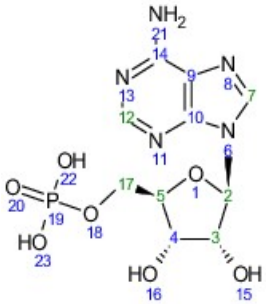
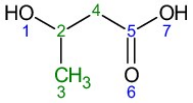
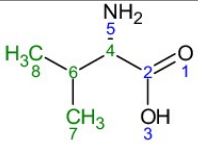
Peak assignment	Name	Chemical structure	HMDB ID	Chemical formula	δ (ppm), multiplicity (J coupling)	Chemical group	Atom(s)
6	Glycine		HMDB0000123	$C_2H_5NO_2$	3.57 s	CH_2	4
7	Guanidinoacetic acid		HMDB0000128	$C_3H_7N_3O_2$	3.76 s	CH_2	4
8	AMP (adenosine monophosphate)		HMDB0000045	$C_{10}H_{14}N_5O_7P$	4.02 m (ND)	CH_2	17
					4.37 m (ND)	CH	5
					4.51 dd (J = 5.1, 3.6 Hz)	CH	3
					6.15 d (J = 5.6 Hz)	CH	2
					8.23 s	CH	12
					8.56 s	CH	7
9	3-Hydroxybutyric acid		HMDB0000357	$C_4H_8O_3$	1.20 d (J = 6.6 Hz)	CH_3	3
					2.36 AB (ND)	CH_2	4
10	Valine		HMDB0000883	$C_5H_{11}NO_2$	0.99 d (J = 7.1 Hz)	CH_3	8
					1.04 d (J = 7.1 Hz)	CH_3	7

Table 4-3 (continued)

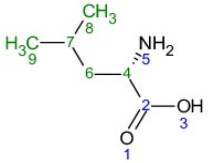
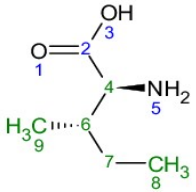
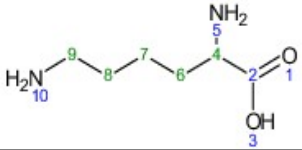
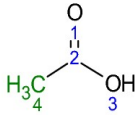
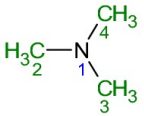
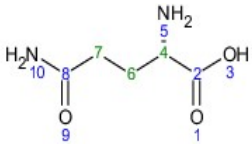
Peak assignment	Name	Chemical structure	HMDB ID	Chemical formula	δ (ppm), multiplicity (J coupling)	Chemical group	Atom(s)
11	Leucine		HMDB0000687	$C_6H_{13}NO_2$	0.96 t (J = 5.7 Hz)	$(CH_3)_2$	8, 9
12	Isoleucine		HMDB0000172	$C_6H_{13}NO_2$	0.94 t (ND)	CH_3	8
					1.01 d (J = 7.1 Hz)	CH_3	9
					3.67 d (ND)	CH	4
13	Lysine		HMDB0000182	$C_6H_{14}N_2O_2$	1.73 m (ND)	CH_2	8
					1.91 m (ND)	CH_2	6
14	Acetic acid		HMDB0000042	$C_2H_4O_2$	1.92 s	CH_3	4
15	Trimethylamine		HMDB0000906	C_3H_9N	2.89 s	$N-(CH_3)_3$	2, 3, 4
16	Glutamine		HMDB0000641	$C_5H_{10}N_2O_3$	2.14 m (ND)	CH_2	6
					2.44 m (ND)	CH_2	7
					3.77 t (ND)	CH	4

Table 4-3 (continued)

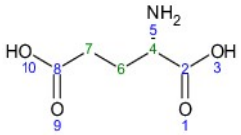
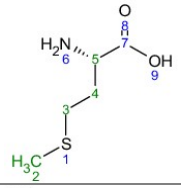
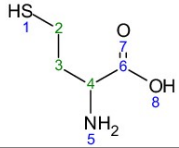
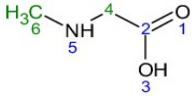
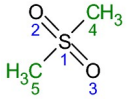
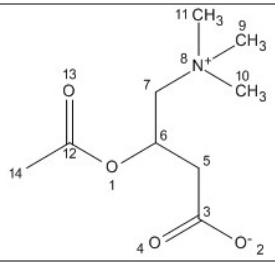
Peak assignment	Name	Chemical structure	HMDB ID	Chemical formula	δ (ppm), multiplicity (J coupling)	Chemical group	Atom(s)
17	Glutamic acid		HMDB0000148	$C_5H_9NO_4$	2.07 m (ND)	CH_2	6
					2.36 m (ND)	CH_2	7
18	Methionine		HMDB0000696	$C_5H_{11}NO_2S$	2.14 s	S-CH_3	2
					2.65 t (J = 6.5 Hz)	CH_2	3
19	Homocysteine		HMDB0000742	$C_4H_9NO_2S$	2.14 m (ND)	CH_2	3
					2.69 m (ND)	CH_2	2
20	Sarcosine		HMDB0000271	$C_3H_7NO_2$	2.75 s	N-CH_3	6
21	Dimethyl sulfone		HMDB0004983	$C_2H_6O_2S$	3.17 s	S-$(CH_3)_2$	4, 5
22	Acetyl-carnitine		HMDB0000201	$C_9H_{17}NO_4$	2.14 s	CH_3	14
					3.19 s	N-$(CH_3)_3$	9, 10, 11
					5.61 m (ND)	CH	6

Table 4-3 (continued)

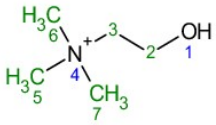
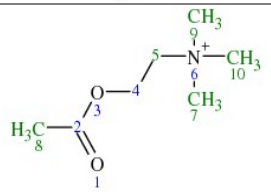
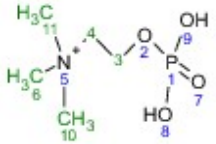
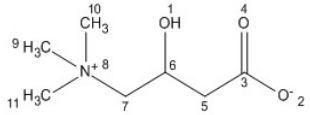
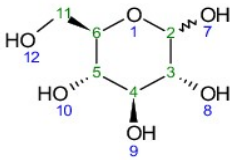
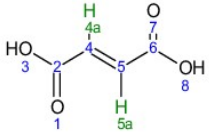
Peak assignment	Name	Chemical structure	HMDB ID	Chemical formula	δ (ppm), multiplicity (J coupling)	Chemical group	Atom(s)
23	Choline		HMDB0000097	$C_5H_{14}NO$	3.20 s	$N\text{-}(CH_3)_3$	5, 6, 7
24	Acetylcholine		HMDB0000895	$C_7H_{16}NO_2$	3.21 s	$N\text{-}(CH_3)_3$	7, 9, 10
25	Phosphocholine		HMDB0001565	$C_5H_{15}NO_4P$	3.21 s	$N\text{-}(CH_3)_3$	6, 10, 11
					4.17 m (ND)	CH_2	3
26	Carnitine		HMDB0000062	$C_7H_{15}NO_3$	3.22 s	$N\text{-}(CH_3)_3$	9, 10, 11
27	Glucose		HMDB0000122	$C_6H_{12}O_6$	3.40 m (ND)	CH	5
					3.75 m (ND)	CH, CH_2	6, 11
					4.63 d (J = 7.9 Hz)	CH	2
					5.22 d (J = 3.7 Hz)	CH	2
28	Fumaric acid		HMDB0000134	$C_4H_4O_4$	6.52 s	$(CH)_2$	4a, 5a

Table 4-3 (continued)

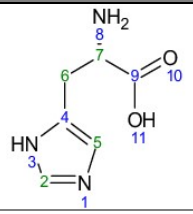
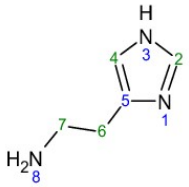
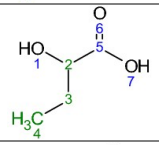
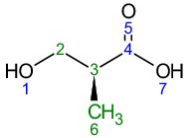
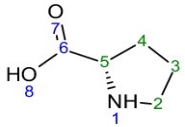
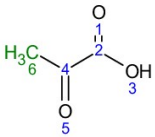
Peak assignment	Name	Chemical structure	HMDB ID	Chemical formula	δ (ppm), multiplicity (J coupling)	Chemical group	Atom(s)
29	Histidine		HMDB0000177	$C_6H_9N_3O_2$	7.03 s	CH	5
					8.09 s	CH	2
30	Histamine		HMDB0000870	$C_5H_9N_3$	7.07 s	CH	4
					8.06 s	CH	2
31	2-Hydroxybutyric acid		HMDB0000008	$C_4H_8O_3$	0.90 t (J = 7.5 Hz)	CH_3	4
32	3-Hydroxyisobutyric acid		HMDB0000023	$C_4H_8O_3$	1.07 d (J = 7.0 Hz)	CH_3	6
33	Proline		HMDB0000162	$C_5H_9NO_2$	2.00 m (ND)	CH, CH	3, 4
34	Pyruvic acid		HMDB0000243	$C_3H_4O_3$	2.37 s	CH_3	6

Table 4-3 (continued)

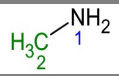
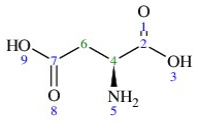
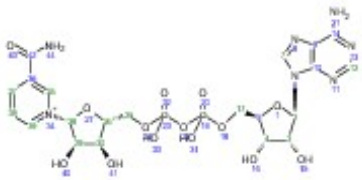
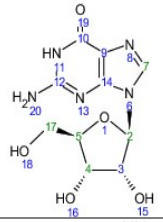
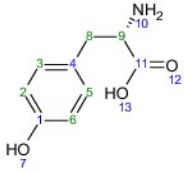
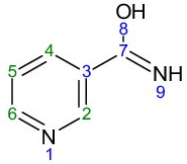
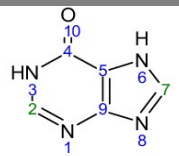
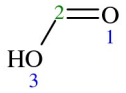
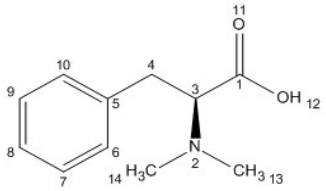
Peak assignment	Name	Chemical structure	HMDB ID	Chemical formula	δ (ppm), multiplicity (J coupling)	Chemical group	Atom(s)
35	Methylamine		HMDB0000164	CH_5N	2.61 s	CH_3	2
36	Aspartic acid		HMDB0000191	$C_4H_7NO_4$	2.80 d (J = 3.8 Hz)	CH_2	6
					2.83 d (J = 3.8 Hz)	CH_2	6
37	NAD (nicotinamide adenine dinucleotide)		HMDB0000902	$C_{21}H_{28}N_7O_{14}P_2$	6.04 d (J = 5.9 Hz)	CH	2
					6.10 d (J = 5.3 Hz)	CH	28
					8.18 s	CH	12
					8.42 s	CH	7
38	Guanosine		HMDB0000133	$C_{10}H_{13}N_5O_5$	5.92 d (ND)	CH	2
					8.01 s	CH	7
39	Tyrosine		HMDB0000158	$C_9H_{11}NO_3$	6.89 dd (J = 6.3 Hz)	CH, CH	2, 6
					7.19 dd (J = 6.5 Hz)	CH, CH	3, 5
40	Nicotinamide		HMDB0001406	$C_6H_6N_2O$	7.60 dd (J = 8.1, 4.9 Hz)	CH	5
					8.72 dd (J = 5.0, 3.8 Hz)	CH	6
					8.94 d (J = 1.9 Hz)	CH	2

Table 4-3 (continued)

Peak assignment	Name	Chemical structure	HMDB ID	Chemical formula	δ (ppm), multiplicity (J coupling)	Chemical group	Atom(s)
41	Hypoxanthine		HMDB0000157	$C_5H_4N_4O$	8.19 s	CH	2
42	Formic acid		HMDB0000142	CH_2O_2	8.46 s	CH	2
IS	*N,N*-DMPA (*N,N*-Dimethylphenylalanine)		N/A		2.93 s	N-$(CH_3)_2$	13, 14
					3.12 dd (J = 13.5, 9.0 Hz)	CH_2	4
					3.34 dd (J = 14.0, 6.0 Hz)	CH	3
					7.37 m (ND)	CH, CH, CH, CH, CH	6, 7, 8, 9, 10

Multiplicity: s − singlet; d − doublet; t – triplet; dd − double doublet; q – quartet; m – multiplet; AB – AB system. ND = not determined; N/A = not available

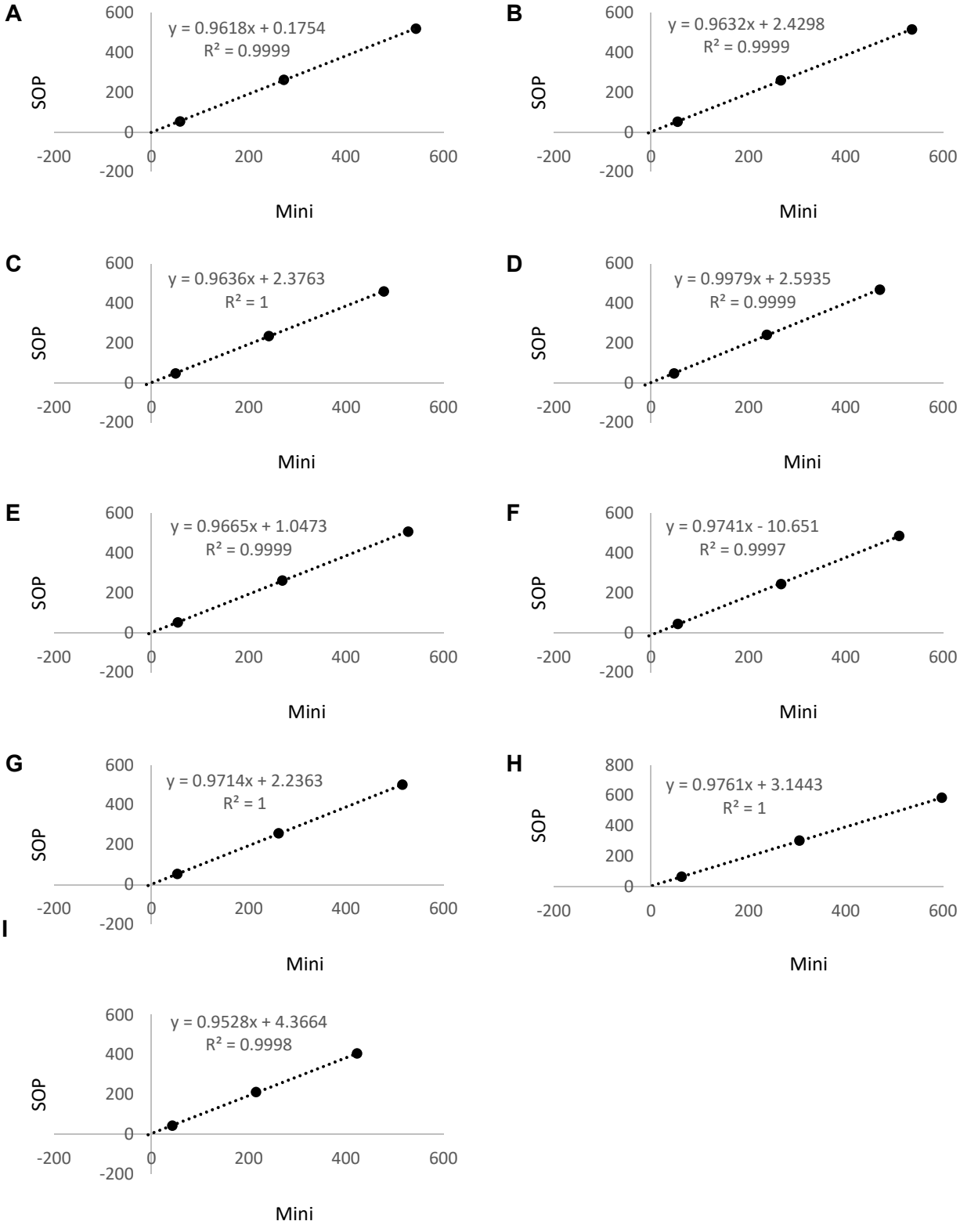


Figure 4-5: Linearity graphs for nine selected metabolites, all with R^2 values ≥0.99. A: lactic acid, **B:** alanine, **C:** 3-hydroxybutyric acid, **D:** choline, **E:** carnitine, **F:** taurine, **G:** glycine, **H:** GAA and **I:** AMP. *Abbreviations: Mini, miniaturised ^{1}H-NMR method; SOP, ^{1}H-NMR standard operating protocol.*

4.6 References

Beckonert, O., Keun, H.C., Ebbels, T.M.D., Bundy, J., Holmes, E., Lindon, J.C. & Nicholson, J.K. 2007. Metabolic profiling, metabolomic and metabonomic procedures for NMR spectroscopy of urine, plasma, serum and tissue extracts. *Nature Protocols*, 2(11):2692-2703.

Cassiède, M., Nair, S., Dueck, M., Mino, J., McKay, R., Mercier, P., Quémerais, B. & Lacy, P. 2017. Assessment of ^{1}H NMR-based metabolomics analysis for normalization of urinary metals against creatinine. *Clinica Chimica Acta*, 464:37-43.

Chambers, D., Kelly, G., Limentani, G., Lister, A., Lung, K.R. & Warner, E. 2005. Analytical method equivalency an acceptable analytical practice. *Pharmaceutical Technology*, 29:64-80.

Chan, C.C., Lee, Y.C., Lam, H. & Zhang, X.M. 2004. Analytical method validation and instrument performance verification. Hoboken, NJ: Wiley.

Dona, A.C., Jiménez, B., Schäfer, H., Humpfer, E., Spraul, M., Lewis, M.R., Pearce, J.T.M., Holmes, E., Lindon, J.C. & Nicholson, J.K. 2014. Precision high-throughput proton NMR Spectroscopy of human urine, serum, and plasma for large-scale metabolic phenotyping. *Analytical Chemistry*, 86(19):9887-9894.

Dunn, W.B., Wilson, I.D., Nicholls, A.W. & Broadhurst, D. 2012. The importance of experimental design and QC samples in largescale and MS-driven untargeted metabolomic studies of humans. *Bioanalysis*, 4(18):2249-2264.

Esterhuizen, K., van der Westhuizen, F.H. & Louw, R. 2017. Metabolomics of mitochondrial disease. *Mitochondrion*, 35:97-110.

FDA (Food and Drug Administration). 2001. Guidance for industry, bioanalytical method validation. https://www.fda.gov/downloads/Drugs/GuidanceComplianceRegulatoryInformation/Guidances/ucm070107.pdf, Date accessed: 12 Apr. 2017.

Figueira, J., Jonsson, P., Adolfsson, A.N., Adolfsson, R., Nyberg, L. & Öhman, A. 2016. NMR analysis of the human saliva metabolome distinguishes dementia patients from matched controls. *Molecular BioSystems*, 12(8):2562-2571.

Fratila, R.M. & Velders, A.H. 2011. Small-volume nuclear magnetic resonance spectroscopy. *Annual Review of Analytical Chemistry*, 4:227-249.

Glaves, J.P., Li, M.X., Mercier, P., Fahlman, R.P. & Sykes, B.D. 2014. High-throughput, multi-platform metabolomics on very small volumes: ^{1}H-NMR metabolite identification in an unadulterated tube-in-tube system. *Metabolomics*, 10(6):1145-1151.

Gullberg, J., Jonsson, P., Nordström, A., Sjöström, M. & Moritz, T. 2004. Design of experiments: an efficient strategy to identify factors influencing extraction and derivatization of *Arabidopsis thaliana* samples in metabolomic studies with gas chromatography/mass spectrometry. *Analytical Biochemistry*, 331(2):283-295.

Hohmann, M., Felbinger, C., Christoph, N., Wachter, H., Wiest, J. & Holzgrabe, U. 2014. Quantification of taurine in energy drinks using ^{1}H NMR. *Journal of Pharmaceutical and Biomedical Analysis*, 93:156-160.

Johansson, T., Jurva, U., Grönberg, G., Weidolf, L. & Masimirembwa, C. 2009. Novel metabolites of amodiaquine formed by CYP1A1 and CYP1B1: structure elucidation using electrochemistry, mass spectrometry, and NMR. *Drug Metabolism and Disposition*, 37(3):571-579.

Kayser, E.-B., Sedensky, M.M. & Morgan, P.G. 2016. Region-specific defects of respiratory capacities in the Ndufs4(KO) mouse brain. *Public Library of Science One*, 11(1):1-18.

Koves, T.R., Noland, R.C., Bates, A.L., Henes, S.T., Muoio, D.M. & Cortright, R.N. 2005. Subsarcolemmal and intermyofibrillar mitochondria play distinct roles in regulating skeletal muscle fatty acid metabolism. *American Journal of Physiology — Cell Physiology*, 288(5):C1074-C1082.

Li, H., Kumar Sharma, L., Li, Y., Hu, P., Idowu, A., Liu, D. Lu, J. & Bai, Y. 2013. Comparative bioenergetic study of neuronal and muscle mitochondria during aging. *Free Radical Biology and Medicine*, 63:30-40.

Limentani, G.B., Ringo, M.C., Ye, F., Bergquist, M.L. & McSorley, E.O. 2005. Beyond the t-test: statistical equivalence testing. *Analytical Chemistry*, 77(11):221A-226A.

Lindon, J.C., Holmes, E., Bollard, M.E., Stanley, E.G. & Nicholson, J.K. 2004. Metabonomics technologies and their applications in physiological monitoring, drug safety assessment and disease diagnosis. *Biomarkers*, 9(1):1-31.

Madji Hounoum, B., Mavel, S., Coque, E., Patin, F., Vourc'h, P., Marouillat, S., Nadal-Desbarats, L., Emond, P., Corcia, P., Andres, C.R., Raoul, C. & Blasco, H. 2017. Wildtype motoneurons, ALS-Linked SOD1 mutation and glutamate profoundly modify astrocyte metabolism and lactate shuttling. *Glia*, 65(4):592-605.

Martin, G.E. 2005. Small-volume and high-sensitivity NMR probes. *Annual Reports on NMR Spectroscopy*, 56:1-96.

Schmitt-Kopplin, P., Harir, M., Kanawati, B., Tziozis, D., Hertkorn, N. & Gabelica, Z. 2012a. Chemical footprint of the solvent soluble extraterrestrial organic matter occluded in Sołtmany ordinary chondrite. *Meteorites*, 2:79-92.

Schmitt-Kopplin, P., Liger-Belair, G., Koch, B.P., Flerus, R., Kattner, G., Harir, M., Kanawati, B., Lucio, M., Tziotis, D., Hertkorn, N. & Gebefügi, I. 2012b. Dissolved organic matter in sea spray: a transfer study from marine surface water to aerosols. *Biogeosciences*, 9(4):1571-1582.

Xia, J., Sinelnikov, I., Han, B. & Wishart, D.S. 2015. MetaboAnalyst 3.0 — making metabolomics more meaningful. *Nucleic Acids Research*, 43(W1):W251-W257.

CHAPTER 5

Metabolomics of *Ndufs4*$^{-/-}$ skeletal muscle: adaptive mechanisms converge at the ubiquinone-cycle

This chapter was published in

Terburgh, K., Lindeque, J.Z., Mason, S.W., van der Westhuizen, F.H. & Louw, R. 2019. Metabolomics of *Ndufs4*$^{-/-}$ skeletal muscle: adaptive mechanisms converge at the ubiquinone-cycle. *Biochimica et Biophysica Acta — Molecular Basis of Disease, 1865(1):98-106.*

5.1 Introduction

Mitochondria play a vital role in a myriad of processes involved in metabolism, cellular bioenergetics, and metabolic cell signalling (Greaves *et al.*, 2012; Shaughnessy *et al.*, 2014; Cherry & Piantadosi, 2015; Shokolenko & Alexeyev, 2015). The mitochondrial oxidative phosphorylation (OXPHOS) system, which comprises complexes I–IV and ATP synthase (CV), is the major contributor to cellular energy production and sustains most mitochondrial functions. The dysfunction of complex I (CI) (OMIM 252010) of the OXPHOS system, is the most common defect in mitochondrial energy metabolism, often resulting in progressive, severe multi-system deterioration. Due to the extreme complexity and heterogeneous nature (genetically and clinically) of human CI deficiency, the underlying pathogenic mechanisms thereof remain poorly understood (Distelmaier et al., 2009; Fassone & Rahman, 2012).

Current studies on mouse models of CI dysfunction, such as the whole-body *Ndufs4*$^{-/-}$ (knockout) mouse, attempt to better comprehend mitochondrial disease. The nuclear DNA-encoded NDUFS4 protein is essential to CI assembly, stability, and activity (Valsecchi *et al.*, 2010; Calvaruso *et al.*, 2012). *Ndufs4*$^{-/-}$ mice present with symptoms similar to human CI deficiency at around postnatal day (P) 35 and develop a progressive Leigh-like phenotype, including developmental delays, failure to thrive, lethargy, ophthalmoplegia, locomotor impairment, hearing loss, as well as progressive ataxia, and necrotising encephalomyopathy leading to early death (P50-60) (Kruse *et al.*, 2008; Johnson *et al.*, 2013; Jin *et al.*, 2014). Since the development of whole-body *Ndufs4*$^{-/-}$ mice, several conditional knockouts (neuronal, glial, cardiac, hematopoietic, and hepatic) have been developed in order to gain insight into tissue-specific consequences of CI dysfunction [reviewed by Torraco *et al.* (2015)]. However, due to the main interest in the predominant neurological phenotype of this disease model, limited information is available on skeletal muscle-specific consequences of the *Ndufs4* knockout.

A recent study by Foriel *et al.* (2018) highlighted the involvement of skeletal muscle in *Ndufs4* knockout pathology. The authors reported similarities between the phenotypes of skeletal muscle-specific and whole-body *Ndufs4* knockout *Drosophila*, such as reduced lifespan, feeding difficulties, locomotor impairment, and climbing defects. Given the important, often underappreciated, role of the muscular system in health and disease (Wolfe, 2006), as well as its integration and interdependence with the nervous system (Goody & Henry, 2018), it is imperative to elucidate the effects of a *Ndufs4* knockout on muscle metabolism. Skeletal muscle not only facilitates breathing and locomotion but also plays an essential role in various systemic, energy-demanding processes such as whole-body protein metabolism, glucose and fatty acid consumption, thermoregulation, immunity, as well as the maintenance of adequate bone strength and density (Wolfe, 2006; Schiaffino & Reggiani, 2011; Goody & Henry, 2018). As

Ndufs4$^{-/-}$ mice display weight loss (Kruse *et al.*, 2008), a significant decrease in body fat (Johnson *et al.*, 2013), decreases in body temperature (Kruse *et al.*, 2008), as well as systemic inflammation and osteoporosis (Jin *et al.*, 2014), it can be hypothesised that aberrant skeletal muscle metabolism might also play an important role in murine *Ndufs4*$^{-/-}$ phenotypes.

We aimed to gain insight into the consequences of a *Ndufs4*$^{-/-}$ on skeletal muscle bioenergetics and metabolism by combining biochemical strategies (respiratory chain enzyme assays) and multi-platform metabolic profiling (LC-MS/MS, GC-TOF-MS, and NMR analyses). Since the metabolic properties and subpopulations of muscle mitochondria depend on muscle fibre type composition (Schiaffino & Reggiani, 2011), both glycolytic (white quadriceps; primarily type IIB myofibres) and oxidative (soleus; primarily type I myofibres) muscles were investigated. To the best of our knowledge, this is the first report of fibre type-specific enzymatic and metabolic data in *Ndufs4*$^{-/-}$ skeletal muscles. We report a metabolic signature consisting of 48 compounds in white quadriceps and 34 compounds in soleus muscles that distinguish whole-body *Ndufs4* knockout mice from wild-types. These metabolic alterations provide insight into skeletal muscle-specific changes in metabolic pathways that result from whole-body mitochondrial dysfunction. These pathways could possibly be targeted in therapeutic interventions to promote muscle health in mitochondrial disorders and improve locomotion, metabolism, and quality of life.

5.2 Materials and methods

Detailed information regarding the described methods, can be found in the supplementary data (Section 5.5).

5.2.1 Animals and sampling

Male whole-body *Ndufs4* knockout mice (B6.129S4-*Ndufs4*$^{tm1.1Rpa}$/J; referred to as *Ndufs4*$^{-/-}$) along with age- and sex-matched controls (*Ndufs4*$^{+/+}$; referred to as WT) were used. *Ndufs4*$^{-/-}$ mice were born from heterozygous (*Ndufs4*$^{+/-}$) crosses obtained from Jackson Laboratory (ME, USA) (JAX stock #027058, https://www.jax.org/strain/027058). It should be noted that this mouse strain is BL6/J-derived and, therefore, potentially contains the *Nnt*$^{C57BL/6J}$ mutation. *Ndufs4* genotypes were confirmed by polymerase chain reaction (PCR) using tail snips. The animals were bred and housed at the specific pathogen-free (SPF) unit of the Vivarium (SAVC reg. no. FR15/13458) of the Pre-Clinical Drug Development Platform (PCDDP; NWU, RSA) and approval (NWU-00378-16-A5) for this study was obtained from the Animal Research Ethics Committee of the NWU. Animals were group housed under temperature- (22 ± 1°C), humidity- (55 ± 10 %) and light-controlled (12:12 hour light/dark cycle) conditions with standard laboratory chow (Laboratory animal food: Rodent Breeder, Cat. #RM1845, LabChef, Nutritionhub) and

water provided *ad libitum*. Mice were euthanised between postnatal day (P) 45-50 via cervical dislocation at the same time of day (8:00-9:00 AM) after overnight (12 hours) fasting. From both hind-limbs, white muscle portions of quadriceps femoris, as well as soleus muscles, were collected. Tissues were snap-frozen in liquid nitrogen (within 15 minutes *post-mortem*) and stored at − 80°C until used.

5.2.2 Enzyme assays

The enzyme activities of complex I (EC 1.6.5.3), complex II (EC 1.3.5.1), complex III (EC 1.10.2.2), and complex IV (EC 1.9.3.1) of the respiratory chain, as well as citrate synthase (EC 2.3.3.1), were measured in 700 ×g supernatants of white quadriceps and soleus muscle homogenates. Analyses were performed on *Ndufs4*$^{-/-}$ (n = 12) and WT (n = 10) samples via standard operating procedures based on existing methods (Shepherd & Garland, 1969; Rahman *et al.*, 1996; Janssen *et al.*, 2007).

5.2.3 Metabolic profiling

Metabolic profiles were obtained from the white quadriceps and soleus muscles of *Ndufs4*$^{-/-}$ (n = 19) and WT (n = 20) mice using a multi-platform metabolomics approach. The analytical techniques were performed as previously described and comprised of targeted liquid chromatography-tandem mass spectrometry (LC-MS/MS) (Mels *et al.*, 2011), untargeted gas chromatography time-of-flight mass spectrometry (GC-TOF-MS) (Lindeque *et al.*, 2013), and proton nuclear magnetic resonance (^{1}H-NMR) spectroscopy (Mason *et al.*, 2018). However, ^{1}H-NMR spectroscopy could not be performed on soleus muscles, due to limited sample quantity. The data obtained in this study (Terburgh *et al.*, 2018) can be accessed at the NIH Common Fund's Data Repository and Coordinating Center (supported by NIH grant, U01-DK097430) website, the Metabolomics Workbench, http://www.metabolomicsworkbench.org.

5.2.3.1 Extract preparation and derivatisation

Muscle tissues were finely minced and homogenised in the presence of internal standards using a vibration mill. Metabolite extraction was achieved using a modified monophasic Bligh–Dyer extraction method (Gullberg *et al.*, 2004) with a solvent ratio of 3:1:1 (methanol:water:chloroform). Details regarding the exact solvent volumes used for white quadriceps (~ 80 mg) and soleus (~ 5 mg) muscles can be found in the supplementary data (Section 5.5). The water used for extraction contained a mixture of internal standards consisting of *N, N*-dimethyl-L-phenylalanine and 3-phenylbutyric acid. Quality control (QC) samples were prepared from aliquots of all samples within a tissue type. Tissue extracts were divided into several vials (one for each analytical platform) and dried under nitrogen. Preparation per

platform, in short, was: reconstitution in water for ^{1}H-NMR; oximation and silylation for GC-TOF-MS; as well as the addition of stable isotopes and butylation for LC-MS/MS.

5.2.4 Data processing

All data processing were done using Excel 2013 (Microsoft) and MetaboAnalyst 3.0 (Xia *et al.*, 2015).

5.2.4.1 Enzyme assays

Enzyme activities were normalised to total protein (mg), reflecting tissue mass. Pretreatment of data involved generalised logarithm (glog) transformation.

5.2.4.2 Metabolic profiling

Spectral data obtained from the analytical platforms were extracted into matrices. Data matrices were individually inspected (correct peak picking and alignment, batch effect and data integrity) as well as preprocessed (data filtering, missing value imputation and normalisation). Metabolites were normalised to tissue mass. This was achieved through normalisation with either *N, N*-dimethyl-L-phenylalanine (LC-MS/MS and ^{1}H-NMR data) or 3-phenylbutyric acid (GC-TOF-MS data). In addition, metabolites measured with LC-MS/MS were further normalised to stable isotopes, which were added to samples before derivatisation. Each metabolite was either normalised to its own isotope (where possible) or to an isotope with a similar retention time to which the metabolite strongly correlated. No batch corrections were needed as the QCs showed no significant batch effects. Thereafter, data pretreatment (glog transformation and mean centering) and outlier detection [principal component analysis (PCA) and heatmaps] were done.

5.2.5 Statistical analyses

5.2.5.1 Enzyme assays

Differences between *Ndufs4*$^{-/-}$ and WT enzyme activities were regarded as statistically significant with a Student's *t* test p-value of < 0.05.

5.2.5.2 Metabolic profiling

Significantly discriminatory features between *Ndufs4*$^{-/-}$ and WT metabolic profiles were determined via univariate analyses. Statistically important differences (Student's *t* test p-values) were inspected at a 5 % and 10 % significance level, and false discovery rate-adjusted p-values were calculated. The cut-off threshold for practical significance (Ellis & Steyn, 2003) was set at an effect size D-value of ≥ 0.5. The important features were visually investigated regarding their clustering, covariance and discriminatory power via PCA performed as well as volcano plots.

PCA was performed in MetaboAnalyst 3.0 (Xia *et al.*, 2015) on a glog-transformed and autoscaled dataset — comprising only the important metabolites identified on each platform. Finally, metabolite identities were assigned to spectral features, with high confidence levels (Sumner *et al.*, 2007; Schymanski *et al.*, 2014). Dataset features were identified via spectral and retention time matching using commercial and in-house spectral libraries together with public databases.

5.3 Results and discussion

5.3.1 Respiratory chain enzyme activities in *Ndufs4*$^{-/-}$ muscles of different fibre type composition

The average (± SD) mitochondrial enzyme activities (respiratory chain complexes I-IV and citrate synthase) in *Ndufs4*$^{-/-}$ (n = 12) and WT (n = 10) white quadriceps and soleus muscles are summarised in Table 5-1. Enzyme activities were normalised to total protein (mg) content, rather than citrate synthase (CS) content, in order to focus on the relative enzyme capacity per tissue mass — thereby emphasising the relative mitochondrial content of the two muscle fibre types, which was relevant to our metabolic results. In addition, Alam and colleagues (Alam *et al.*, 2015) recently called into question whether CS activity could be considered a measure of mitochondrial volume in *Ndufs4*$^{-/-}$ mice. Through experimental and computational strategies, the authors reported significantly increased (72 %) CS activity in *Ndufs4*$^{-/-}$ muscles — suggested to reflect an increase in Krebs cycle enzyme levels rather than mitochondrial content. With regard to our data, no significant difference in CS activity was found in *Ndufs4*$^{-/-}$ white quadriceps muscles compared to WTs; whereas a moderate decrease (12 %, $p = 0.0149$) in CS activity was observed in *Ndufs4*$^{-/-}$ soleus muscles. Therefore, since a statistically significant difference was detected between WT and *Ndufs4*$^{-/-}$ soleus samples, normalisation to CS would more than likely skew enzymatic data and lead to a distorted picture of the results. The lower *Ndufs4*$^{-/-}$ soleus CS activity we report, is in stark contrast to the 72 % increase in CS activity previously reported for *Ndufs4*$^{-/-}$ (P35) hind-limb muscles (Alam *et al.*, 2015) — the difference could possibly be ascribed to the age difference between the mice studied or differences in the experimental procedures employed. However, several studies (Kruse *et al.*, 2008; Leong *et al.*, 2012; Valsecchi *et al.*, 2012; de Haas *et al.*, 2017) on other *Ndufs4*$^{-/-}$ tissues have reported no alterations in CS activity, similar to the results we report here. This discrepancy should thus be investigated further.

Our data revealed a severe reduction (80 %) in rotenone-sensitive CI activity ($p < 0.0001$) in both *Ndufs4*$^{-/-}$ white quadriceps and soleus muscles, compared to WTs. These results correspond with that reported for *Ndufs4*$^{-/-}$ skeletal muscle (Calvaruso *et al.*, 2012; Alam *et al.*,

2015). Although CI activity is reduced by the same factor in both muscles, glycolytic fibres have approximately 2-3 times fewer mitochondria than oxidative fibres (Schiaffino & Reggiani, 2011). Accordingly, with a *Ndufs4* knockout, our data demonstrate that glycolytic fibres display a much lower residual CI activity (4.58 ± 1.67 nmol/min/mg) than oxidative fibres (14.74 ± 6.67 nmol/min/mg). As evident from our metabolomics data (discussed in Section 5.3.4), this difference in residual CI activity reflects a biochemical threshold effect with the metabolic consequences of CI deficiency considerably more apparent in white quadriceps compared to soleus muscles. In agreement, model predictions by Alam *et al.* (2015) (on entire hind-limb *Ndufs4*$^{-/-}$ muscle) suggested that CI activity could be inhibited up to a critical value (90 % of normal levels) before major metabolic consequences become apparent.

Table 5-1: Mitochondrial respiratory chain enzyme activities in skeletal muscles from WT and *Ndufs4*$^{-/-}$ mice

Enzyme activity	White quadriceps			Soleus		
(nmol/min/mg)	WT	*Ndufs4*$^{-/-}$	*Ndufs4*$^{-/-}$ /WT	WT	*Ndufs4*$^{-/-}$	*Ndufs4*$^{-/-}$ /WT
CI	22.9 ± 5.9	4.58 ± 1.7 *	0.20	81.2 ± 15.1	14.7 ± 6.7 *	0.19
CII	29.9 ± 4.2	31.3 ± 5.0	1.05	63.1 ± 9.8	63.6±10.3	1.01
CIII	430.2 ± 57.1	455.6 ± 47.8	1.06	1430.1 ± 105.1	1170.7 ± 97.4 *	0.82
CIV	275.1 ± 32.4	273.8 ± 30.6	1.00	1033.1 ± 168.7	1077.0 ± 199.1	1.04
CS	233.4 ± 48.4	229.7 ± 50.6	0.98	636.7 ± 51.5	562.9 ± 75.3 *	0.88

Enzyme activities normalised to mg protein. Average values (± SD) were obtained from 12 *Ndufs4*$^{-/-}$ and 10 WT animals. Significant differences in *Ndufs4*$^{-/-}$ enzyme activity relative to WTs are indicated with an asterisk (* $p < 0.05$). *Abbreviations: CI, Complex I; CII, Complex II; CIII, Complex III; CIV, Complex IV; CS, Citrate synthase; WT, Wild-type (Ndufs4*$^{+/+}$*).*

We found no significant differences in CII–CIV activities in *Ndufs4*$^{-/-}$ white quadriceps compared to WTs. However, in *Ndufs4*$^{-/-}$ soleus muscles, CIII activity was moderately decreased (18 %, $p < 0.0001$). CIII has been shown to form a functional, albeit unstable, supercomplex with CI subassemblies in *Ndufs4*$^{-/-}$ muscle (Calvaruso *et al.*, 2012) and slight decreases in CIII activity have been reported in other tissues from *Ndufs4*$^{-/-}$ mice (Kruse *et al.*, 2008; de Haas *et al.*, 2017) as well as patients (Budde *et al.*, 2003; Valsecchi *et al.*, 2012). Literature reports on respiratory chain (RC) enzyme activities in *Ndufs4*$^{-/-}$ mice are quite diverse, with multiple studies (Kruse *et al.*, 2008; Calvaruso *et al.*, 2012; Valsecchi *et al.*, 2012; Alam *et al.*, 2015; de Haas *et al.*, 2017) reporting variations in CII-CIV activity. This variation can possibly be attributed to tissue-specific differences, variances in sample preparation resulting in different amounts of functional enzyme (especially in the case of CI and supercomplexes thereof, due to its instability), as well as differences in the age of the mice at which point they were studied.

5.3.2 Statistical significance and discriminative power of *Ndufs4*$^{-/-}$ metabolic profiles

At 95 % and 90 % significance, univariate statistical analyses revealed a respective 48 (Table 5-3) and 34 (Table 5-4) discriminatory metabolites between *Ndufs4*$^{-/-}$ and WT white quadriceps and soleus muscles. Volcano plots (Figure 5-1 A and B) depict the practical significance of all analytes detected by multi-platform metabolomics in white quadriceps and soleus muscles respectively. Significantly altered metabolites are indicated as decreased (green) or increased (red), while insignificant alterations are shown in grey. The five most decreased and increased metabolites are highlighted with ellipses and listed according to rank. As evident in the volcano plots, the majority of important metabolites were decreased in *Ndufs4*$^{-/-}$ muscles compared to WTs, with the white quadriceps (Figure 5-1 A) displaying a more pronounced metabolic profile. The highest relative fold change was attributed to decreased levels of *N, N*-dimethylglycine (DMG), creatinine, and 2-aminoadipate (2AA), while the most prominent increases in metabolite levels (common to both muscles) were seen in lysine (Lys) and its catabolic product — pipecolate (Pip), as well as *N*-acetylaspartate (NAA). Multivariate PCA (Figure 5-2) of significant metabolites revealed a partial separation in the clustering of *Ndufs4*$^{-/-}$ and WT groups in both muscles, indicating a distinct metabolic profile in *Ndufs4*$^{-/-}$ muscle.

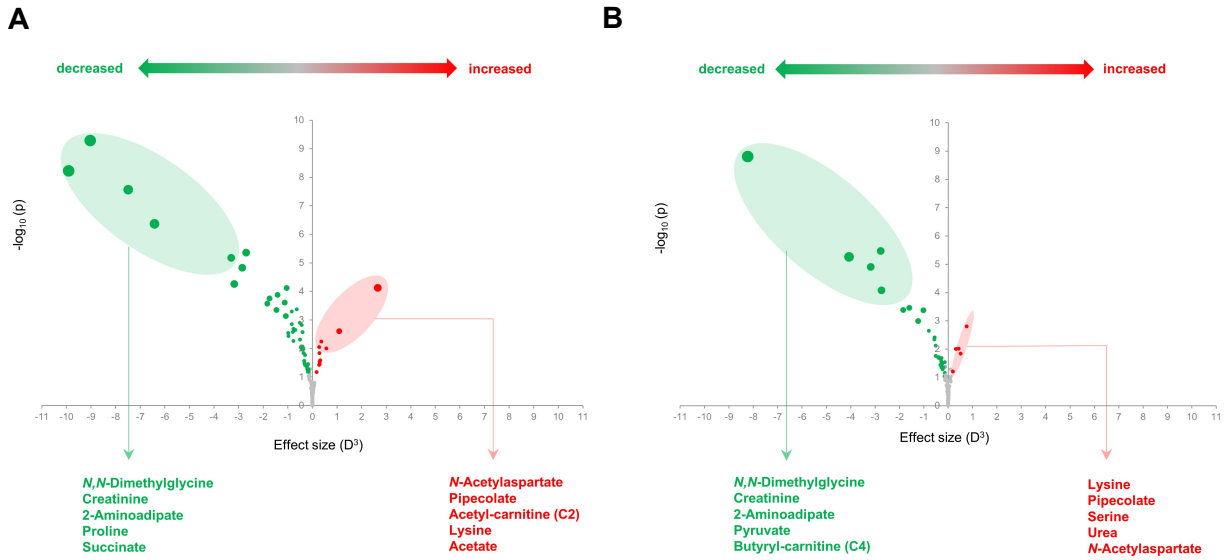


Figure 5-1: Univariate analyses indicating the practical significance of important skeletal muscle metabolites. Volcano plots depicting multi-platform metabolomics results of **A:** white quadriceps muscles and **B:** soleus muscles from *Ndufs4*$^{-/-}$ mice (n = 19) compared to WTs (n = 20). The x-axis specifies the effect size raised to the third power (D^3) and the y-axis specifies the negative logarithm to the base 10 of the *t* test p-values. Green and red symbols respectively indicate metabolites significantly lower or higher in *Ndufs4*$^{-/-}$ mice compared to WTs ($p < 0.1$ and $D \geq 0.5$). The five most significantly decreased and increased metabolites are highlighted and listed according to rank.

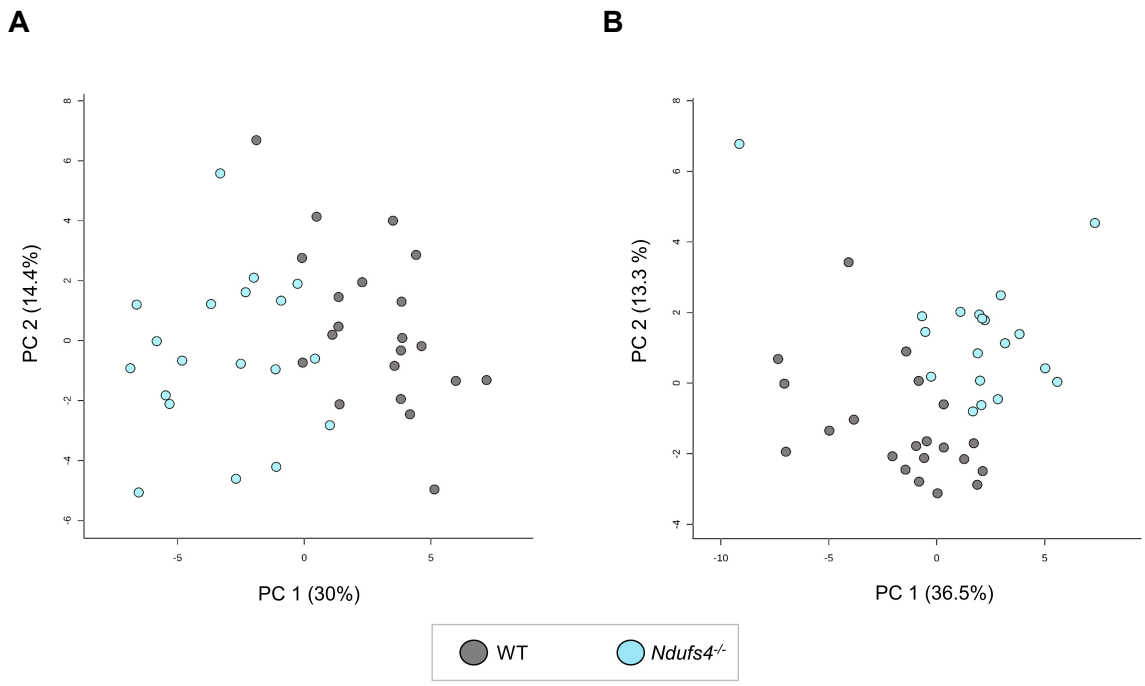


Figure 5-2: Multivariate analyses indicating the discriminative power of important skeletal muscle metabolites. Principal component analysis (PCA) scores plots depicting significant metabolites ($p < 0.1$, $D \geq 0.5$) identified in **A:** white quadriceps muscles and **B:** soleus muscles. Partial separation in the clustering of *Ndufs4*$^{-/-}$ (n = 19, blue) and WT groups (n = 20, grey) are visible in both cases. White quadriceps: PC1 and PC2 account for 30.0 % and 14.4 % of variation respectively. Soleus: PC1 and PC2 account for 36.5 % and 13.3 % of variation respectively.

5.3.3 Common metabolic alterations in *Ndufs4*$^{-/-}$ skeletal muscles of different fibre type composition

Numerous alterations in the levels of amino acids, acylcarnitines and organic acids were evident in *Ndufs4*$^{-/-}$ skeletal muscles. The Venn diagram in Figure 5-3 illustrates the number of similarities, as well as differences, observed between *Ndufs4*$^{-/-}$ metabolic profiles in the two muscles. Among the metabolites differing between genotypes, the majority (n = 26) were common to both white quadriceps and soleus muscles. Taken together, these adaptions revealed a similar bioenergetic flexibility in skeletal muscles of different fibre type composition. The most prominent changes in metabolite levels could be organised into several non-classical pathways involved in oxidative metabolism and redox regulation as depicted in Figure 5-4. These pathways seem to participate in an attempt to increase (and restore) the electron flux to the RC via the ubiquinone (Q) pool, fuelling CIII and allowing oxidative ATP production while bypassing CI in the process. A more in-depth discussion of the adaptive mechanisms involved in *Ndufs4*$^{-/-}$ skeletal muscle follows.

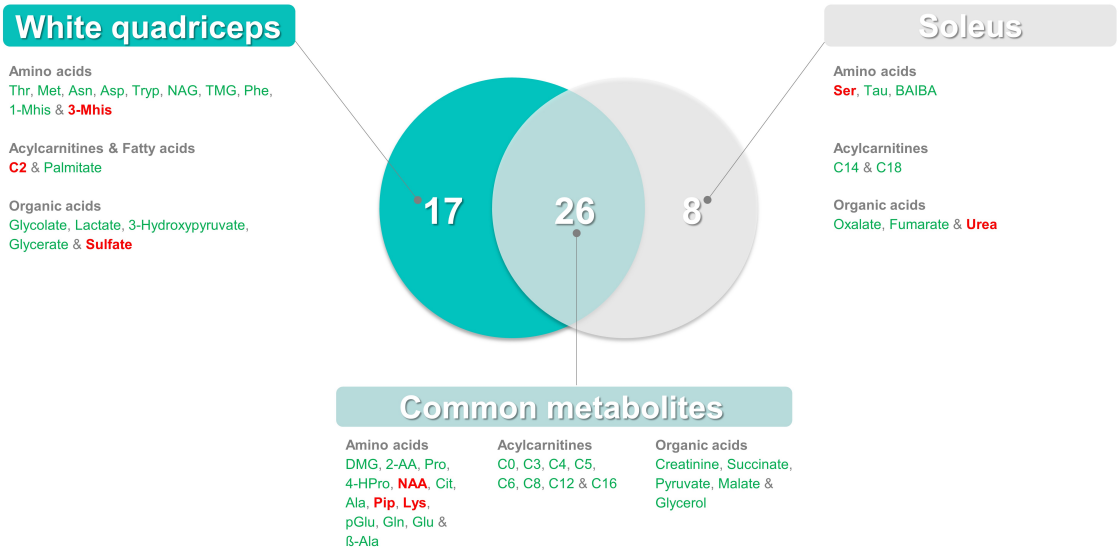


Figure 5-3: Venn diagram of important metabolites discriminating *Ndufs4*$^{-/-}$ and WT groups in skeletal muscles. Green and red respectively indicate metabolites significantly ($p < 0.1$ and $D \geq 0.5$) lower or higher in *Ndufs4*$^{-/-}$ mice (n = 19) compared to WTs (n = 20). Among the important metabolites identified, 26 were common to both muscles, while several alterations were unique to the white quadriceps (n = 17) and soleus (n = 8). Important metabolites (n = 5) identified in white quadriceps muscles by NMR spectroscopy were excluded from the comparison as soleus samples were not analysed on that analytical platform due to limited sample quantity. *Abbreviations: 1-Mhis, 1-Methylhistidine; 2-AA, 2-Aminoadipate; 2-Mhis, 2-Methylhistidine; Ala, Alanine; Asn, Asparagine; Asp, Aspartate; BAIBA, β-aminoisobutyrate; β-Ala, Beta-alanine; C0, Carnitine; C2, Acetyl-carnitine; C3, Propionyl-carnitine; C4, Butyryl-carnitine; C5, Isovaleryl-carnitine; C6, Hexanoyl-carnitine; C8, Octanoyl-carnitine; C12, Dodecanoyl-carnitine; C14, Myristoyl-carnitine; C16, Palmitoyl-carnitine; C18, Stearoyl-carnitine; Cit, Citrulline; DMG, N, N-Dimethylglycine; Gln; Glutamine; Glu, Glutamate; Hpro, Hydroxyproline; Lys, Lysine; Met, Methionine; NAA, N-Acetylaspartate; NAG, N-Acetylglutamate; pGlu, Pyroglutamate; Phe, Phenylalanine; Pip, Pipecolate; Pro, Proline; Ser, Serine; Tau, Taurine, Thr, Threonine; TMG, Trimethylglycine; Tryp, Tryptophan.*

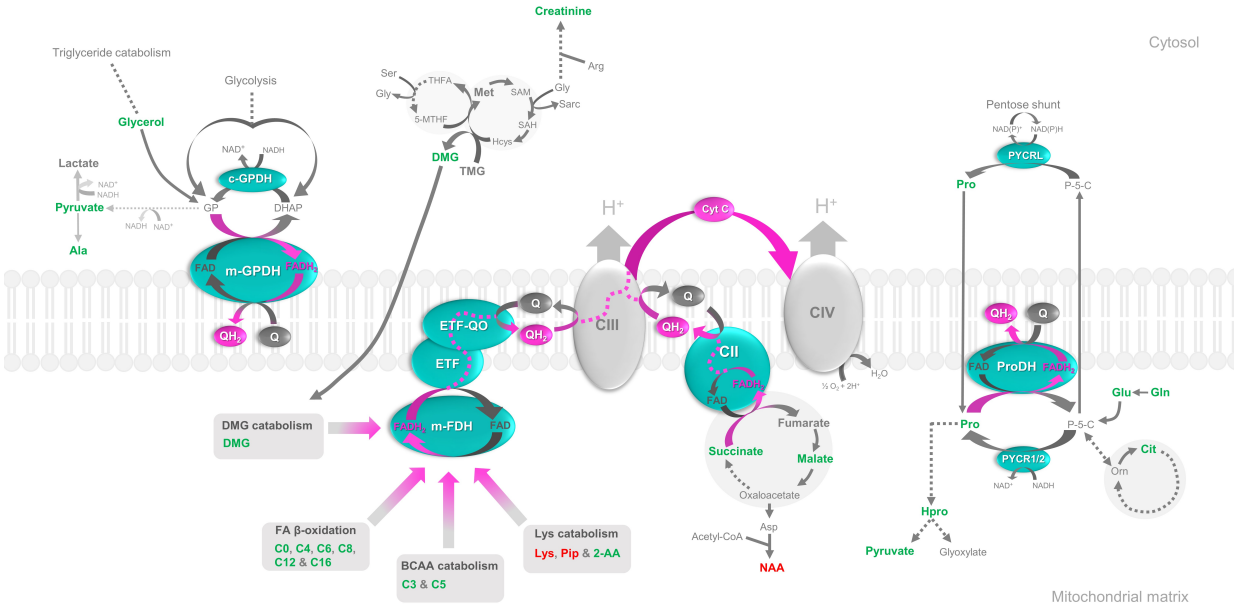


Figure 5-4: Common metabolic alterations in *Ndufs4*$^{-/-}$ skeletal muscles. *Ndufs4*$^{-/-}$ white quadriceps and soleus skeletal muscles both show a metabolic shift towards several non-classical pathways involved in oxidative metabolism and redox regulation, in an attempt to restore electron delivery to the respiratory chain via the ubiquinone (Q) pool. Green and red indicate metabolite levels significantly lower or higher,

respectively, in *Ndufs4*$^{-/-}$ mice (n = 19) compared to WTs (n = 20). Pink arrows indicate electron flow. Dashed lines reflect multi-step reactions not fully shown. Multi-platform metabolic profiling of *Ndufs4*$^{-/-}$ skeletal muscles indicates (from left to right): 1) a shift in glycolysis and triglyceride catabolism towards the glycerol-3-phosphate shuttle, which re-oxidises cytosolic NADH while serving as an electron donor to the respiratory chain via the mitochondrial enzyme glycerol-3-phosphate dehydrogenase (m-GPDH); 2) a shift in flux through several mitochondrial flavoprotein dehydrogenases (m-FDH) involved in one-carbon metabolism (dimethylglycine dehydrogenase), fatty acid β-oxidation (short-, medium- and long-chain acyl-CoA dehydrogenase) and amino acid catabolism (isobutyryl-, isovaleryl- and glutaryl-CoA dehydrogenase) which supply electrons to the respiratory chain via the electron transfer flavoprotein (ETF/ETF-QO) system; 3) a shift in flux through the Krebs cycle to increase electron delivery to the respiratory chain via complex II (CII; succinate dehydrogenase); and 4) increased mitochondrial cycling of proline and pyrroline-5-carboxylate (P-5-C) to directly provide electrons to the respiratory chain via proline dehydrogenase and sustain NAD^+ levels. *Abbreviations:* ***Enzymes in blue****: ETF, Electron transfer flavoprotein; ETF-QO, Electron transfer flavoprotein:ubiquinone oxidoreductase; m-FDH(s), Mitochondrial flavoprotein dehydrogenase(s); m-GPDH, Mitochondrial glycerol-3-phosphate dehydrogenase; c-GPDH, Cytosolic glycerol-3-phosphate dehydrogenase; CII, Complex II or succinate dehydrogenase; ProDH, Proline dehydrogenase; PYCR, Pyrroline-5-carboxylate reductase; Cyt c, Cytochrome c.* ***Electron carriers:*** *FAD, Oxidised flavin adenine dinucleotide; $FADH_2$, Reduced flavin adenine dinucleotide; NAD^+, Oxidised nicotine amide adenine dinucleotide; NADH, Reduced nicotine amide adenine dinucleotide; Q, Ubiquinone (oxidised coenzyme Q10); QH_2, Ubiquinol (reduced coenzyme Q10).* ***Metabolites:*** *2-AA, 2-Aminoadipate; 5-MTHF, 5-Methyltetrahydrofolate; Ala, Alanine; Arg, Arginine; Asp, Aspartate; C0, Carnitine; C12, Dodecanoyl-carnitine; C16, Palmitoyl-carnitine; C3, Propionyl-carnitine; C4, Butyryl-carnitine; C5, Isovaleryl-carnitine; C6, Hexanoyl-carnitine; C8, Octanoyl-carnitine; Cit, Citrulline; DHAP, Dihydroxyacetone phosphate; DMG, N, N-Dimethylglycine; GP, Glycerol-3-phosphate; Gln; Glutamine; Glu, Glutamate; Gly, Glycine; Hcys, Homocysteine; Hpro, Hydroxyproline; Lys, Lysine; Met, Methionine; NAA, N-Acetylaspartate; Orn, Ornithine; P-5-C, Pyrroline-5-carboxylate; Pip, Pipecolate; Pro, Proline; SAH, S-adenosylhomocysteine; SAM, S-adenosylmethionine; Sar, Sarcosine; Ser, Serine; THFA, Tetrahydrofolate.*

5.3.3.1 Glycolysis, triglyceride catabolism and the glycerol-3-phosphate (GP) shuttle

The accumulation of pyruvate and its derivatives, lactate and alanine, is considered a hallmark feature of mitochondrial metabolic dysfunction attributed to a disturbed redox balance (decreased NAD^+/NADH ratio) (Esterhuizen *et al.*, 2017). In agreement with this hallmark, Johnson *et al.* (2013) reported the accumulation of pyruvate, lactate, and glycolytic intermediates in *Ndufs4*$^{-/-}$ whole-brain (P30). However, in *Ndufs4*$^{-/-}$ skeletal muscles, we observed significantly decreased levels of pyruvate, glycerol, and alanine along with significantly (white quadriceps) and moderately (soleus) decreased lactate levels. A possible mechanistic explanation for these observations is the activity of the glycerol-3-phosphate (GP) shuttle. Like lactate dehydrogenase, the GP shuttle rapidly re-oxidises cytosolic NADH produced by glycolysis. However, an important difference between these redox regulatory mechanisms is the oxidative ATP producing capacity of the GP shuttle. Lying at the intersection of glycolysis, fatty acid metabolism and oxidative phosphorylation, the GP shuttle serves as an alternative electron donor to the RC at the ubiquinone (Q) pool by transferring reducing equivalents from the cytosol to mitochondria. In this shuttle, the cytosolic enzyme, glycerol-3-phosphate dehydrogenase (c-GPDH, EC 1.1.1.8), oxidises NADH to NAD^+ during the synthesis of GP from dihydroxyacetone phosphate (DHAP) — formed from either glycolysis or the phosphorylation of glycerol derived from triglyceride catabolism. GP can then be used as a substrate for the synthesis of either pyruvate, triglycerides, or phospholipids, however, in the case of the GP shuttle, GP is converted back to DHAP via the inner-membrane bound

mitochondrial form of GPDH (m-GPDH) which reduces FAD to $FADH_2$. $FADH_2$ then reduces ubiquinone (Q) to ubiquinol (QH_2). The resulting DHAP is then recycled to again oxidise cytosolic NADH. Although understanding of the structure, function, and regulation of this system is still limited (reviewed by McDonald *et al.* (2018)), several studies have suggested the important role of m-GPDH in thermogenesis and have shown it to be an important site of ROS production. Among the various metabolite shuttles responsible for the transfer of reducing equivalents from the cytosol to mitochondria, the GP shuttle is the most important in skeletal muscle (Schiaffino & Reggiani, 2011). Therefore, we postulate that the metabolic alterations we observed indicate the diversion of the glycolytic and triglyceride catabolic fluxes towards the GP shuttle in an attempt to not only restore the redox balance but also electron delivery to the RC at the Q pool. This mechanism could also possibly be involved in aberrant ROS production, a feature often reported in mitochondrial disease.

5.3.3.2 β-oxidation, amino acid catabolism and the electron transfer flavoprotein (ETF/ETF-QO) system

Both *Ndufs4*$^{-/-}$ skeletal muscle types displayed dramatic decreases in the levels of *N, N*-dimethylglycine (DMG), fatty acid acylcarnitines of even (C0, C4, C6, C8, C12 and C16) and odd (C3 and C5) chain length, as well as 2-aminoadipate (2-AA). Although previous metabolomics investigations on mitochondrial disease have reported disturbances in one-carbon metabolism, the catabolism of fatty acids, branched chain amino acids (BCAA), as well as the ketogenic amino acid, lysine, the underlying mechanisms remain unclear (Esterhuizen *et al.*, 2017). We postulate that these diverse metabolic alterations point to several pathways that converge at the electron transfer flavoprotein (ETF/ETF-QO*)* system. The ETF/ETF-QO system functions as an electron transfer pathway conducting electrons from eleven mitochondrial flavoprotein dehydrogenases (m-FDHs) to the Q pool of the RC. These m-FDHs include enzymes involved in mitochondrial one-carbon metabolism (dimethylglycine dehydrogenase, EC 1.5.99.2; and sarcosine dehydrogenase, EC 1.5.99.1), fatty acid β-oxidation (short-chain acyl-CoA dehydrogenase, EC 1.3.99.2; medium-chain acyl-CoA dehydrogenase, EC 1.3.99.3; and long-chain acyl-CoA dehydrogenase, EC 1.3.99.13), as well as branched-chain amino acid catabolism (isovaleryl-CoA dehydrogenase, EC 1.3.99.10; and isobutyryl-CoA dehydrogenase) and lysine catabolism (glutaryl-CoA dehydrogenase, EC 1.3.99.7) [reviewed by Watmough and Frerman (2010)]. Therefore we hypothesise that, in *Ndufs4*$^{-/-}$ skeletal muscle, there is an increased flux through these m-FDHs supplying the ETF/ETF-QO system with electrons in order to compensate for decreased electron transfer from CI. This increased flux, in part, could lead to the observed decreased metabolite levels. However, this switch in flux cannot effectively compensate for the CI defect as all of these $FADH_2$ producing pathways also require NAD^+ as a

co-factor. NADH levels could build up due to CI inactivity as well as these compensatory reactions themselves. The hypothesised result of the altered redox state and shortage of NAD^+ is seen in the lysine catabolic pathway. Lysine is normally catabolised to 2-AA via the saccharopine pathway, which requires $NADP^+$ and two NAD^+ molecules. The subsequent conversion of 2-AA to glutaryl-CoA (substrate for ETF/ETF-QO system) requires an additional NAD^+ molecule. In addition to decreased 2-AA levels, we observed the accumulation of lysine and its alternative catabolite, pipecolate (Pip), in *Ndufs4*$^{-/-}$ skeletal muscles — indicating that an alternative non-NAD^+-consuming catabolic route is preferred, resulting in an even larger reduction in 2-AA levels. Altogether, the data suggest that β-oxidation and amino acid catabolism might fuel the Q-cycle via the ETF/ETF-QO system, even though a disturbed redox balance might limit the efficacy of some of the reactions.

When comparing previous metabolomics studies on *Ndufs4* knockout mice with our current observations, similar ambiguous effects on lipid metabolism are noticeable. In *Ndufs4*$^{-/-}$ liver, markedly reduced levels of fat droplets and free fatty acids were reported (Johnson *et al.*, 2013); while significantly increased blood hydroxy-acylcarnitine (C4:0, C16:0, and C18:1) levels were reported in a comparable *Ndufs4* knockout mouse model (*Ndufs4*$^{fky/fky}$) (Leong *et al.*, 2012). The latter observation was postulated to reflect a blockage in the NAD^+-dependent (third) step of β-oxidation. However, upon further investigation, *Ndufs4*$^{fky/fky}$ liver and heart revealed no alterations in carnitine species, while skeletal muscle displayed no detectable lipid accumulation via Oil Red O staining (Leong *et al.*, 2012). These observations could fit into our combined hypotheses of decreased lipogenesis and increased lipolysis due to the activity of the GP shuttle, as well as increased fatty acid β-oxidation, albeit inefficient due to a redox imbalance.

5.3.3.3 One-carbon metabolism, the methylation cycle and the transsulfuration pathway

The altered redox state as well as the postulated use of DMG by the ETF/ETF-QO system, seem to contribute to the disruption of one-carbon metabolism, the methylation cycle and the transsulfuration pathway. These disturbances were more prominent in white quadriceps muscles, which along with decreased levels of DMG, displayed significantly decreased levels of trimethylglycine (betaine), methionine, threonine, and the accumulation of choline. Trimethylglycine (TMG) originates from the NAD^+ dependent catabolism of choline, which takes place in mitochondria. DMG is then produced from TMG in a folate-independent cytosolic reaction during which homocysteine is re-methylated to methionine. NAD^+ shortage could, therefore, cause choline build up and a further reduction in DMG levels. As DMG also has the ability to yield one carbon units via folate-dependent mitochondrial reactions involving dimethylglycine dehydrogenase (which produces sarcosine) and sarcosine dehydrogenase

(which produces glycine) this metabolite links one-carbon metabolism to the ETF/ETF-QO system.

Furthermore, in both *Ndufs4*$^{-/-}$ skeletal muscle types, dramatic decreases were seen in creatinine levels along with slightly (not significantly) reduced creatine levels. Creatine biosynthesis takes place chiefly in the liver and kidneys, however, a small amount of skeletal muscle creatine stores have been shown to be produced in the muscles themselves (Russell *et al.*, 2014). Creatine biosynthesis is a two-step reaction involving the conversion of arginine and glycine to guanidinoacetate, which is then methylated via SAM to form creatine and SAH. A disturbance in one-carbon metabolism could lead to lowered SAM available for methylation reactions, therefore dramatic decreases in creatinine could reflect the disrupted methylation of guanidinoacetate to creatine. In agreement, significantly reduced levels of 1-methylhistidine (1-Mhis) and increased levels of histamine in *Ndufs4*$^{-/-}$ white quadriceps could also reflect disturbed methylation reactions. On the whole, the observed metabolic alterations indicate disturbances in one-carbon metabolism and methylation reactions, possibly due to a disturbed redox balance and derangements in DMG metabolism.

5.3.3.4 The Krebs cycle and mitochondrial complex II (succinate dehydrogenase)

We observed significantly decreased levels of succinate and malate in both muscles along with significant (soleus) and moderate (white quadriceps) reductions in fumarate levels. A similar observation was made in *Ndufs4*$^{-/-}$ (P35) hind-limb skeletal muscle by Alam *et al.* (2015), who reported decreased succinate levels along with an increase in flux (10-11 %) through reactions providing substrates to CII and a slight decrease in the other (generally NAD^+ consuming) reactions which mainly fuel CI. The reduction in metabolite levels we observed could, therefore, reflect an increased use of succinate to fuel CII and the respiratory chain via the Q pool together with a decreased re-supply thereof due to a congested Krebs cycle. In addition, we observed increased levels of *N*-acetylasparte (NAA) which is hypothesised to be an alternative storage and transport form of acetate and has been suggested to play a role in lipid metabolism and post-translational protein modification (Bogner-Strauss, 2017). Although the physiological functions of NAA are still poorly understood, it was recently discovered that NAA metabolism is not exclusive to the brain as previously thought. Aberrant NAA metabolism has been reported in mitochondrial disease, however, to the best of our knowledge, this is the first report thereof in skeletal muscle. NAA is synthesised from aspartate and acetyl-CoA by aspartate *N*-acetyltransferase (Asp-NAT, EC 2.3.1.17). In skeletal muscle, the expression of *Nat8l* mRNA (encoding Asp-NAT) has been observed, although levels were reported to be negligible (Bogner-Strauss, 2017). We, therefore, hypothesise that the rate of acetyl-CoA synthesis from sources like β-oxidation and lysine catabolism (which fuel the ETF/ETF-QO system) exceeds

the rate at which the Krebs cycle can utilise the molecule, therefore acetyl-CoA accumulates and is converted to NAA.

5.3.3.5 Proline metabolism and the proline cycle

Although there is still much to be learned about the precise mechanism and functions of the proline cycle, the vital role of this relatively novel pathway in health and disease is becoming increasingly clear [reviewed by Phang (2017)]. Some of the most striking metabolic alterations we observed in *Ndufs4*$^{-/-}$ skeletal muscles included the reduction of proline, hydroxyproline (Hpro), citrulline, glutamate, and glutamine levels. These alterations could reflect aberrant proline metabolism, which is strongly associated with the pentose phosphate pathway, urea cycle, and Krebs cycle. The mitochondrial flavin-dependent enzyme, proline dehydrogenase (ProDH, EC 1.5.99.8), together with the cytosolic (PYCRL) and mitochondrial (PYCR1/2) isoforms of pyrroline-5-carboxylate reductase (EC 1.5.1.2) are responsible for the interconversions of proline and pyrroline-5-carboxylate (P-5-C) constituting the proline cycle. Proline can directly act as an alternative source of electron delivery to the RC Q pool, through its catabolism to P-5-C via ProDH. P-5-C can also be synthesised from either glutamate or ornithine while its conversion back to proline regenerates $NAD(P)^+$. We, therefore, postulate that the adaptive increased cycling of proline and P-5-C might serve to sustain QH_2 and $NAD(P)^+$ levels. In addition to energy production and redox homeostasis, proline metabolism has been shown to be involved in ROS production, the initiation of apoptosis, autophagy, as well as protein and nucleotide synthesis while proline's post-translational product, hydroxyproline, has recently been recognised as a substrate for the synthesis of pyruvate, glucose and glycine [reviewed by Wu *et al.* (2011)]. Taken together, proline metabolism might play a central role in several metabolic pathway derangements often reported in mitochondrial disease.

5.3.4 Fibre type-specific metabolic alterations in *Ndusf4*$^{-/-}$ skeletal muscles

When looking at the difference between the important metabolites identified in *Ndufs4*$^{-/-}$ muscles (Figure 5-3), seventeen metabolites were uniquely altered in the white quadriceps while eight alterations were unique to the soleus. This comparison excludes the five important metabolites detected with NMR spectroscopy as soleus samples were not analysed on that analytical platform due to limited sample quantity. Altogether, glycolytic fibres (white quadriceps) seemed to show more pronounced metabolic disturbances in response to CI deficiency with NAA accumulation being more than two-fold higher than in soleus muscles, along with an additional accumulation of acetyl-CoA derivatives, acetate and acetyl-carnitine (C2). In addition, *Ndufs4*$^{-/-}$ white quadriceps muscles showed significant 3-methylhistidine accumulation, which is indicative of myofibrillar protein breakdown (Qureshi *et al.*, 1986). This observation agrees with literature

reports of glycolytic fibres showing more pronounced atrophy than oxidative fibres in pathological conditions affecting muscle protein balance, and ageing (Schiaffino & Reggiani, 2011). Taken together with the greater disturbance in methylation reactions we observed in white quadriceps muscles (discussed in Section 5.3.3.3), these alterations could indicate more profound disruptions of the redox balance (NAD^+/NADH ratio), Krebs cycle congestion and possible acetyl-CoA accumulation in more glycolytic muscle fibres. In addition to less dramatic metabolic alterations than in the white quadriceps, we saw significantly increased levels of serine along with decreased levels of taurine and pyroglutamate in *Ndufs4*$^{-/-}$ soleus muscles. These alterations could indicate a shift in glycolysis towards serine production, which could be used for glutathione synthesis — a phenomenon often described in mitochondrial disease due to increased electron leak and ROS production. As oxidative fibres have been shown to have a greater supply of substrates, oxygen and more mitochondria (with greater oxidative capacity) (Schiaffino & Reggiani, 2011), it can be postulated that mitochondrial ROS levels — due to the CI deficiency — are higher in *Ndufs4*$^{-/-}$ soleus muscles and therefore the need for glutathione ROS scavenging is greater. Furthermore, our results suggest that BCAA catabolism might be more dramatically affected in soleus muscles as we observed moderately (but not significantly) increased levels of valine and leucine, significant decreases in β-aminoisobutyrate (BAIBA) levels, and much greater decreases in C5 and C3 carnitine levels than in the white quadriceps muscles. Hence, the data could point to a more effectively functioning Krebs cycle and a better metabolic adaption of soleus muscles to the CI defect.

5.4 Conclusions

We report the first fibre type-specific enzymatic and metabolic data in *Ndufs4*$^{-/-}$ skeletal muscles. Enzyme assays revealed a severe reduction (80 %) in CI activity in both glycolytic (white quadriceps) and oxidative (soleus) muscles from whole-body *Ndufs4*$^{-/-}$ mice. Such an extreme reduction in CI activity would greatly reduce the electron flux to the rest of the respiratory chain (RC). As an adaptive response in both tissues, our metabolic data suggest that alternative fuels and non-classical pathways serve to sustain the RC ubiquinol (QH_2) pool, thereby restoring electron flux to CIII through the ubiquinone (Q) cycle. However, despite these metabolic adaptions in skeletal muscle, a disturbed redox balance still seems to result in congested mitochondrial pathways. Metabolic and bioenergetic disturbances due to CI deficiency seem to be more evident in glycolytic fibres, possibly due to their innately lower mitochondrial content. Some of the most significant metabolic alterations we observed in *Ndufs4*$^{-/-}$ muscles implicate the involvement of the glycerol-3-phosphate (GP) shuttle, the electron transfer flavoprotein (ETF/ETF-QO) system, complex II of the RC, and the proline cycle in electron delivery to the Q pool. Some of these mechanisms might also serve to restore NAD^+ levels (GP shuttle and

proline cycle), while others could contribute to redox imbalance (NAD^+ consuming reactions fuelling ETF/ETF-QO and the Krebs cycle) in CI deficiency. Altogether, the observed adaptive mechanisms could explain the apparent lack of an obvious muscle phenotype in *Ndufs4*$^{-/-}$ mice, as well as the reported ability of skeletal muscle to maintain normal ATP production, despite CI deficiency (Kruse *et al.*, 2008; Alam *et al.*, 2015). (Kruse *et al.*, 2008; Alam *et al.*, 2015). However, the hypotheses generated in this study need to be followed up/validated in more targeted metabolic studies on *Ndufs4*$^{-/-}$ mice. For now, it remains unclear whether these adaptive responses are capable of sustaining energy homeostasis when challenged with exercise or nutrient deprivation. A comparison of these and related metabolic pathways in other tissues (e.g. the brain) could possibly provide answers to tissue-specific phenotypes and novel insight in targeted therapeutic interventions.

5.5 Supplementary information

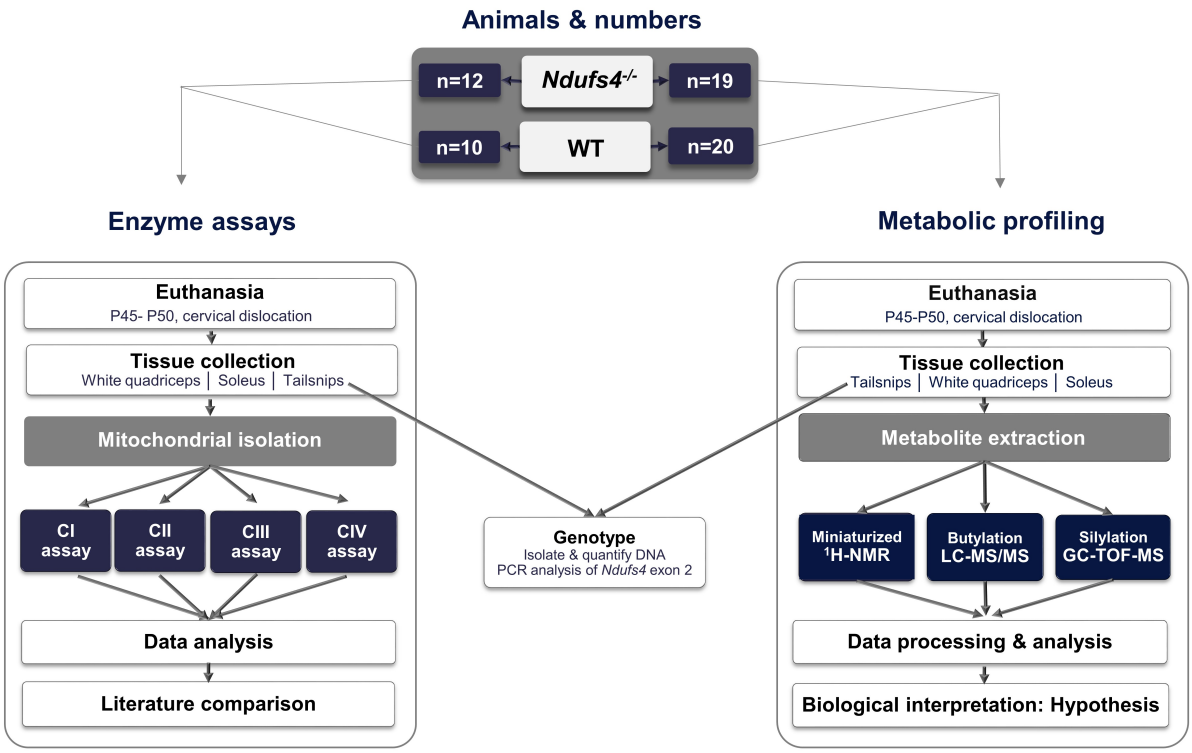


Figure 5-5: Experimental workflow

5.5.1 Enzyme assays

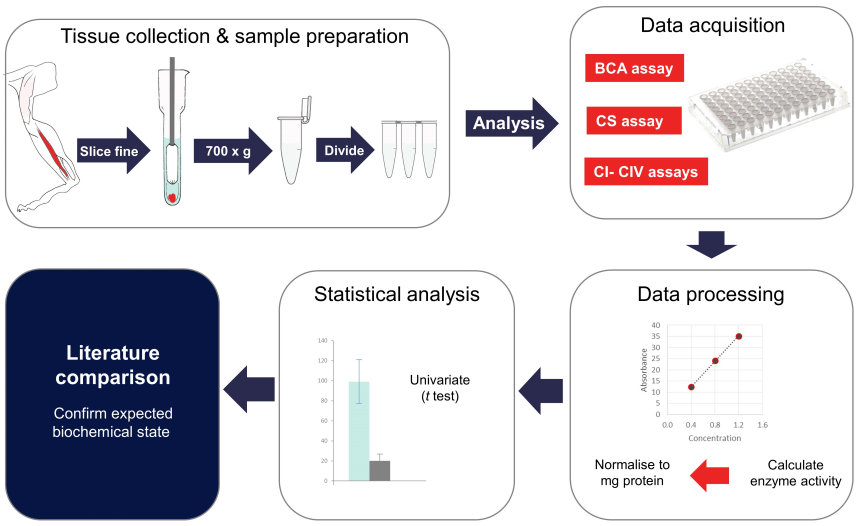


Figure 5-6: Enzyme assays workflow

5.5.1.1 Mitochondrial isolation

White quadriceps (WQ) and soleus (SOL) muscles were minced (~ 2 minutes) using scalpel blades, weighed (WQ: 148.05 ± 25.5 mg and SOL: 9.59 ± 3.0 mg), and mechanically homogenised in Zheng buffer (WQ: 10 % w/v and SOL: 2 % w/v) using a Teflon® pestle attached to a motor-driven tissue homogeniser (~ 15 passes at 164 rpm). Homogenates were centrifuged at 700 ×g (10 minutes; 4 °C) to obtain a fraction enriched in intact mitochondria. Supernatants were then freeze-thawed twice in liquid nitrogen and water and stored at − 80 °C. Zheng buffer (pH 7.2) for tissue homogenate preparation consisted of 210 mM mannitol, 70 mM sucrose, 5 mM HEPES, and 0.1 mM EGTA. The pH of the buffer was set to 7.2 using KOH.

5.5.1.2 CI enzyme assay

The assay was performed at 30 °C with triplicate reactions for each of the biological replicates in a 96-well UV microtiter plate with a final reaction volume of 200 µL per well. The reaction consisted of 120 µL of CI master mixture consisting of 50 mM KPi-buffer, 1 µM antimycin A, 70 µM decylubiquinone in DMSO, 60 µM DCIP, 0.35 % (w/v) BSA, and 700 ×g supernatant (10 µL of 9:1 diluted WQ or undiluted SOL supernatant). Each sample was analysed in the presence of 2.5 µM DMSO (ν_1) and 2.5 µM rotenone (ν_2) respectively (50 µL). After a 10 minute incubation (30 °C) period, 0.2 mM NADH (20 µL; preheated to 33 °C) was used to initiate the reaction and the reduction of the coloured substrate (DCIP) to colourless was kinetically measured at 600 nm in 1 minute intervals for 5 minutes.

5.5.1.3 CII enzyme assay

The assay was performed at 30 °C with duplicate reactions for each of the biological replicates in a 96-well UV microtiter plate with a final reaction volume of 200 µL per well. The reaction consisted of 162 µL of CII master mixture consisting of 50 mM KPi-buffer, 1 µM antimycin A, 2.5 µM rotenone, 50 µM decylubiquinone in DMSO, 80 µM DCIP, 0.2 mM ATP, 0.08 % (w/v) EDTA, 0.10 % (w/v) BSA, and 700 ×g supernatant (8 µL of undiluted WQ or SOL supernatant). After a 10 minute incubation (30 °C) period, 10 mM succinate (30 µL; preheated to 33 °C) was used to initiate the reaction and the reduction of the coloured substrate (DCIP) to colourless was kinetically measured at 600 nm in 1 minute intervals for 5 minutes.

5.5.1.4 CIII enzyme assay

The assay was performed at 30 °C with duplicate reactions for each of the biological replicates in a 96-well UV microtiter plate with a final reaction volume of 200 µL per well. The reaction mixture consisted of 125 µL cytochrome c (83.3 µM) and 700 ×g supernatant (10 µL of a 1:9 dilution of WQ or SOL supernatant). After a 10 minute incubation (30 °C) period, the reaction was initiated by the addition of 65 µL of CIII master mixture consisting of 250 mM KPi buffer, 20 mM NaN_3, 0.05 %, (w/v) BSA, 0.25 % (v/v) Tween® 20, and 0.25 mM decylubiqiunol. The reduction (increase in absorbance) of the coloured substrate (cytochrome c) was kinetically measured at 550 nm in 1 minute intervals for 5 minutes.

5.5.1.5 CIV enzyme assay

The assay was performed at 30 °C with duplicate reactions for each of the biological replicates in a 96-well UV microtiter plate with a final reaction volume of 200 µL per well. The reaction mixture consisted of 42.5 µL or 45 µL of Kpi buffer and 700 ×g supernatant (7.5 µL of a 1:9 dilution of WQ and 5 µL of 1:9 a dilution of SOL supernatant). After a 10 minute incubation (3 °C) period, the reaction was initiated by the addition of 150 µL of CIV master mixture consisting of 50 mM Kpi buffer, 0.5 mM dodecylmaltoside, and 25 µM reduced cytochrome c. The oxidation (decrease in absorbance) of the coloured substrate (reduced cytochrome c) was kinetically measured at 550 nm in 1 minute intervals for 5 minutes.

5.5.2 Metabolic profiling

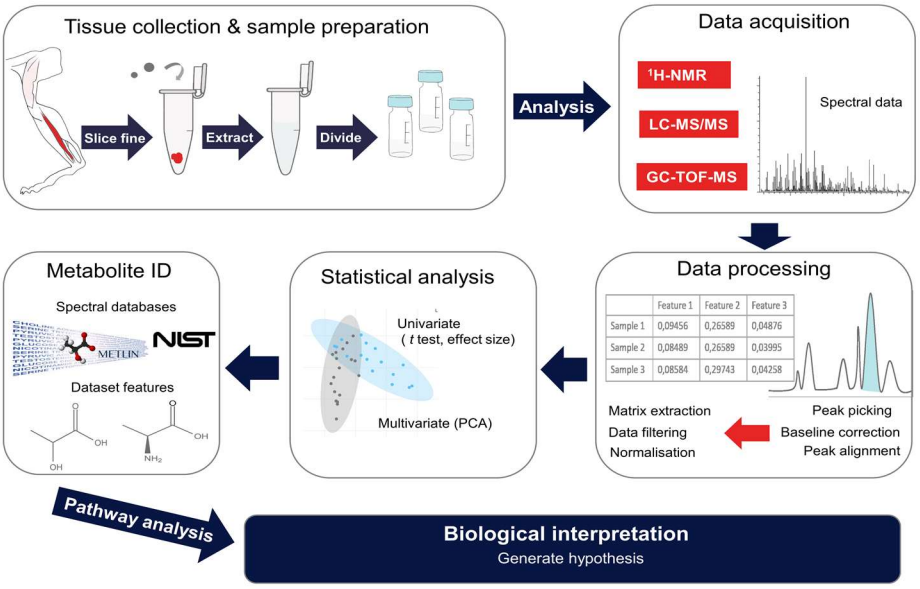


Figure 5-7: Metabolic profiling workflow

5.5.2.1 Metabolite extraction

A modified monophasic Bligh–Dyer extraction method (Gullberg *et al.*, 2004) using a solvent ratio of 3:1:1 (methanol:water:chloroform) was employed. Due to the limited quantity of soleus samples, the solvent volumes used were increased by a factor of ten compared to the white quadriceps muscles in order to obtain a sufficient sample volume. Because approximately 75 % of the wet muscle samples consist of water (i.e. 0.75 µL/mg tissue), cold methanol (WQ: 6 µL/mg tissue; SOL: 60 µL/mg tissue) and water (WQ: 1.25 µL/mg tissue; SOL:19.25 µL/mg tissue) containing an internal standard mixture [*N, N*-dimethyl-L-phenylalanine (DMPA) and 3-phenylbutyric acid (3-PBA)] were added to the pre-minced and pre-weighed (WQ: ~ 80 mg; SOL: ~ 5 mg) frozen muscle tissues. As indicated in Table 5-2, the concentrations of internal standards in the mixture were calculated to allow the analysis of 50 ng DMPA in NMR samples, 25 ng DMPA in LC samples, and 25 ng 3-PBA in GC samples. Subsequently, tungsten carbide and stainless steel beads (3 mm Ø and 5 mm Ø, respectively, ~ 7:1 (w/w), Qiagen) were added to the tissues in Safe-Lock microcentrifuge tubes (Eppendorf®). Tissues were pulverised in a vibration mill (MM 400, Retsch©) for 2 minutes at 30 Hz. After the addition of chloroform (WQ: 2 µL/mg tissue; SOL: 20 µL/mg tissue), homogenates were thoroughly vortexed (1 minute) and incubated on ice (10 minutes). Samples were then centrifuged at 20 000 ×g (10 minutes; 4 °C) and the supernatant transferred to a new tube.

Table 5-2: Volume extracts and mass internal standard mixture analysed on various platforms

Analytical platform	Tissue type	Extract volume (µL)	Final sample volume (µL)	Injection volume (µL)	Mass IS analysed (ng)
^{1}H-NMR	WQ	70	70	N/A	50
LC-MS/MS	WQ	50	100	1	25
	SOL	50	25	2.5	25
GC-TOF-MS	WQ	40	100	1	25
	SOL	200	50	1	25

5.5.2.2 Quality control samples

Quality control (QC) samples were prepared for the white quadriceps and soleus muscles respectively by pooling equal amounts of the *Ndufs4*$^{-/-}$ and control sample extracts. The QC samples were then aliquoted, stored and prepared for each analytical platform in the same manner as the other samples. For LC-MS/MS and GC-TOF-MS analyses, QC samples were analysed in the beginning, after every 5 samples, and at the end of each batch. For NMR analyses QC samples were analysed at the beginning, middle, and end of each batch. In addition, for LC-MS/MS, an in-house standard mixture (consisting of all metabolites analysed) as well as a QC sample spiked with this standard mixture, was analysed at the end of each batch.

5.5.2.3 ^{1}H-NMR sample preparation and analysis

For ^{1}H-NMR spectroscopy, white quadriceps muscle extracts (70 µL) were transferred to glass vials (2 mL, Agilent©) and evaporated under a stream of nitrogen gas at 37 °C. On the day of analysis, each dried extract was resuspended in sterile, filtered water (70 µL) and centrifuged at 12 000 ×g (5 minutes, 25 °C) to remove macromolecules and other particulates. A buffer solution (pH 7.4) was prepared as described by Dona *et al.* (2014) containing 1.5 M KH_2PO_4 dissolved in D_2O together with 100 ppm trimethylsilyl-2,2,3,3-tetradeuteropropionic acid (TSP) as chemical shift standard. Using an eVol® NMR digital syringe, the sample ultra-filtrate (54 µL) together with 10 % buffer solution (6 µL) was aspirated and the total volume (60 µL) was purged into a 2 mm NMR tube (outside Ø 2.0 mm, inside Ø 1.6 mm, length 100 mm). The sample was then mixed once inside the 2 mm NMR tube to ensure homogeneity by aspirating and purging the entire volume. Thereafter, a wash sequence was used to clean the syringe before the next sample was prepared: (1) aspirate 100 µL distilled water, (2) purge 100 µL (waste), (3) aspirate 100 µL distilled water, (4) purge 100 µL (waste), (5) aspirate 100 µL distilled water, (6) purge 100 µL (waste). Next, the NMR tubes were assembled using the Bruker MATCH system, which is an adapter with a gripper to hold the 2 mm NMR tube, inserted into a 10 mm spinner. Finally, each NMR MATCH assembly was loaded onto a SampleXpress autosampler for NMR analysis.

^{1}H-NMR spectroscopy was performed according to the miniaturised method described by Mason *et al.* (2018). ^{1}H spectra were acquired as 128 transients in 32K data points with a spectral width of 6000 Hz (12.0 ppm). The sample temperature was maintained at a constant 300 K. The H_2O resonance at 4.70 ppm was suppressed using the pulse sequence program NOESY-presat, which presaturates the H_2O resonance by single-frequency irradiation during a relaxation delay of 4 seconds, with a 90° excitation pulse of 10 µs. The acquisition time and receiver gain were set for 2.7 seconds and 64, respectively. The number of dummy scans (n= 4) and scans (n= 128) yielded a run time of 15 minutes and 45 seconds per sample. Each sample was automatically shimmed on the deuterium signal, locked, probe tuned and matched, and pulse calibrated.

The NMR system consisted of a 500 MHz Bruker Avance III HD NMR spectrometer equipped with a 5 mm triple-resonance inverse (TXI) [^{1}H,^{15}N, ^{13}C] probe head and x, y, z gradient coils with the inner coil of the TXI optimised for ^{1}H observation. The eVol® NMR digital syringe was equipped with a 100 µL syringe and a 180-mm-long bevel-tipped needle. The Bruker Topspin (v 3.1) and Bruker AMIX (v 3.9.12) software were used for spectral processing and metabolite identification respectively while the Bruker pH 7.0 spectral library was used to confirm metabolite identities.

5.5.2.4 LC-MS/MS sample preparation and analysis

For LC-MS/MS, muscle extracts (50 µL) were transferred to a glass vial (WQ: 2 mL Agilent©; SOL: 250 µL insert with polymer feet) together with 2.5 ppm (WQ: 100 µL; SOL: 50 µL) of isotope mixture and evaporated under a stream of nitrogen gas at 37 °C. To derivatise the samples, *N*-butanol:acetyl chloride (WQ: 300 µL; SOL: 200 µL) was added and the samples were incubated at 50 °C for 1 h. Thereafter the butylated samples were evaporated to dryness under a stream of nitrogen gas at 37 °C. Finally, the dried residue was reconstituted in a final volume of water:acetonitrile (50:50) (v/v) containing 0.1 % formic acid (WQ: 100 µL; SOL: 25 µL). The samples were thoroughly vortex mixed to dissolve the dried compounds. In the case of white quadriceps samples, the final volume was transferred 250 µL pulled point glass inserts. Due to the small volumes used during derivatisation, soleus samples were derivatised in inserts to maximise recovery for small sample volumes, therefore, sample transfer to inserts was not necessary. Finally, each vial was loaded onto an Agilent© 1200 series auto sampler for LC-MS/MS analysis.

LC-MS/MS was performed as described by Mels *et al.* (2011) with slight modifications. For separation, a C18 Zorbax SB-Aq reverse phase column (2.1mm x 150 mm x 3.5 µm, Agilent©) was used. The column was kept at 30 °C during the entire run. One µL and 2.5 µL of the

sample were injected respectively for the white quadriceps and soleus samples. The chromatographic gradient started at 95 % solvent A (water with 0.1 % formic acid) with a flow of 0.3 mL/min and maintained for 1 minute before the gradient was increased to 20 % solvent B (acetonitrile with 0.1 % formic acid) over a period of 2 minutes. The gradient was then kept constant for 3 minutes after which it was increased linearly to 100 % solvent B at 13 minutes. Over this period, the flow was linearly increased to 0.35 mL/min at 13.1 minutes. After maintaining these conditions for 5 minutes, the gradient was decreased to 5 % solvent B at 18.5 minutes and kept constant for 1.5 minutes. A post-run of 10 minutes was allowed to ensure equilibration of the column to give a total run time of 30 minutes (20 minute gradient and 10 minute post-run) per sample. The electrospray ionisation (ESI) source gas temperature was kept at 300 °C, with a flow rate of 7.5 L/min. Nebuliser pressure was kept at 30 psi and the capillary voltage at 3500 V.

The LC-MS/MS system consisted of an Agilent© 1200 series LC front end with binary pump coupled to an Agilent© 6410 series triple quadrupole mass analyser with electrospray ionisation (ESI) source operated in positive ionisation mode. The system is equipped with a vacuum degasser as well as thermostatted autosampler and column compartments. Agilent©'s MassHunter Workstation Software (v B02.01; Data acquisition for 6400 Series Triple Quadrupole) and MassHunter Optimiser software (v B02.01) were used for data acquisition in the multiple reaction monitoring (MRM) configuration settings while data extraction was done using Agilent©'s MassHunter Workstation software (v B06.00; Qualitative Analysis and Quantitative Analysis).

5.5.2.5 GC-TOF-MS sample preparation and analysis

For GC-TOF-MS sample extracts (WQ: 40 µL; SOL: 200 µL) were transferred to a glass vial (WQ: 2 mL Agilent©; SOL: 1.1 mL microvial Separations) and evaporated under a stream of nitrogen gas at 37 °C. Derivatisation was achieved via oximation and silylation. To oximate the samples, methoxyamine hydrochloride (20 mg/mL in pyridine, WQ: 50 µL; SOL: 25 µL) was added and the samples were vortex mixed for ~ 1 minute to dissolve the dried compounds. The samples were then incubated at 60 °C for 1 hour. Thereafter the samples were silylated by adding BSTFA (WQ: 50 µL; SOL: 25 µL) containing 1 % (v/v) TMCS (catalyst for silylation reaction) and incubated at 60 °C for 1 hour. For the white quadriceps samples, the final volume (100 µL) was then transferred to 250 µL pulled point glass inserts. Due to the small volumes used during derivatisation, soleus samples (50 µL) were derivatised in microvials designed to maximise recovery for small sample volumes, therefore, sample transfer to inserts was not necessary. Finally, each vial was loaded onto an Agilent© 7693 auto sampler for GC-TOF-MS analysis.

The GC-TOF-MS protocol described by Lindeque *et al.* (2013) was slightly modified for this study. Chromatographic separation was done with an Rxi®-5Sil MS, 28.6 m x 250 µm x 0.25 µm (Restek, Cat. #13620) capillary column. The derivatised samples (1 µL for both muscle types) were injected with the injector operating in splitless mode (hold 30 seconds) and the inlet temperature set to hold at 250 °C throughout the entire run. A 4.0 mm ID x 6.3 mm OD x 78.5 mm length split/splitless, single taper deactivated FocusLiner® with glass wool (Phenomenex, Cat. #AGO-4680) was used. The initial GC oven temperature was held at 70 °C for 1 minute. Thereafter the oven temperature was increased by 7 °C/min until 120 °C, then 10 °C/min until 230 °C and finally 13 °C/min until 300 °C where the temperature was held for 1 minute before cooling to 70 °C in a total run time of ~ 25.53 minutes. Helium was used as carrier gas with a pressure-programmed constant flow rate of 1.5 mL/min. Throughout the entire run, the transferline and ion source temperatures were held at 225 °C and 200 °C respectively. In order to detect metabolites, mass spectrometry was operated in electron impact (EI) ionisation (- 70 V) mode which enabled the fragmentation of all eluting compounds. After an acquisition (solvent) delay of 250 seconds, data were acquired at a rate of 20 spectra/second using a mass-to-charge (m/z) ratio scan range of 50–950 amu. Peaks with 5 apexing masses were detected using an expected peak width of 3 seconds and a signal-to-noise (S/N) ratio of > 20.

The GC-TOF-MS system consisted of an Agilent© 7890A series gas chromatograph with Agilent© 7693 autosampler coupled to a LECO Pegasus HT time-of-flight mass analyser with an electron impact (EI) ionisation source. The LECO Corporation ChromaTOF® software (v 4.5x) was used for data acquisition and extraction. This included automatic baseline removal via the “spanning” tracking method (offset of 1; just above the noise) and auto smoothing, with the software’s Statistical Compare feature used to align peaks. Spectral matching was done using the NIST11 commercial- and an in-house mass spectral library in order to identify important analytes

Table 5-3: List of 48 significant discriminatory metabolites between *Ndufs4*$^{-/-}$ and WT white quadriceps muscles

Metabolite	Δ direction	*t* test p-value (p < 0.1)		Effect size D-value (D ≥ 0.5)	Platform	ID level	Alternative platforms
AMINO ACIDS AND DERIVATIVES							
1-Methylhistidine	↓	0.0023	**	0.882	LC-MS/MS	1	
2-Aminoadipate	↓	<0.0001	**	1.957	LC-MS/MS	1	
3-Methylhistidine	↑	0.0379	**	0.656	LC-MS/MS	1	
4-Hydroxyproline	↓	<0.0001	**	1.389	LC-MS/MS	1	GC-TOF-MS
Alanine	↓	0.0007	**	1.026	LC-MS/MS	1	NMR & GC-TOF-MS
Asparagine	↓	0.0029	**	0.993	LC-MS/MS	1	
Aspartate	↓	0.0775		0.499	GC-TOF-MS	3	
Beta-Alanine	↓	0.0276	**	0.693	LC-MS/MS	1	
Choline	↑	0.0368	*	0.670	NMR	1	
Citrulline	↓	0.0001	**	1.123	LC-MS/MS	1	
Glutamate	↓	0.0379	**	0.666	LC-MS/MS	1	
Glutamine	↓	0.0111	**	0.738	LC-MS/MS	1	NMR
Histamine	↑	0.0684	*	0.564	NMR	1	
Lysine	↑	0.0058	**	0.718	LC-MS/MS	1	NMR
Methionine	↓	0.0027	**	0.924	LC-MS/MS	1	
N,N-Dimethylglycine	↓	<0.0001	**	2.082	LC-MS/MS	1	
N-Acetylaspartate	↑	0.0001	**	1.386	LC-MS/MS	1	
N-Acetylglutamate	↓	0.0094	**	0.771	LC-MS/MS	1	
Phenylalanine	↓	0.0935		0.530	LC-MS/MS	1	
Pipecolate	↑	0.0025	**	1.028	LC-MS/MS	1	
Proline	↓	<0.0001	**	1.858	LC-MS/MS	1	GC-TOF-MS
Pyroglutamate	↓	0.0088	**	0.767	LC-MS/MS	1	GC-TOF-MS
Threonine	↓	0.0002	**	1.039	LC-MS/MS	1	GC-TOF-MS
Trimethylglycine (Betaine)	↓	0.0144	**	0.713	LC-MS/MS	1	
Tryptophan	↓	0.0584	*	0.564	LC-MS/MS	1	

Table 5-3 (continued)

Metabolite	Δ direction	*t* test p-value (p < 0.1)		Effect size D-value (D ≥ 0.5)	Platform	ID level	Alternative platforms
FATTY ACIDS AND ACYLCARNITINES							
Acetyl-carnitine (C2)	↑	0.0100	**	0.831	LC-MS/MS	1	
Butyryl-carnitine (C4)	↓	<0.0001	**	1.417	LC-MS/MS	1	
Carnitine (C0)	↓	0.0003	**	1.224	NMR	1	LC-MS/MS
Dodecanoyl-carnitine (C12)	↓	0.0425	*	0.616	LC-MS/MS	1	
Hexanoyl-carnitine (C6)	↓	0.0037	**	0.987	LC-MS/MS	1	
Isovaleryl-carnitine (C5)	↓	0.0171	**	0.661	LC-MS/MS	1	
Octanoyl-carnitine (C8)	↓	0.0001	**	1.470	LC-MS/MS	1	
Palmitate (C16:0)	↓	0.0438	*	0.602	GC-TOF-MS	1	
Palmitoyl-carnitine (C16)	↓	0.0334	**	0.682	LC-MS/MS	1	
Propionyl-carnitine (C3)	↓	0.0659	*	0.567	LC-MS/MS	1	
ORGANIC ACIDS AND DERIVATIVES							
3-Hydroxypyruvate	↓	0.0105	**	0.713	GC-TOF-MS	3	
Acetate	↑	0.0145	**	0.662	NMR	1	
Creatinine	↓	<0.0001	**	2.147	GC-TOF-MS	3	
Glycerate	↓	0.0015	**	0.753	GC-TOF-MS	1	
Glycerol	↓	0.0049	**	0.791	GC-TOF-MS	1	
Glycolate	↓	0.0005	**	1.135	GC-TOF-MS	3	
Lactate	↓	0.0013	**	0.798	NMR	1	GC-TOF-MS
Malate	↓	0.0055	**	0.913	GC-TOF-MS	1	
Methylmalonate	↑	0.0300	**	0.670	NMR	1	
Pyruvate	↓	0.0001	**	1.015	GC-TOF-MS	1	NMR
Succinate	↓	<0.0001	**	1.488	NMR	1	GC-TOF-MS
OTHER							
Adenosine monophosphate	↓	0.0099	**	0.721	NMR	1	
Sulfate	↑	0.0260	*	0.688	GC-TOF-MS	1	

Average values were obtained from 19 *Ndufs4*$^{-/-}$ and 20 WT animals, FDR adjusted p-values are indicated with an asterisk (* FDR-adjusted p < 0.1; ** FDR-adjusted p < 0.05).
Symbols and abbreviations: Δ direction, change in Ndufs4$^{-/-}$ *metabolite levels relative to WT; ↑ indicates increased levels in the Ndufs4*$^{-/-}$*; ↓ indicates decreased levels in the Ndufs4*$^{-/-}$*; ID level, metabolite identification level on relevant platform; alternative platform, if a metabolite was detected as significant by more than one analytical platform the platform will be listed under this column.*

Table 5-4: List of 34 significant discriminatory metabolites between *Ndufs4*$^{-/-}$ and WT soleus muscles

Metabolite	Δ direction	*t* test p-value (p < 0.1)		Effect size D-value (D ≥ 0.5)	Platform	ID level	Alternative platforms
AMINO ACIDS AND DERIVATIVES							
2-Aminoadipate	↓	<0.0001	**	1.469	LC-MS/MS	1	
3-Aminoisobutyrate	↓	0.0198		0.737	GC-TOF-MS	3	
4-Hydroxyproline	↓	0.0003	**	1.169	LC-MS/MS	1	
Alanine	↓	0.0023	**	0.923	LC-MS/MS	1	GC-TOF-MS
Beta-Alanine	↓	0.0210	**	0.722	LC-MS/MS	1	
Citrulline	↓	0.0010	**	1.073	LC-MS/MS	1	
Glutamate	↓	0.0174	**	0.797	LC-MS/MS	1	
Glutamine	↓	0.0529	*	0.603	LC-MS/MS	1	
Lysine	↑	0.0016	**	0.912	LC-MS/MS	1	
N,N-Dimethylglycine	↓	<0.0001	**	2.018	LC-MS/MS	1	
N-Acetylaspartate	↑	0.0627	*	0.586	LC-MS/MS	1	
Pipecolate	↑	0.0097	**	0.760	LC-MS/MS	1	
Proline	↓	0.0428	*	0.500	LC-MS/MS	1	
Pyroglutamate	↓	0.0368	*	0.681	LC-MS/MS	1	
Serine	↑	0.0147		0.802	GC-TOF-MS	1	
Taurine	↓	0.0922		0.468	LC-MS/MS	1	
FATTY ACIDS AND ACYLCARNITINES							
Butyryl-carnitine (C4)	↓	0.0001	**	1.398	LC-MS/MS	1	
Carnitine (C0)	↓	0.0339	*	0.623	LC-MS/MS	1	
Dodecanoyl-carnitine (C12)	↓	0.0456	*	0.582	LC-MS/MS	1	
Hexanoyl-carnitine (C6)	↓	0.0045	**	0.826	LC-MS/MS	1	
Isovaleryl-carnitine (C5)	↓	0.0004	**	1.227	LC-MS/MS	1	
Myristoyl-carnitine (C14)	↓	0.0211	**	0.645	LC-MS/MS	1	
Octanoyl-carnitine (C8)	↓	0.0213	**	0.700	LC-MS/MS	1	
Palmitoyl-carnitine (C16)	↓	0.0076	**	0.798	LC-MS/MS	1	
Propionyl-carnitine (C3)	↓	0.0041	**	0.817	LC-MS/MS	1	
Stearoyl-carnitine (C18)	↓	0.0275	*	0.651	LC-MS/MS	1	

Table 5-4 (continued)

Metabolite	Δ direction	*t* test p-value (p < 0.1)		Effect size D-value (D ≥ 0.5)	Platform	ID level	Alternative platforms
ORGANIC ACIDS AND DERIVATIVES							
Creatinine	↓	<0.0001	**	1.597	GC-TOF-MS	3	
Fumarate	↓	0.0460		0.642	GC-TOF-MS	1	
Glycerol	↓	0.0195		0.720	GC-TOF-MS	3	
Malate	↓	0.0004	**	1.006	GC-TOF-MS	1	
Oxalate	↓	0.0703		0.508	GC-TOF-MS	1	
Pyruvate	↓	<0.0001	**	1.404	GC-TOF-MS	1	
Succinate	↓	0.0296		0.508	GC-TOF-MS	1	
Urea	↑	0.0100	*	0.685	GC-TOF-MS	1	

Average values were obtained from 19 *Ndufs4*$^{-/-}$ and 20 WT animals, FDR adjusted p-values are indicated with an asterisk (* FDR-adjusted p < 0.1; ** FDR-adjusted p < 0.05).
Symbols and abbreviations: Δ direction, change in Ndufs4$^{-/-}$ *metabolite levels relative to WT; ↑ indicates increased levels in the Ndufs4*$^{-/-}$*; ↓ indicates decreased levels in the Ndufs4*$^{-/-}$*; ID level, metabolite identification level on relevant platform; alternative platform, if a metabolite was detected as significant by more than one analytical platform the platform will be listed under this column.*

5.6 References

Alam, M.T., Manjeri, G.R., Rodenburg, R.J., Smeitink, J.A.M., Notebaart, R.A., Huynen, M., Willems, P.H.G.M. & Koopman, W.J.H. 2015. Skeletal muscle mitochondria of NDUFS4$^{-/-}$ mice display normal maximal pyruvate oxidation and ATP production. *Biochimica et Biophysica Acta — Bioenergetics*, 1847(6-7):526-533.

Bogner-Strauss, J.G. 2017. N-Acetylaspartate metabolism outside the brain: lipogenesis, histone acetylation, and cancer. *Frontiers in Endocrinology (Lausanne)*, 8:5.

Budde, S.M.S., van den Heuvel, L.P.W.J., Smeets, R.J.P., Skladal, D., Mayr, J.A., Boelen, C., Petruzzella, V., Papa, S. & Smeitink, J.A.M. 2003. Clinical heterogeneity in patients with mutations in the NDUFS4 gene of mitochondrial complex I. *Journal of Inherited Metabolic Disease*, 26(8):813-815.

Calvaruso, M.A., Willems, P., van den Brand, M., Valsecchi, F., Kruse, S., Palmiter, R., Smeitink, J. & Nijtmans, L. 2012. Mitochondrial complex III stabilizes complex I in the absence of NDUFS4 to provide partial activity. *Human Molecular Genetics*, 21(1):115-120.

Cherry, A.D. & Piantadosi, C.A. 2015. Regulation of mitochondrial biogenesis and its intersection with inflammatory responses. *Antioxidants & Redox Signaling*, 22(12):965-976.

de Haas, R., Das, D., Garanto, A., Renkema, H.G., Greupink, R., van den Broek, P., Pertijs, J., Collin, R.W.J., Willems, P., Beyrath, J., Heerschap, A., Russel, F.G. & Smeitink, J.A.M. 2017. Therapeutic effects of the mitochondrial ROS-redox modulator KH176 in a mammalian model of Leigh disease. *Scientific Reports*, 7(1):11733.

Distelmaier, F., Koopman, W.J.H., van den Heuvel, L.P., Rodenburg, R.J., Mayatepek, E., Willems, P.H.G.M. & Smeitink, J.A.M. 2009. Mitochondrial complex I deficiency: from organelle dysfunction to clinical disease. *Brain*, 132(4):833-842.

Dona, A.C., Jiménez, B., Schäfer, H., Humpfer, E., Spraul, M., Lewis, M.R., Pearce, J.T.M., Holmes, E., Lindon, J.C. & Nicholson, J.K. 2014. Precision high-throughput proton NMR Spectroscopy of human urine, serum, and plasma for large-scale metabolic phenotyping. *Analytical Chemistry*, 86(19):9887-9894.

Ellis, S.M. & Steyn, H.S. 2003. Practical significance (effect sizes) versus or in combination with statistical significance (p-values). *Management Dynamics*, 12(4):51-53.

Esterhuizen, K., van der Westhuizen, F.H. & Louw, R. 2017. Metabolomics of mitochondrial disease. *Mitochondrion*, 35:97-110.

Fassone, E. & Rahman, S. 2012. Complex I deficiency: clinical features, biochemistry and molecular genetics. *Journal of Medical Genetics*, 49(9):578-590.

Foriel, S., Beyrath, J., Eidhof, I., Rodenburg, R.J., Schenck, A. & Smeitink, J.A.M. 2018. Feeding difficulties, a key feature of the *Drosophila* NDUFS4 mitochondrial disease model. *Disease Models & Mechanisms*, 11:10.

Goody, M.F. & Henry, C.A. 2018. A need for NAD^+ in muscle development, homeostasis, and aging. *Skeletal Muscle*, 8:14.

Greaves, L.C., Reeve, A.K., Taylor, R.W. & Turnbull, D.M. 2012. Mitochondrial DNA and disease. *Journal of Pathology*, 226(2):274-286.

Gullberg, J., Jonsson, P., Nordström, A., Sjöström, M. & Moritz, T. 2004. Design of experiments: an efficient strategy to identify factors influencing extraction and derivatization of *Arabidopsis thaliana* samples in metabolomic studies with gas chromatography/mass spectrometry. *Analytical Biochemistry*, 331(2):283-295.

Janssen, A.J.M., Trijbels, F.J.M., Sengers, R.C.A., Smeitink, J.A.M., van den Heuvel, L.P., Wintjes, L.T.M., Stoltenborg-Hogenkamp, B.J.M. & Rodenburg, R.J.T. 2007. Spectrophotometric assay for complex I of the respiratory chain in tissue samples and cultured fibroblasts. *Clinical Chemistry*, 53(4):729-734.

Jin, Z., Wei, W., Yang, M., Du, Y. & Wan, Y. 2014. Mitochondrial complex I activity suppresses inflammation and enhances bone resorption by shifting macrophage-osteoclast polarization. *Cell Metabolism*, 20(3):483-498.

Johnson, S.C., Yanos, M.E., Kayser, E.B., Quintana, A., Sangesland, M., Castanza, A., Uhde, L., Hui, J., Wall, V.Z., Gagnidze, A., Oh, K., Wasko, B.M., Ramos, F.J., Palmiter, R.D., Rabinovitch, P.S., Morgan, P.G., Sedensky, M.M. & Kaeberlein, M. 2013. mTOR inhibition alleviates mitochondrial disease in a mouse model of Leigh syndrome. *Science*, 342(6165):1524.

Kruse, S.E., Watt, W.C., Marcinek, D.J., Kapur, R.P., Schenkman, K.A. & Palmiter, R.D. 2008. Mice with mitochondrial complex i deficiency develop a fatal encephalomyopathy. *Cell Metabolism*, 7(4):312-320.

Leong, D.W., Komen, J.C., Hewitt, C.A., Arnaud, E., McKenzie, M., Phipson, B., Bahlo, M., Laskowski, A., Kinkel, S.A., Davey, G.M., Heath, W.R., Voss, A.K., Zahedi, R.P., Pitt, J.J., Chrast, R., Sickmann, A., Ryan, M.T., Smyth, G.K., Thorburn, D.R. & Scott, H.S. 2012. Proteomic and metabolomic analyses of mitochondrial complex I-deficient mouse model generated by spontaneous B2 short interspersed nuclear element (SINE) insertion into NADH dehydrogenase (ubiquinone) Fe-S protein 4 (Ndufs4) gene. *Journal of Biological Chemistry*, 287(24):20652-20663.

Lindeque, J.Z., Hidalgo, J., Louw, R. & van der Westhuizen, F.H. 2013. Systemic and organ specific metabolic differences in metallothionein knockout mice when challenged with exercise. *Metabolomics*, 9(2):418-432.

Mason, S.W., Terburgh, K. & Louw, R. 2018. Miniaturized ^{1}H-NMR method for analyzing limited-quantity samples applied to a mouse model of Leigh disease. *Metabolomics*, 14:1-12.

McDonald, A.E., Pichaud, N. & Darveau, C.A. 2018. "Alternative" fuels contributing to mitochondrial electron transport: importance of non-classical pathways in the diversity of animal metabolism. *Comparative Biochemistry and Physiology Part B: Biochemistry and Molecular Biology*, 224:185-194.

Mels, C.M.C., Jansen van Rensburg, P., van der Westhuizen, F.H., Pretorius, P.J. & Erasmus, E. 2011. Increased excretion of C4-carnitine species after a therapeutic acetylsalicylic acid dose: evidence for an inhibitory effect on short-chain fatty acid metabolism. *International Scholarly Research Network Pharmacology*:8.

Phang, J. 2017. Proline metabolism in cell regulation and cancer biology: recent advances and hypotheses. *Antioxidants & Redox Signaling*, (In press).

Qureshi, G.A., Gutierrez, A. & Bergström, J. 1986. Determination of histidine, 1-methylhistidine and 3-methylhistidine in biological samples by high-performance liquid chromatography: clinical application of urinary 3-methylhistidine in evaluating the muscle protein breakdown in uraemic patients. *Journal of Chromatography B: Biomedical Sciences and Applications*, 374:363-369.

Rahman, S., Blok, R.B., Dahl, H.H., Danks, D.M., Kirby, D.M., Chow, C.W., Christodoulou, J. & Thorburn, D.R. 1996. Leigh syndrome: clinical features and biochemical and DNA abnormalities. *Annals of Neurology*, 39(3):343-351.

Russell, A.P., Ghobrial, L., Wright, C.R., Lamon, S., Brown, E.L., Kon, M., Skelton, M.R. & Snow, R.J. 2014. Creatine transporter (SLC6A8) knockout mice display an increased capacity for in vitro creatine biosynthesis in skeletal muscle. *Frontiers in Physiology*, 5.

Schiaffino, S. & Reggiani, C. 2011. Fiber types in mammalian skeletal muscles. *Physiological Reviews*, 91(4):1447-1531.

Schymanski, E.L., Jeon, J., Gulde, R., Fenner, K., Ruff, M., Singer, H.P. & Hollender, J. 2014. Identifying small molecules via high resolution mass spectrometry: communicating confidence. *Environmental Science & Technology*, 48(4):2097-2098.

Shaughnessy, D.T., McAllister, K., Worth, L., Haugen, A.C., Meyer, J.N., Domann, F.E., van Houten, B., Mostoslavsky, R., Bultman, S.J., Baccarelli, A.A., Begley, T.J., Sobol, R.W., Hirschey, M.D., Ideker, T., Santos, J.H., Copeland, W.C., Tice, R.R. & Balshaw, D.M. 2014. Mitochondria, energetics, epigenetics, and cellular responses to stress. *Environmental Health Perspectives*, 122(12):1271-1278.

Shepherd, D. & Garland, P.B. 1969. The kinetic properties of citrate synthase from rat liver mitochondria. *Biochemistry Journal*, 114(3):597-610.

Shokolenko, I.N. & Alexeyev, M.F. 2015. Mitochondrial DNA: a disposable genome? *Biochimica et Biophysica Acta*, 1852(9):1805-1809.

Sumner, L.W., Amberg, A., Barrett, D., Beale, M.H., Beger, R., Daykin, C.A., Fan, T.W.M., Fiehn, O., Goodacre, R., Griffin, J.L., Hankemeier, T., Hardy, N., Harnly, J., Higashi, R., Kopka, J., Lane, A.N., Lindon, J.C., Marriott, P., Nicholls, A.W., Reily, M.D., Thaden, J.J. & Viant, M.R. 2007. Proposed minimum reporting standards for chemical analysis Chemical Analysis Working Group (CAWG) Metabolomics Standards Initiative (MSI). *Metabolomics*, 3(3):211-221.

Terburgh, K., Lindeque, J.Z., Mason, S.W., van der Westhuizen, F.H. & Louw, R. 2018. Multi-platform metabolomics data from *Ndufs4*$^{-/-}$ skeletal muscles. Metabolomics Workbench. https://doi.org/10.21228/M8GM4Z

Torraco, A., Peralta, S., Iommarini, L. & Diaz, F. 2015. Mitochondrial diseases part I: mouse models of OXPHOS deficiencies caused by defects on respiratory complex subunits or assembly factors. *Mitochondrion*:76-91.

Valsecchi, F., Koopman, W.J.H., Manjeri, G.R., Rodenburg, R.J., Smeitink, J.A.M. & Willems, P.H.G.M. 2010. Complex I disorders: Causes, mechanisms, and development of treatment strategies at the cellular level. *Developmental Disabilities Research Reviews*, 16(2):175-182.

Valsecchi, F., Monge, C., Forkink, M., de Groof, A.J.C., Benard, G., Rossignol, R., Swarts, H.G., van Emst-de Vries, S.E., Rodenburg, R.J., Calvaruso, M.A., Nijtmans, L.G.J., Heeman, B., Roestenberg, P., Wieringa, B., Smeitink, J.A.M., Koopman, W.J.H. & Willems, P.H.G.M. 2012. Metabolic consequences of NDUFS4 gene deletion in immortalized mouse embryonic fibroblasts. *Biochimica et Biophysica Acta — Bioenergetics*, 1817(10):1925-1936.

Watmough, N.J. & Frerman, F.E. 2010. The electron transfer flavoprotein: ubiquinone oxidoreductases. *Biochimica et Biophysica Acta — Bioenergetics*, 1797(12):1910-1916.

Wolfe, R.R. 2006. The underappreciated role of muscle in health and disease. *American Journal of Clinical Nutrition*, 84(3):475-482.

Wu, G., Bazer, F.W., Burghardt, R.C., Johnson, G.A., Kim, S.W., Knabe, D.A., Li, P., Li, X., McKnight, J.R., Satterfield, M.C. & Spencer, T.E. 2011. Proline and hydroxyproline metabolism: implications for animal and human nutrition. *Amino Acids*, 40(4):1053-1063.

Xia, J., Sinelnikov, I., Han, B. & Wishart, D.S. 2015. MetaboAnalyst 3.0 — making metabolomics more meaningful. *Nucleic Acids Research*, 43(W1):W251-W257.

CHAPTER 6

Summary and conclusions

6.1 Introduction

CI deficiency is the most prevalent mitochondrial disease (MD) manifesting in a devastating, often multisystemic phenotype for which there is currently no effective treatment. The main factors impeding our understanding of this progressive disease, and its underlying mechanisms, is its extreme complexity on a genetic-, biochemical- and clinical level. As the most frequent form of CI deficiency, childhood-onset Leigh syndrome (LS) currently lies at the forefront of MD research. Although neuromuscular manifestation is a hallmark feature of LS (and MD), the effect of CI deficiency on skeletal muscle remains poorly investigated. This is largely due to the notion that the whole-body *Ndufs4*$^{-/-}$ mouse model, used to study human LS, does not display muscle involvement.

Therefore, with this study, we aimed to comprehensively investigate the *in vivo* effect of CI deficiency in skeletal muscles with different fibre type compositions (i.e. white quadriceps femoris and soleus muscles) from *Ndufs4*$^{-/-}$ mice via the combination of biochemical strategies and multi-platform metabolomics. In order to achieve this aim, several objectives — organised into three study phases — had to be met. An in-depth discussion of the results obtained for each objective of the study is provided in Chapters 4 and 5 (together with Annexures A and B) of the dissertation. The current chapter aims to provide a summary of the key findings and final conclusions from this study. First, a summary of the research findings is presented; organised into three sections corresponding to the three study phases. Thereafter, the strengths and limitations of the study are provided, followed by proposed future research prospects stemming from this study.

6.2 Summary of the findings from this study

6.2.1 Phase I: sample collection — Annexure A

The study commenced with the sample collection phase, which was a time-consuming process due to i) the large amount (n = 61) of animals required; ii) the low genetic probability (12.25 %) of obtaining mice of both the correct genotype and sex; and iii) the waiting period (45-50 days) required before euthanasia to allow the disease to reach appropriate severity. The animal breeding- and genotyping strategy (**Objective 1.1**) was successfully set up and managed to optimise the probability of obtaining the desired mice. From the litter of several heterozygous carrier (*Ndufs4*$^{+/-}$) breeding trios[40], an adequate amount of male *Ndufs4*$^{-/-}$ and WT animals were obtained for the study. Euthanasia and sample collection (**Objective 1.2**) took place rapidly and

[40] Two female mice per male

efficiently, with tissue dissection and snap-freezing completed under 15 minutes *post-mortem*. The genotyping method employed for both animal selection and *post-mortem* genotype confirmation (**Objective 1.3**), successfully distinguished between the different genotypes (*Ndufs4*$^{-/-}$, *Ndufs4*$^{+/-}$, and *Ndufs4*$^{+/+}$) of the *Ndufs4* strain, with results corresponding to those described by Valsecchi *et al.* (2012). Furthermore, it was established that the correct animals were euthanised since the *post-mortem* determined genotype of each animal corresponded to that which was previously determined. Conclusively, all the objectives of the first phase of the study were successfully met.

6.2.2 Phase II: biochemical evaluation — Chapter 5 and Annexure B

In the second phase of the study, *Ndufs4*$^{-/-}$ white quadriceps and soleus skeletal muscles were characterised on a biochemical level by evaluating RC enzyme activity. To ensure that all the spectrophotometric assays could be acceptably performed on a single sample — the assays were first standardised for both muscle types (**Objective 2.1**). Method standardisation was successfully done and demonstrated that all six assays (BCA, CS, and CI-CIV) could be performed in replicate using a single sample, with high linearity ($R^2 > 0.99$) and repeatability (CV < 10 %). Thereafter, the spectrophotometric assays were effectively performed on white quadriceps and soleus skeletal muscles from *Ndufs4*$^{-/-}$ (n = 12) and WT (n = 10) mice (P45-50) (**Objective 2.2**). Data processing and statistical analyses (**Objective 2.3**) revealed an equally severe reduction (80 %) in CI activity in both *Ndufs4*$^{-/-}$ muscle types compared to WTs. However, it was found that *Ndufs4*$^{-/-}$ glycolytic fibres ultimately exhibit dramatically lower residual levels of CI activity, compared to *Ndufs4*$^{-/-}$ oxidative fibres, due to their inherently lower mitochondrial content. This observation was later linked to a more severely altered metabolic profile in *Ndufs4*$^{-/-}$ glycolytic fibres, which could possibly be ascribed to a biochemical threshold effect. The severe reduction in CI activity did not seem to dramatically affect the activities of citrate synthase (CS) or the rest of RC (CII-CIV). However, *Ndufs4*$^{-/-}$ solei did display a moderate decrease in the activity of two of these enzymes. The first, CIII (18 % reduction), is known to partially stabilise CI subassemblies in *Ndufs4*$^{-/-}$ muscle (Calvaruso *et al.*, 2012); while the second, CS (12 % reduced), has been suggested to reflect alterations in *Ndufs4*$^{-/-}$ muscle Krebs cycle activity rather than mitochondrial content (Alam *et al.*, 2015). Although we report the first muscle fibre type-specific enzymatic data in *Ndufs4*$^{-/-}$ mice, our CI activity results agree well with previous literature reports in *Ndufs4*$^{-/-}$ muscles (Calvaruso *et al.*, 2012; Alam *et al.*, 2015). Altogether, the objectives of the second phase of the study were well achieved, thereby confirming that the *Ndufs4* knockout dramatically reduces CI activity in both glycolytic (white quadriceps) and oxidative (soleus) muscles, while possibly leaving glycolytic fibres more vulnerable. Hence, our observations on a biochemical level warranted the further investigation

of *Ndufs4*$^{-/-}$ skeletal muscle on a metabolic level in order to elucidate how the tissue phenotypically appears unaffected, despite having a greatly reduced electron flux from CI to the RC.

6.2.3 Phase III: metabolic profiling — Chapter 4, Chapter 5 and Annexure B

The third phase of the study entailed the in-depth metabolic profiling of glycolytic and oxidative muscles from *Ndufs4*$^{-/-}$ mice (P45-50). The selected metabolomics approach required the analysis of a single sample on multiple analytical platforms i.e., ^{1}H-NMR, LC-MS/MS and GC-TOF-MS. Due to the insensitivity of NMR spectroscopy and the limited sample quantity obtained from mice — especially in the case of aged *Ndufs4*$^{-/-}$ mice who lose a significant amount of body weight — we required a financially feasible NMR protocol suited for limited-quantity biological samples. Consequently, we developed a novel miniaturised ^{1}H-NMR protocol (**Objective 3.1**), which requires only one-tenth (60 µL) of the sample volume normally needed, with no additional costly adjustments to instrument hardware. This resulted in a publication in *Metabolomics* (Mason *et al.*, 2018) in which we demonstrated, via statistical equivalence testing, that the novel method performs acceptably compared to an established SOP. Equivalence testing was done on samples of spiked synthetic urine as well as *Ndufs4*$^{-/-}$ muscle extracts, which therefore took into account the effect of biological matrices in downscaling the NMR method. Furthermore, we demonstrated the novel method's advantages for large-scale metabolomics as it is able to increase metabolome coverage when adequate sample quantities are available (through sample concentration); and produce reliable metabolic profiles from minute sample quantities (~ 4 mg) with strong discriminative power.

After establishing the suitability of our novel method for multi-platform metabolomics, we standardised the metabolomics analyses (miniaturised ^{1}H-NMR, LC-MS/MS and GC-TOF-MS protocols) for both mouse muscle types (**Objectives 3.1 to 3.3**). During this process, we determined the sample quantity required for each analysis. While quadriceps sample quantities were adequate, it was concluded that soleus samples were too minute for tri-platform analysis. Consequently, soleus samples could only be analysed on the two most sensitive platforms (LC-MS/MS and GC-TOF-MS). Next, we evaluated the repeatability with which the various analyses could be performed on the two mouse muscle types. All three metabolomics platforms demonstrated good intra- and inter-batch repeatability as well as metabolome coverage; however, soleus samples displayed moderately higher variance compared to quadriceps samples — possibly due to the difference in sample quantity.

Once method standardisation was complete, multi-platform metabolic profiling of white quadriceps and soleus skeletal muscles from *Ndufs4*$^{-/-}$ (n = 19) and WT (n = 20) mice was

carried out successfully (**Objectives 3.4**). Next, a suitable bioinformatics workflow was selected and the data from all platforms were individually preprocessed and pretreated (**Objectives 3.5**). The data proved to be of good quality, with no obvious batch effects or biases evident. Statistical analyses revealed a respective 48 and 34 metabolites discriminating *Ndufs4*$^{-/-}$ and WT white quadriceps and soleus muscles (**Objectives 3.6**). The obtained metabolic profiles were then extensively investigated via pathway analysis and from our biological interpretations, several novel hypotheses were generated (**Objectives 3.7**). These results, together with the enzymatic data obtained in Phase II of the study, were published in *Biochimica et Biophysica Acta (BBA) — Molecular Basis of Disease* (Terburgh *et al.,* 2019). In the aforementioned publication, we report the first empirical evidence of an adaptive response in *Ndufs4*$^{-/-}$ skeletal muscles aimed at compensating for the lack of CI-mediated electron input into the RC. Our metabolic data suggests that this adaptive response attempts to restore electron flux to CIII through alternative fuels and non-classical pathways that supply the RC ubiquinone (Q) pool with electrons. However, a disturbed redox balance still seemed to result in congested mitochondrial pathways. Some of the most noteworthy metabolic alterations observed in *Ndufs4*$^{-/-}$ muscles identified the glycerol-3-phosphate (GP) shuttle, the electron transfer flavoprotein (ETF/ETF-QO) system, complex II of the RC, and the proline cycle as key adaptive pathways fuelling the Q pool. In addition to supplying electrons, some of these mechanisms potentially replenish NAD^+ levels (GP shuttle and proline cycle), while others might contribute to redox imbalance (NAD^+ consuming reactions fuelling ETF/ETF-QO and the Krebs cycle) or ROS production (m-GPDH, ETF-QO, CII, CIII, and ProDH) in CI deficiency. Although these metabolic and bioenergetic adaptations were surprisingly similar between *Ndufs4*$^{-/-}$ glycolytic and oxidative muscle types, the disturbances due to CI deficiency seemed to be more evident in glycolytic fibres, possibly due to their low (biochemical threshold-breaching) residual CI activity.

Conclusively, all objectives of the third phase of this study were fittingly achieved. Our research successfully provided an explanatory metabolic basis for the lack of an obvious muscle phenotype in *Ndufs4*$^{-/-}$ mice. In addition, our observations also make sense of previous puzzling reports of normal ATP production capacity in CI deficient skeletal muscles (Kruse *et al.*, 2008; Alam *et al.*, 2015). Furthermore, as the ability of skeletal muscle to compensate for a reduction in CI-mediated electron transfer via the Q-cycle is previously undocumented, our findings open up new areas of MD disease research that should be further explored. It currently remains unclear whether the adaptive responses we identified are capable of efficiently sustaining muscle energy homeostasis in cases of nutrient deprivation, exercise challenges, or insults to the immune system; how this change in muscle metabolism affects whole-body health; and whether similar adaptive mechanisms take place in other tissues.

6.3 Strengths and limitations of the study

6.3.1 Animals and sampling

6.3.1.1 Strengths

A great strength of the study is found in the number of animals used, which provided high statistical power. Obtaining such a relatively large, genetically homogenous MD cohort, is currently not feasible for human samples due to the rare and heterogeneous nature of these disorders. In addition, the relative absence of genetic background-, medication- or diet-induced variability among highly interbred, genetically modified mice, greatly simplifies the interpretation of metabolomics data. Another strength of the study lies in the inclusion of two different muscle types. In addition to this being the first metabolomics study on *Ndufs4*$^{-/-}$ skeletal muscle, ours is also the first research on fibre type-specific metabolic and enzymatic alterations due to CI deficiency. Furthermore, identifying similar metabolic alterations in *Ndufs4*$^{-/-}$ two skeletal muscles, with vast differences in fibre type composition and size, greatly increases the credibility of our results.

6.3.1.2 Limitations

Although phenotypic studies on such a large animal group were not within the scope of this study, it proved to be a limitation in two ways. First, in retrospect, we observed that animal age did not seem to best indicate disease progression and severity — as the biological variation (phenotypic, enzymatic and metabolic) among *Ndufs4*$^{-/-}$ mice was greater than expected within such a tight age range (P45-50). Although the inter-group variation and statistical power of our sample sizes were enough to overcome this intra-group variation, we strongly recommend the use of phenotype score sheets, rather than age, to determine uniform disease progression and animal endpoints. Second, with a recent publication (Foriel *et al.*, 2018) highlighting the possibility of feeding difficulties in animal models of MD, we realised that animal feeding habits should have been better monitored to ensure that differential nutrient intake did not complicate results, especially in the case of metabolomics analyses. Further limitations include the exclusion of female mice from the study as well as the inherent difference in the metabolism of mice and humans. While we acknowledge the need and importance of including females in research, we have to emphasise the known hormonal and metabolic differences between sexes (Wells *et al.*, 2016; Ruoppolo *et al.*, 2018). As mentioned in Section 3.2.1, research should focus on comparing sex-specific mechanisms and metabolic responses to disease, rather than combining both sexes into a single group. However, this was beyond the scope of our study as we merely aimed to generate hypotheses on the basic underlying mechanisms of a very

complex disease. Therefore, in order to minimise sex-related metabolic variation, we decided to focus on one sex-group. Once the basic mechanisms of the disease are clearer, sex-specific targeted metabolic investigations should most certainly be done.

6.3.2 Multi-platform metabolomics approach

6.3.2.1 Strengths

A key strength of the study was the use of various analytical platforms, as opposed to one, to enable large-scale metabolomics of *Ndufs4*$^{-/-}$ skeletal muscles. As different metabolomics platforms favour the detection of compounds with different chemical properties, we could obtain a larger metabolome coverage by combining untargeted (^{1}H-NMR spectrometry and GC-TOF-MS) as well as targeted (LC-MS/MS) analyses. In addition, identifying important discriminatory metabolites on more than one metabolomics platform considerably increases the confidence in results and adds credibility to the data. Furthermore, the application of large-scale metabolomics in MD research is uncommon, even though it is an information-rich tool with great potential for elucidating disease mechanisms — hence, our multi-platform metabolomics approach provided the opportunity to obtain novel information on MD mechanisms. Another strength lies in the miniaturised ^{1}H-NMR method we developed, which enabled the inclusion of this valuable technique in the multi-platform metabolomics of mouse white quadriceps samples — something not previously feasible in our department.

6.3.2.2 Limitations

One of the limitations associated with multi-platform metabolomics in this study is the sample quantities required. Generally, sample quantities do not present a problem for metabolomics analyses, however, difficulties arise when working with limited amounts of biological samples e.g. mouse tissues or biofluids. Although more sensitive techniques, such as targeted LC-MS/MS, do not require large sample volumes individually, the combination of this technique with other methods — such as innately insensitive NMR — greatly increases the sample quantities needed. Consequently, we were unable to analyse soleus samples on all three analytical platforms, thereby losing valuable information on metabolites solely detected with the excluded technique i.e. ^{1}H-NMR spectroscopy.

6.3.3 Metabolomics data and bioinformatics

6.3.3.1 Strengths

Although the bioinformatics of metabolomics data is a daunting, often ambiguous process — one strength of this study includes the fact that our metabolomics data was processed and

analysed via different methods (Annexure B). This included the pipeline discussed in Section 3.5.4, with and without missing value imputation, using different normalisation methods (single internal standard- and mass spectrum total useful signal-normalisation); as well as the XERp variable selection and classification method for metabolomics data described by van Reenen *et al.* (2017). Although there were clear differences in mean values, variation and metabolite rank, ultimately, the shortlist of discriminatory metabolites obtained in each case, was quite similar. Obtaining such similar results using various data analyses methods greatly increased the reliability of our findings and confirmed the biological relevance of our results.

6.3.3.2 Limitations

Selecting the most suitable metabolomics data preprocessing and pretreatment methods, proved to be the greatest bottleneck of the study. As there are currently no standardised bioinformatics guidelines or pipelines for metabolomics datasets, the choice of method largely depends on the dataset properties, the selected data analysis methods and the research question (van den Berg *et al.*, 2006). Starting with data preprocessing methods, it is known that missing value imputation, and the various methods[41] with which to achieve this, have different effects on the number and rank of metabolites identified as important. Selecting a single missing value imputation method was, therefore, difficult as each available technique has inherent merits and disadvantages regarding the assumptions it makes and biases it introduces into data. The same was observed for different normalisation methods[42], of which some methods seemed to greatly reduce the technical variation of certain metabolites, while not affecting or increasing errors in others. From our observations, it became clear that no single internal standard or normalisation method is appropriate for all classes of chemical compounds in a dataset. Furthermore, different data pretreatment methods[43] also seemed to differentially affect the data means and variances, the influence of technical errors and ultimately, the statistical conclusions — again each method having its own advantages and drawbacks. An additional shortcoming lies in the fact that metabolite identification from untargeted metabolomics studies, remains considerably problematic to the field (Dunn *et al.*, 2013; Beisken *et al.*, 2015; Schrimpe-Rutledge *et al.*, 2016). This limitation was evident in our untargeted metabolomics data, as some of the important features detected, could not be identified. These unknown, albeit important, metabolites were excluded from our biological interpretation. Consequently, by

[41] e.g. half smallest value, mean, K-nearest neighbours (KNN), fuzzy K-means (FKM), singular value decomposition (SVD), bayesian principal component, analysis (bPCA), and multiple imputations by chained equations (MICE) etc. (Schmitt *et al.*, 2015).

[42] e.g. internal standard-, isotope internal standard-, mass spectrum total useful signal (MTUS)-, interquartile range (IQR)- normalisation etc.

[43] .e.g. centering, autoscaling, pareto scaling, range scaling etc. (van den Berg *et al.*, 2006).

essentially ignoring the contribution of these unknowns, important information is lost and an incomplete metabolic profile is used to generate hypotheses.

6.4 Future prospects

6.4.1 Applying the novel miniaturised ^{1}H-NMR method

The miniaturised ^{1}H-NMR method we presented in Chapter 4 provides researchers with a cost-effective way to analyse limited-quantity biological samples or increase metabolome coverage with a standard machine set up — a previously impossible task. This opens up the possibilities for research projects at our department as well as other research groups that do not have a dedicated NMR spectrometer for small-volume analyses or the funding to obtain such a set-up. In this manner, our technique could enable researchers to easily obtain more information from biological samples.

6.4.2 Investigating the adaptive pathways identified

Our extensive metabolic profiles of *Ndufs4*$^{-/-}$ skeletal muscles, discussed in Chapter 5, provide new insight into LS disease mechanisms, which paves the way for future research and new experimental approaches in the field of MD research. Our results highlight several possible key players in CI deficiency, of which many metabolites and pathways (such as *N*-acetylasparte, proline and the proline cycle, as well as the glycerol-3-phosphate shuttle) are poorly researched in general. Hence, our work emphasises the need to elucidate the over-all functional mechanisms and physiological roles of these pathways in addition to their possible roles in MD. As this was a discovery-phase, hypothesis-generating study, further investigations of our postulations are required to validate our findings. These validation studies should include more targeted techniques such as metabolic flux analyses of the adaptive pathways that we identified. Furthermore, a comparison of these and related metabolic pathways in other tissues (e.g. the brain) could possibly provide answers to the variety of tissue-specific phenotypes observed. Such investigations should examine the tissue-specific availability of metabolites (certain amino acids, -derivatives, fatty- or organic acids etc.) that fuel these pathways, as well as the capacity of these metabolic fuels and adaptive pathways to rescue ATP production in different CI deficient tissues. Ultimately, future studies building upon our findings could provide novel insight into targeted therapeutic interventions, which may help to compensate for CI deficiency and LS.

6.5 References

Alam, M.T., Manjeri, G.R., Rodenburg, R.J., Smeitink, J.A.M., Notebaart, R.A., Huynen, M., Willems, P.H.G.M. & Koopman, W.J.H. 2015. Skeletal muscle mitochondria of NDUFS4$^{-/-}$ mice display normal maximal pyruvate oxidation and ATP production. *Biochimica et Biophysica Acta — Bioenergetics*, 1847(6-7):526-533.

Beisken, S., Eiden, M. & Salek, R.M. 2015. Getting the right answers: understanding metabolomics challenges. *Expert Review of Molecular Diagnostics*, 15(1):97-109.

Calvaruso, M.A., Willems, P., van den Brand, M., Valsecchi, F., Kruse, S., Palmiter, R., Smeitink, J.A.M. & Nijtmans, L.G.J. 2012. Mitochondrial complex III stabilizes complex I in the absence of NDUFS4 to provide partial activity. *Human Molecular Genetics*, 21(1):115-120.

Dunn, W.B., Erban, A., Weber, R.J.M., Creek, D.J., Brown, M., Breitling, R., Hankemeier, T., Goodacre, R., Neumann, S. & Kopka, J. 2013. Mass appeal: metabolite identification in mass spectrometry-focused untargeted metabolomics. *Metabolomics*, 9(1): 44-66.

Foriel, S., Beyrath, J., Eidhof, I., Rodenburg, R.J., Schenck, A. & Smeitink, J.A.M. 2018. Feeding difficulties, a key feature of the *Drosophila* NDUFS4 mitochondrial disease model. *Disease Models & Mechanisms*, 11:10.

Kruse, S.E., Watt, W.C., Marcinek, D.J., Kapur, R.P., Schenkman, K.A. & Palmiter, R.D. 2008. Mice with mitochondrial complex I deficiency develop a fatal encephalomyopathy. *Cell Metabolism*, 7(4):312-320.

Mason, S.W., Terburgh, K. & Louw, R. 2018. Miniaturized ^{1}H-NMR method for analyzing limited-quantity samples applied to a mouse model of Leigh disease. *Metabolomics*, 14:1-12.

Ruoppolo, M., Caterino, M., Albano, L., Pecce, R., Di Girolamo, M.G., Crisci, D., Costanzo, M., Milella, L., Franconi, F. & Campesi, I. 2018. Targeted metabolomic profiling in rat tissues reveals sex differences. *Scientific Reports*, 8(1):4663.

Schmitt, P., Mandel, J. & Guedj, M. (2015) A comparison of six methods for missing data imputation. *Journal of Biometrics & Biostatistics*, 6(1):2155-6180.

Schrimpe-Rutledge, A.C., Codreanu, S.G., Sherrod, S.D. & McLean, J.A. 2016. Untargeted Metabolomics Strategies—Challenges and Emerging Directions. *Journal of the American Society for Mass Spectrometry*, 27(12):1897-1905.

Terburgh, K., Lindeque, J.Z., Mason, S.W., van der Westhuizen, F.H. & Louw, R. 2019. Metabolomics of *Ndufs4*$^{-/-}$ skeletal muscle: adaptive mechanisms converge at the ubiquinone-cycle. *Biochimica et Biophysica Acta — Molecular Basis of Disease*, 1865(1):98-106.

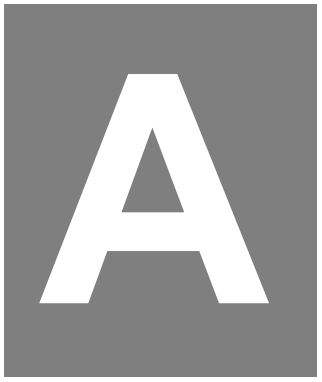
Valsecchi, F., Monge, C., Forkink, M., de Groof, A.J.C., Benard, G., Rossignol, R., Swarts, H.G., van Emst-de Vries, S.E., Rodenburg, R.J., Calvaruso, M.A., Nijtmans, L.G.J., Heeman, B., Roestenberg, P., Wieringa, B., Smeitink, J.A.M., Koopman, W.J.H. & Willems, P.H.G.M. 2012. Metabolic consequences of NDUFS4 gene deletion in immortalized mouse embryonic fibroblasts. *Biochimica et Biophysica Acta — Bioenergetics*, 1817(10):1925-1936.

van den Berg, R.A., Hoefsloot, H.C., Westerhuis, J.A., Smilde, A.K. & van der Werf, M.J. 2006. Centering, scaling, and transformations: improving the biological information content of metabolomics data. *BioMed Central — Genomics*, 7(1):142.

van Reenen, M., Westerhuis, J.A., Reinecke, C.J. & Venter, J.H. 2017. Metabolomics variable selection and classification in the presence of observations below the detection limit using an extension of ERp. *BioMed Central — Bioinformatics*, 18(1):83.

Wells, A., Barrington, W., Threadgill, D., Dearth, S., Campagna, S., Saxton, A. & Voy, B. 2016. Gene, sex and diet interact to control the tissue metabolome. *Federation of American Societies for Experimental Biology Journal*, 30(1_supplement):122-127.

ANNEXURE



Animal information

A.1 Introduction

This section contains information on the animals used in the study. First, the results from the genotypic characterisation of the mice are discussed. Second, the animals used in phase II (Table A-1) and phase III (Table A-2) of the study are described, regarding their specific animal ID- and litter numbers, age, and the time *post-mortem* at which their skeletal muscle tissues were snap frozen.

A.2 Genotypic characterisation of Ndufs4 mice

The genotype of each mouse (n = 61) selected for this study was confirmed via polymerase chain reaction (PCR) amplification of a section spanning the second exon of the mouse *Ndufs4* gene using *post-mortem* collected tail snips (as discussed in Section 3.3). Genotyping results from this study corresponded to that initially used to select the mice and therefore confirmed that the correct animals were euthanised. During each analysis, tailsnip derived DNA from control mice (*Ndufs4*$^{-/-}$, *Ndufs4*$^{+/+}$, and *Ndufs4*$^{+/-}$) were amplified along with that of the collected samples. The resulting PCR products were then separated via agarose gel electrophoresis along with a DNA size marker (ladder) used to estimate amplicon sizes. All DNA samples were acceptably pure with an A_{260}/A_{280} ratio of ~ 1.8. Figure A-1 represents the typical PCR genotyping results obtained in the study. For a complete list of sample names and confirmed genotypes (all gel results not shown) refer to Table A-1 and Table A-2.

The first lane in the gel (Figure A-1) contains a 100-1000 bp DNA ladder, with lanes three to five depicting controls. *Ndufs4*$^{-/-}$ DNA (lane 3) display an intense band corresponding to a 429 bp fragment of the *Ndufs4* gene from which an 800 bp region (including exon two) was removed. *Ndufs4*$^{+/+}$ DNA (lane 4) display an intense band at 1229 bp, as exon two is present in *Ndufs4* gene fragments, while *Ndufs4*$^{+/-}$ DNA (lane 5) display both the disrupted (429 bp) and intact (1229 bp) *Ndufs4* amplicons. However, it should be noted that very faint, non-specific bands were observed in the lanes containing *Ndufs4*$^{+/+}$ (~ 429 bp) and *Ndufs4*$^{+/-}$ (~ 813 bp) DNA. Despite previous attempts[44] to prevent non-specific DNA amplification, these bands were ascribed to non-specific PCR amplification, as they were consistently observed across all samples during the initial genotyping (performed by a laboratory analyst) as well as the genotype confirmation done in this study. Nevertheless, our genotyping results agreed with that

[44] The laboratory analyst who optimised the used PCR method tried to resolve the observed non-specific DNA amplification by varying several parameters including: different primer preparations, annealing temperatures, cycling times, concentrations, thermal cycler ramp rate, and employing a DMSO gradient (Mereis, 2017).

reported by Valsecchi *et al.* (2012) and could be successfully used to clearly distinguished *Ndufs4*$^{+/-}$ from *Ndufs4*$^{+/+}$ genotypes.

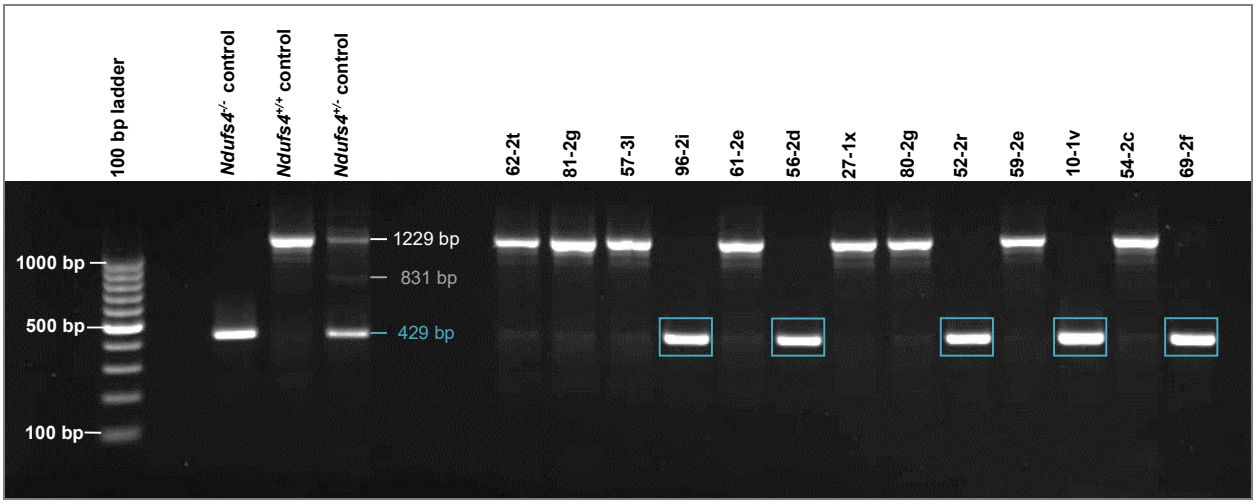


Figure A-1: Agarose gel electrophoretogram depicting PCR genotyping results obtained from mouse tailsnip-DNA. A representative 1.0 % agarose gel electrophoretogram illustrating the amplified PCR products from 13 of the mice used in the study (lanes numbered according to sample name, see Tables A-1 and A-2 for details) along with a 100-1000 bp DNA ladder (lane 1), and amplified PCR products for control DNA: *Ndufs4*$^{-/-}$ (lane 3; 429 bp), *Ndufs4*$^{+/+}$ (lane 4; 1229 bp) and *Ndufs4*$^{+/-}$ (lane 5; 1229 bp, 831 bp, and 429 bp). *Ndufs4*$^{-/-}$ samples are highlighted with blue rectangles.

Table A-1: Animals used for biochemical evaluation

Genotype	ID number	Litter number	Postnatal day	Time[45] (min)
Ndufs4$^{-/-}$	39	5g	48	08:30
	48	5h	48	07:28
	90	5o	46	07:30
	2	5p	46	07:40
	14	5q	46	06:45
	17	5q	46	06:58
	35	5s	46	07:40
	43	5t	46	08:14
	44	5t	46	09:33
	46	5t	46	08:26
	52	5v	46	09:06
	60	5w	46	09:10
WT	65	5j	48	08:50
	67	5j	48	10:19
	93	5o	46	08:08
	1	5p	46	08:08
	3	5p	46	08:50
	25	5r	46	07:59
	34	5s	46	07:50
	42	5t	46	09:00
	67	5x	46	07:30
	69	5x	46	08:35

[45] Time from euthanasia to liquid nitrogen quenching

Table A-2: Animals used for metabolic profiling

Genotype	ID number	Litter number	Postnatal day	Time[46] (min)
Ndufs4$^{-/-}$	68	1o	46	11:00
	70	1o	46	08:00
	10	1v	48	09:36
	56	2d	46	12:42
	69	2f	48	10:00
	96	2i	46	14:01
	52	2r	49	11:57
	28	3g	49	12:50
	37	3j	48	13:20
	44	3k	46	10:00
	86	3q	49	11:44
	2	3s	49	12:10
	54	4a	46	09:58
	2	4i	48	10:16
	8	4j	48	09:24
	20	4m	47	09:51
	34	4o	47	09:53
	42	4q	49	08:20
	50	4s	45	10:15
WT	8	1v	48	08:22
	27	1x	47	09:25
	54	2c	47	11:00
	59	2e	46	11:23
	61	2e	47	12:02
	80	2g	48	12:27
	81	2g	48	12:27
	62	2t	48	10:58
	2	3c	47	09:48
	9	3d	47	12:40
	42	3k	46	09:58
	57	3l	46	10:08
	83	3p	49	10:53
	88	3q	49	11:05
	9	3t	49	09:00
	19	3u	49	08:49
	35	3x	49	08:42
	40	3y	49	08:27
	48	3z	46	08:34
	63	4b	46	08:20
	62	4b	46	08:59

[46] Time from euthanasia to liquid nitrogen quenching

A.3 References

Mereis, M. 2017. Evaluating the involvement of metallothionein I in complex I deficiency: an *in vitro* study. Potchefstroom: NWU. (Dissertation — MSc).

Valsecchi, F., Monge, C., Forkink, M., de Groof, A.J.C., Benard, G., Rossignol, R., Swarts, H.G., van Emst-de Vries, S.E., Rodenburg, R.J., Calvaruso, M.A., Nijtmans, L.G.J., Heeman, B., Roestenberg, P., Wieringa, B., Smeitink, J.A.M., Koopman, W.J.H. & Willems, P.H.G.M. 2012. Metabolic consequences of NDUFS4 gene deletion in immortalized mouse embryonic fibroblasts. *Biochimica et Biophysica Acta — Bioenergetics*, 1817(10):1925-1936.

ANNEXURE B

Method standardisation and data integrity

B.1 Standardising the spectrophotometric enzyme assays

B.1.1 Introduction

In this section, the standardisation of the various spectrophotometric assays (BCA, CS, CI, CII, CIII, and CIV) will be discussed. As mentioned in Section 3.4, these assays were performed according to standard operating protocols of the Mitochondria Research Laboratory (NWU) standardised on human muscle samples. Therefore, here the aim of standardisation was to establish the mouse sample volume required for each assay, while confirming assay operation within the linear range. Thereby, comparable and reproducible results were ensured. Due to the difference in oxidative capacity of different muscle types (explained in Section 2.8), it was necessary to standardise the assays for both the white quadriceps (WQ) and soleus (SOL) muscles respectively. Standardisation was done using mitochondria-enriched 700 ×g supernatant prepared from 10 % (w/v) murine muscle homogenate (as described in Section 3.4). Due to the small size of SOL muscles (~ 5 mg), preparing a 10 % (w/v) homogenate from a single mouse was not practically feasible. Therefore, the SOL muscles from six WT mice (~ 53 mg) were pooled to prepare a 10 % (w/v) homogenate used to standardise the first few assays (BCA, CS, and CI). Consequently, these results were used to calculate the sample volumes required when using a 2 % (w/v) homogenate (as was the case during the final analysis). Thereafter, a 2 % (w/v) homogenate was used to standardise the rest of the RC enzyme assays for the SOL muscles.

B.1.2 Standardising the protein assay (BCA method)

The optimal protein content (µg) per well and assay linearity were evaluated by analysing different volumes (5, 10, and 15 µL) of a 1:5 working dilution of 700 ×g supernatants, in triplicate. The BCA assay was performed as described in Section 3.4. Results are visible in Figure B-1, with each data point representing the mean (n = 3) absorbance vs. protein content per well obtained for each volume. The protein content of the two skeletal muscle supernatants were quite similar (~ 4 µg/µL). For both the WQ (Figure B-1 A) and the SOL (Figure B-1 B) muscles, a sufficiently linear relationship ($R^2 > 0.99$) was observed between the volume supernatant added per well (i.e. µg protein) and the absorbance measured. The optimal protein content per well was selected to be ~ 8 µg, thereby accommodating experimental variation on either side of the midpoint in the protein concentration range (Figure B-1 A and B).

To demonstrate that the BCA assay performed with acceptable repeatability and precision, the protein content from 22 (n = 10 WT and n = 12 *Ndufs4*$^{-/-}$) WQ (Figure B-1 C) and SOL (Figure B-1 D) samples were determined and displayed in relation to the BSA standard curve. The assays were done using 10 µL of a 700 ×g supernatant from a 10 % (w/v) WQ homogenate

(diluted 1:5) and a 2 % (w/v) SOL homogenate (undiluted). All 22 data points of each muscle type were shown to be quantified within the linear range of the BSA standard curve (R^2 > 0.999). The average protein concentration for the WQ and SOL muscles were respectively determined as 3.90 ± 0.2 µg/µL (CV = 5.9 %) and 0.85 ± 0.8 µg/µL (CV = 8.9 %).

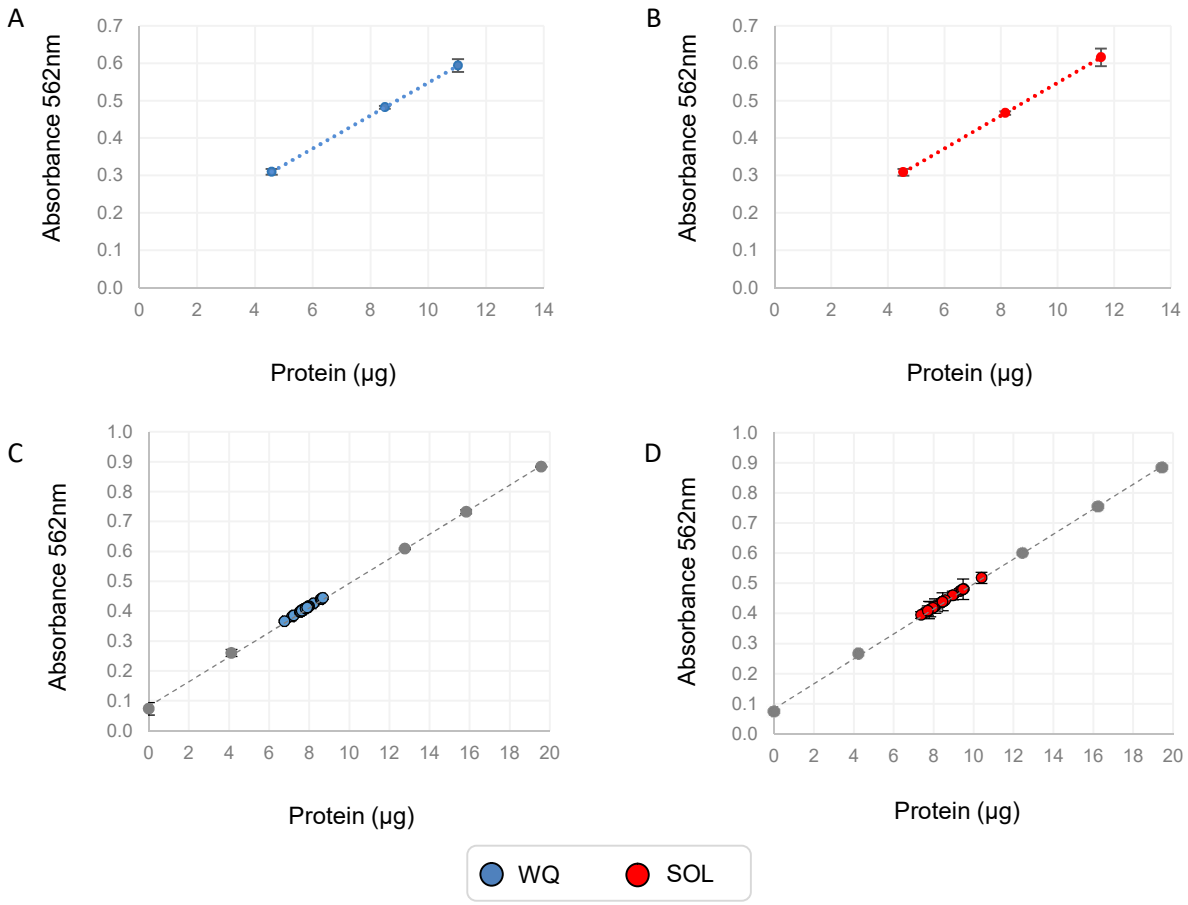


Figure B-1: BCA assay linearity for mitochondria-enriched 700 ×g supernatants of mouse skeletal muscle homogenates. A-B: Assay linearity (R^2 > 0.99) shown for **A:** white quadriceps (WQ) and **B:** soleus (SOL) by analysing different volumes (5, 10, and 15 µL) of a 1:5 dilution of a 700 ×g supernatant prepared from a 10 % (w/v) homogenate. Each volume was analysed in triplicate and protein content was determined from a BSA standard curve. Each data point represents the average absorbance (± SD, too small to be visualised in some cases) vs. the average protein content per well obtained for each volume. **C-D:** Protein determination of 700 ×g supernatants from 22 mice shown to be quantified within the linear range of the BSA standard curve (R^2 > 0.999). Grey symbols represent different volumes of BSA standard (0, 4, 8, 12, 16, and 20 µL), while coloured symbols represent 700 ×g supernatant of muscle homogenates. Each data point represents the average absorbance (± SD, too small to be visualised in some cases) vs. the average protein content per well obtained for 10 µL triplicates of **C:** a 1:5 dilution of WQ supernatant (10 %, w/v homogenate) and **D:** undiluted SOL supernatant (2 %, w/v homogenate).

B.1.3 Standardising the citrate synthase assay

For the citrate synthase (CS) assay, the optimal sample volume required per well and assay linearity were evaluated by analysing different volumes (2.5, 3.3, and 5 µL) of a working dilution (WQ: 1:10 dilution and SOL: 1:15 dilution) of 700 ×g supernatants, in triplicate. The CS assay was performed as described in Section 3.4. Results are visible in Figure B-2 with each data

point representing the mean (n = 3) initial reaction velocity (v_0 in mAbs/min) measured over 3 minutes vs. the effective sample volume (µL) added per well. As expected, CS activity was considerably higher in the oxidative SOL muscles compared to the glycolytic WQ muscles. The assays for both muscle types displayed a sufficiently linear relationship (R^2 > 0.99) between the initial reaction velocity and sample volume added per well. Therefore, the optimal effective sample volume per well was selected to be 0.4 µL and 0.3 µL of WQ and SOL supernatants, respectively — allowing experimental variation on either side of the dilution range.

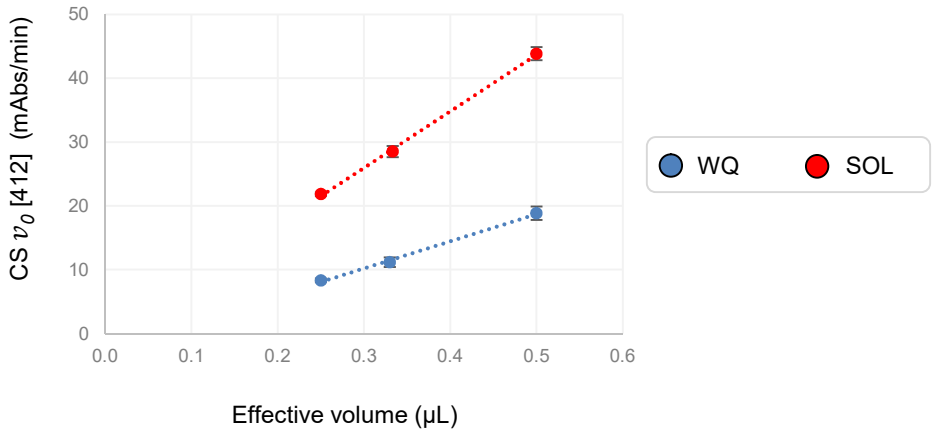


Figure B-2: CS assay linearity for mitochondria-enriched 700 ×g supernatants of mouse skeletal muscle homogenates. Assay linearity (R^2 > 0.99) shown for the WQ and SOL by analysing different volumes (2.5, 3.3, and 5 µL) of a 1:10 dilution for the WQ and a 1:15 dilution for the SOL 700 ×g supernatant prepared from a 10 % (w/v) homogenate. Each volume was analysed in triplicate with data expressed as an average of v_0 ± SD (too small to be visualised in some cases). *Abbreviations: SOL, soleus; WQ, white quadriceps.*

B.1.4. Standardising the respiratory chain enzyme assays

For each skeletal muscle type, the optimal amount of RC enzyme (CI, CII, CIII, and CIV) per well and assay linearity were evaluated by analysing the initial reaction velocity (v_0 in mAbs/min) of the assays of a sample dilution series. Each assay was performed as described in Section 3.4, with results visible in Figure B-3 as the mean (n = 3) v_0 measured over 3 minutes vs. the effective sample volume (µL) loaded per well for each data point.

For the CI assay, the dilution series contained 4, 6, 8, and 10 µL of undiluted WQ supernatant and 2, 4, and 6 µL of 1:2 diluted SOL supernatant. For both the WQ (Figure B-3 A) and the SOL (Figure B-3 B) muscles, an adequately linear relationship (R^2 > 0.99) was observed between the volume supernatant added per well and the initial reaction velocity measured for the entire dilution series. The optimal volume per well was selected based on the desired CI v_0 values in the absence of rotenone (or v_1 values, as defined in Section 3.4.4) of WT mice in order to have that of *Ndufs4*$^{-/-}$ mice (which is expected to be lower) still fall within the linear range of the assay. Therefore, effective sample volumes corresponding to CI v_0 values of ~ 50 mAbs/min were

selected — thereby accommodating experimental variation on either side of the dilution series (Figure B-3 A and B). The selected effective volumes were, therefore, 9 µL and 2 µL for the WQ and SOL, respectively. Hence, 10 µL of 9:1 diluted supernatant is required for the WQ (10 %, w/v homogenate) while 10 µL of undiluted supernatant is required for the SOL muscles (2 %, w/v homogenate).

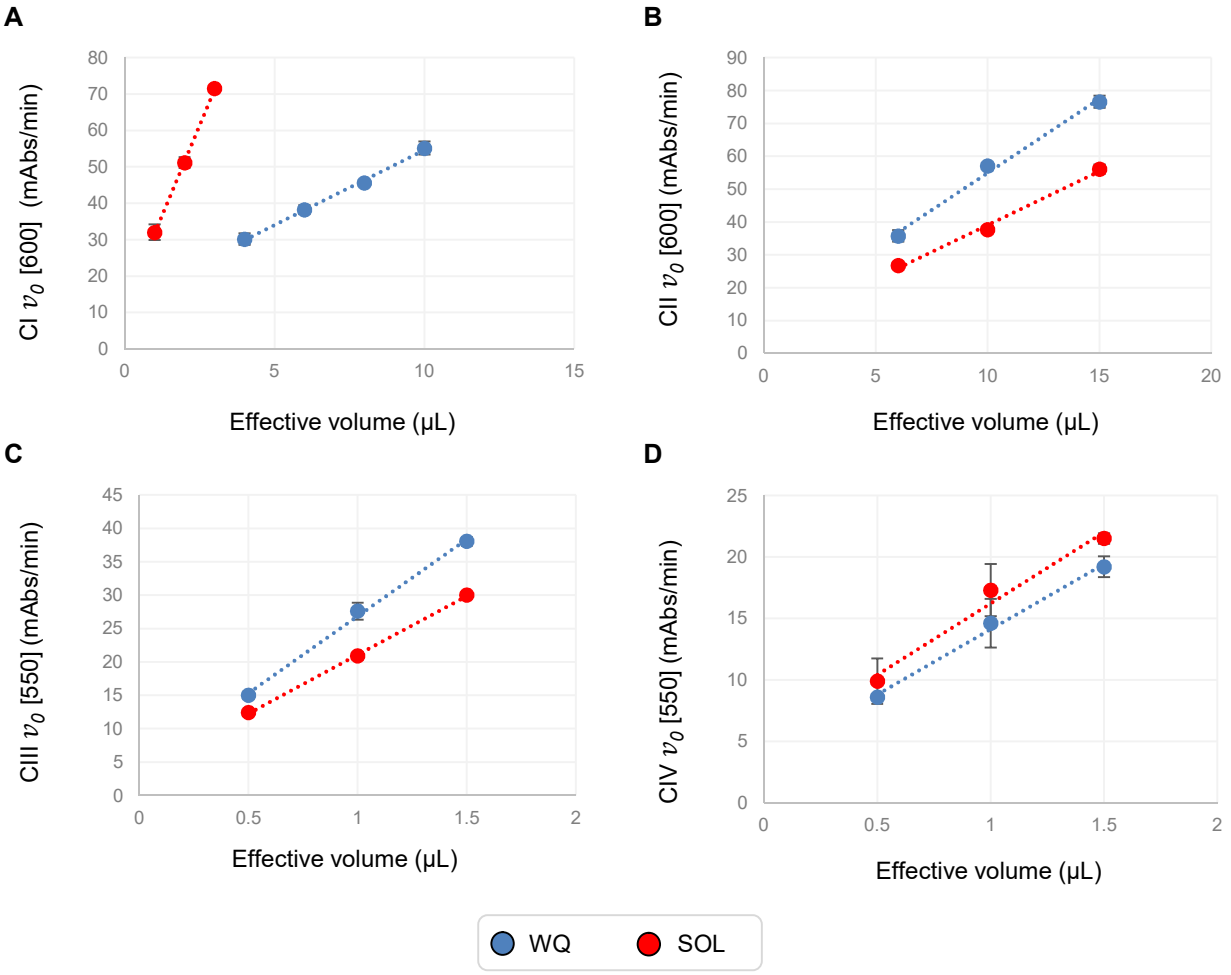


Figure B-3: Respiratory chain enzyme assay linearity for mitochondria-enriched 700 ×g supernatants of mouse skeletal muscle homogenates. Plots of initial reaction velocity (v_0) measured at a specific wavelength vs effective supernatant volume analysed per well for CI, CII, CIII, and CIV assays. Assay linearity ($R^2 > 0.99$) was shown for **A:** CI by analysing 4, 6, 8, and 10 µL of undiluted WQ and 2, 4 and 6 µL of 1:2 diluted SOL supernatants; **B:** CII by analysing 6, 10, and 15 µL of undiluted WQ and SOL supernatants; **C:** CIII and **D:** CIV by analysing 5, 10, and 15 µL of 1:10 diluted WQ and SOL supernatants. For the CI assay, supernatants were prepared from a 10 % (w/v) homogenate for both muscle types and each volume was analysed in triplicate. The assays for the rest of the RC enzymes were prepared from a 10 % (w/v) WQ homogenate and 2 % (w/v) SOL homogenate respectively, with each volume analysed in duplicate. Data were expressed as the average v_0 values ± SD (too small to be visualised in some cases). *Abbreviations: SOL, soleus; WQ, white quadriceps.*

The dilution series for the rest of the RC enzymes were performed on 10 % (w/v) and 2 % (w/v) WQ and SOL 700 ×g supernatants, respectively. The dilution series consisted of duplicate reactions containing 6, 10, and 15 µL of undiluted WQ and SOL 700 ×g supernatant for CII; and 5, 10, and 15 µL of a 1:10 diluted WQ and SOL 700 ×g supernatant for CIII and CIV. As evident

in Figures B-3 B to D, all assays were sufficiently linear (R^2 > 0.99) for the entire dilution series. The volumes selected for the final assays were, therefore, near the midpoint of the linearity graph with 8 µL of undiluted WQ and SOL supernatant selected for the CII assay; 10 µL of a 1:9 dilution of WQ and SOL supernatant selected for the CIII assay; as well as 7.5 µL of a 1:9 dilution of WQ and 5 µL of a 1:9 dilution of SOL supernatant selected for the CIV assay.

B.2 Standardising the metabolic profiling methods

B.2.1 Introduction

Standardisation of the metabolic profiling methods (^{1}H-NMR, GC-TOF-MS, and LC-MS/MS) entailed, firstly, determining the sample volume and internal standard (IS) concentration required for each analysis via a sample dilution series (data not shown) and secondly, performing repeatability studies to determine intra- and inter-batch precision. The latter will be discussed in this section, along with the data quality of the final analyses.

B.2.2 Repeatability and intermediate precision studies

Repeatability and intermediate precision studies were carried out by firstly preparing a single pooled sample extract for each muscle type (WQ and SOL). For each analytical platform, five replicates of each muscle extract were then separately prepared (as described in Section 3.5) and analysed on the same day (repeatability [intra-batch]) after which, muscle extract samples were prepared and analysed on two separate days (intermediate precision [inter-batch]). The amount of intra- and inter-batch variability for each metabolite detected, was then described relative to the mean value obtained from the replicates, by determining the percentage coefficient of variance (CV) as seen in Equation B-1. The mean ($\bar{x}$) and standard deviation (SD) values were calculated using the abundances of each metabolite detected in the sample replicates.

Equation B-1: Percentage coefficient of variance

$$\% \, CV = \frac{SD}{\bar{x}} \times 100$$

$\bar{x}$ = average and SD = standard deviation

Figure B-4 depicts the CV distribution of metabolites identified via GC-TOF-MS (A-B), LC-MS/MS (C-D) and miniaturised ^{1}H-NMR spectroscopy (E). Table B-3 provides a summary of these CV distribution values. The typical precision cut-off for targeted analyses is a CV-value of > 15-20 % (FDA, 2001), while that for untargeted metabolomics analyses is a CV-value of > 50 % (Dunn *et al.*, 2012). The targeted metabolomics approach (LC-MS/MS) proved to be the most precise technique with more than 85 % of the detected metabolites in both muscles having an intra-and inter-batch CV-value of < 10 %. Between the two untargeted techniques, the

miniaturised ^{1}H-NMR method had the highest precision with intra- and inter-batch CV-values of < 10 % for more than 80 % and 70 % respectively of the metabolites identified in both muscle types. Although still adequately high for an untargeted metabolomics technique, the precision of the GC-TOF-MS was the lowest, with more than 80 % of the metabolites detected having an intra-and inter-batch CV-value of < 40 %. This relatively higher CV distribution can be ascribed to the untargeted nature the analysis, and mainly, sample derivatisation — as the silylation reaction continues over time[47] (Erban *et al.*, 2007; Fiehn, 2008) and ultimately leads to differences in the extent of compound derivatisation or decomposition among samples analysed throughout a batch. Furthermore, it was evident from the results that white quadriceps samples were prepared and analysed with less variability than soleus samples, which is most likely due to the tenfold greater sample quantity available for that muscle type. Altogether, it was clear from the repeatability studies that the total variation (from sample workup to analysis) for each metabolomics technique was sufficiently low and that the methods were adequately repeatable to yield good quality data.

B.2.3 Data quality

To establish whether the various methods did indeed perform with acceptable repeatability, the final dataset for each tissue type, obtained from each analytical platform, was visually inspected for between-batch effects — as the final muscle extract samples [*Ndufs4*$^{-/-}$ (n = 19), WT (n = 20) and QC (n = 6) samples] were analysed in two batches, over two days. Figure B-5 provides an overview of the data quality obtained in each case, using a scatter plot of the samples in the order that they were analysed on the instrument (x-axis) vs the total signal obtained for each sample (y-axis). The total signal of each sample was calculated as the sum of the relative peak intensities (after IS normalisation) of all metabolites measured in the sample. Figures B-5 A to E were inspected regarding the distribution of QC samples and the general scatter of the rest of the samples in the batches. From the distribution of the QC samples, it was clear that there were no obvious intra- or inter-batch drift throughout the analyses — as all QC samples horizontally aligned with each other. Regarding the remaining samples, there were no noticeable trends in the overall scatter of the data points that could be attributed to technical variation. Therefore, visible differences in the data distribution were ascribed to inherit biological variance along with variations due to sample preparation. After important metabolite selection, the individual data matrices were then combined for each muscle type and inspected according

[47] The derivatisation reaction is not quenched, since the silylation solvent (BSTFA/TMCS) is never removed from the samples. Therefore, the silylation reaction is able to continue as the samples are standing in the auto sampler prior to their analysis. Considering the runtime per sample and the amount of samples in a batch, the samples analysed at the begging, middle and end of a batch are subjected to significantly different derivatisation lengths before analysis.

to the clustering of *Ndufs4*$^{-/-}$, WT, and QC groups using principal component analysis (PCA) scores plots (Figure B-6). The close clustering of QC samples in both Figures B-6 A and B-6 B indicates good data quality for the white quadriceps and soleus respectively. Altogether, both the repeatability study as well as the evaluation of the final data matrix demonstrated that the metabolomics methods provided repeatable data with good quality

Table B-1: GC-TOF-MS intra- and inter-batch CV-values for the quadriceps and soleus

CV range (%)	Percentage of total metabolites (%)			
	Quadriceps		Soleus	
	Intra-batch	Inter-batch	Intra-batch	Inter-batch
<10	52	8	35	14
10-20	19	30	24	27
20-30	14	27	18	32
30-40	5	16	13	14
40-50	3	9	4	7
>50	7	10	6	6

Table B-2: LC-MS/MS intra- and inter-batch CV-values for the quadriceps and soleus

CV range (%)	Percentage of total metabolites (%)			
	Quadriceps		Soleus	
	Intra-batch	Inter-batch	Intra-batch	Inter-batch
<10	95	95	96	87
10-20	5	5	4	11
20-30	0	0	0	0
30-40	0	0	0	2
>40	0	0	0	0

Table B-3: ^{1}H-NMR spectroscopy intra- and inter-batch CV-values for the quadriceps

CV range (%)	Percentage of total metabolites (%)	
	Quadriceps	
	Intra-batch	Inter-batch
<10	87	71
10-20	8	18
20-30	3	3
30-40	3	3
40-50	0	3
>50	0	3

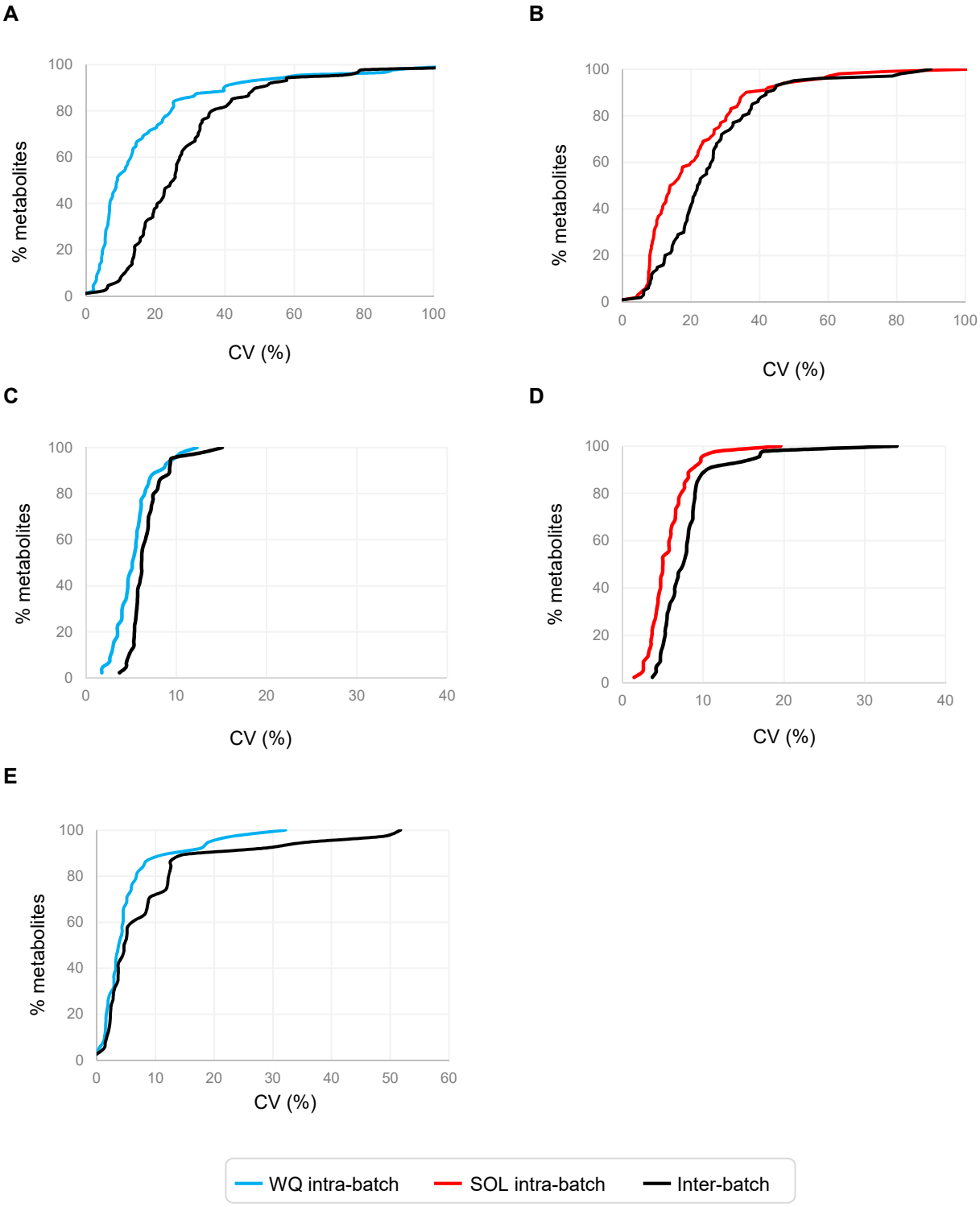


Figure B-4: Performance of the various metabolic profiling methods. The intra-batch (WQ: blue, SOL: red) and inter-batch (black) relative coefficient of variance (CV) of sample replicates from GC-TOF-MS analysis of pooled **A:** white quadriceps and **B:** soleus samples; LC-MS/MS analysis of pooled **C:** white quadriceps and **D:** soleus samples; and **E:** miniaturised ^{1}H-NMR spectroscopy analysis of pooled white quadriceps samples. Pooled sample replicates were separately prepared and analysed in two batches over two days. For GC-TOF-MS and LC-MS/MS, each batch consisted of seven samples, while ^{1}H-NMR QC batches consisted of three samples. *Abbreviations: SOL, soleus; WQ, white quadriceps.*

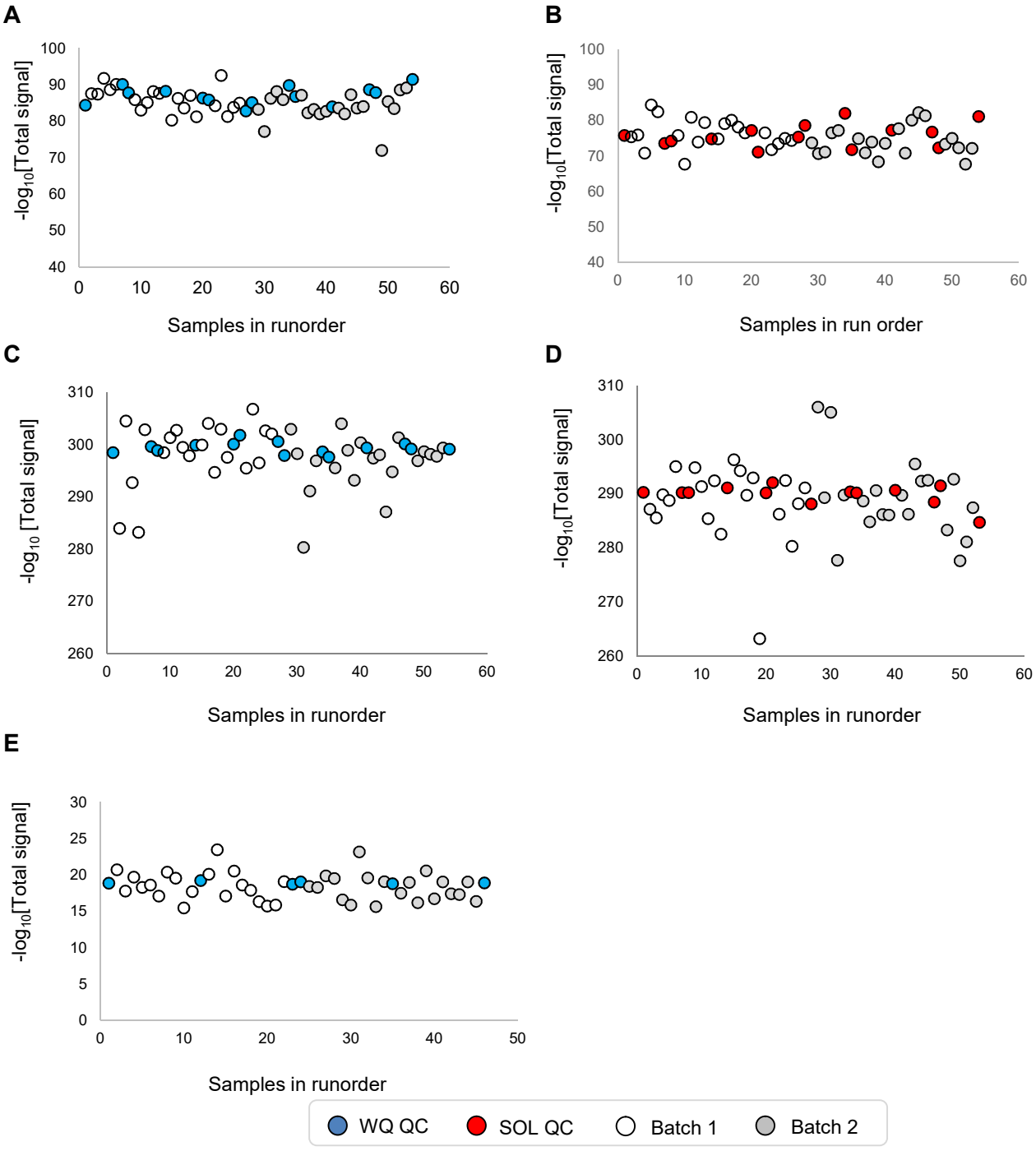


Figure B-5: Sequential total signal scatter plot of various metabolic profiling methods. Scatter plots depicting the total signal obtained for GC-TOF-MS analysis of **A:** WQ and **B:** SOL samples; LC-MS/MS analysis of **C:** WQ and **D:** SOL samples; and **E:** miniaturised ^{1}H-NMR spectroscopy analysis of WQ samples. Samples were analysed in two batches over two days and consisted of *Ndufs4*$^{-/-}$ (n = 19), WT (n = 20) and QC (n = 14/6) samples. The x-axis specifies the sample run order on each analytical platform, while the y-axis specifies the negative logarithm to the base 10 of the total signal obtained for each sample i.e. the sum of the relative peak intensities of all metabolites measured in the sample. White and grey symbols respectively indicate samples of batch one and batch two, while blue or red symbols indicate QC samples analysed throughout the batches. *Abbreviations: Ndufs4*$^{-/-}$*, Ndufs4 knockout; SOL, soleus; QC, quality control; WT, wild-type; WQ, white quadriceps.*

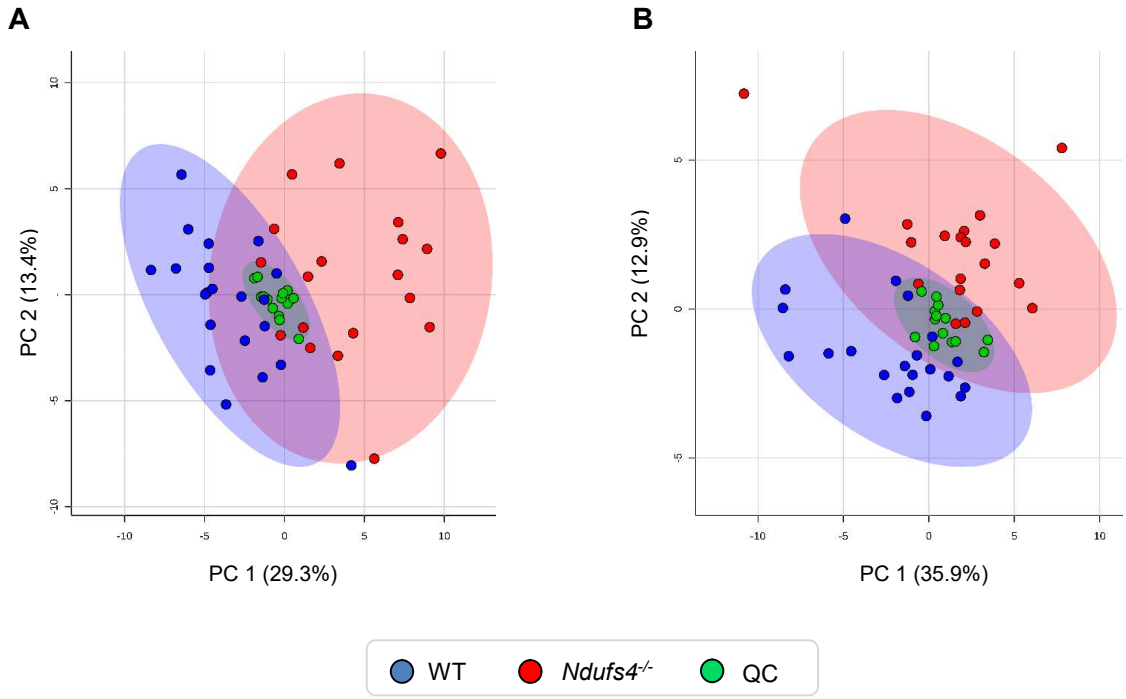


Figure B-6: Multivariate analyses indicating the clustering of groups after important metabolite selection. Principal component analysis (PCA) scores plots depicting the clustering of *Ndufs4*$^{-/-}$ (n = 19, red), WT (n = 20, blue) and QC (n = 14, green) samples after significant metabolite were selected ($p < 0.1$, $D \geq 0.5$) in A: WQ muscles and B: SOL muscles. The close clustering of QC samples indicates good data quality. *Abbreviations: Ndufs4*$^{-/-}$*, Ndufs4 knockout; SOL, soleus; QC, quality control; WT, wild-type; WQ, white quadriceps.*

B.2.4 Bioinformatics approaches

In order to ensure the selection of a suitable bioinformatics pipeline, several data preprocessing steps were assessed. First, different methods were used to normalise the data obtained from each analytical platform. The effect of each normalisation method was then investigated using i) sequential total signal scatter plots for each individual metabolite detected; and ii) the important metabolite shortlist obtained after statistical analysis. In the case of LC-MS/MS data, normalisation with DMPA and stable isotope internal standards (respectively and in combination), as well as normalisation with mass spectrum total useful signal (MSTUS), were investigated. For GC-TOF-MS data, the effect of 3-PBA-, MSTUS- and interquartile range-normalisation were inspected. For ^{1}H-NMR data, DMPA-, MSTUS- and TSP-normalisation were investigated. While all of the results cannot be reported here, Figure B-7, along with Tables B-4 and B-5, demonstrate the manner in which the different methods were compared. From our results, it was clear that no single normalisation method seemed to be appropriate for all classes of chemical compounds in the datasets. However, for the majority of metabolites, the chosen normalisation methods (as discussed in Section 3.5.4) seemed to best adjust for differences among samples and between batches.

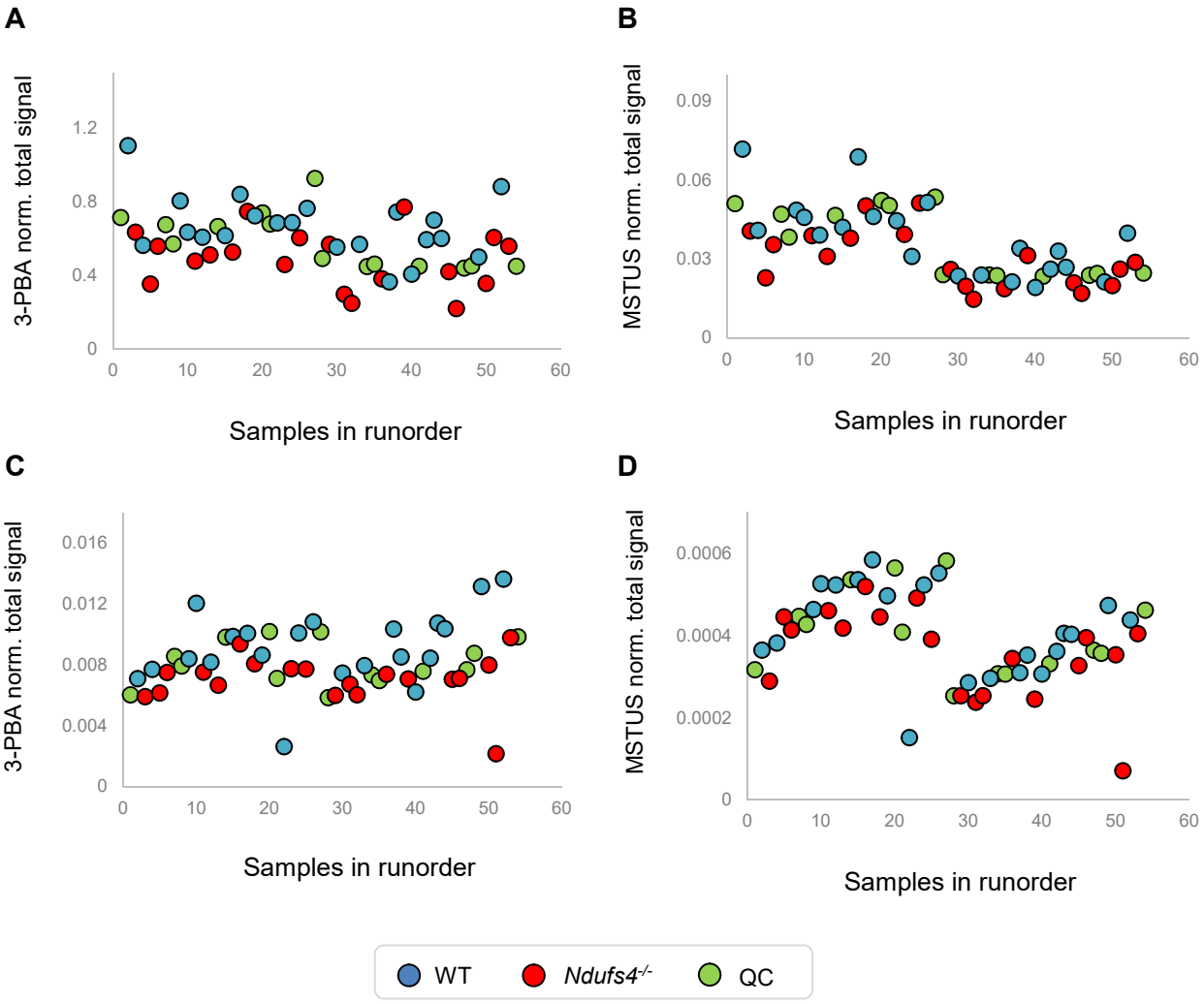


Figure B-7: The effect of different normalisation methods on the total signal scatter plots for individual metabolites. Scatter plots depicting the total signal obtained for GC-TOF-MS analysis of **A-B:** alanine in WQ samples and **C-D:** BAIBA in SOL samples when normalised using 3-PBA (A and C) vs MSTUS (B and D). Blue, red and green symbols indicate WT, *Ndufs4*$^{-/-}$ and QC samples, respectively. All metabolites were investigated in this manner. In these two cases, MSTUS normalisation enhanced inter-batch variation, while 3-PBA better compensated for the variation between batches. *Abbreviations: 3-PBA, 3-phenylbutyric acid; BAIBA, β-aminoisobutyrate; MSTUS, mass spectrum total useful signal; Ndufs4*$^{-/-}$*, Ndufs4 knockout; SOL, soleus; QC, quality control; WT, wild-type; WQ, white quadriceps.*

Next, the effect of dataset zero values on metabolite shortlists, were investigated. This was done by i) excluding the missing value replacement step from our bioinformatics pipeline; and ii) using the XERp method described by van Reenen *et al.* (2017) to select and classify discriminatory metabolites, as this extension of ERp[48] is better suited for datasets containing missing values. From these results, it was evident that the most significant discriminatory metabolites between *Ndufs4*$^{-/-}$ and WT muscles, identified via the XERp method (Table B-6),

[48] "ERp uses minimised classification error rates, based on data from a control and experimental group, to test the null hypothesis of no difference between the distributions of variables over the two groups" (van Reenen et al., 2017).

were quite similar to that obtained using the selected pipeline (described in Section 3.5.4.) with, and without, missing value replacement. Although the mean values, variation and rank of a few metabolites were considerably affected by missing value replacement, ultimately the discriminatory metabolite shortlists obtained in each case were very similar. Therefore, the replacement of dataset zero values, was included in the bioinformatics pipeline.

Table B-4: Effect of different normalisation methods on important metabolites for the white quadriceps

Selected pipeline				MSTUS normalisation			
Metabolite	**Δ direction**	**p-value**	**D-value**	**Metabolite**	**Δ direction**	**p-value**	**D-value**
GC-TOF-MS							
Creatinine	↓	0.000	2.15	Creatinine	↓	0.000	2.37
Pyruvate	↓	0.000	1.02	Succinate	↓	0.000	1.62
Proline	↓	0.000	1.20	Pyruvate	↓	0.000	0.99
Succinate	↓	0.000	0.86	Proline	↓	0.001	1.05
Glycolate	↓	0.000	1.13	4-Hydroxyproline	↓	0.002	1.00
Alanine	↓	0.001	0.94	Sulfate	↑	0.010	0.86
Glycerate	↓	0.002	0.75	Phosphate	↑	0.011	0.84
Glycerol	↓	0.005	0.79	Glycerate	↓	0.012	0.80
Malic acid	↓	0.006	0.91	Mannose	↑	0.017	0.63
3-Hydroxypyruvate	↓	0.010	0.71				
Sulfate	↑	0.026	0.69				
Pyroglutamate	↓	0.036	0.56				
Palmitate	↓	0.044	0.60				
LC-MS/MS							
Dimethylglycine	↓	0.000	2.08	Dimethylglycine	↓	0.000	2.43
2-Aminoadipate	↓	0.000	1.96	N-Acetylglutamate	↑	0.000	1.81
Proline	↓	0.000	1.86	2-Aminoadipate	↓	0.000	1.66
4-Hydroxyproline	↓	0.000	1.39	Proline	↓	0.000	1.37
C4-carnitine	↓	0.000	1.42	C2-carnitine	↑	0.000	1.47
C8-carnitine	↓	0.000	1.47	C4-carnitine	↓	0.000	1.33
N-Acetylaspartate	↑	0.000	1.39	4-Hydroxyproline	↓	0.000	1.28
Citrulline	↓	0.000	1.12	Pipecolate	↑	0.000	1.01
Threonine	↓	0.000	1.04	Citrulline	↓	0.002	1.05
Alanine	↓	0.001	1.03	Lysine	↑	0.003	0.72
Carnitine	↓	0.002	0.92	C6-carnitine	↓	0.003	0.78
1-Methylhistidine	↓	0.002	0.88	3-Methylhistidine	↑	0.008	0.87
Pipecolate	↑	0.002	1.03	1-Methylhistidine	↓	0.018	0.77
Methionine	↓	0.003	0.92	Threonine	↓	0.020	0.67
Asparagine	↓	0.003	0.99	Creatine	↑	0.029	0.68
C6-carnitine	↓	0.004	0.99	Asparagine	↓	0.036	0.65
Lysine	↑	0.006	0.72	N-Acetylglutamate	↓	0.038	0.60
Pyroglutamate	↓	0.009	0.77	C8-carnitine	↓	0.040	0.57
N-Acetylglutamate	↓	0.009	0.77	Alanine	↓	0.042	0.66
C2-carnitine	↑	0.010	0.83				
Glutamine	↓	0.011	0.74				

Table B-4 (continued)

Selected pipeline				MSTUS normalisation			
Metabolite	Δ direction	p-value	D-value	Metabolite	Δ direction	p-value	D-value
LC-MS/MS							
Trimethylglycine	↓	0.014	0.71				
C5-carnitine	↓	0.017	0.66				
Beta-Alanine	↓	0.028	0.69				
C16-carnitine	↓	0.033	0.68				
3-Methylhistidine	↑	0.038	0.66				
Glutamate	↓	0.038	0.67				
C12-carnitine	↓	0.043	0.62				
NMR							
Succinate	↓	0.000	1.49	Carnitine	↓	0.000	1.76
Carnitine	↓	0.000	1.22	Succinate	↓	0.000	1.60
Dimethyl sulfone	↑	0.000	1.03	AMP	↓	0.000	1.38
Pyruvate	↓	0.001	0.94	Dimethyl sulfone	↑	0.000	1.12
Lactate	↓	0.001	0.80	Lactic acid	↓	0.000	0.87
Alanine	↓	0.009	0.73	Alanine	↓	0.002	0.92
Lysine	↑	0.009	0.65	Glutamine	↓	0.004	0.89
AMP	↓	0.010	0.72	Pyruvate	↓	0.022	0.81
Acetate	↑	0.015	0.66	Lysine	↑	0.034	0.54
Glutamine	↓	0.015	0.71				
Methylmalonate	↑	0.030	0.67				
Choline	↑	0.037	0.67				

Symbols and abbreviations: Δ direction, change in Ndufs4$^{-/-}$ metabolite levels relative to WT; ↑ indicates increased levels in the Ndufs4$^{-/-}$; ↓ indicates decreased levels in the Ndufs4$^{-/-}$; MSTUS, mass spectrum total useful signal.

Table B-5: Effect of different normalisation methods on important metabolites for the soleus

Selected pipeline				MSTUS normalisation			
Metabolite	Δ direction	p-value	D-value	Metabolite	Δ direction	p-value	D-value
GC-TOF-MS							
Pyruvate	↓	0.000	1.40	Creatinine	↓	0.000	1.59
Creatinine	↓	0.000	1.60	Pyruvate	↓	0.000	1.22
Malate	↓	0.000	1.01	BAIBA	↓	0.001	1.08
Alanine	↓	0.004	0.82	Malate	↓	0.001	1.01
Urea	↑	0.010	0.69	Serine	↑	0.002	0.97
Serine	↑	0.015	0.80	Succinate	↓	0.002	0.91
Glycerol	↓	0.019	0.72	Urea	↑	0.003	0.89
BAIBA	↓	0.020	0.74	Alanine	↓	0.008	0.72
Succinate	↓	0.030	0.51				
Fumarate	↓	0.046	0.64				
LC-MS/MS							
Dimethylglycine	↓	0.000	2.02	Dimethylglycine	↓	0.000	2.29
2-Aminoadipate	↓	0.000	1.47	2-Aminoadipate	↓	0.000	1.08
C4-carnitine	↓	0.000	1.40	Lysine	↑	0.001	0.94
4-Hydroxyproline	↓	0.000	1.17	Pipecolate	↑	0.001	0.89
C5-carnitine	↓	0.000	1.23	C4-carnitine	↓	0.001	0.93
Citrulline	↓	0.001	1.07	Citrulline	↓	0.002	0.97
Lysine	↑	0.002	0.91	4-Hydroxyproline	↓	0.002	0.88
Alanine	↓	0.002	0.92	C5-carnitine	↓	0.003	0.91

Table B-5 (continued)

Selected pipeline				MSTUS normalisation			
Metabolite	Δ direction	p-value	D-value	Metabolite	Δ direction	p-value	D-value
LC-MS/MS							
Alanine	↓	0.002	0.92	C5-carnitine	↓	0.003	0.91
C3-carnitine	↓	0.004	0.82	C3-carnitine	↓	0.008	0.77
C6-carnitine	↓	0.005	0.83	Alanine	↓	0.008	0.83
C16-carnitine	↓	0.008	0.80	Histidine	↑	0.015	0.62
Pipecolate	↑	0.010	0.76	3-Methylhistidine	↑	0.016	0.67
Glutamate	↓	0.017	0.80	Beta-Alanine	↓	0.022	0.65
Beta-Alanine	↓	0.021	0.72	Glutamate	↓	0.035	0.59
C14-carnitine	↓	0.021	0.64	C18-carnitine	↓	0.049	0.51
C8-carnitine	↓	0.021	0.70				
C18-carnitine	↓	0.028	0.65				
C0-Carnitine	↓	0.034	0.62				
Pyroglutamate	↓	0.037	0.68				
Proline	↓	0.043	0.50				
C12-carnitine	↓	0.046	0.58				

Symbols and abbreviations: Δ direction, change in Ndufs4$^{-/-}$ metabolite levels relative to WT; ↑ indicates increased levels in the Ndufs4$^{-/-}$; ↓ indicates decreased levels in the Ndufs4$^{-/-}$; MSTUS, mass spectrum total useful signal.

Table B-6: List of important metabolites for white quadriceps and soleus muscles determined using the XERp method

Platform	Metabolite	Minimised ER	ER threshold	ER Δ direction	Observed p-value	Observed pi WT	*Ndufs4*$^{-/-}$	All	FDR threshold
WHITE QUADRICEPS									
GC-TOF-MS	Creatinine	0.10	0.00	↓	<0.0001	0	0	0	0.0001
	Succinate	0.16	0.04	↓	<0.0001	0	0.211	0	0.0001
	Proline	0.16	0.07	↓	<0.0001	0	0	0	0.0001
	Glycerate	0.17	0.00	↓	<0.0001	0	0.263	0.125	0.0001
LC-MS/MS	*N,N*-Dimethylglycine	0.03	0.00	↓	<0.0001	0	0.158	0.075	0.0031
	4-Hydroxyproline	0.13	0.00	↓	<0.0001	0	0	0	0.0031
	2-Aminoadipate	0.08	0.00	↓	<0.0001	0	0	0	0.0031
	Citrulline	0.16	0.00	↓	<0.0001	0	0	0	0.0031
	Proline	0.15	0.00	↓	<0.0001	0	0	0	0.0031
	N-Acetylaspartate	0.15	0.00	↑	<0.0001	0	0	0	0.0031
	Butyryl-carnitine (C4)	0.18	0.00	↓	0.0002	0	0	0	0.0031
	Threonine	0.20	0.00	↓	0.0003	0	0	0	0.0031
	Octanoyl-carnitine (C8)	0.20	0.00	↓	0.0003	0	0	0	0.0031
	Asparagine	0.21	0.00	↓	0.0008	0	0	0	0.0031
	N-Acetylglutamate	0.22	0.00	↓	0.0009	0.048	0.158	0.100	0.0031
	Pipecolate	0.22	0.00	↑	0.0011	0	0	0	0.0031
	Pyroglutamate	0.22	0.00	↓	0.0011	0	0	0	0.0031
	Methionine	0.22	0.00	↓	0.0014	0	0	0	0.0031
	Hexanoyl-carnitine (C6)	0.23	0.00	↓	0.0015	0.095	0.053	0.075	0.0031
	Alanine	0.24	0.00	↓	0.0025	0	0	0	0.0031
	1-Methylhistidine	0.24	0.00	↓	0.0031	0	0	0	0.0031
	Glutamine	0.24	0.00	↓	0.0031	0	0	0	0.0031
^{1}H-NMR	Succinate	0.16	0.07	↓	0.0000	0	0	0	0.0023
	Lactate	0.18	6.84	↓	0.0002	0	0	0	0.0023
	Dimethyl sulfone	0.19	0.13	↑	0.0002	0	0	0	0.0023

Table B-6 (continued)

Platform	Metabolite	Minimised ER	ER threshold	ER Δ direction	Observed p-value	Observed pi			FDR threshold
						WT	*Ndufs4*$^{-/-}$	All	
WHITE QUADRICEPS									
^{1}H-NMR	Pyruvate	0.22	0.06	↓	0.0010	0.048	0.474	0.250	0.0023
	Carnitine (C0)	0.23	0.41	↓	0.0013	0	0	0	0.0023
	Glutamine	0.24	0.72	↓	0.0023	0	0	0	0.0023
SOLEUS									
GC-TOF-MS	Pyruvate	0.16	0.01	↓	<0.0001	0	0	0	0.0003
	Creatinine	0.19	0.01	↓	0.0002	0	0	0	0.0003
	BAIBA	0.20	0.12	↓	0.0003	0	0	0	0.0003
LC-MS/MS	*N,N*-Dimethylglycine	0.07	0.00	↓	0.0000	0.048	0.211	0.125	0.0007
	2-Aminoadipate	0.14	0.00	↓	0.0000	0	0	0	0.0007
	Pipecolate	0.21	0.00	↑	0.0007	0	0	0	0.0007

Important metabolites discriminating between *Ndufs4*$^{-/-}$ and WT muscles are listed according to the rank of their significant observed p-values. The third column lists the minimised error rate (ER), while and the fourth and fifth columns list the associated ER threshold and ER direction, respectively. The three columns listed under "Observed pi" report the proportion of zeros in each group as well as in the combined data set ("All"). The last column lists the false discovery rate (FDR) threshold. *Abbreviations: ER Δ direction, direction of the minimised error rate; BAIBA, β-aminoisobutyrate; Ndufs4*$^{-/-}$*, Ndufs4 knockout; WT, wild-type.*

B.3 References

Dunn, W.B., Wilson, I.D., Nicholls, A.W. & Broadhurst, D. 2012. The importance of experimental design and QC samples in largescale and MS-driven untargeted metabolomic studies of humans. *Bioanalysis*, 4(18):2249-2264.

Erban, A., Schauer, N., Fernie, A.R. & Kopka, J. 2007. Nonsupervised construction and application of mass spectral and retention time index libraries from time-of-flight gas chromatography-mass spectrometry metabolite profiles. *(In* Weckwerth, W., *ed.* Metabolomics — Methods in Molecular Biology. Clifton, NJ: Humana Press. p. 19-38).

FDA (Food and Drug Administration). 2001. Guidance for industry, bioanalytical method validation. https://www.fda.gov/downloads/Drugs/GuidanceComplianceRegulatoryInformation/Guidances/ucm070107.pdf, Date accessed: 12 Apr. 2017.

Fiehn, O. 2008. Extending the breadth of metabolite profiling by gas chromatography coupled to mass spectrometry. *Trends in Analytical Chemistry*, 27(3):261-269.

van Reenen, M., Westerhuis, J.A., Reinecke, C.J. & Venter, J.H. 2017. Metabolomics variable selection and classification in the presence of observations below the detection limit using an extension of ERp. *BioMed Central — Bioinformatics*, 18(1):83.

ANNEXURE C

Published peer-reviewed article I

Metabolomics (2018) 14:74
https://doi.org/10.1007/s11306-018-1372-6

ORIGINAL ARTICLE

Miniaturized ^{1}H-NMR method for analyzing limited-quantity samples applied to a mouse model of Leigh disease

Shayne Mason[1] · Karin Terburgh[1] · Roan Louw[1]

Received: 18 December 2017 / Accepted: 15 May 2018
© Springer Science+Business Media, LLC, part of Springer Nature 2018

Abstract

Introduction The analysis of limited-quantity samples remains a challenge associated with mouse models, especially for multi-platform metabolomics studies. Although inherently insensitive, the highly specific characteristics of nuclear magnetic resonance (NMR) spectroscopy make it an advantageous platform for global metabolite profiling, particularly in mitochondrial disease research.

Objectives Show method equivalency between a well-established standard operating protocol (SOP) and our novel miniaturized ^{1}H-NMR method.

Method The miniaturized method was performed in a 2 mm NMR tube on a standard 500 MHz NMR spectrometer with a 5 mm triple-resonance inverse TXI probe at room temperature.

Results Firstly, using synthetic urine spiked with low (50 µM), medium (250 µM) and high (500 µM) levels (n = 10) of nine standards, both the SOP and miniaturized method were shown to have acceptable precision (CV < 15%), relative accuracy (80–120%), and linearity ($R^2 > 0.95$), except for taurine. Furthermore, statistical equivalence was shown using the two one-sided test. Secondly, pooled mouse quadriceps muscle extract was used to further confirm method equivalence (n = 3), as well as explore the analytical dynamics of this novel approach by analyzing more-concentrated versions of samples (up to 10× concentration) to expand identification of metabolites qualitatively, with quantitative linearity. Lastly, we demonstrate the new technique's application in a pilot metabolomics study using minute soleus muscle tissue from a mouse model of Leigh syndrome using *Ndufs4* KO mice.

Conclusion We demonstrate method equivalency, supporting our novel miniaturized ^{1}H-NMR method as a financially feasible alternative to cryoprobe technology—for limited-quantity biological samples in metabolomics studies that requires a volume one-tenth of the SOP.

Keywords Nuclear magnetic resonance (NMR) spectroscopy · Miniaturized · Metabolomics · *Ndufs4* KO mice, Leigh disease · Mouse model studies

1 Introduction

Nuclear magnetic resonance (NMR) spectroscopy is one of the most information-rich analytical techniques available (Lindon et al. 2004). In contrast to its highly specific nature, however, NMR is inherently insensitive—a restriction that precludes its application when samples are very limited in quantity (Fratila and Velders 2011). Here, limited-quantity samples are defined as < 20 mg of tissue. Increases in the sensitivity of NMR experiments have been achieved by improving upon the hardware, in particular by the use of miniaturized coils and greater field strength. In the late 1990s, the first examples of cryogenic NMR probe technology became available, and these high-sensitivity NMR

Electronic supplementary material The online version of this article (https://doi.org/10.1007/s11306-018-1372-6) contains supplementary material, which is available to authorized users.

✉ Shayne Mason
nmr.nwu@gmail.com

[1] Centre for Human Metabolomics, Faculty of Natural and Agricultural Sciences, North-West University (Potchefstroom Campus), Private Bag X6001, Potchefstroom, South Africa

Published online: 21 May 2018

probes have now become more readily available to investigators faced with small samples (Martin 2005). All these developments in the analysis by NMR of small volumes and improvements in sensitivity have ultimately relied upon advances in technology and spectrometers. Often, however, it is not financially feasible to set up a dedicated NMR spectrometer for small-volume analyses. Compromise is achieved by developing new analytical methods.

In a 2014 study, Glaves et al. addressed the issue of limited-quantity samples from animal models in metabolomics studies. These authors developed a tube-in-tube system (2 mm NMR tube containing sample biofluid within a 5 mm NMR tube containing NMR standards) to analyze ~ 30 µL biofluids (probe not reported) in high-throughput, longitudinal, multimodal metabolomics studies of small animals. The compartmentalization of sample and NMR standards in this tube-in-tube method, however, had the limitation of requiring chemical shift correction due to bulk magnetic susceptibility and ionic strength changes. Further improvements in the analytical method came from the Bruker company (Rheinstetten, Germany) and their development of the MATCH adaptor system, which consisted of a gripper that holds NMR tubes < 5 mm in diameter and can be loaded into a standard 5 mm probe. Indeed, as small as 3 mm NMR tubes have been used for analysis of various biofluids, but require ~ 200 µL of sample, for example (most recently): saliva (190 µL; Figueira et al. 2016); urine (250 µL; Cassiède et al. 2017); astrocyte–motor neuron co-cultures (250 µL; Madji Hounoum et al. 2017). Furthermore, these studies utilizing 3 mm NMR tubes were all done using cryoprobes. In the study reported here, we specifically explored the uses of 2 mm NMR tubes, capable of holding a 60 µL sample, with the Bruker MATCH adaptor system on a room temperature probe.

The use of 2 mm NMR MATCH tubes itself is not novel, as it has been adopted elsewhere, for example in: biogeosciences (Schmitt-Kopplin et al. 2012a); a drug metabolism study (Johansson et al. 2009); and characterization of meteorite material (Schmitt-Kopplin et al. 2012b). These three studies reported using 2 mm NMR MATCH systems, although, also all relied upon cryoprobes, and none were used for murine models in metabolomics. In our case, we report the first use of the 2 mm NMR MATCH system in the broad analysis of the metabolite profile in biofluids in the field of metabolomics, demonstrated first using spiked synthetic urine, followed by extracted muscle tissue samples from *Ndufs4* KO (knockout) mice. Muscle tissues were chosen as they are among the most metabolically active and, consequently, the most affected by mitochondrial disorders such as Leigh disease (Li et al. 2013). Comprehensive multi-platform metabolomics of tissues from mouse models remains a challenge due to the limited quantities of analyte obtained from mice. Multi-platform metabolomics of skeletal muscles with different fiber compositions is required to understand better the pathophysiological consequences of complex I deficiency in this tissue. Since the oxidative properties and unique subpopulations of muscle mitochondria depend on the muscle fiber composition (Koves et al. 2005), it is imperative to investigate both glycolytic and oxidative muscles. Glycolytic muscles, for example quadriceps, can be found in adequate quantities for metabolomics, whereas the primarily oxidative soleus is quite small (~ 4 mg in total in *Ndufs4* KO mice). However, because complex I deficiency influences oxidative phosphorylation, it is imperative to investigate the muscle type most reliant on this pathway for energy production, which is the soleus muscles.

Here, we use a routine 500 MHz NMR setup with a 5 mm triple-resonance inverse (TXI) probe head in a biofluid analysis laboratory at room temperature and present a novel miniaturized method for limited-quantity samples (just 60 µL) that yields a result with equivalence with that of an established standard operating protocol (SOP) using a sample ten times greater. First, we tested the analytical parameters of this miniaturized method by using spiked synthetic urine. We show that there is acceptable equivalence between our miniaturized method and a well-established SOP, with the advantage of requiring ten times less sample. Next, using the more-abundant mouse quadriceps muscle, we further confirmed method equivalency and explored the analytical dynamics of the miniaturized method by concentrating samples up to ten times and demonstrating, qualitatively, increased identification of metabolites, with quantitative linearity. Finally, we concluded by applying this miniaturized method to the limited-quantity samples of minute soleus muscle from *Ndufs4* KO mice in a pilot metabolomics study of Leigh disease.

2 Materials and methods

2.1 Spiked synthetic urine

A biological matrix in the form of synthetic urine (surine) was used to spike with nine commercially available metabolites commonly found in muscle tissue, namely: lactic acid (Lac), alanine (Ala), taurine (Tau), glycine (Gly), adenosine 5′-monophosphate (AMP), guanidineacetic acid (GAA), 3-hydroxybutyric acid (3-HB), carnitine (Car) and choline (Chol). Using stock solutions of each of the nine metabolites, prepared in surine, a combined stock concentration of 500 µM of each metabolite was created—designated high concentration. Thereafter, medium (250 µM) and low (50 µM) concentration spiked surine mixtures were prepared from the high concentration mixture by diluting 2× and 10× respectively with surine.

2.2 Animals and sampling

The AnimCare animal research ethics committee of North-West University approved (NWU-00378-16-A5) the animal protocols used here. All animals were maintained and all procedures performed in accordance with the code of ethics in research, training and testing of drugs in South Africa and complied with national legislation. *Ndufs4* KO mice (B6.129S4-*Ndufs4*$^{tm1.1Rpa}$/J) along with age- and sex-matched controls (wild type; WT) born from heterozygous crosses (https://www.jax.org/strain/027058; Jackson Laboratories, Maine, USA) were used. Mice were held under controlled conditions of temperature (22 ± 1 °C), humidity (55 ± 10%) and light (12:12-h light/dark cycle) at the Vivarium (SAVC reg. no. FR15/13458) of the Pre-Clinical Drug Development Platform (PCDDP; NWU, RSA). The animals were fed a standard laboratory diet with food and water provided ad libitum. Mice were euthanized between P45–P50 as significant central nervous system symptoms are only apparent at this age (Kayser et al. 2016). After euthanasia via cervical dislocation, skeletal muscle tissues were rapidly dissected and snap-frozen in liquid nitrogen. Thereafter, tissues were stored at − 80 °C until extraction.

2.3 Metabolite extraction

A slightly modified monophasic Bligh–Dyer extraction method (Gullberg et al. 2004) using a solvent ratio of 6:2:2 (methanol:water:chloroform) was employed. Because approximately 80% of the wet tissue samples consists of water (i.e. 0.8 L/mg tissue), cold methanol (6 L/mg tissue), water (0.7 L/mg tissue) and internal standard (DMPA) solution (0.5µL/mg tissue; 1840 ppm in water) were added to pre-minced and pre-weighed frozen muscle tissues. Subsequently, tungsten carbide and stainless steel beads (3 mm Ø and 5 mm Ø, respectively, ~ 7:1 (w/w), Qiagen) were added to the muscle tissues in safe-lock microcentrifuge tubes (Eppendorf). Muscle tissues were pulverized in a vibration mill (MM 400, Retsch) for 2 min at 30 Hz. After the addition of chloroform (2 L/mg tissue), homogenates were thoroughly vortexed (1 min) and incubated on ice (10 min). Samples were then centrifuged at 20,000×*g* (10 min; 4 °C) and the supernatant transferred to a new tube. Quadriceps skeletal muscle tissues were used to prepare extracts for further testing of method equivalency and exploration of the miniaturized method (Sect. 3.2). A minute muscle type (both soleus muscles) were used to prepare extracts for the application of the miniaturized method in a metabolomics pilot study (Sect. 3.3).

2.4 ^{1}H-NMR sample preparation

2.4.1 NMR buffer solution

Buffer solution (1.5 M KH_2PO_4) was prepared by dissolving 20.4 g of the reagent in 80 mL of D_2O. Then 100 mg of TSP and 13 mg of NaN_3 were dissolved in 6–10 mL of D_2O and added to the solution before mixing well. After adjusting the pH to 7.4 (by adding KOH pellets), the solution was transferred to a volumetric flask and the volume adjusted to 100 mL with D_2O (Dona et al. 2014).

2.4.2 Established standard operating protocol

Of the muscle tissue extracts, 600 µL was transferred to a 2 mL screw-top glass vial (Agilent) and dried under N_2(g) at 37 °C. Solvent evaporation ensured the removal of organic solvents (methanol and chloroform) that would cause ^{1}H-NMR signal interference. Dried extracts were therefore resuspended in 600 µL sterile, filtered water to achieve single signal suppression (NOSEY pre-saturation). Sample preparation followed for both spiked surine (600 µL) and muscle tissues. Samples were centrifuged at 12,000×*g* at room temperature to remove particulates and other macromolecules. From this, 540 µL ultrafiltrate was collected and 60 µL NMR buffer solution added. Samples were then mixed in a vortex to ensure complete homogeneity and, finally, the entire volume transferred to 5 mm NMR tubes. Each tube was placed in a 5 mm spinner and loaded onto a SampleXpress autosampler for NMR analysis.

2.4.3 Miniaturized ^{1}H-NMR protocol

Of the muscle tissue extracts, 60 µL was transferred to a 2 mL screw-top glass vial (Agilent) and dried under N_2(g) at 37 °C. Each dried extract was resuspended in 60 µL sterile, filtered water. Apart from removing organic solvents, as described in 2.4.2, this resuspension step provides an opportunity to concentrate a sample (as described in Sect. 3.2.2). Sample preparation followed for both spiked surine (600 µL) and muscle tissues. Samples were centrifuged at 12,000×*g* at room temperature to remove particulates and other macromolecules. Each sample for the miniaturized method was prepared in a 2 mm NMR tube (outside Ø 2.0 mm, inside Ø 1.6 mm, length 100 mm) using the eVol® NMR digital syringe equipped with a 100 µL syringe and a 180-mm-long bevel-tipped needle. The programmed pipetting sequence of the eVol® NMR digital syringe was as follows: (1) aspirate 6 µL NMR buffer solution; (2) aspirate 54 µL sample—maintaining the 10:90% ratio of D_2O:H_2O as per standard protocol; (3) purge 60 µL (this dispenses prepared sample into 2 mm NMR tube); (4) aspirate 60 µL; (5) purge 60 µL (mix sample once inside 2 mm NMR tube to ensure

homogeneity); followed by a wash sequence: (6) aspirate 100 µL distilled water, (7) purge 100 µL (waste), (8) aspirate 100 µL distilled water, (9) purge 100 µL (waste), (10) aspirate 100 µL distilled water, (11) purge 100 µL (waste). For the miniaturized method the Bruker MATCH system was used—an adapter with a gripper to hold the 2 mm NMR tube, inserted into a 10 mm spinner. Each NMR MATCH assembly was loaded onto a SampleXpress autosampler for NMR analysis.

2.5 ^{1}H-NMR spectroscopy

Samples were measured at 500 MHz on a Bruker Avance III HD NMR spectrometer equipped with a 5 mm triple-resonance inverse (TXI) {^{1}H, ^{15}N, ^{13}C} probe head and x, y, z gradient coils. The inner coil of the TXI was optimized for ^{1}H observation, the focus of our study. ^{1}H spectra were acquired as 128 transients in 32K data points with a spectral width of 12,000 Hz (24.0 ppm) for the standard 600 µL method and 6000 Hz (12.0 ppm) for the miniaturized 60 µL method. The sample temperature was maintained at a constant 300 K. The H_2O resonance at 4.70 ppm was suppressed using the pulse sequence program NOESY-presat, which presaturates the H_2O resonance by single-frequency irradiation during a relaxation delay of 4 s, with a 90° excitation pulse of 10 µs. The acquisition time and receiver gain were set for 2.7 s and 64, respectively. The number of dummy scans = 4 and number of scans = 128, yielding a run time of 15 min and 45 s per sample. These settings follow those given by established SOPs (Beckonert et al. 2007; Dona et al. 2014).

As in the traditional NMR protocol, each sample was automatically shimmed on the deuterium signal, locked, probe tuned and matched, and pulse calibrated. NMR analysis and processing were performed using Bruker Topspin (V3.5), and further processing conducted using Bruker AMIX (V3.9.14).

2.6 Statistics

Both untargeted and targeted metabolomics approaches were used to compare methods. For the untargeted data analysis, each NMR spectrum was quantified across 376 spectral bins of equal size—0.02 ppm bins, excluding the water region of 4.0–6.0 ppm. For the targeted data analysis, nine clearly discernible, common metabolites were identified and quantified from the NMR spectra obtained for the quadriceps muscle tissue extract for both methods. The univariate analyses were performed in Excel 2013 (Microsoft), while the multivariate analyses were conducted using the online metabolomics suite MetaboAnalyst 3.0 (Xia et al. 2015).

For the pilot study, the data were investigated with a targeted and untargeted approach. The data were normalized to the IS before an 80% zero filter was applied. Thereafter, the data were log transformed and variables important in projection (VIPs) were selected using the Student's *t* test ($p < 0.05$). Principle component analyses (PCA) score plots (MetaboAnalyst 3.0) were used to illustrate the natural separation in the data.

3 Results and discussion

The experimental workflow can be divided into three phases (illustrated in Fig. 1). First, acceptable equivalence between the ^{1}H-NMR SOP and miniaturized method was established

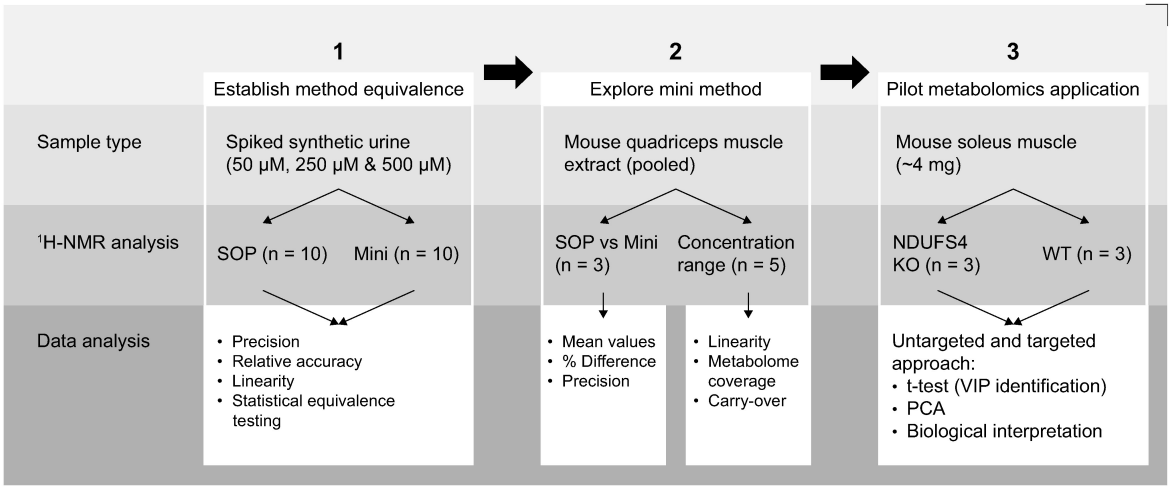


Fig. 1 Experimental design and workflow

by analyzing surine spiked with nine standards at low, medium, and high levels (n = 10). Second, pooled mouse muscle extract was used to further confirm this method equivalence (n = 3), as well as explore the capability of the miniaturized ^{1}H-NMR method. A concentration range (up to 10×) prepared from a pooled muscle extract in replicates of five was used to show quantitative linearity for nine metabolites, as well as the ability of the miniaturized method to effectively increase analytical sensitivity (i.e. metabolome coverage) through sample concentration. In addition, water blanks were analyzed in between samples in order to show no carry-over when using the same eVol® syringe. Third, the applicability of the miniaturized ^{1}H-NMR method on the metabolomics of limited-quantity samples was demonstrated in a pilot study on the soleus muscle from a mouse model of Leigh syndrome.

3.1 Establishing method equivalency

The aim of method equivalency here was to prove that one method performs within an acceptable range of another for the intended application. Therefore, the acceptability of the miniaturized ^{1}H-NMR method as an alternative to the current SOP, when faced with limited sample quantities, was investigated. The samples used in the equivalency tests were chosen based on the desired application (i.e. metabolomics analysis of biological matrices) and therefore consisted of surine spiked with low (50 µM), medium (250 µM) and high (500 µM) levels of standards. Ten replicate samples were prepared at each of the three concentrations, per method. Hence, from the generated ^{1}H-NMR spectra, 30 data points were available for each method to test method equivalency. Again, due to the intended metabolomics application, the miniaturized method's acceptability was judged based upon: precision (coefficient of variation (CV) < 15%), relative accuracy (80–120%), linearity ($R^2 > 0.95$), and statistical equivalence ($p < 0.05$) to the SOP using the two one-sided test (TOST).

3.1.1 Precision

As a measure of precision, the CV was determined for each method at each concentration level (low, medium and high). The results (Table 1) were weighed against predefined acceptable limits of variation. For samples spiked with low levels of standards (near the detection limit) a CV < 15% was considered acceptable while CVs < 10 and < 5% were considered acceptable for the medium and high concentration levels, respectively. These precision cut-off values lie below the specified levels set out by the FDA for targeted studies: "the precision determined at each concentration level should not exceed 15% of the CV except for the lower limit of quantification, where it should not exceed 20% of the CV." (US FDA 2001), and far below the CV cut-off value of 50% typically used in metabolomics studies (Dunn et al. 2012). As expected, the SOP proved to be more precise than the miniaturized method, which despite having slightly higher variance still performed with excellent precision. For both methods CVs fell well below the predefined limits in almost all cases (< 2% in high and medium levels, and

Table 1 Measure of precision and accuracy

Standards CV% (recovery %)	Low		Medium		High	
	SOP	Mini	SOP	Mini	SOP	Mini
Lactic acid	5.1 (95–114)	5.5 (95–114)	0.3 (100–101)	1.1 (101–105)	0.3 (100–101)	1.1 (102–106)
Alanine	1.8 (98–105)	6.0 (89–108)	0.1 (100)	1.2 (100–104)	0.2 (100)	1.2 (101–105)
3-Hydroxybutyric acid	3.0 (93–103)	7.5 (91–118)	0.3 (100–100)	0.8 (101–103)	0.2 (100)	0.7 (102–104)
Choline	0.6 (99–101)	1.5 (96–100)	0.1 (100)	0.6 (98–99)	0.2 (100)	0.9 (98–102)
Carnitine	2.0 (98–106)	1.8 (101–106)	0.1 (100)	0.4 (102–103)	0.2 (100)	0.6 (103–104)
Taurine	15.0 (77–135)	16.0 (89–149)	1.7 (98–102)	4.1 (102–115)	0.7 (99–101)	2.2 (102–108)
Glycine	5.1 (91–113)	7.1 (85–113)	0.4 (100–101)	1.5 (99–104)	0.2 (100)	0.8 (102–104)
GAA	1.4 (99–104)	5.0 (90–108)	0.2 (100)	1.2 (99–102)	0.2 (100)	1.5 (99–104)
AMP	4.5 (90–105)	12.8 (79–122)	0.3 (99–100)	2.4 (97–104)	0.3 (99–100)	1.2 (101–106)

Percentage coefficient of variation (CV) and relative percentage recovery (%) for the two methods in spiked synthetic urine at low, medium and high concentrations (n = 10)

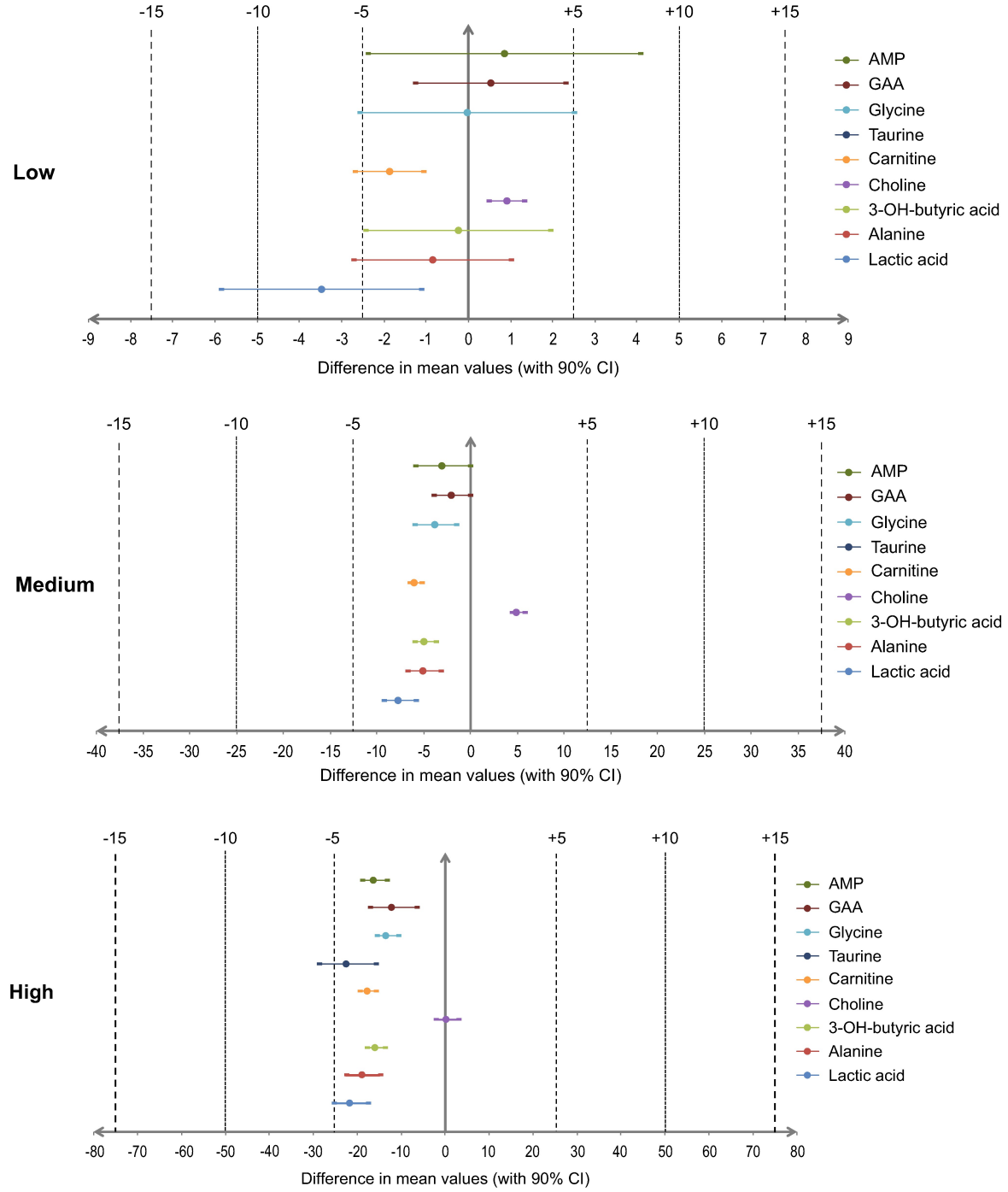


Fig. 2 Test of equivalence. TOST ($\alpha = 0.05$) comparing the two methods in spiked synthetic urine (at a low, medium and high concentration). The graphs at each concentration level display the 90% CI on the difference between the mean values ($n = 10$) obtained from the two methods for nine standards (from bottom to top: lactic acid, alanine, 3-hydroxybutyric acid, choline, carnitine, taurine, glycine, GAA, and adenosine 5′-monophosphate). Equivalence margins ($\pm\theta$) for ± 5, ± 10 and $\pm 15\%$ difference between mean values are displayed. If $|CI| < \theta$, reject H0 and conclude equivalence

< 10% in low levels). The only exceptions were seen with taurine and AMP. Taurine had a relatively high CV in both the SOP and miniaturized methods (clearly visible at low level). The higher CV observed for taurine is known, previously reported in quantitative ^{1}H-NMR analysis (Hohmann et al. 2014) to have mean recovery rates ranged between 97.1 and 108.2%, yielding an average value of 104.2 ± 4.9%. For AMP, the SOP performed better than the miniaturized method (4.5 vs. 12.8%) at the lowest level.

3.1.2 Relative accuracy

Relative recovery (Table 1) was used as a measure of accuracy at each concentration level. Recovery using the miniaturized method was compared to that of the SOP (where the average recovery of the SOP was taken as 100%). A recovery range of 80–120% was deemed acceptable as per bioanalytical method validation standards (Chan et al. 2004). The miniaturized method performed well within these parameters for the medium and high concentrations. However, again, taurine, and to a small degree AMP, fell outside this acceptable recovery range at low concentrations.

3.1.3 Linearity

Linear least squares regression was used to measure the correlation between the results obtained from the SOP and miniaturized method. For each standard the average (n = 10) concentration obtained using the SOP was plotted against that obtained from the miniaturized method across varying concentration levels (low, medium, and high). A coefficient of determination (R^2) larger than 0.95 was considered to describe a sufficiently linear relationship between the two methods. The results obtained were as follows: lactic acid ($y = 0.96x + 0.17$; $R^2 = 0.999$); alanine ($y = 0.96x + 2.43$; $R^2 = 0.999$); 3-HB ($y = 0.96x + 2.37$; $R^2 = 1.000$), choline ($y = 0.99x + 2.59$; $R^2 = 0.999$), carnitine ($y = 0.97x + 1.04$; $R^2 = 0.999$), taurine ($y = 0.97x - 10.65$; $R^2 = 0.9997$), glycine ($y = 0.97x + 2.23$; $R^2 = 1.000$), GAA ($y = 0.97x + 3{,}14$; $R^2 = 1.000$), and AMP ($y = 0.95x + 4.36$; $R^2 = 0.9998$). See Fig. S1 for linearity graphs. Hence, linearity between the methods is evident for all nine metabolites with R^2 values ≥ 0.99. These results further confirm acceptable equivalency between the SOP and miniaturized method.

3.1.4 Statistical equivalence testing

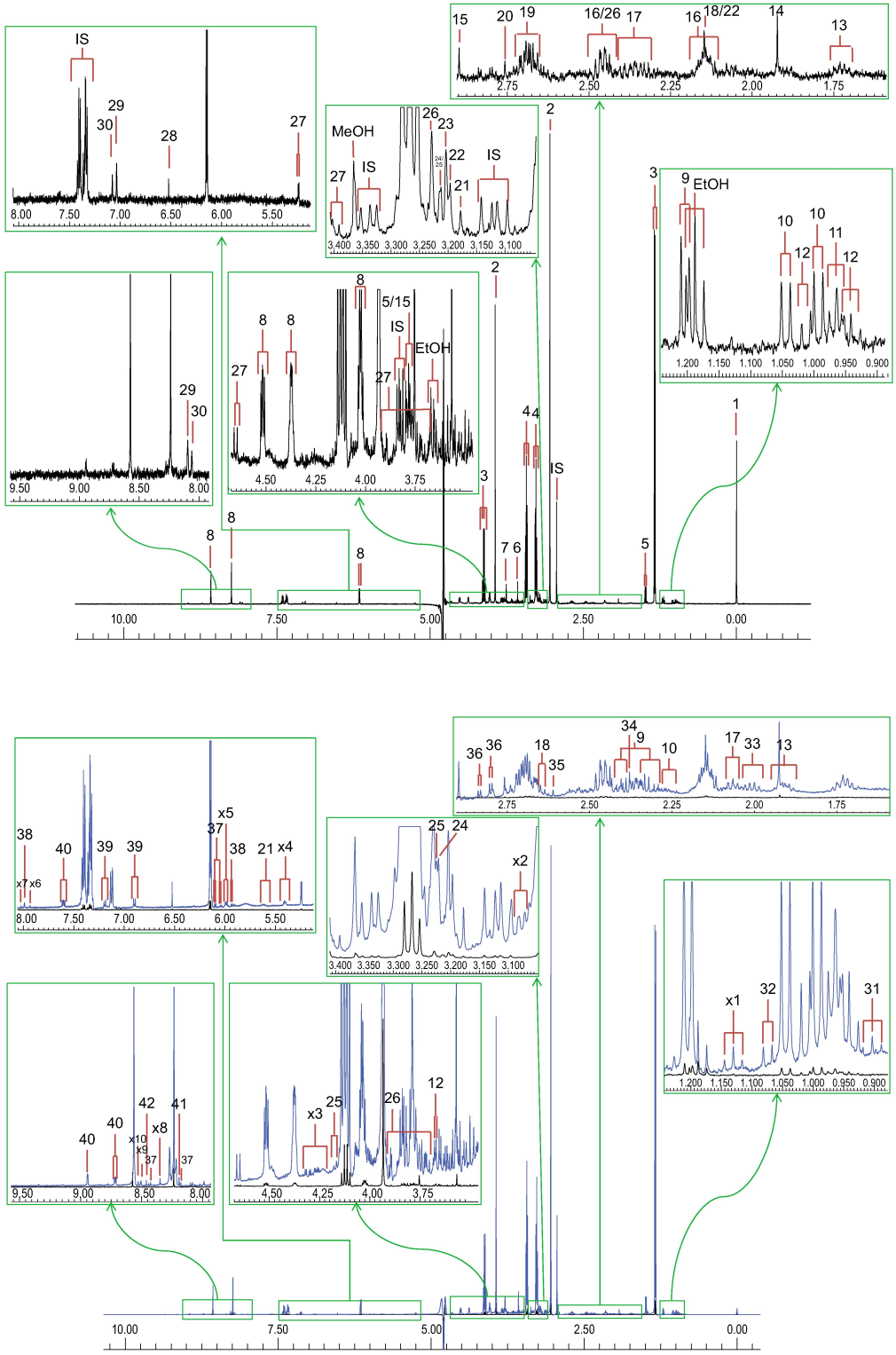
Although commonly used in statistical hypothesis testing, the two-sample t test proves problematic when trying to establish equivalence. Since the aim of a t-test is to determine whether a difference exists, the null hypothesis (H0: means are equivalent) is inappropriate for equivalence testing. As only an alternative hypothesis can be statistically proven, failure to reject H0 does not prove that equivalence truly exists (Chambers et al. 2005). In the case of equivalency testing, incorrectly retaining a false H0 (Type II error: conclude equivalence) has more severe consequences than incorrectly rejecting a true H0 (Type I error: conclude difference). Therefore the TOST approach was used as a statistical means to evaluate the equivalency between the two methods. TOST begins with a H0 that the two mean values are not equivalent. Next, TOST determines an upper and lower confidence interval (CI). Finally, TOST attempts to demonstrate that the mean values are equivalent within a practical, pre-set limit (designated as ±θ). Hence, TOST is conceptually opposite to the two-sample *t* test procedure.

Table 2 Test of equivalence

Metabolites	SOP versus Mini						H0: difference
	Low θ = ± 15%		Medium θ = ± 10%		High θ = ± 5%		
	|%D| between means	*p* value	|%D| between means	*p* value	|%D| between means	*p* value	
Lactic acid	6.3	0.0010	2.9	< 0.0001	4.2	0.0190	Reject
Alanine	1.6	0.0001	1.9	< 0.0001	3.5	0.0012	Reject
3-Hydroxybutyric acid	0.5	0.0001	2.1	< 0.0001	3.4	< 0.0001	Reject
Choline	1.8	0.0001	2.1	< 0.0001	0.1	< 0.0001	Reject
Carnitine	3.6	< 0.0001	2.3	< 0.0001	3.4	< 0.0001	Reject
Taurine	21.4	0.7908	9.0	0.2527	4.5	0.2396	Accept
Glycine	0.1	< 0.0001	1.5	< 0.0001	2.6	< 0.0001	Reject
GAA	0.8	< 0.0001	0.7	< 0.0001	2.1	< 0.0001	Reject
AMP	1.9	0.0030	1.4	< 0.0001	4.1	0.0281	Reject

TOST (α = 0.05) approach to determine if the two methods are sufficiently equivalent in spiked synthetic urine (low, medium and high concentrations) at selected equivalence margins

\|%D\| = absolute percentage difference between mean concentrations (n = 10) obtained with SOP and Mini method, θ = acceptable limit for equivalence


IS
29
30
28
27
MeOH
IS
26
23
22
21
IS
15
20
19
16/26
17
16
18/22
14
13
2
3
9
EtOH
10
10
11
12
12
8
5/15
IS
EtOH
27
27
8
8
29
30
44
IS
1
3
8
8
8
7 6
5
10.00
7.50
5.00
2.50
0.00
38
40
39
39
x5
37
38
21
x4
x7
x6
36
36
18
35
34
9
10
17
33
13
25
24
x2
x1
32
31
42
41
40
40
x8
x10
x9
37
37
x3
25
26
12

◂**Fig. 3** Representative ^{1}H-NMR spectra from the miniaturized method on muscle tissue scaled relative to TSP for (top) normal concentration (black spectrum), with windows A–F zoomed in 32×, and (bottom) 10× concentration (blue spectrum) compared to normal concentration, with windows A–F showing peaks that are either not clearly discernible or not detectable at all in normal concentration [windows: A = 0.90–1.25 ppm, B = 1.60–2.82 ppm, C = 3.05–3.41 ppm, D = 3.55–4.65 ppm, E = 5.00–8.00 ppm, F = 8.00–9.50 ppm]. Peak assignments: 1 = TSP (0.00 s), 2 = creatine (3.04 s, 3.93 s), 3 = lactic acid (1.33 d, 4.12 q), 4 = taurine (3.26 t, 3.42 t), 5 = alanine (1.48 d, 3.78 q), 6 = glycine (3.57 s), 7 = guanidinoacetic acid (3.76 s), 8 = AMP (4.02 m, 4.37 m, 4.51 dd, 6.15 d, 8.23 s, 8.56 s), 9 = 3-hydroxybutyric acid (1.20 d, 2.36 AB), 10 = valine (0.99 d, 1.04 d), 11 = leucine (0.96 t), 12 = isoleucine (0.94 t, 1.01 d, 3.67 d), 13 = lysine (1.73 m, 1.91 m), 14 = acetic acid (1.92 s), 15 = trimethylamine (2.89 s), 16 = glutamine (2.14 m, 2.44 m, 3.77 t), 17 = glutamic acid (2.07 m, 2.36 m), 18 = methionine (2.14 s, 2.65 t), 19 = homocysteine (2.14 m, 2.69 m), 20 = sarcosine (2.75 s), 21 = dimethyl sulfone (3.17 s), 22 = acetylcarnitine (2.14 s, 3.19 s, 5.61 m), 23 = choline (3.20 s), 24 = acetylcholine (3.21 s), 25 = phosphocholine (3.21 s, 4.17 m), 26 = carnitine (3.22 s), 27 = glucose (3.40 m, 3.75 m, 4.63 d, 5.22 d), 28 = fumaric acid (6.52 s), 29 = histidine (7.03 s, 8.09 s), 30 = histamine (7.07 s, 8.06 s), 31 = 2-hydroxybutyric acid (0.90 t), 32 = 3-hydroxyisobutyric acid (1.07 d), 33 = proline (2.00 m), 34 = pyruvic acid (2.37 s), 35 = methylamine (2.61 s), 36 = aspartic acid (2.80 d, 2.83 d), 37 = NAD (6.04 d, 6.10 d, 8.18 s, 8.42 s), 38 = guanosine (5.92 d, 8.01 s), 39 = tyrosine (6.89 dd, 7.19 dd), 40 = nicotinamide (7.60 dd, 8.72 dd, 8.94 d), 41 = hypoxanthine (8.19 s), 42 = formic acid (8.46 s). IS = internal standard (*N,N*-dimethylphenylalanine (2.93 s, 3.12 dd, 3.34 dd, 7.37 m)), MeOH = methanol (3.36 s), EtOH = ethanol (1.19 t, 3.64 q), x1–x10 = unassigned. See Table S1 for additional chemical information on assigned peaks

Unlike the two-sample t-test, TOST appropriately penalizes poor precision and/or small n values and places the burden on the analyst to prove that the data sets are equivalent (Limentani et al. 2005).

Therefore TOST was used to evaluate the equivalence between the SOP and miniaturized method at each concentration level. For each standard the difference between mean values (n = 10) along with the calculated 90% CI was plotted (Fig. 2). Margins were drawn at ± 5, ± 10, and ± 15%, as per the precision cut-off CV values. At low concentration levels the methods showed to be equivalent even within the ± 10% margin for most of the standards (with lactic acid and taurine (not displayed) being the only exceptions). Similarly, at medium and high concentration levels the methods showed to be equivalent for all standards (except taurine) within the ± 5% margin. When excluding taurine, the absolute percentage difference between mean values (Table 2) obtained from both methods was < 7% at low levels, and < 5% at medium and high levels. Table 2 also displays the p values obtained from TOST when using the different preset equivalence margins for each concentration level. Thus acceptable equivalence between the methods was shown statistically ($p < 0.05$) at a 5% significance level for all metabolites (except taurine) at each concentration level.

3.2 Exploring the miniaturized ^{1}H-NMR method

After establishing the miniaturized ^{1}H-NMR method as an acceptable alternative for metabolomics studies using limited quantity samples, the miniaturized method's capabilities were further explored in a true biological matrix, namely, murine skeletal muscle extract.

3.2.1 Method comparability

In order to further confirm acceptable method equivalency, a pooled skeletal muscle extract was analyzed using both the SOP and miniaturized ^{1}H-NMR methods in replicates of three. Nine clearly discernible targeted metabolites (same nine used for method equivalence testing in surine) were quantified from the ^{1}H-NMR spectra and used to further evaluate method equivalency. Firstly, the observed difference between the mean values obtained from each method were between 0.06 and 4.01%. Secondly, comparing the precision of the two methods, as seen before, the SOP operated with higher precision than the miniaturized method in most cases [except for 3-HB (SOP: 8.32% CV; Mini 4.82% CV) and carnitine (SOP: 2.17% CV; Mini 1.66% CV)]. However, the CV values for both methods were below 5% (except for 3-HB in the SOP). Thus, the miniaturized protocol produced quantified data close to that of the current SOP, with acceptably equal precision.

3.2.2 Quantitative linearity

In order to validate whether the miniaturized ^{1}H-NMR protocol performed linearly with sample concentration, a muscle extract concentration range was analyzed. Six different extract concentrations (1×, 2×, 4×, 6×, 8× and 10× concentrated) were prepared from a pooled muscle sample by transferring and drying [in N_2(g) at 37 °C] various extract volumes (80, 160, 320, 480, 640 and 800 µL) in a glass vial and resuspending each in 80 µL of water. Five replicates of each concentration were analyzed using the miniaturized protocol. A total of ten compounds, varying in composition and signal intensity, were identified from the NMR spectrum and their absolute concentrations determined. The linear relationship between instrument response and level of concentration for all nine metabolites ($R^2 > 0.98$) was clear: acetic acid ($R^2 = 0.979$); alanine ($R^2 = 0.991$); taurine ($R^2 = 0.990$); glycine ($R^2 = 0.990$); creatine ($R^2 = 0.990$); lactic acid ($R^2 = 0.991$); fumaric acid ($R^2 = 0.991$); AMP ($R^2 = 0.989$); carnitine ($R^2 = 0.990$); valine ($R^2 = 0.986$).

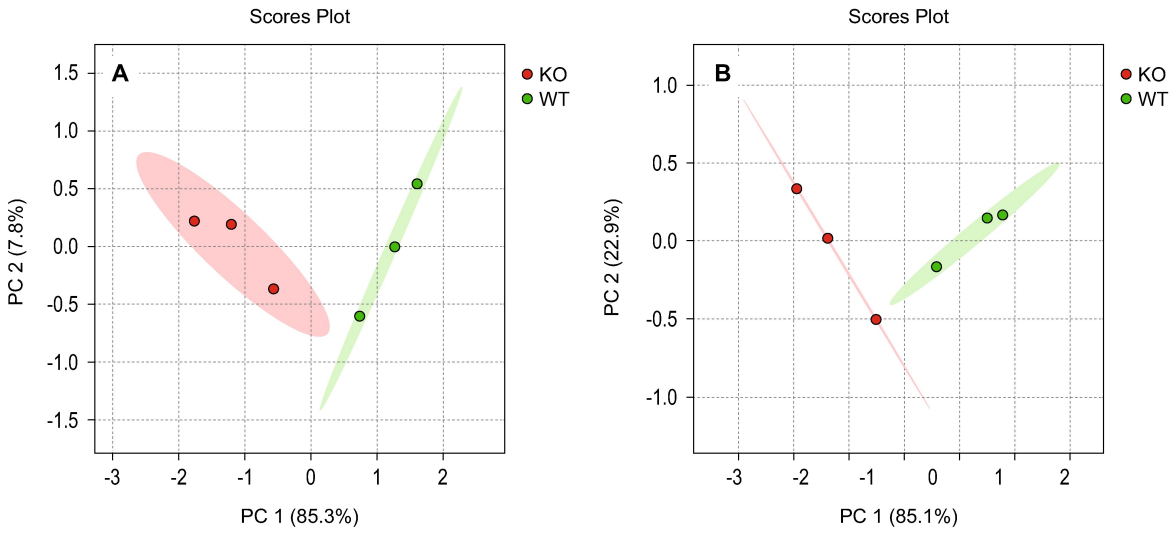


Fig. 4 Application of the miniaturized ^{1}H-NMR method in pilot metabolomics study of *Ndufs4* KO mice. PCA score plots of extracts of soleus muscle and olfactory bulb tissues from *Ndufs4* WT and KO mice. **a** Untargeted approach (using VIPs) for soleus muscles. **b** Targeted approach (using VIPs) for soleus muscles. Ellipses indicate 90% confidence

3.2.3 Metabolome coverage

In addition to analyzing limited-quantity samples, another advantage of the miniaturized protocol is the possibility of concentrating samples to such an extent that essentially there is an increase in the analytical sensitivity, and consequently metabolome coverage. To illustrate this, ^{1}H-NMR spectra of normal (1×) and concentrated (10×) muscle extracts were analyzed and investigated in terms of metabolome coverage. Representative ^{1}H-NMR spectra, scaled relative to TSP, are given in Fig. 3. The top spectrum represents a normal concentration extract (black spectrum), with windows A–F zoomed in 32×. The bottom spectrum shows the comparison between normal and 10× concentrated (blue spectrum) extracts, with windows A–F showing peaks that are either not clearly discernible or not detectable at all in the normal concentration. Qualitative inspection of Fig. 3 shows that some of the identified metabolites not clearly discernible or detectable in the normal concentration are: 2-hydroxybutyric acid (0.90 t), 3-hydroxyisobutyric acid (1.07 d), proline (2.00 m), pyruvic acid (2.37 s), methylamine (2.61 s), aspartic acid (2.80 d, 2.83 d), NAD (6.04 d, 6.10 d, 8.18 s, 8.42 s), guanosine (5.92 d, 8.01 s), tyrosine (6.89 dd, 7.19 dd), nicotinamide (7.60 m, 8.72 dd, 8.94 d), hypoxanthine (8.19 s), and formic acid (8.46 s). Also present were at least 10 non-annotated peak assignments. Of interest, it was noted that some remaining methanol (3.36 s) from the extraction process, and ethanol (1.19 t, 3.64 q) from the cleaning of the instruments used during tissue sample collection and workup, were detected. These two alcohols were classified as exogenous.

3.2.4 Sample carry-over

An analytical question raised whilst examining the linearity of the miniaturized method was: Is there any potential carry-over from the same eVol® syringe being used during sample preparation? To test for carry-over, a clean water sample (blank) was drawn by the same eVol® syringe after the preparation of each muscle extract sample (concentrations: 1×, 2×, 4×, 6×, 8× and 10×). These blank samples were analyzed as per experimental protocol and qualitatively there was no evidence of carry-over. Hence, the wash procedure (flushing the syringe with water three times) of the experimental method used was considered adequate.

3.3 Pilot metabolomics application on limited quantity samples

To further examine the applicability of the miniaturized ^{1}H-NMR protocol, we conducted a pilot metabolomics study using soleus muscle tissue (~4 mg) of wild-type (WT) and KO *Ndufs4* mice. Metabolites were extracted as described earlier, with some adjustments. Owing to the limited sample quantity, the solvent ratio of 6:2:2 (methanol:water:chloroform) was multiplied by a factor of 10 for the soleus muscles. After drying, the tissue extracts were resuspended in water to obtain a final concentration of 0.05 mg tissue/µL. Although 0.1 mg tissue/µL is equal

to that obtained from an unadjusted extraction (used earlier for quadriceps), this concentration could not be obtained for the soleus muscles due to the limited sample quantities. The samples were analyzed using the miniaturized ^{1}H-NMR protocol and the data were investigated using an untargeted and targeted metabolomics approach.

For the untargeted approach, each NMR spectrum was again quantified across 376 spectral bins of equal size—0.02 ppm bins, excluding the water region 4.0–6.0 ppm. Statistical analyses (Student's *t* test) of the bins indicated that 14 bins differed significantly (VIPs) in the muscle samples. PCA score plots of the untargeted data (using only the VIPs) show clear separation between the WT and KO groups (Fig. 4a).

For the targeted approach, ten clearly discernible metabolites were selected for quantification. Univariate statistical analysis (Student's *t* test) was used to identify variables that differed significantly ($p < 0.05$) between the WT and KO groups. Five compounds differed significantly in the muscle samples: alanine, AMP, choline, fumaric acid and valine. The compounds detected as significant were used for PCA. Figure 4b shows clear separation between the WT and KO muscle samples. All of the metabolites identified as important have previously been linked to mitochondrial disease (Esterhuizen et al. 2017). Understandably, one cannot draw definitive conclusions for a population from a sample size of only three. However, the preliminary findings of this pilot metabolomics study using the miniaturized ^{1}H-NMR protocol indicates information in line with the current knowledge of altered metabolism observed in mitochondrial disease.

4 Conclusion

We have presented a novel miniaturized ^{1}H-NMR protocol, which requires a sample volume of only 60 µL. This new method was compared with an established SOP, which requires a sample volume of at least 600 µL. Method equivalency was tested using spiked synthetic urine samples, as well as muscle tissue extracts from *Ndufs4* KO mice. We demonstrated an acceptable equivalence between the two methods at a 95% confidence level. Spectral data of equal quality from the two methods was obtained but with the new technique requiring only one-tenth of the sample of the other. We went further and analytically tested this miniaturized ^{1}H-NMR method by: (1) analyzing samples up to 10× concentration, yielding qualitatively more identified metabolites (effectively addressing the sensitivity issues that attend NMR technology), with quantitative linearity ($R^2 > 0.98$), and (2) examining post-analysis blank samples to show no detectable carry-over from the miniaturized ^{1}H-NMR analytical method.

Finally, we applied the miniaturized method in a pilot metabolomics study using a very small tissue sample (as little as 4 mg), something that would not have been possible with an established SOP, which requires more sample, on a room temperature 5 mm NMR probe. In this pilot study we were able to generate data that could separate the WT and KO groups from *Ndufs4* mice, using both an untargeted and targeted approach. Furthermore, the metabolites detected as important with the targeted approach have all been linked to mitochondrial disease in previous studies, indicating important variables with biological relevance.

Acknowledgements This work is based on the research supported by the National Research Foundation of South Africa (Grant No. 92736) and the Technological Innovation Agency of the Department of Science and Technology of South Africa.

Author contributions The manuscript was written with equal contributions from all authors.

Compliance with ethical standards

Conflict of interest All authors declare that they have no conflict of interest.

Ethical approval The AnimCare animal research ethics committee of North-West University approved (NWU-00378-16-A5) the animal protocols used here. All animals were maintained and all procedures performed in accordance with the code of ethics in research, training and testing of drugs in South Africa and complied with national legislation.

References

Beckonert, O., Keun, H. C., Ebbels, T. M. D., Bundy, J., Holmes, E., Lindon, J. C., et al. (2007). Metabolic profiling, metabolomic and metabonomic procedures for NMR spectroscopy of urine, plasma, serum and tissue extracts. *Nature Protocols, 2*, 2692–2703.

Cassiède, M., Nair, S., Dueck, M., Mino, J., McKay, R., Mercier, P., et al. (2017). Assessment of 1H NMR-based metabolomics analysis for normalization of urinary metals against creatinine. *Clinica Chimica Acta, 464*, 37–43.

Chambers, D., Kelly, G., Limentani, G., Lister, A., Lung, K. R., & Warner, E. (2005). Analytical method equivalency. *Pharmaceutical Technology, 29*, 64–80.

Chan, C. C., Lee, Y. C., Lam, H., & Zhang, X. M. (Eds.). (2004). *Analytical method validation and instrument performance verification*. Hoboken: Wiley.

Dona, A. C., Jiménez, B., Schäfer, H., Humpfer, E., Spraul, M., Lewis, M. R., et al. (2014). Precision high-throughput proton NMR spectroscopy of human urine, serum, and plasma for large-scale metabolic phenotyping. *Analytical Chemistry, 86*, 9887–9894.

Dunn, W. B., Wilson, I. D., Nicholls, A. W., & Broadhurst, D. (2012). The importance of experimental design and QC samples in large-scale and MS-driven untargeted metabolomic studies of humans. *Bioanalysis, 4*, 2249–2264.

Esterhuizen, K., van der Westhuizen, F. H., & Louw, R. (2017). Metabolomics of mitochondrial disease. *Mitochondrion, 35*, 97–110.

Figueira, J., Jonsson, P., Adolfsson, A. N., Adolfsson, R., Nyberg, L., & Öhman, A. (2016). NMR analysis of the human saliva metabolome distinguishes dementia patients from matched controls. *Molecular BioSystems, 12*, 2562–2571.

Fratila, R. M., & Velders, A. H. (2011). Small-volume nuclear magnetic resonance spectroscopy. *Annual Review of Analytical Chemistry, 4*, 227–249.

Glaves, J. P., Li, M. X., Mercier, P., Fahlman, R. P., & Sykes, B. D. (2014). High-throughput, multi-platform metabolomics on very small volumes: ^{1}H NMR metabolite identification in an unadulterated tube-in-tube system. *Metabolomics, 10*, 1145–1151.

Gullberg, J., Jonsson, P., Nordström, A., Sjöström, M., & Moritz, T. (2004). Design of experiments: An efficient strategy to identify factors influencing extraction and derivatization of *Arabidopsis thaliana* samples in metabolomic studies with gas chromatography/mass spectrometry. *Analytical Biochemistry, 331*, 283–295.

Hohmann, M., Felbinger, C., Christoph, N., Wachter, H., Wiest, J., & Holzgrabe, U. (2014). Quantification of taurine in energy drinks using 1 H NMR. *Journal of Pharmaceutical and Biomedical Analysis, 93*, 156–160.

Johansson, T., Jurva, U., Grönberg, G., Weidolf, L., & Masimirembwa, C. (2009). Novel metabolites of amodiaquine formed by CYP1A1 and CYP1B1: Structure elucidation using electrochemistry, mass spectrometry, and NMR. *Drug Metabolism and Disposition, 37*, 571–579.

Kayser, E., Sedensky, M. M., & Morgan, P. G. (2016). Region-specific defects of respiratory capacities in the Ndufs4(KO) mouse brain. *PLoS ONE, 11*, 1–18.

Koves, T. R., Noland, R. C., Bates, A. L., Henes, S. T., Muoio, D. M., & Cortright, R. N. (2005). Subsarcolemmal and intermyofibrillar mitochondria play distinct roles in regulating skeletal muscle fatty acid metabolism. *American Journal of Physiology-Cell Physiology, 288*, C1074–C1082.

Li, H., Kumar Sharma, L., Li, Y., Hu, P., Idowu, A., Liu, D., et al. (2013). Comparative bioenergetic study of neuronal and muscle mitochondria during aging. *Free Radical Biology and Medicine, 63*, 30–40.

Limentani, G. B., Ringo, M. C., Ye, F., Bergquist, M. L., & McSorley, E. O. (2005). Beyond the t-test: Statistical equivalence testing. *Analytical Chemistry, 77*, 221A–226A.

Lindon, J. C., Holmes, E., Bollard, M. E., Stanley, E. G., & Nicholson, J. K. (2004). Metabonomics technologies and their applications in physiological monitoring, drug safety assessment and disease diagnosis. *Biomarkers, 9*, 1–31.

Madji Hounoum, B., Mavel, S., Coque, E., Patin, F., Vourc'h, P., Marouillat, S., et al. (2017). Wildtype motoneurons, ALS-Linked SOD1 mutation and glutamate profoundly modify astrocyte metabolism and lactate shuttling. *Glia, 65*, 592–605.

Martin, G. E. (2005). Small-volume and high-sensitivity NMR probes. *Annual Reports on NMR Spectroscopy, 56*, 1–96.

Schmitt-Kopplin, P., Harir, M., Kanawati, B., Tziozis, D., Hertkorn, N., & Gabelica, Z. (2012b). Chemical footprint of the solvent soluble extraterrestrial organic matter occluded in Sołtmany ordinary chondrite. *Meteorites, 2*, 79–92.

Schmitt-Kopplin, P., Liger-Belair, G., Koch, B. P., Flerus, R., Kattner, G., Harir, M., Kanawati, B., Lucio, M., Tziotis, D., Hertkorn, N., & Gebefügi, I. (2012a). Dissolved organic matter in sea spray: A transfer study from marine surface water to aerosols. *Biogeosciences, 9*, 1571–1582.

US FDA. Guidance for industry, bioanalytical method validation. US FDA, MD, USA (2001).

Xia, J., Sinelnikov, I., Han, B., & Wishart, D. S. (2015). MetaboAnalyst 3.0—making metabolomics more meaningful. *Nucleic Acids Research, 43*, W251–W257.

ANNEXURE D

Published peer-reviewed article II

ANNEXURE D

BBA - Molecular Basis of Disease 1865 (2019) 98–106

Contents lists available at ScienceDirect

BBA - Molecular Basis of Disease

journal homepage: www.elsevier.com/locate/bbadis

Metabolomics of *Ndufs4*$^{-/-}$ skeletal muscle: Adaptive mechanisms converge at the ubiquinone-cycle

Karin Terburgh, Zander Lindeque, Shayne Mason, Francois van der Westhuizen, Roan Louw*

Human Metabolomics, Faculty of Natural and Agricultural Sciences, North-West University (Potchefstroom Campus), South Africa

ARTICLE INFO

Keywords:
Ndufs4 knockout mice
Skeletal muscle
Metabolomics
Mitochondrial disease
Complex I deficiency
Ubiquinone-cycle

ABSTRACT

Leigh syndrome is one of the most common childhood-onset neurometabolic disorders resulting from a primary oxidative phosphorylation dysfunction and affecting mostly brain tissues. *Ndufs4*$^{-/-}$ mice have been widely used to study the neurological responses in this syndrome, however the reason why these animals do not display strong muscle involvement remains elusive. We combined biochemical strategies and multi-platform metabolomics to gain insight into the metabolism of both glycolytic (white quadriceps) and oxidative (soleus) skeletal muscles from *Ndufs4*$^{-/-}$ mice. Enzyme assays confirmed severely reduced (80%) CI activity in both *Ndufs4*$^{-/-}$ muscle types, compared to WTs. No significant alterations were evident in other respiratory chain enzyme activities; however, *Ndufs4*$^{-/-}$ solei displayed moderate decreases in citrate synthase (12%) and CIII (18%) activities. Through hypothesis-generating metabolic profiling, we provide the first evidence of adaptive responses to CI dysfunction involving non-classical pathways fueling the ubiquinone (Q) cycle. We report a respective 48 and 34 discriminatory metabolites between *Ndufs4*$^{-/-}$ and WT white quadriceps and soleus muscles, among which the most prominent alterations indicate the involvement of the glycerol-3-phosphate shuttle, electron transfer flavoprotein system, CII, and proline cycle in fueling the Q cycle. By restoring the electron flux to CIII via the Q cycle, these adaptive mechanisms could maintain adequate oxidative ATP production, despite CI deficiency. Taken together, our results shed light on the underlying pathogenic mechanisms of CI dysfunction in skeletal muscle. Upon further investigation, these pathways could provide novel targets for therapeutic intervention in CI deficiency and potentially lead to the development of new treatment strategies.

1. Introduction

Mitochondria play a vital role in a myriad of processes involved in metabolism, cellular bioenergetics, and metabolic cell signaling [1–4]. The mitochondrial oxidative phosphorylation (OXPHOS) system, which comprises complexes I–IV and ATP synthase (CV), is the major contributor to cellular energy production and sustains most mitochondrial functions. The dysfunction of complex I (CI) (OMIM 252010) of the

Abbreviations: ^{1}H NMR, Proton nuclear magnetic resonance spectroscopy; 1-Mhis, 1-Methylhistidine; 2-AA, 2-Aminoadipate; 2-Mhis, 2-Methylhistidine; 5MTHF, 5-Methyl-tetrahydrofolate; Ala, Alanine; Arg, Arginine; Asn, Asparagine; Asp, Aspartate; BAIBA, β-Aminoisobutyrate; β-Ala, Beta-Alanine; C0, Carnitine; CI, complex I; C2, Acetyl-carnitine; CII, complex II; C3, Propionyl-carnitine; CIII, complex III; C4, Butyryl-carnitine; CIV, complex IV; C5, Isovalerylcarnitine; C6, Hexanoyl-carnitine; C8, Octanoyl-carnitine; C12, Dodecanoyl-carnitine; C14, Myristoyl-carnitine; C16, Palmitoyl-carnitine; C18, Stearoyl-carnitine; c-GPDH, Cytosolic glycerol-3-phosphate dehydrogenase; Cit, Citrulline; CS, Citrate synthase; Cyt c, Cytochrome c; DHAP, Dihydroxyacetone phosphate; DMG, N, *N*-Dimethylglycine; ETF, Electron transfer flavoprotein; ETF-QO, Electron transfer flavoprotein:ubiqionone oxidoreductase; FAD, Oxidized flavin adenine dinucleotide; $FADH_2$, Reduced flavin adenine dinucleotide; GC–TOF–MS, Gas chromatography time-of-flight mass spectrometry; GP, Glycerol-3-phosphate; Gln, Glutamine; Glu, Glutamate; Gly, Glycine; Hcys, Homocysteine; Hpro, Hydroxyproline; LC–MS/MS, Liquid chromatography tandem mass spectrometry; Lys, Lysine; Met, Methionine; m-FDH(s), Mitochondrial flavoprotein dehydrogenase(s); m-GPDH, Mitochondrial glycerol-3-phosphate dehydrogenase; NAA, *N*-Acetylaspartate; NAD^+, Oxidized nicotine amide adenine dinucleotide; NADH, Reduced nicotine amide adenine dinucleotide; NAG, *N*-Acetylglutamate; *Ndufs4*, NADH dehydrogenase (ubiquinone) iron-sulphur protein 4; *Ndufs4*$^{-/-}$, Homozygous *Ndufs4* knockout; Orn, Ornithine; OXPHOS, Oxidative phosphorylation; P-5-C, Pyrroline-5-carboxylate; pGlu, Pyroglutamate; Phe, Phenylalanine; Pip, Pipecolate; Pro, Proline; ProDH, Proline dehydrogenase; PYCR, Pyrroline-5-carboxylate reductase; Q, Ubiquinone (oxidized coenzyme Q10); QH_2, Ubiquinol (reduced coenzyme Q10); RC, Respiratory chain; SAH, *S*-Adenosylhomocysteine; SAM, *S*-Adenosylmethionine; Sar, Sarcosine; Ser, Serine; Tau, Taurine; THFA, Tetrahydrofolate; Thr, Threonine; TMG, Trimethylglycine; Tryp, Tryptophan; WT, Wild type (*Ndufs4*$^{+/+}$)

* Corresponding author at: Human Metabolomics, Faculty of Natural and Agricultural Sciences, North-West University (Potchefstroom Campus), Private Bag X6001, Potchefstroom, South Africa.

E-mail address: Roan.Louw@nwu.ac.za (R. Louw).

https://doi.org/10.1016/j.bbadis.2018.10.034
Received 4 September 2018; Received in revised form 23 October 2018; Accepted 29 October 2018
Available online 31 October 2018
0925-4439/ © 2018 Elsevier B.V. All rights reserved.

OXPHOS system, is the most common defect in mitochondrial energy metabolism, often resulting in progressive, severe multi-system deterioration. Due to the extreme complexity and heterogeneous nature (genetically and clinically) of human CI deficiency, the underlying pathogenic mechanisms thereof remain poorly understood [5,6].

Current studies on mouse models of CI dysfunction, such as the whole-body *Ndufs4*$^{-/-}$ (knockout) mouse, attempt to better comprehend mitochondrial disease. The nuclear DNA-encoded NDUFS4 protein is essential to CI assembly, stability, and activity [7,8]. *Ndufs4*$^{-/-}$ mice present with symptoms similar to human CI deficiency at around postnatal day (P) 35 and develop a progressive Leigh-like phenotype, including developmental delays, failure to thrive, lethargy, ophthalmoplegia, locomotor impairment, hearing loss, as well as progressive ataxia, and necrotizing encephalomyopathy leading to early death (P50–60) [9–11]. Since the development of whole-body *Ndufs4*$^{-/-}$ mice, several conditional knockouts (neuronal, glial, cardiac, hematopoietic, and hepatic) have been developed in order to gain insight into tissue-specific consequences of CI dysfunction (reviewed by Toracco et al. [12]). However, due to the main interest in the predominant neurological phenotype of this disease model, limited information is available on skeletal muscle-specific consequences of the *Ndufs4* knockout.

A recent study by Foriel and colleagues [13] highlighted the involvement of skeletal muscle in *Ndufs4* knockout pathology. The authors reported similarities between the phenotypes of skeletal muscle-specific and whole-body *Ndufs4* knockout *Drosophila*, such as reduced lifespan, feeding difficulties, locomotor impairment, and climbing defects. Given the important, often underappreciated, role of the muscular system in health and disease [14], as well as its integration and interdependence with the nervous system [15], it is imperative to elucidate the effects of a *Ndufs4* knockout on muscle metabolism. Skeletal muscle not only facilitates breathing and locomotion but also plays an essential role in various systemic, energy-demanding processes such as whole-body protein metabolism, glucose, and fatty acid consumption, thermoregulation, immunity, as well as the maintenance of adequate bone strength and density [14–16]. As *Ndufs4*$^{-/-}$ mice display weight loss [9], a significant decrease in body fat [11], decreases in body temperature [9], as well as systemic inflammation and osteoporosis [10], it can be hypothesized that aberrant skeletal muscle metabolism might also play an important role in murine *Ndufs4*$^{-/-}$ phenotypes.

We aimed to gain insight into the consequences of a *Ndufs4*$^{-/-}$ on skeletal muscle bioenergetics and metabolism by combining biochemical strategies (respiratory chain enzyme assays) and multi-platform metabolic profiling (LC–MS/MS, GC–TOF–MS, and NMR analyses). Since the metabolic properties and subpopulations of muscle mitochondria depend on muscle fiber type composition [16], both glycolytic (white quadriceps; primarily type IIB myofibers) and oxidative (soleus; primarily type I myofibers) muscles were investigated. To the best of our knowledge, this is the first report of fiber type-specific enzymatic and metabolic data in *Ndufs4*$^{-/-}$ skeletal muscles. We report a metabolic signature consisting of 48 compounds in white quadriceps and 34 compounds in soleus muscles that distinguish whole-body *Ndufs4* knockout mice from wild types. These metabolic alterations provide insight into skeletal muscle-specific changes in metabolic pathways that result from whole-body mitochondrial dysfunction. These pathways could possibly be targeted in therapeutic interventions to promote muscle health in mitochondrial disorders and improve locomotion, metabolism, and quality of life.

2. Materials and methods

Detailed information regarding the described methods can be found in the supplementary data (Appendix A).

2.1. Animals and sampling

Male whole-body *Ndufs4* knockout mice (B6.129S4-*Ndufs4*$^{tm1.1Rpa}$/J; referred to as *Ndufs4*$^{-/-}$) along with age- and sex-matched controls (*Ndufs4*$^{+/+}$; referred to as WT) were used. *Ndufs4*$^{-/-}$ mice were born from heterozygous (*Ndufs4*$^{+/-}$) crosses obtained from Jackson Laboratory (ME, USA) (JAX stock #027058, https://www.jax.org/strain/027058). It should be noted that this mouse strain is BL6/J-derived and, therefore, potentially contains the *Nnt*$^{C57BL/6J}$ mutation. *Ndufs4* genotypes were confirmed by polymerase chain reaction (PCR) using tail snips. The animals were bred and housed at the specific pathogen-free (SPF) unit of the Vivarium (SAVC reg. no. FR15/13458) of the Pre-Clinical Drug Development Platform (PCDDP, NWU, RSA) and approval (NWU-00378-16-A5) for this study was obtained from the Animal Research Ethics Committee of the NWU. Animals were group housed under temperature- (22 ± 1 °C), humidity- (55 ± 10%) and light-controlled (12:12-h light/dark cycle) conditions with standard laboratory chow (Laboratory animal food: Rodent Breeder, Cat. #RM1845, LabChef, Nutritionhub) and water provided ad libitum. Mice were euthanized between postnatal day (P) 45–50 via cervical dislocation at the same time of day (8:00–9:00 AM) after overnight (12-h) fasting. From both hind limbs, white muscle portions of quadriceps femoris, as well as soleus muscles, were collected. Tissues were snap-frozen in liquid nitrogen (within 15 min *post-mortem*) and stored at −80 °C until used.

2.2. Enzyme assays

The enzyme activities of complex I (EC 1.6.5.3), complex II (EC 1.3.5.1), complex III (EC 1.10.2.2), and complex IV (EC 1.9.3.1) of the respiratory chain, as well as citrate synthase (EC 2.3.3.1), were measured in 700 × *g* supernatants of white quadriceps and soleus muscle homogenates. Analyses were performed on *Ndufs4*$^{-/-}$ (n = 12) and WT (n = 10) samples via standard operating procedures based on existing methods [17–19].

2.3. Metabolic profiling

Metabolic profiles were obtained from the white quadriceps and soleus muscles of *Ndufs4*$^{-/-}$ (n = 19) and WT (n = 20) mice using a multi-platform metabolomics approach. The analytical techniques were performed as previously described and comprised of targeted liquid chromatography-tandem mass spectrometry (LC–MS/MS) [20], untargeted gas chromatography time-of-flight mass spectrometry (GC–TOF–MS) [21], and proton nuclear magnetic resonance (^{1}H NMR) spectroscopy [22]. However, ^{1}H NMR spectroscopy could not be performed on soleus muscles, due to limited sample quantity. The data obtained in this study [23] can be accessed at the NIH Common Fund's Data Repository and Coordinating Center (supported by NIH grant, U01-DK097430) website, the Metabolomics Workbench, http://www.metabolomicsworkbench.org.

2.3.1. Extract preparation and derivatization

Muscle tissues were finely minced and homogenized in the presence of internal standards using a vibration mill. Metabolite extraction was achieved using a modified monophasic Bligh–Dyer extraction method [24] with a solvent ratio of 3:1:1 (methanol:water:chloroform). Details regarding the exact solvent volumes used for white quadriceps (~80 mg) and soleus (~5 mg) muscles can be found in the supplementary data (Appendix A). The water used for extraction contained a mixture of internal standards consisting of *N*, *N*-dimethyl-L-phenylalanine and 3phenylbutyric acid. Quality control (QC) samples were prepared from aliquots of all samples within a tissue type. Tissue extracts were divided into several vials (one for each analytical platform) and dried under nitrogen. Preparation per platform, in short, was: reconstitution in water for ^{1}H NMR; oximation and silylation for

GC–TOF–MS; as well as the addition of stable isotopes and butylation for LC–MS/MS.

2.4. Data processing

All data processing were done using Excel 2013 (Microsoft Inc.) and MetaboAnalyst 3.0 [25].

2.4.1. Enzyme assays

Enzyme activities were normalized to total protein (mg) content, reflecting tissue mass. Pretreatment of data involved generalized logarithm (glog) transformation.

2.4.2. Metabolic profiling

Spectral data obtained from the analytical platforms were extracted into matrices. Data matrices were individually inspected (correct peak picking and alignment, batch effect, and data integrity) as well as preprocessed (data filtering, missing value imputation, and normalization). Metabolites were normalized to tissue mass. This was achieved through normalization with either *N*, *N*-dimethyl-L-phenylalanine (GC–TOF–MS and LC–MS/MS data) or 3-phenylbutyric acid (^{1}H NMR data). In addition, metabolites measured with LC–MS/MS were further normalized to stable isotopes, which were added to samples before derivatization. Each metabolite was either normalized to its own isotope (where possible) or to an isotope with a similar retention time to which the metabolite strongly correlated. No batch corrections were needed as the QCs showed no significant batch effects. Thereafter, data pretreatment (glog transformation and mean centering) and outlier detection (principal component analysis (PCA) and heatmaps) were done.

2.5. Statistical analyses

2.5.1. Enzyme assays

Differences between *Ndufs4*$^{-/-}$ and WT enzyme activities were regarded as statistically significant with a Student's *t*-test p-value of < 0.05.

2.5.2. Metabolic profiling

Significantly discriminatory features between *Ndufs4*$^{-/-}$ and WT metabolic profiles were determined via univariate analyses. Statistically important differences (Student's *t*-test p-values) were inspected at a 5% and 10% significance level, and false discovery rate-adjusted p-values were calculated. The cut-off threshold for practical significance [26] was set at an effect size D-value of ≥ 0.5. The important features were visually investigated regarding their clustering, covariance, and discriminatory power via PCA as well as volcano plots. PCA was performed in MetaboAnalyst 3.0 [25] on a log-transformed and autoscaled dataset — comprising only the important metabolites identified on each platform. Finally, metabolite identities were assigned to spectral features, with high confidence levels [27,28]. Data set features were identified via spectral and retention time matching using commercial and in-house spectral libraries together with public databases.

3. Results and discussion

3.1. Respiratory chain enzyme activities in *Ndufs4*$^{-/-}$ muscles of different fiber type composition

The average (± SD) mitochondrial enzyme activities (respiratory chain complexes I-IV and citrate synthase) in *Ndufs4*$^{-/-}$ ($n = 12$) and WT ($n = 10$) white quadriceps and soleus muscles are summarized in Table 1. Enzyme activities were normalized to total protein (mg) content, rather than citrate synthase (CS) content, in order to focus on the relative enzyme capacity per tissue mass — thereby emphasizing the relative mitochondrial content of the two muscle fiber types, which was relevant to our metabolic results. In addition, Alam and colleagues [29] recently called into question whether CS activity could be considered a measure of mitochondrial volume in *Ndufs4*$^{-/-}$ mice. Through experimental and computational strategies, the authors reported significantly increased (72%) CS activity in *Ndufs4*$^{-/-}$ muscles — suggested to reflect an increase in Krebs cycle enzyme levels rather than mitochondrial content. With regard to our data, no significant difference in CS activity was found in *Ndufs4*$^{-/-}$ white quadriceps muscles compared to WTs; whereas a moderate decrease (12%, $p = 0.0149$) in CS activity was observed in *Ndufs4*$^{-/-}$ soleus muscles. Therefore, since a statistically significant difference was detected between WT and *Ndufs4*$^{-/-}$ soleus samples, normalization to CS would more than likely skew enzymatic data and lead to a distorted picture of the results. The lower *Ndufs4*$^{-/-}$ soleus CS activity we report, is in stark contrast to the 72% increase in CS activity previously reported for *Ndufs4*$^{-/-}$ (P35) hind limb muscles [29] — the difference could possibly be ascribed to the age difference between the mice studied or differences in the experimental procedures employed. However, several studies [9,30–32] on other *Ndufs4*$^{-/-}$ tissues have reported no alterations in CS activity, similar to the results we report here. This discrepancy should thus be investigated further.

Our data revealed a severe reduction (80%) in rotenone-sensitive CI activity ($p < 0.0001$) in both *Ndufs4*$^{-/-}$ white quadriceps and soleus muscles, compared to WTs. These results correspond with that reported for *Ndufs4*$^{-/-}$ skeletal muscle [7,29]. Although CI activity is reduced by the same factor in both muscles, glycolytic fibers have approximately 2–3 times fewer mitochondria than oxidative fibers [16]. Accordingly, with a *Ndufs4* knockout, our data demonstrate that glycolytic fibers display a much lower residual CI activity (4.58 ± 1.67 nmol/min/mg) than oxidative fibers (14.74 ± 6.67 nmol/min/mg). As evident from our metabolomics data (discussed in Section 3.4), this difference in residual CI activity reflects a biochemical threshold effect with the metabolic consequences of CI deficiency considerably more apparent in white quadriceps compared to soleus muscles. In agreement, model predictions by Alam and colleagues [29] (on entire hind limb *Ndufs4*$^{-/-}$ muscle) suggested that CI activity could be inhibited up to a critical value (90% of normal levels) before major metabolic consequences become apparent.

We found no significant differences in CII–CIV activities in *Ndufs4*$^{-/-}$ white quadriceps compared to WTs. However, in *Ndufs4*$^{-/-}$ soleus muscles, CIII activity was moderately decreased (18%, $p < 0.0001$). CIII has been shown to form a functional, albeit unstable, supercomplex with CI subassemblies in *Ndufs4*$^{-/-}$ muscle [7] and slight decreases in CIII activity have been reported in other tissues from *Ndufs4*$^{-/-}$ mice [9,31] as well as patients [30,33–36]. Literature reports on respiratory chain (RC) enzyme activities in *Ndufs4*$^{-/-}$ mice are quite diverse, with multiple studies [7,9,29–31] reporting variations in CII–CIV activity. This variation can possibly be attributed to tissue-specific differences, variances in sample preparation resulting in different amounts of functional enzyme (especially in the case of CI and supercomplexes thereof, due to its instability), as well as differences in the age of the mice at which point they were studied.

3.2. Statistical significance and discriminative power of *Ndufs4*$^{-/-}$ metabolic profiles

At 95% and 90% significance, univariate statistical analyses revealed a respective 48 (Table A.2) and 34 (Table A.3) discriminatory metabolites between *Ndufs4*$^{-/-}$ and WT white quadriceps and soleus muscles. Volcano plots (Fig. 1 A and B) depict the practical significance of all analytes detected by multi-platform metabolomics in white quadriceps and soleus muscles respectively. Significantly altered metabolites are indicated as decreased (green) or increased (red), while insignificant alterations are shown in gray. The five most decreased and increased metabolites are highlighted with ellipses and listed according to rank. As evident in the volcano plots, the majority of important

Table 1
Mitochondrial respiratory chain enzyme activities in skeletal muscles from WT and *Ndufs4*$^{-/-}$ mice.

Enzyme activity	White quadriceps			Soleus		
(nmol/min/mg)	WT	*Ndufs4*$^{-/-}$	*Ndufs4*$^{-/-}$/WT	WT	*Ndufs4*$^{-/-}$	*Ndufs4*$^{-/-}$/WT
CI	22.9 ± 5.9	4.58 ± 1.7*	0.20	81.2 ± 15.1	14.7 ± 6.7*	0.19
CII	29.9 ± 4.2	31.3 ± 5.0	1.05	63.1 ± 9.8	63.6 ± 10.3	1.01
CIII	430.2 ± 57.1	455.6 ± 47.8	1.06	1430.1 ± 105.1	1170.7 ± 97.4*	0.82
CIV	275.1 ± 32.4	273.8 ± 30.6	1.00	1033.1 ± 168.7	1077.0 ± 199.1	1.04
CS	233.4 ± 48.4	229.7 ± 50.6	0.98	636.7 ± 51.5	562.9 ± 75.3*	0.88

Enzyme activities normalized to mg protein. Average values (± SD) were obtained from 12 Ndufs4$^{-/-}$ and 10 WT animals. Significant differences in Ndufs4$^{-/-}$ enzyme activity relative to WTs are indicated with an asterisk (*p < 0.05). Abbreviations: CI, Complex I; CII, Complex II; CIII, Complex III; CIV, Complex IV; CS, Citrate synthase; WT, Wild type (Ndufs4$^{+/+}$).

metabolites were decreased in *Ndufs4*$^{-/-}$ muscles, compared to WTs, with the white quadriceps (Fig. 1A) displaying a more pronounced metabolic profile. The highest relative fold change was attributed to decreased levels of *N*, *N*-dimethylglycine (DMG), creatinine, and 2-aminoadipate (2AA), while the most prominent increases in metabolite levels (common to both muscles) were seen in lysine (Lys) and its catabolic product — pipecolate (Pip), as well as *N*-acetylaspartate (NAA). Multivariate PCA (Fig. 2) of significant metabolites revealed a partial separation in the clustering of *Ndufs4*$^{-/-}$ and WT groups in both muscles, indicating a distinct metabolic profile in *Ndufs4*$^{-/-}$ muscle.

3.3. Common metabolic alterations in *Ndufs4*$^{-/-}$ skeletal muscles of different fiber type composition

Numerous alterations in the levels of amino acids, acylcarnitines, and organic acids were evident in *Ndufs4*$^{-/-}$ skeletal muscles. The Venn diagram in Fig. 3 illustrates the number of similarities, as well as differences, observed between *Ndufs4*$^{-/-}$ metabolic profiles in the two muscles. Among the metabolites differing between genotypes, the majority (n = 26) were common to both white quadriceps and soleus muscles. Taken together, these adaptions revealed a similar bioenergetic flexibility in skeletal muscles of different fiber type composition. The most prominent changes in metabolite levels could be organized into several non-classical pathways involved in oxidative metabolism and redox regulation as depicted in Fig. 4. These pathways seem to participate in an attempt to increase (and restore) the electron flux to the RC via the ubiquinone (Q) pool, fueling CIII and allowing oxidative ATP production while bypassing CI in the process. A more in-depth discussion of the adaptive mechanisms involved in *Ndufs4*$^{-/-}$ skeletal muscle follows.

3.3.1. Glycolysis, triglyceride catabolism and the glycerol-3-phosphate (GP) shuttle

The accumulation of pyruvate and its derivatives, lactate, and alanine is considered a hallmark feature of mitochondrial metabolic dysfunction attributed to a disturbed redox balance (decreased NAD$^+$/NADH ratio) [37]. In agreement with this hallmark, Johnson and colleagues [11] reported the accumulation of pyruvate, lactate, and glycolytic intermediates in *Ndufs4*$^{-/-}$ whole-brain (P30). However, in *Ndufs4*$^{-/-}$ skeletal muscles, we observed significantly decreased levels of pyruvate, glycerol, and alanine along with significantly (white quadriceps) and moderately (soleus) decreased lactate levels. A possible mechanistic explanation for these observations is the activity of the glycerol-3-phosphate (GP) shuttle. Like lactate dehydrogenase, the GP shuttle rapidly re-oxidizes cytosolic NADH produced by glycolysis. However, an important difference between these redox regulatory mechanisms is the oxidative ATP producing capacity of the GP shuttle. Lying at the intersection of glycolysis, fatty acid metabolism, and oxidative phosphorylation, the GP shuttle serves as an alternative electron donor to the RC at the ubiquinone (Q) pool by transferring reducing equivalents from the cytosol to mitochondria. In this shuttle, the cytosolic enzyme, glycerol-3-phosphate dehydrogenase (c-GPDH, EC 1.1.1.8), oxidizes NADH to NAD$^+$ during the synthesis of GP from dihydroxyacetone phosphate (DHAP) — formed from either glycolysis or the phosphorylation of glycerol derived from triglyceride catabolism. GP can then be used as a substrate for the synthesis of either pyruvate, triglycerides, or phospholipids, however, in the case of the GP shuttle, GP is converted back to DHAP via the inner-membrane bound mitochondrial form of GPDH (m-GPDH) which reduces FAD to $FADH_2$. $FADH_2$ then reduces ubiquinone (Q) to ubiquinol (QH_2). The resulting DHAP is then recycled to again oxidize cytosolic NADH. Although understanding of the structure, function, and regulation of this system is still limited (reviewed by McDonald et al. [38]), several studies have suggested the important role of m-GPDH in thermogenesis and have shown it to be an important site of ROS production. Among the various metabolite shuttles responsible for the transfer of reducing equivalents from the cytosol to mitochondria, the GP shuttle is the most important in skeletal muscle [16]. Therefore, we postulate that the metabolic alterations we observed indicate the diversion of the glycolytic and triglyceride catabolic fluxes towards the GP shuttle in an attempt to not only restore the redox balance but also electron delivery to the RC at the Q pool. This mechanism could also possibly be involved in aberrant

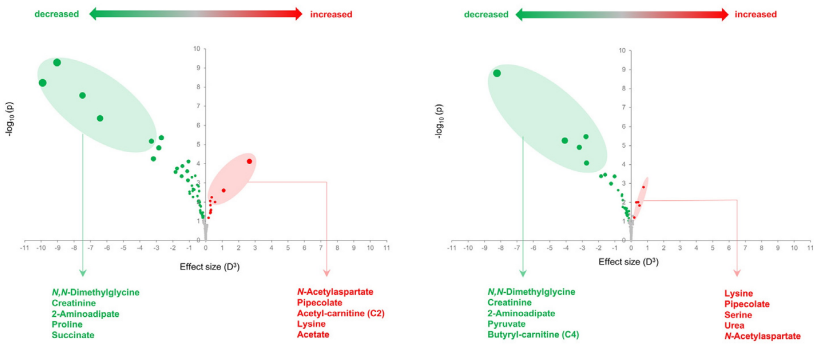


Fig. 1. Univariate analyses indicating the practical significance of important skeletal muscle metabolites. Volcano plots depicting multi-platform metabolomics results of A: white quadriceps muscles and B: soleus muscles from *Ndufs4*$^{-/-}$ mice (n = 19) compared to WTs (n = 20). The x-axis specifies the effect size raised to the third power (D^3) and the y-axis specifies the negative logarithm to the base 10 of the *t*-test p-values. Green and red symbols respectively indicate metabolites significantly lower or higher in *Ndufs4*$^{-/-}$ mice compared to WTs ($p < 0.1$ and $D \geq 0.5$). The five most significantly decreased and increased metabolites are highlighted and listed according to rank.

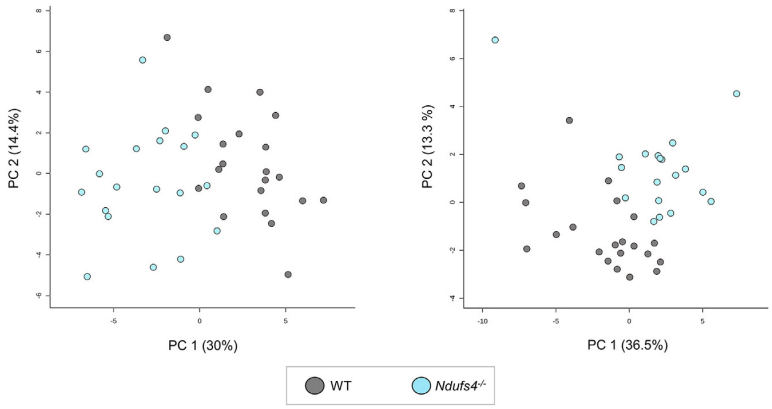


Fig. 2. Multivariate analyses indicating the discriminative power of important skeletal muscle metabolites. Principal component analysis (PCA) scores plots depicting significant metabolites ($p < 0.1$, $D \geq 0.5$) identified in A: white quadriceps muscles and B: soleus muscles. Partial separation in the clustering of *Ndufs4*$^{-/-}$ (n = 19, blue) and WT (n = 20, gray) groups are visible in both cases. White quadriceps: PC1 and PC2 account for 30.0% and 14.4% of variation respectively. Soleus: PC1 and PC2 account for 36.5% and 13.3% of variation respectively.

ROS production, a feature often reported in mitochondrial disease.

3.3.2. β-oxidation, amino acid catabolism, and the electron transfer flavoprotein (ETF/ETF-QO) system

Both *Ndufs4*$^{-/-}$ skeletal muscle types displayed dramatic decreases in the levels of *N*, *N*-dimethylglycine (DMG), fatty acid acylcarnitines of even (C0, C4, C6, C8, C12, and C16) and odd (C3 and C5) chain length, as well as 2-aminoadipate (2-AA). Although previous metabolomics investigations on mitochondrial disease have reported disturbances in one-carbon metabolism, the catabolism of fatty acids, branched-chain amino acids (BCAA), as well as the ketogenic amino acid, lysine, the underlying mechanisms remain unclear [37]. We postulate that these diverse metabolic alterations point to several pathways that converge at the electron transfer flavoprotein (ETF/ETF-QO) system. The ETF/ETF-QO system functions as an electron transfer pathway conducting electrons from eleven mitochondrial flavoprotein dehydrogenases (m-FDHs) to the Q pool of the RC. These m-FDHs include enzymes involved in mitochondrial one-carbon metabolism (dimethylglycine dehydrogenase, EC 1.5.99.2; and sarcosine dehydrogenase, EC 1.5.99.1), fatty acid β-oxidation (short-chain acyl-CoA dehydrogenase, EC 1.3.99.2; medium-chain acyl-CoA dehydrogenase, EC 1.3.99.3; and long-chain acyl-CoA dehydrogenase, EC 1.3.99.13), as well as branched-chain amino acid catabolism (isovaleryl-CoA dehydrogenase, EC 1.3.99.10; and isobutyryl-CoA dehydrogenase) and lysine catabolism (glutaryl-CoA dehydrogenase, EC 1.3.99.7) (reviewed by Watmough et al. [39]). Therefore we hypothesize that, in *Ndufs4*$^{-/-}$ skeletal muscle, there is an increased flux through these m-FDHs supplying the ETF/ETF-QO system with electrons in order to compensate for decreased electron transfer from CI. This increased flux, in part, could lead to the observed decreased metabolite levels. However, this switch in flux cannot effectively compensate for the CI defect as all of these $FADH_2$ producing pathways also require NAD^+ as a co-factor. NADH levels could build up due to CI inactivity as well as these compensatory reactions themselves. The hypothesized result of the altered redox state and shortage of NAD^+ is seen in the lysine catabolic pathway. Lysine is normally catabolized to 2AA via the saccharopine pathway, which requires $NADP^+$ and two NAD^+ molecules. The subsequent conversion of 2-AA to glutaryl-CoA (substrate for ETF/ETF-QO system) requires an additional NAD^+ molecule. In addition to decreased 2-AA levels, we observed the accumulation of lysine and its alternative catabolite, pipecolate (Pip), in *Ndufs4*$^{-/-}$ skeletal muscles — indicating that an alternative non-NAD^+-consuming catabolic route is preferred, resulting in an even larger reduction in 2-AA levels. Altogether, the data suggest that βoxidation and amino acid catabolism might fuel the Q cycle via the ETF/ETF-QO system, even though a disturbed redox balance might limit the efficacy of some of the reactions.

When comparing previous metabolomics studies on *Ndufs4* knockout mice with our current observations, similar ambiguous effects on lipid metabolism are noticeable. In *Ndufs4*$^{-/-}$ liver, markedly reduced levels of fat droplets and free fatty acids were reported [11];

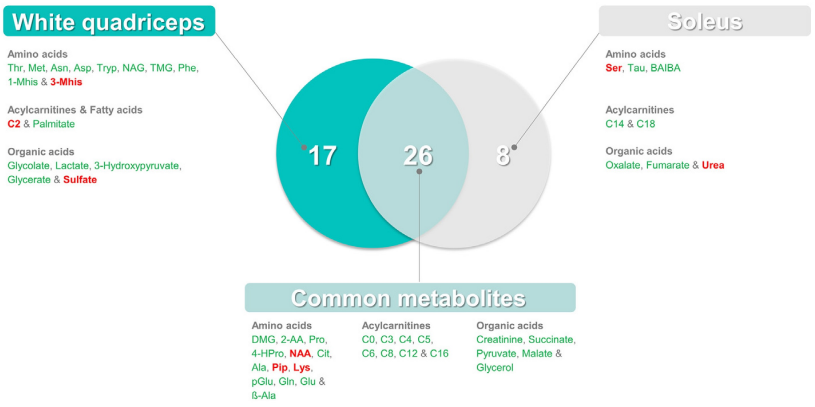


Fig. 3. Venn diagram of important metabolites discriminating *Ndufs4*$^{-/-}$ and WT groups in skeletal muscles. Green and red respectively indicate metabolites significantly ($p < 0.1$ and $D \geq 0.5$) lower or higher in *Ndufs4*$^{-/-}$ mice (n = 19) compared to WTs (n = 20). Among the important metabolites identified, 26 were common to both muscles, while several alterations were unique to the quadriceps (n = 17) and soleus (n = 8). Important metabolites (n = 5) identified in white quadriceps muscles by NMR spectroscopy were excluded from the comparison as soleus samples were not analyzed on that analytical platform due to limited sample quantity. Abbreviations: 1-Mhis, 1-Methylhistidine; 2-AA, 2-Aminoadipate; 2-Mhis, 2-Methylhistidine; Ala, Alanine; Asn, Asparagine; Asp, Aspartate; BAIBA, β-aminoisobutyrate; β-Ala, Beta-alanine; C0, Carnitine; C2, Acetyl-carnitine; C3, Propionyl-carnitine; C4, Butyryl-carnitine; C5, Isovaleryl-carnitine; C6, Hexanoyl-carnitine; C8, Octanoyl-carnitine; C12, Dodecanoyl-carnitine; C14, Myristoyl-carnitine; C16, Palmitoyl-carnitine; C18, Stearoyl-carnitine; Cit, Citrulline; DMG, N, *N*-Dimethylglycine; Gln; Glutamine; Glu, Glutamate; Hpro, Hydroxyproline; Lys, Lysine; Met, Methionine; NAA, N-Acetylaspartate; NAG, N-Acetylglutamate; pGlu, Pyroglutamate; Phe, Phenylalanine; Pip, Pipecolate; Pro, Proline; Ser, Serine; Tau, Taurine, Thr, Threonine; TMG, Trimethylglycine; Tryp, Tryptophan.

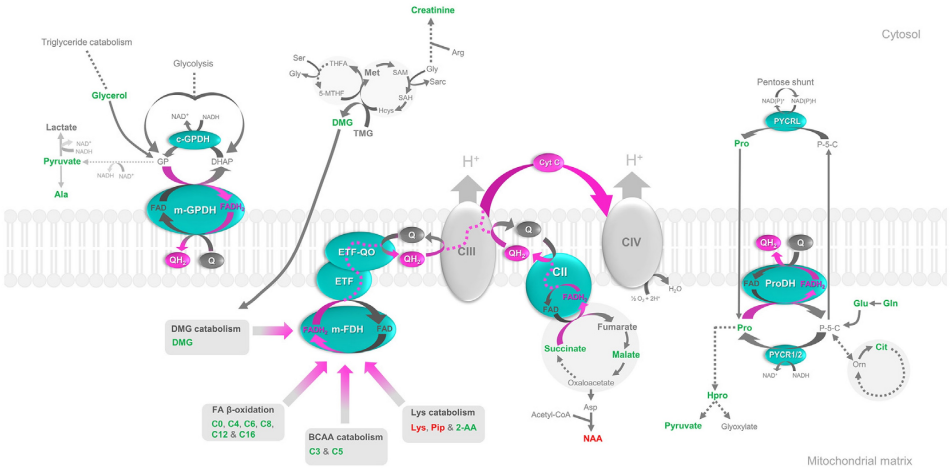


Fig. 4. Common metabolic alterations in *Ndufs4*$^{-/-}$ skeletal muscles. *Ndufs4*$^{-/-}$ quadriceps and soleus skeletal muscles both show a metabolic shift towards several non-classical pathways involved in oxidative metabolism and redox regulation, in an attempt to restore electron delivery to the respiratory chain via the ubiquinone (Q) pool. Green and red indicate metabolite levels significantly lower or higher, respectively, in *Ndufs4*$^{-/-}$ mice (n = 19) compared to WTs (n = 20). Pink arrows indicate electron flow. Dashed lines reflect multi-step reactions not fully shown. Multi-platform metabolic profiling of *Ndufs4*$^{-/-}$ skeletal muscles indicates (from left to right): 1) a shift in glycolysis and triglyceride catabolism towards the glycerol-3-phosphate shuttle, which re-oxidizes cytosolic NADH while serving as an electron donor to the respiratory chain via the mitochondrial enzyme glycerol-3-phosphate dehydrogenase (m-GPDH); 2) a shift in flux through several mitochondrial flavoprotein dehydrogenases (m-FDH) involved in one-carbon metabolism (dimethylglycine dehydrogenase), fatty acid β-oxidation (short-, medium- and long-chain acyl-CoA dehydrogenase), and amino acid catabolism (isobutyryl-, isovaleryl- and glutaryl-CoA dehydrogenase) which supply electrons to the respiratory chain via the electron transfer flavoprotein (ETF/ETF-QO) system; 3) a shift in flux through the Krebs cycle to increase electron delivery to the respiratory chain via complex II (CII; succinate dehydrogenase); and 4) increased mitochondrial cycling of proline and pyrroline-5-carboxylate (P-5-C) to directly provide electrons to the respiratory chain via proline dehydrogenase and sustain NAD^+ levels. Abbreviations: Enzymes in blue: ETF, Electron transfer flavoprotein; ETF-QO, Electron transfer flavoprotein:ubiquinone oxidoreductase; m-FDH(s), Mitochondrial flavoprotein dehydrogenase(s); m-GPDH, Mitochondrial glycerol-3-phosphate dehydrogenase; c-GPDH, Cytosolic glycerol-3-phosphate dehydrogenase; CII, Complex II or succinate dehydrogenase; ProDH, Proline dehydrogenase; PYCR, Pyrroline-5-carboxylate reductase; Cyt c, Cytochrome c. Electron carriers: FAD, Oxidized flavin adenine dinucleotide; $FADH_2$, Reduced flavin adenine dinucleotide; NAD^+, Oxidized nicotine amide adenine dinucleotide; NADH, Reduced nicotine amide adenine dinucleotide; Q, Ubiquinone (oxidized coenzyme Q); QH_2, Ubiquinol (reduced coenzyme Q). Metabolites: 2-AA, 2-Aminoadipate; 5-MTHF, 5-Methyltetrahydrofolate; Ala, Alanine; Arg, Arginine; Asp, Aspartate; C0, Carnitine; C12, Dodecanoyl-carnitine; C16, Palmitoyl-carnitine; C3, Propionyl-carnitine; C4, Butyryl-carnitine; C5, Isovaleryl-carnitine; C6, Hexanoyl-carnitine; C8, Octanoyl-carnitine; Cit, Citrulline; DHAP, Dihydroxyacetone phosphate; DMG, *N*, *N*-Dimethylglycine; GP, Glycerol-3-phosphate; Gln; Glutamine; Glu, Glutamate; Gly, Glycine; Hcys, Homocysteine; Hpro, Hydroxyproline; Lys, Lysine; Met, Methionine; NAA, N-Acetylaspartate; Orn, Ornithine; P-5-C, Pyrroline-5-carboxylate; Pip, Pipecolate; Pro, Proline; SAH, S-adenosylhomocysteine; SAM, S-adenosylmethionine; Sar, Sarcosine; Ser, Serine; THFA, Tetrahydrofolate.

while significantly increased blood hydroxy-acylcarnitine (C4:0, C16:0, and C18:1) levels were reported in a comparable *Ndufs4* knockout mouse model (*Ndufs4*$^{fky/fky}$) [32]. The latter observation was postulated to reflect a blockage in the NAD^+-dependent (third) step of βoxidation. However, upon further investigation, *Ndufs4*$^{fky/fky}$ liver and heart revealed no alterations in carnitine species, while skeletal muscle displayed no detectable lipid accumulation via Oil Red O staining [32]. These observations could fit into our combined hypotheses of decreased lipogenesis and increased lipolysis due to the activity of the GP shuttle, as well as increased fatty acid βoxidation, albeit inefficient due to a redox imbalance.

3.3.3. One-carbon metabolism, the methylation cycle, and the transsulfuration pathway

The altered redox state, as well as the postulated use of DMG by the ETF/ETF-QO system, seem to contribute to the disruption of one-carbon metabolism, the methylation cycle, and the transsulfuration pathway. These disturbances were more prominent in white quadriceps muscles which, along with decreased levels of DMG, displayed significantly decreased levels of trimethylglycine (betaine), methionine, threonine, and the accumulation of choline. Trimethylglycine (TMG) originates from the NAD^+ dependent catabolism of choline, which takes place in mitochondria. DMG is then produced from TMG in a folate-independent cytosolic reaction during which homocysteine is re-methylated to methionine. NAD^+ shortage could, therefore, cause choline build up and a further reduction in DMG levels. As DMG also has the ability to yield one-carbon units via folate-dependent mitochondrial reactions involving dimethylglycine dehydrogenase (which produces sarcosine) and sarcosine dehydrogenase (which produces glycine), this metabolite links one-carbon metabolism to the ETF/ETF-QO system.

Furthermore, in both *Ndufs4*$^{-/-}$ skeletal muscle types, dramatic decreases were seen in creatinine levels along with slightly (not significantly) reduced creatine levels. Creatine biosynthesis takes place chiefly in the liver and kidneys, however, a small amount of skeletal muscle creatine stores have been shown to be produced in the muscles themselves [40]. Creatine biosynthesis is a two-step reaction involving the conversion of arginine and glycine to guanidinoacetate, which is then methylated via SAM to form creatine and SAH. A disturbance in one-carbon metabolism could lead to lowered SAM available for methylation reactions, therefore dramatic decreases in creatinine could reflect the disrupted methylation of guanidinoacetate to creatine. In agreement, significantly reduced levels of 1-methylhistidine (1-Mhis) and increased levels of histamine in *Ndufs4*$^{-/-}$ white quadriceps could also reflect disturbed methylation reactions. On the whole, the observed metabolic alterations indicate disturbances in one-carbon metabolism and methylation reactions, possibly due to a disturbed redox balance and derangements in DMG metabolism.

3.3.4. The Krebs cycle and mitochondrial complex II (succinate dehydrogenase)

We observed significantly decreased levels of succinate and malate in both muscles along with significant (soleus) and moderate (white quadriceps) reductions in fumarate levels. A similar observation was made in *Ndufs4*$^{-/-}$ (P35) hind limb skeletal muscle by Alam and

colleagues [29], who reported decreased succinate levels along with an increase in flux (10–11%) through reactions providing substrates to CII and a slight decrease in the other (generally NAD^+ consuming) reactions which mainly fuel CI. The reduction in metabolite levels we observed could, therefore, reflect an increased use of succinate to fuel CII and the respiratory chain via the Q pool together with a decreased resupply thereof due to a congested Krebs cycle. In addition, we observed increased levels of *N*-acetylasparte (NAA) which is hypothesized to be an alternative storage and transport form of acetate and has been suggested to play a role in lipid metabolism and posttranslational protein modification [41]. Although the physiological functions of NAA are still poorly understood, it was recently discovered that NAA metabolism is not exclusive to the brain as previously thought. Aberrant NAA metabolism has been reported in mitochondrial disease, however, to the best of our knowledge this is the first report thereof in skeletal muscle. NAA is synthesized from aspartate and acetyl-CoA by aspartate *N*-acetyltransferase (Asp-NAT, EC 2.3.1.17). In skeletal muscle, the expression of *Nat8l* mRNA (encoding Asp-NAT) has been observed, although levels were reported to be negligible [41]. We, therefore, hypothesize that the rate of acetyl-CoA synthesis from sources like β-oxidation and lysine catabolism (which fuel the ETF/ETF-QO system) exceeds the rate at which the Krebs cycle can utilize the molecule, therefore acetyl-CoA accumulates and is converted to NAA [41].

3.3.5. Proline metabolism and the proline cycle

Although there is still much to be learned about the precise mechanism and functions of the proline cycle, the vital role of this relatively novel pathway in health and disease is becoming increasingly clear (reviewed by Phang et al. [42]). Some of the most striking metabolic alterations we observed in *Ndufs4*$^{-/-}$ skeletal muscles included the reduction of proline, hydroxyproline (Hpro), citrulline, glutamate, and glutamine levels. These alterations could reflect aberrant proline metabolism, which is strongly associated with the pentose phosphate pathway, urea cycle, and Krebs cycle. The mitochondrial flavin-dependent enzyme, proline dehydrogenase (ProDH, EC 1.5.99.8), together with the cytosolic (PYCRL) and mitochondrial (PYCR1/2) isoforms of pyrroline-5-carboxylate reductase (EC 1.5.1.2) are responsible for the interconversions of proline and pyrroline-5-carboxylate (P-5-C) constituting the proline cycle. Proline can directly act as an alternative source of electron delivery to the RC Q pool, through its catabolism to P-5-C via ProDH. P-5-C can also be synthesized from either glutamate or ornithine while its conversion back to proline regenerates $NAD(P)^+$. We, therefore, postulate that the adaptive increased cycling of proline and P-5-C might serve to sustain QH_2 and $NAD(P)^+$ levels. In addition to energy production and redox homeostasis, proline metabolism has been shown to be involved in ROS production, the initiation of apoptosis, autophagy, as well as protein and nucleotide synthesis while proline's post-translational product, hydroxyproline, has recently been recognized as a substrate for the synthesis of pyruvate, glucose, and glycine (reviewed by Wu et al. [43]). Taken together, proline metabolism might play a central role in several metabolic pathway derangements often reported in mitochondrial disease.

3.4. Fiber type-specific metabolic alterations in *Ndusf4*$^{-/-}$ skeletal muscles

When looking at the difference between the important metabolites identified in *Ndufs4*$^{-/-}$ muscles (Fig. 3), seventeen metabolites were uniquely altered in the white quadriceps while eight alterations were unique to the soleus. This comparison excludes the five important metabolites detected with NMR spectroscopy as soleus samples were not analyzed on that analytical platform due to limited sample quantity. Altogether, glycolytic fibers (white quadriceps) seemed to show more pronounced metabolic disturbances in response to CI deficiency with NAA accumulation being more than two-fold higher than in soleus muscles, along with an additional accumulation of acetyl-CoA derivatives, acetate, and acetyl-carnitine (C2). In addition, *Ndufs4*$^{-/-}$ white quadriceps muscles showed significant 3-methylhistidine accumulation, which is indicative of myofibrillar protein breakdown [44]. This observation agrees with literature reports of glycolytic fibers showing more pronounced atrophy than oxidative fibers in pathological conditions affecting muscle protein balance, and aging [16]. Taken together with the greater disturbance in methylation reactions we observed in white quadriceps muscles (discussed in Section 3.3.3), these alterations could indicate more profound disruptions of the redox balance (NAD^+/NADH ratio), Krebs cycle congestion and possible acetyl-CoA accumulation in more glycolytic muscle fibers. In addition to less dramatic metabolic alterations than in the white quadriceps, we saw significantly increased levels of serine along with decreased levels of taurine and pyroglutamate in *Ndufs4*$^{-/-}$ soleus muscles. These alterations could indicate a shift in glycolysis towards serine production, which could be used for glutathione synthesis — a phenomenon often described in mitochondrial disease due to increased electron leak and ROS production. As oxidative fibers have been shown to have a greater supply of substrates, oxygen, and more mitochondria (with greater oxidative capacity) [16], it can be postulated that mitochondrial ROS levels — due to the CI deficiency — are higher in *Ndufs4*$^{-/-}$ soleus muscles and therefore the need for glutathione ROS scavenging is greater. Furthermore, our results suggest that BCAA catabolism might be more dramatically affected in soleus muscles as we observed moderately (but not significantly) increased levels of valine and leucine, significant decreases in β-aminoisobutyrate (BAIBA) levels, and much greater decreases in C5- and C3-carnitine levels than in the white quadriceps muscles. Hence, the data could point to a more effectively functioning Krebs cycle and a better metabolic adaption of soleus muscles to the CI defect.

4. Conclusions

We report the first fiber type-specific enzymatic and metabolic data in *Ndufs4*$^{-/-}$ skeletal muscles. Enzyme assays revealed a severe reduction (80%) in CI activity in both glycolytic (white quadriceps) and oxidative (soleus) muscles from whole-body *Ndufs4*$^{-/-}$ mice. Such an extreme reduction in CI activity would greatly reduce the electron flux to the rest of the respiratory chain (RC). As an adaptive response in both tissues, our metabolic data suggest that alternative fuels and non-classical pathways serve to sustain the RC ubiquinol (QH_2) pool, thereby restoring electron flux to CIII through the ubiquinone (Q) cycle. However, despite these metabolic adaptions in skeletal muscle, a disturbed redox balance still seems to result in congested mitochondrial pathways. Metabolic and bioenergetic disturbances due to CI deficiency seem to be more evident in glycolytic fibers, possibly due to their innately lower mitochondrial content. Some of the most significant metabolic alterations we observed in *Ndufs4*$^{-/-}$ muscles implicate the involvement of the glycerol-3-phosphate (GP) shuttle, the electron transfer flavoprotein (ETF/ETF-QO) system, complex II of the RC, and the proline cycle in electron delivery to the Q pool. Some of these mechanisms might also serve to restore NAD^+ levels (GP shuttle and proline cycle), while others could contribute to redox imbalance (NAD^+ consuming reactions fueling ETF/ETF-QO and the Krebs cycle) in CI deficiency. Altogether, the observed adaptive mechanisms could explain the apparent lack of an obvious muscle phenotype in *Ndufs4*$^{-/-}$ mice, as well as the reported ability of skeletal muscle to maintain normal ATP production, despite CI deficiency [9,29]. However, the hypotheses generated in this study need to be followed up/validated in more targeted metabolic studies on *Ndufs4*$^{-/-}$ mice. For now, it remains unclear whether these adaptive responses are capable of sustaining energy homeostasis when challenged with exercise or nutrient deprivation. A comparison of these and related metabolic pathways in other tissues (e.g. the brain) could possibly provide answers to tissue-specific phenotypes and novel insight in targeted therapeutic interventions.

Transparency document

The Transparency document associated with this article can be found, in online version.

Acknowledgments

Funding: This work was supported by the National Research Foundation of South Africa (NRF; Grant numbers 92736 and 111247) and the Technological Innovation Agency of the Department of Science and Technology, Republic of South Africa (TIA; Grant number Metabol. 01). Opinions expressed and conclusions arrived at, are those of the authors and are not necessarily to be attributed to the NRF or the TIA. We thank Kobus Venter and Antoinette Fick from the Pre-Clinical Drug Development Platform (PCDDP, NWU, RSA), for their assistance regarding animal handling.

Conflict of interest

All authors declare that they have no conflict of interest.

Ethical approval

The AnimCare animal research ethics committee of North-West University approved (NWU-00378-16-A5) the animal protocols used in this study. All animals were maintained and all procedures performed in accordance with the code of ethics in research, training, and testing of drugs in South Africa and complied with national legislation.

Appendix A. Supplementary data

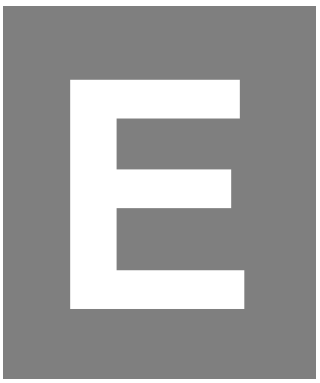
Supplementary data to this article can be found online at https://doi.org/10.1016/j.bbadis.2018.10.034.

References

[1] D.T. Shaughnessy, K. McAllister, L. Worth, A.C. Haugen, J.N. Meyer, F.E. Domann, B. Van Houten, R. Mostoslavsky, S.J. Bultman, A.A. Baccarelli, T.J. Begley, R.W. Sobol, M.D. Hirschey, T. Ideker, J.H. Santos, W.C. Copeland, R.R. Tice, D.M. Balshaw, Mitochondria, energetics, epigenetics, and cellular responses to stress, Environ. Health Perspect. 122 (2014) 1271–1278.
[2] I.N. Shokolenko, M.F. Alexeyev, Mitochondrial DNA: a disposable genome? Biochim. Biophys. Acta 1852 (2015) 1805–1809.
[3] L.C. Greaves, A.K. Reeve, R.W. Taylor, D.M. Turnbull, Mitochondrial DNA and disease, J. Pathol. 226 (2012) 274–286.
[4] A.D. Cherry, C.A. Piantadosi, Regulation of mitochondrial biogenesis and its intersection with inflammatory responses, Antioxid. Redox Signal. 22 (2015) 965–976.
[5] E. Fassone, S. Rahman, Complex I deficiency: clinical features, biochemistry and molecular genetics, J. Med. Genet. 49 (2012) 578–590.
[6] F. Distelmaier, W.J.H. Koopman, L.P. van den Heuvel, R.J. Rodenburg, E. Mayatepek, P.H.G.M. Willems, J.A.M. Smeitink, Mitochondrial complex I deficiency: from organelle dysfunction to clinical disease, Brain 132 (2009) 833–842.
[7] M.A. Calvaruso, P. Willems, M. van den Brand, F. Valsecchi, S. Kruse, R. Palmiter, J. Smeitink, L. Nijtmans, Mitochondrial complex III stabilizes complex I in the absence of NDUFS4 to provide partial activity, Hum. Mol. Genet. 21 (2012) 115–120.
[8] F. Valsecchi, W.J.H. Koopman, G.R. Manjeri, R.J. Rodenburg, J.A.M. Smeitink, P.H.G.M. Willems, Complex I disorders: causes, mechanisms, and development of treatment strategies at the cellular level, Dev. Disabil. Res. Rev. 16 (2010) 175–182.
[9] S.E. Kruse, W.C. Watt, D.J. Marcinek, R.P. Kapur, K.A. Schenkman, R.D. Palmiter, Mice with mitochondrial complex I deficiency develop a fatal encephalomyopathy, Cell Metab. 7 (2008) 312–320.
[10] Z. Jin, W. Wei, M. Yang, Y. Du, Y. Wan, Mitochondrial complex I activity suppresses inflammation and enhances bone resorption by shifting macrophage-osteoclast polarization, Cell Metab. 20 (2014) 483–498.
[11] S.C. Johnson, M.E. Yanos, E.–.B. Kayser, A. Quintana, M. Sangesland, A. Castanza, L. Uhde, J. Hui, V.Z. Wall, A. Gagnidze, K. Oh, B.M. Wasko, F.J. Ramos, R.D. Palmiter, P.S. Rabinovitch, P.G. Morgan, M.M. Sedensky, M. Kaeberlein, mTOR inhibition alleviates mitochondrial disease in a mouse model of Leigh syndrome, Science 342 (2013) 1524–1528.
[12] A. Torraco, S. Peralta, L. Iommarini, F. Diaz, Mitochondrial diseases part I: mouse models of OXPHOS deficiencies caused by defects on respiratory complex subunits or assembly factors, Mitochondrion (2015) 76–91.
[13] S. Foriel, J. Beyrath, I. Eidhof, R.J. Rodenburg, A. Schenck, J.A.M. Smeitink, Feeding difficulties, a key feature of the *Drosophila* NDUFS4 mitochondrial disease model, Dis. Model. Mech. 11 (2018).
[14] R.R. Wolfe, The underappreciated role of muscle in health and disease, Am. J. Clin. Nutr. 84 (2006) 475–482.
[15] M.F. Goody, C.A. Henry, A need for NAD^+ in muscle development, homeostasis, and aging, Skelet. Muscle 8 (2018) 9.
[16] S. Schiaffino, C. Reggiani, Fiber types in mammalian skeletal muscles, Physiol. Rev. 91 (2011) 1447–1531.
[17] D. Shepherd, P.B. Garland, The kinetic properties of citrate synthase from rat liver mitochondria, Biochem. J. 114 (1969) 597–610.
[18] A.J.M. Janssen, F.J.M. Trijbels, R.C.A. Sengers, J.A.M. Smeitink, L.P. van den Heuvel, L.T.M. Wintjes, B.J.M. Stoltenborg–Hogenkamp, R.J.T. Rodenburg, Spectrophotometric assay for complex I of the respiratory chain in tissue samples and cultured fibroblasts, Clin. Chem. 53 (2007) 729–734.
[19] S. Rahman, R.B. Blok, I.H.-H.M. Dah, D.M. Danks, D.M. Kirby, C.W. Chow, J. Christodoulou, D.R. Thorburn, Leigh syndrome: clinical features and biochemical and DNA abnormalities, Ann. Neurol. 39 (1996) 343–351.
[20] C.M.C. Mels, P. Jansen Van Rensburg, F.H. van der Westhuizen, P.J. Pretorius, E. Erasmus, Increased excretion of C4–carnitine species after a therapeutic acetylsalicylic acid dose: evidence for an inhibitory effect on short–chain fatty acid metabolism, ISRN Pharmacol. 2011 (2011) 851870.
[21] J.Z. Lindeque, J. Hidalgo, R. Louw, F.H. van der Westhuizen, Systemic and organ specific metabolic differences in metallothionein knockout mice when challenged with exercise, Metabolomics 9 (2013) 418–432.
[22] S.W. Mason, K. Terburgh, R. Louw, Miniaturized ^{1}H–NMR method for analyzing limited–quantity samples applied to a mouse model of Leigh disease, Metabolomics 14 (2018) 74.
[23] K. Terburgh, J.Z. Lindeque, S.W. Mason, F.H. Van der Westhuizen, R. Louw, Multi-platform metabolomics data from Ndufs4$^{-/-}$ skeletal muscles, Metabolomics Workbench, http://www.metabolomicsworkbench.org, (2018).
[24] J. Gullberg, P. Jonsson, A. Nordström, M. Sjöström, T. Moritz, Design of experiments: an efficient strategy to identify factors influencing extraction and derivatization of *Arabidopsis thaliana* samples in metabolomic studies with gas chromatography/mass spectrometry, Anal. Biochem. 331 (2004) 283–295.
[25] J. Xia, I. Sinelnikov, B. Han, D.S. Wishart, MetaboAnalyst 3.0–making metabolomics more meaningful, Nucleic Acids Res. 43 (2015) W251–W257.
[26] S.M. Ellis, H.S. Steyn, Practical significance (effect sizes) versus or in combination with statistical significance (p–values), Manag. Dyn. 12 (2003) 51–53.
[27] L.W. Sumner, A. Amberg, D. Barrett, M.H. Beale, R. Beger, C.A. Daykin, T.W.M. Fan, O. Fiehn, R. Goodacre, J.L. Griffin, T. Hankemeier, N. Hardy, J. Harnly, R. Higashi, J. Kopka, A.N. Lane, J.C. Lindon, P. Marriott, A.W. Nicholls, M.D. Reily, J.J. Thaden, M.R. Viant, Proposed minimum reporting standards for chemical analysis chemical analysis working group (CAWG) metabolomics standards initiative (MSI), Metabolomics 3 (2007) 211–221.
[28] E.L. Schymanski, J. Jeon, R. Gulde, K. Fenner, M. Ruff, H.P. Singer, J. Hollender, Identifying small molecules via high resolution mass spectrometry: communicating confidence, Environ. Sci. Technol. 48 (2014) 2097–2098.
[29] M.T. Alam, G.R. Manjeri, R.J. Rodenburg, J.A.M. Smeitink, R.A. Notebaart, M. Huynen, P.H.G.M. Willems, W.J.H. Koopman, Skeletal muscle mitochondria of NDUFS4$^{-/-}$ mice display normal maximal pyruvate oxidation and ATP production, Biochim. Biophys. Acta Bioenerg. 1847 (2015) 526–533.
[30] F. Valsecchi, C. Monge, M. Forkink, A.J.C. de Groof, G. Benard, R. Rossignol, H.G. Swarts, S.E. van Emst-De Vries, R.J. Rodenburg, M.A. Calvaruso, L.G.J. Nijtmans, B. Heeman, P. Roestenberg, B. Wieringa, J.A.M. Smeitink, W.J.H. Koopman, P.H.G.M. Willems, Metabolic consequences of NDUFS4 gene deletion in immortalized mouse embryonic fibroblasts, Biochim. Biophys. Acta Bioenerg. 1817 (2012) 1925–1936.
[31] R. de Haas, D. Das, A. Garanto, H.G. Renkema, R. Greupink, P. van den Broek, J. Pertijs, R.W.J. Collin, P. Willems, J. Beyrath, A. Heerschap, F.G. Russel, J.A. Smeitink, Therapeutic effects of the mitochondrial ROS–redox modulator KH176 in a mammalian model of Leigh disease, Sci. Rep. 7 (2017) 11733.
[32] D.W. Leong, J.C. Komen, C.A. Hewitt, E. Arnaud, M. McKenzie, B. Phipson, M. Bahlo, A. Laskowski, S.A. Kinkel, G.M. Davey, W.R. Heath, A.K. Voss, R.P. Zahedi, J.J. Pitt, R. Chrast, A. Sickmann, M.T. Ryan, G.K. Smyth, D.R. Thorburn, H.S. Scott, Proteomic and metabolomic analyses of mitochondrial complex I-deficient mouse model generated by spontaneous B2 short interspersed nuclear element (SINE) insertion into NADH dehydrogenase (ubiquinone) Fe-S protein 4 (Ndufs4) gene, J. Biol. Chem. 287 (2012) 20652–20663.
[33] S.M.S. Budde, L.P.W.J. van den Heuvel, R.J.P. Smeets, D. Skladal, J.A. Mayr, C. Boelen, V. Petruzzella, S. Papa, J.A.M. Smeitink, Clinical heterogeneity in patients with mutations in the NDUFS4 gene of mitochondrial complex I, J. Inherit. Metab. Dis. 26 (2003) 813–815.
[34] C. Ugalde, R.J.R.J. Janssen, L.P. van den Heuvel, J.A.M. Smeitink, L.G.J. Nijtmans, Differences in assembly or stability of complex I and other mitochondrial OXPHOS complexes in inherited complex I deficiency, Hum. Mol. Genet. 13 (2004) 659–667.
[35] S.M.S. Budde, L.P.W.J. van den Heuvel, A.J. Janssen, R.J.P. Smeets, C.A.F. Buskens, L. Demeirleir, R. Van Coster, M. Baethmann, T. Voit, J.M.F. Trijbels, J.A.M. Smeitink, Combined enzymatic complex I and III deficiency associated with mutations in the nuclear encoded NDUFS4 gene, Biochem. Biophys. Res. Commun. 275 (2000) 63–68.
[36] M.E. Breuer, P.H.G.M. Willems, J.A.M. Smeitink, W.J.H. Koopman, M. Nooteboom, Cellular and animal models for mitochondrial complex I deficiency: a focus on the NDUFS4 subunit, IUBMB Life 65 (2013) 202–208.
[37] K. Esterhuizen, F.H. van der Westhuizen, R. Louw, Metabolomics of mitochondrial disease, Mitochondrion 35 (2017) 97–110.
[38] A.E. McDonald, N. Pichaud, C.-A. Darveau, "Alternative" fuels contributing to mitochondrial electron transport: importance of non-classical pathways in the

diversity of animal metabolism, Comp. Biochem. Physiol. B 224 (2018) 185–194.
[39] N.J. Watmough, F.E. Frerman, The electron transfer flavoprotein: ubiquinone oxidoreductases, Biochim. Biophys. Acta Bioenerg. 1797 (2010) 1910–1916.
[40] A.P. Russell, L. Ghobrial, C.R. Wright, S. Lamon, E.L. Brown, M. Kon, M.R. Skelton, R.J. Snow, Creatine transporter (SLC6A8) knockout mice display an increased capacity for in vitro creatine biosynthesis in skeletal muscle, Front. Physiol. 5 (2014) 314.
[41] J.G. Bogner-Strauss, *N*–Acetylaspartate metabolism outside the brain: lipogenesis, histone acetylation, and cancer, Front. Endocrinol. 8 (2017) 240.
[42] J. Phang, Proline metabolism in cell regulation and cancer biology: recent advances and hypotheses, Antioxid. Redox Signal. (2017), https://doi.org/10.1089/ars.2017.7350.
[43] G. Wu, F.W. Bazer, R.C. Burghardt, G.A. Johnson, S.W. Kim, D.A. Knabe, P. Li, X. Li, J.R. McKnight, M.C. Satterfield, T.E. Spencer, Proline and hydroxyproline metabolism: implications for animal and human nutrition, Amino Acids 40 (2011) 1053–1063.
[44] G.A. Qureshi, A. Gutierrez, J. Bergström, Determination of histidine, 1-methylhistidine and 3-methylhistidine in biological samples by high-performance liquid chromatography: clinical application of urinary 3-methylhistidine in evaluating the muscle protein breakdown in uraemic patients, J. Chromatogr. B Biomed. Sci. Appl. 374 (1986) 363–369.

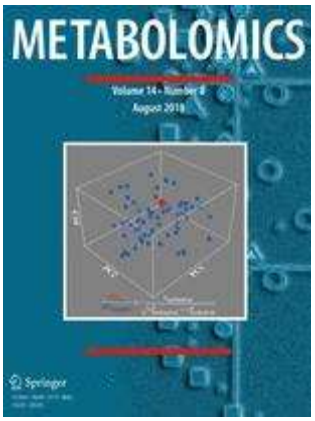
ANNEXURE



Metabolomics author guidelines

Springer METABOLOMICS

Instructions for Authors



TYPES OF PAPERS

Original Articles

The journal publishes Original Research articles that contextualize their hypothesis and research to a broader global issue, and/or present a novel technological approach to the study of metabolomics. All research paper submissions are supported by sound experimental design, methodology, and data interpretation. Submissions of Original Research articles should be 2,500-4,000 words in length (or a maximum of 7 printed pages), should have a maximum of 6 figures/tables (combined), and data should be made accessible via public metabolomics data repositories. Supplementary information is welcome.

ISSN: 1573-3882

Reviews

There are several types of reviews that Metabolomics aims to publish:
Critical Reviews which review an area in a critical fashion. These reviews aim to critique objectively an area and in doing so synthesis knowledge giving the reader a feel for the critical aspects in terms of what has been currently achieved and what is needed to move a particular field forward. These are typically 7-15 pp. printed text.
Tutorial Reviews are used to guide a reader through a particular area, be it analytical in nature, computational, or of a biological/medical focus. These should contain a teaching element aimed at earlier career scientists. These are typically 7-15 pp. printed text.
Mini-reviews are highly focused and report on a current hot topic of importance within metabolomics. These should aim to review and critique a few key papers in the field. These are a maximum of 4 pp. printed text.
Opinion Pieces like mini-reviews are focused on a particular area and should review a few key papers in the field. As these are opinions, if there is potential contention then authors of papers that are criticized may be asked for their views first, and these along with the reviews comments may be published. These are a maximum of 4 printed pages.

Short Communications

• This should follow the same style as a full paper (please refer to section above).
• The Abstract contains less than 100 words.
• This is followed by a brief Introduction section.
• Material and Methods should allow work to be reproduced and extensive material should be provided in supporting Supplementary Information.
• The Results and Discussion must be combined.
• References contain no more than 20 references.
• These are a maximum of 4 pages of printed text, with a combined maximum of 2 Figures and/or Tables.

Software/Databases

These highlight recent developments in software and computer programs along with database developments. Submissions should follow the original article format with structured abstracts and within the abstract and paper details of where to access the software and databases. Articles of this type can also be produced in brief formats as short communications.

GENERAL FORMAT FOR ALL TYPES OF PAPERS

Format

1. Abstract
Original Papers require a structured abstract of less than 250 words arranged under the following headings:
• Introduction: Describe the topic's mechanisms, history, and/or how it relates to a problem.
• Objectives: Explain the purpose. What does the study try to demonstrate?
• Methods: Briefly describe the experimental design.
• Results: Report your findings.
• Conclusion: Analyse your results and link it back to the purpose.
Reviews also require an abstract. Please adhere to the following structure:
• Background
• Aim of Review

• Key Scientific Concepts of Review
An abstract is not required of Commentaries or Letters to the Editor.
Each heading should be composed of 1-2 sentences. All abstracts must not include equations, tables, reference citations, or graphics.

2. Introduction: briefly introduces the area and provides a road map of what is to come.
3. Headed Sections: a series of these are then used to bring various aspects together
4. Overall Conclusions: should be made to bring the review to a conclusion.
5. Figures and Tables: should be used to break up the text.

A well-used figure or table can be used to synthesis knowledge, depict time lines etc. The data presented in these formats should stand-alone and the author should avoid repeating these within the body of the text.

MANUSCRIPT PREPARATION

Ethical Statements and Journal Specific Requirements:

• Conflicts of Interest Statement
• Author Contributions
• Ethical Statements
• Data Availability
• Software Availability

Author Conflict of Interest Statement

Funding: This study was funded by X (grant number X). (optional - could be left out in case no funding was received)
Conflict of Interest: Author1 declares that he/she has no conflict of interest.
Author2 declares that he/she has no conflict of interest. …

Author Contribution Statement

Authors must provide a short description of the contributions made by each listed author (please use initials). This will be published in a separate section in front of the Acknowledgments.For example: AM and DB conceived and designed research. AM and BB conducted experiments. GR contributed new reagents or analytical tools. AM and GR analysed data. AM wrote the manuscript. All authors read and approved the manuscript.

Authorship Policy

Authorship should incorporate and should be restricted to those who have contributed substantially to the work in one or more of the following categories:

• Conceived of or designed study
• Performed research
• Analysed data
• Contributed new methods or models
• Wrote the paper

Compliance with Ethical Standards

Please included a Compliance with Ethical Standards section before the References as shown in the samples below.
In case animals were involved:
“All applicable international, national, and/or institutional guidelines for the care and use of animals were followed.”
And/or in case humans were involved:
“All procedures performed in studies involving human participants were in accordance with the ethical standards of the institutional and/or national research committee and with the 1964 Helsinki declaration and its later amendments or comparable ethical standards.”
Informed consent: “Informed consent was obtained from all individual participants included in the study.
If articles do not contain studies with human participants or animals by any of the authors, please select one of the following statements:
“This article does not contain any studies with human and/or animal participants performed by any of the authors.”

Data Availability Statement

“The metabolomics and metadata reported in this paper are available via [insert repository and URL] study identifier [insert study identifier/project ID etc]"

Software or Database Availability Statement

"The software developed in this study is available via [inset URL]"
and/or
"The database reported in this study is accessible via [inset URL]"

Data Availability Statement

The Metabolomics strongly encourages open data! If you have not already done so, please make your research data available – for example on the following repositories:
Metabolights https://www.ebi.ac.uk/metabolights/
Metabolnote http://metabolonote.kazusa.or.jp/Main_Page
Metabolomics Workbench http://www.metabolomicsworkbench.org/
Metaspace http://metaspace2020.eu/#/about

OFFPRINTS

25 offprints of each article will be provided free of charge. Additional offprints can be ordered by means of an offprint order form supplied with the proofs.

MANUSCRIPT SUBMISSION

Manuscript Submission

Submission of a manuscript implies: that the work described has not been published before; that it is not under consideration for publication anywhere else; that its publication has been approved by all co-authors, if any, as well as by the responsible authorities – tacitly or explicitly – at the institute where the work has been carried out. The publisher will not be held legally responsible should there be any claims for compensation.

Permissions

Authors wishing to include figures, tables, or text passages that have already been published elsewhere are required to obtain permission from the copyright owner(s) for both the print and online format and to include evidence that such permission has been granted when submitting their papers. Any material received without such evidence will be assumed to originate from the authors.

Online Submission

Please follow the hyperlink "Submit online" on the right and upload all of your manuscript files following the instructions given on the screen.

PLAGIARISM CHECK WITH CROSSCHECK

Plagiarism prevention with CrossCheck

Springer is a participant of CrossCheck, a multi-publisher plagiarism detection initiative to screen published and submitted content for originality. CrossCheck consists of two products: a database of scholarly publications (CrossCheck) and a web-based tool (iThenticate) to check an authored work against that database.
This journal uses the plagiarism tool to detect instances of overlapping and similar text in submitted manuscripts and your manuscript may be screened upon submission for plagiarism against previously published works.

TITLE PAGE

Title Page

The title page should include:
The name(s) of the author(s)
A concise and informative title
The affiliation(s) and address(es) of the author(s)
The e-mail address, and telephone number(s) of the corresponding author
If available, the 16-digit ORCID of the author(s)

Abstract

Please provide an abstract of 150 to 250 words. The abstract should not contain any undefined abbreviations or unspecified references.

Keywords

Please provide 4 to 6 keywords which can be used for indexing purposes.

TEXT

Text Formatting

Manuscripts should be submitted in Word.
Use a normal, plain font (e.g., 10-point Times Roman) for text.
Use italics for emphasis.
Use the automatic page numbering function to number the pages.
Do not use field functions.
Use tab stops or other commands for indents, not the space bar.
Use the table function, not spreadsheets, to make tables.
Use the equation editor or MathType for equations.
Save your file in docx format (Word 2007 or higher) or doc format (older Word versions).
Manuscripts with mathematical content can also be submitted in LaTeX.
LaTeX macro package (zip, 182 kB)

Headings

Please use the decimal system of headings with no more than three levels.

Abbreviations

Abbreviations should be defined at first mention and used consistently thereafter.

Footnotes

Footnotes can be used to give additional information, which may include the citation of a reference included in the reference list. They should not consist solely of a reference citation, and they should never include the bibliographic details of a reference. They should also not contain any figures or tables.
Footnotes to the text are numbered consecutively; those to tables should be indicated by superscript lower-case letters (or asterisks for significance values and other statistical data). Footnotes to the title or the authors of the article are not given reference symbols.
Always use footnotes instead of endnotes.

Acknowledgments

Acknowledgments of people, grants, funds, etc. should be placed in a separate section on the title page. The names of funding organizations should be written in full.

SCIENTIFIC STYLE

Please always use internationally accepted signs and symbols for units (SI units).
Nomenclature: Insofar as possible, authors should use systematic names similar to those used by Chemical Abstract Service or IUPAC.
Genus and species names should be in italics.
Generic names of drugs and pesticides are preferred; if trade names are used, the generic name should be given at first mention.
Please use the standard mathematical notation for formulae, symbols, etc.:
Italic for single letters that denote mathematical constants, variables, and unknown quantities
Roman/upright for numerals, operators, and punctuation, and commonly defined functions or abbreviations, e.g., cos, det, e or exp, lim, log, max, min, sin, tan, d (for derivative)
Bold for vectors, tensors, and matrices.

REFERENCES

Citation

Cite references in the text by name and year in parentheses. Some examples:
Negotiation research spans many disciplines (Thompson 1990).
This result was later contradicted by Becker and Seligman (1996).
This effect has been widely studied (Abbott 1991; Barakat et al. 1995; Kelso and Smith 1998; Medvec et al. 1999).

Reference list

The list of references should only include works that are cited in the text and that have been published or accepted for publication. Personal communications and unpublished works should only be mentioned in the text. Do not use footnotes or endnotes as a substitute for a reference list.
Reference list entries should be alphabetized by the last names of the first author of each work.

Journal article
Harris, M., Karper, E., Stacks, G., Hoffman, D., DeNiro, R., Cruz, P., et al. (2001). Writing labs and the Hollywood connection. Journal of Film Writing, 44(3), 213–245.
Article by DOI
Slifka, M. K., & Whitton, J. L. (2000) Clinical implications of dysregulated cytokine production. Journal of Molecular Medicine, https://doi.org/10.1007/s001090000086
Book
Calfee, R. C., & Valencia, R. R. (1991). APA guide to preparing manuscripts for journal publication. Washington, DC: American Psychological Association.
Book chapter
O'Neil, J. M., & Egan, J. (1992). Men's and women's gender role journeys: Metaphor for healing, transition, and transformation. In B. R. Wainrib (Ed.), Gender issues across the life cycle (pp. 107–123). New York: Springer.
Online document
Abou-Allaban, Y., Dell, M. L., Greenberg, W., Lomax, J., Peteet, J., Torres, M., & Cowell, V. (2006). Religious/spiritual commitments and psychiatric practice. Resource document. American Psychiatric Association. http://www.psych.org/edu/other_res/lib_archives/archives/200604.pdf. Accessed 25 June 2007.
Journal names and book titles should be italicized.
For authors using EndNote, Springer provides an output style that supports the formatting of in-text citations and reference list.
EndNote style (zip, 3 kB)

EndNote-Style for Metabolomics

Please find an EndNote citation style that had been customised for the journal at the Link below:

Link (zip, 1 kB)

TABLES

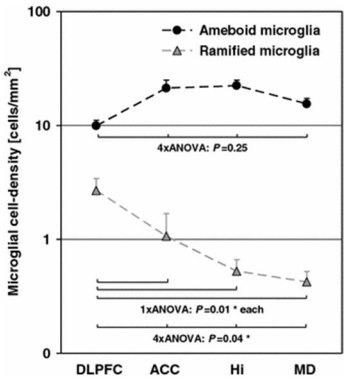
All tables are to be numbered using Arabic numerals.
Tables should always be cited in text in consecutive numerical order.
For each table, please supply a table caption (title) explaining the components of the table.
Identify any previously published material by giving the original source in the form of a reference at the end of the table caption.
Footnotes to tables should be indicated by superscript lower-case letters (or asterisks for significance values and other statistical data) and included beneath the table body.

ARTWORK AND ILLUSTRATIONS GUIDELINES

Electronic Figure Submission

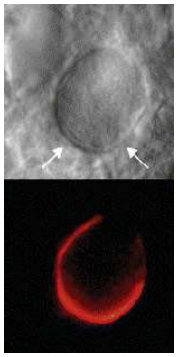
Supply all figures electronically.
Indicate what graphics program was used to create the artwork.
For vector graphics, the preferred format is EPS; for halftones, please use TIFF format. MSOffice files are also acceptable.
Vector graphics containing fonts must have the fonts embedded in the files.
Name your figure files with "Fig" and the figure number, e.g., Fig1.eps.

Line Art



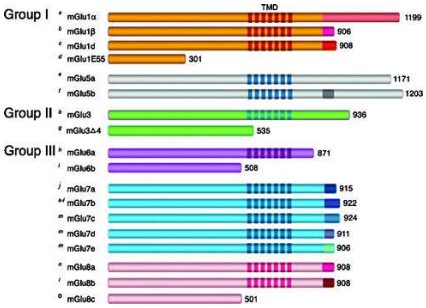
Definition: Black and white graphic with no shading.
Do not use faint lines and/or lettering and check that all lines and lettering within the figures are legible at final size.
All lines should be at least 0.1 mm (0.3 pt) wide.
Scanned line drawings and line drawings in bitmap format should have a minimum resolution of 1200 dpi.
Vector graphics containing fonts must have the fonts embedded in the files.

Halftone Art



Definition: Photographs, drawings, or paintings with fine shading, etc.
If any magnification is used in the photographs, indicate this by using scale bars within the figures themselves.
Halftones should have a minimum resolution of 300 dpi.

Combination Art



Definition: a combination of halftone and line art, e.g., halftones containing line drawing, extensive lettering, color diagrams, etc.
Combination artwork should have a minimum resolution of 600 dpi.

Color Art

Color art is free of charge for online publication.
If black and white will be shown in the print version, make sure that the main information will still be visible. Many colors are not distinguishable from one another when converted to black and white. A simple way to check this is to make a xerographic copy to see if the necessary distinctions between the different colors are still apparent.
If the figures will be printed in black and white, do not refer to color in the captions.
Color illustrations should be submitted as RGB (8 bits per channel).

Figure Lettering

To add lettering, it is best to use Helvetica or Arial (sans serif fonts).
Keep lettering consistently sized throughout your final-sized artwork, usually about 2–3 mm (8–12 pt).
Variance of type size within an illustration should be minimal, e.g., do not use 8-pt type on an axis and 20-pt type for the axis label.
Avoid effects such as shading, outline letters, etc.
Do not include titles or captions within your illustrations.

Figure Numbering

All figures are to be numbered using Arabic numerals.
Figures should always be cited in text in consecutive numerical order.
Figure parts should be denoted by lowercase letters (a, b, c, etc.).
If an appendix appears in your article and it contains one or more figures, continue the consecutive numbering of the main text.
Do not number the appendix figures,
"A1, A2, A3, etc." Figures in online appendices (Electronic Supplementary Material) should, however, be numbered separately.

Figure Captions

Each figure should have a concise caption describing accurately what the figure depicts. Include the captions in the text file of the manuscript, not in the figure file.
Figure captions begin with the term Fig. in bold type, followed by the figure number, also in bold type.
No punctuation is to be included after the number, nor is any punctuation to be placed at the end of the caption.
Identify all elements found in the figure in the figure caption; and use boxes, circles, etc., as coordinate points in graphs.

Identify previously published material by giving the original source in the form of a reference citation at the end of the figure caption.

Figure Placement and Size

Figures should be submitted separately from the text, if possible.
When preparing your figures, size figures to fit in the column width.
For most journals the figures should be 39 mm, 84 mm, 129 mm, or 174 mm wide and not higher than 234 mm.
For books and book-sized journals, the figures should be 80 mm or 122 mm wide and not higher than 198 mm.

Permissions

If you include figures that have already been published elsewhere, you must obtain permission from the copyright owner(s) for both the print and online format. Please be aware that some publishers do not grant electronic rights for free and that Springer will not be able to refund any costs that may have occurred to receive these permissions. In such cases, material from other sources should be used.

Accessibility

In order to give people of all abilities and disabilities access to the content of your figures, please make sure that
All figures have descriptive captions (blind users could then use a text-to-speech software or a text-to-Braille hardware)
Patterns are used instead of or in addition to colors for conveying information (colorblind users would then be able to distinguish the visual elements)
Any figure lettering has a contrast ratio of at least 4.5:1

ELECTRONIC SUPPLEMENTARY MATERIAL

Springer accepts electronic multimedia files (animations, movies, audio, etc.) and other supplementary files to be published online along with an article or a book chapter. This feature can add dimension to the author's article, as certain information cannot be printed or is more convenient in electronic form.
Before submitting research datasets as electronic supplementary material, authors should read the journal's Research data policy.
We encourage research data to be archived in data repositories wherever possible.

Submission

Supply all supplementary material in standard file formats.
Please include in each file the following information: article title, journal name, author names; affiliation and e-mail address of the corresponding author.
To accommodate user downloads, please keep in mind that larger-sized files may require very long download times and that some users may experience other problems during downloading.

Audio, Video, and Animations

Aspect ratio: 16:9 or 4:3
Maximum file size: 25 GB
Minimum video duration: 1 sec
Supported file formats: avi, wmv, mp4, mov, m2p, mp2, mpg, mpeg, flv, mxf, mts, m4v, 3gp

Text and Presentations

Submit your material in PDF format; .doc or .ppt files are not suitable for long-term viability.
A collection of figures may also be combined in a PDF file.

Spreadsheets

Spreadsheets should be submitted as .csv or .xlsx files (MS Excel).

Specialized Formats

Specialized format such as .pdb (chemical), .wrl (VRML), .nb (Mathematica notebook), and .tex can also be supplied.

Collecting Multiple Files

It is possible to collect multiple files in a .zip or .gz file.

Numbering

If supplying any supplementary material, the text must make specific mention of the material as a citation, similar to that of figures and tables.
Refer to the supplementary files as "Online Resource", e.g., "... as shown in the animation (Online Resource 3)", "... additional data are given in Online Resource 4".
Name the files consecutively, e.g. "ESM_3.mpg", "ESM_4.pdf".

Captions

For each supplementary material, please supply a concise caption describing the content of the file.

Processing of supplementary files

Electronic supplementary material will be published as received from the author without any conversion, editing, or reformatting.

Accessibility

In order to give people of all abilities and disabilities access to the content of your supplementary files, please make sure that:
The manuscript contains a descriptive caption for each supplementary material
Video files do not contain anything that flashes more than three times per second (so that users prone to seizures caused by such effects are not put at risk)

ETHICAL RESPONSIBILITIES OF AUTHORS

This journal is committed to upholding the integrity of the scientific record. As a member of the Committee on Publication Ethics (COPE) the journal will follow the COPE guidelines on how to deal with potential acts of misconduct.
Authors should refrain from misrepresenting research results which could damage the trust in the journal, the professionalism of scientific authorship, and ultimately the entire scientific endeavour. Maintaining integrity of the research and its presentation can be achieved by following the rules of good scientific practice, which include:
The manuscript has not been submitted to more than one journal for simultaneous consideration.
The manuscript has not been published previously (partly or in full), unless the new work concerns an expansion of previous work (please provide transparency on the re-use of material to avoid the hint of text-recycling ("self-plagiarism")).
A single study is not split up into several parts to increase the quantity of submissions and submitted to various journals or to one journal over time (e.g. "salami-publishing").
No data have been fabricated or manipulated (including images) to support your conclusions
No data, text, or theories by others are presented as if they were the author's own ("plagiarism"). Proper acknowledgements to other works must be given (this includes material that is closely copied (near verbatim), summarized and/or paraphrased), quotation marks are used for verbatim copying of material, and permissions are secured for material that is copyrighted.
Important note: the journal may use software to screen for plagiarism.
Consent to submit has been received explicitly from all co-authors, as well as from the responsible authorities - tacitly or explicitly - at the institute/organization where the work has been carried out, **before** the work is submitted.
Authors whose names appear on the submission have contributed sufficiently to the scientific work and therefore share collective responsibility and accountability for the results.
Authors are strongly advised to ensure the correct author group, corresponding author, and order of authors at submission. Changes of authorship or in the order of authors are **not** accepted **after** acceptance of a manuscript.
Adding and/or deleting authors and/or changing the order of authors **at revision stage** may be justifiably warranted. A letter must accompany the revised manuscript to explain the reason for the change(s) and the contribution role(s) of the added and/or deleted author(s). Further documentation may be required to support your request.
Requests for addition or removal of authors as a result of authorship disputes after acceptance are honored after formal notification by the institute or independent body and/or when there is agreement between all authors.
Upon request authors should be prepared to send relevant documentation or data in order to verify the validity of the results. This could be in the form of raw data, samples, records, etc. Sensitive information in the form of confidential proprietary data is excluded.
If there is a suspicion of misconduct, the journal will carry out an investigation following the COPE guidelines. If, after investigation, the allegation seems to raise valid concerns, the accused author will be contacted and given an opportunity to address the issue. If misconduct has been established beyond reasonable doubt, this may result in the Editor-in-Chief's implementation of the following measures, including, but not limited to:
If the article is still under consideration, it may be rejected and returned to the author.
If the article has already been published online, depending on the nature and severity of the infraction, either an erratum will be placed with the article or in severe cases complete retraction of the article will occur. The reason must be given in the published erratum or retraction note. Please note that retraction means that the paper is **maintained on the platform**, watermarked "retracted" and explanation for the retraction is provided in a note linked to the watermarked article.
The author's institution may be informed.

COMPLIANCE WITH ETHICAL STANDARDS

To ensure objectivity and transparency in research and to ensure that accepted principles of ethical and professional conduct have been followed, authors should include information regarding sources of funding, potential conflicts of interest (financial or non-financial), informed consent if the research involved human participants, and a statement on welfare of animals if the research involved animals.
Authors should include the following statements (if applicable) in a separate section entitled "Compliance with Ethical Standards" when submitting a paper:
Disclosure of potential conflicts of interest
Research involving Human Participants and/or Animals
Informed consent

Please note that standards could vary slightly per journal dependent on their peer review policies (i.e. single or double blind peer review) as well as per journal subject discipline. Before submitting your article check the instructions following this section carefully.
The corresponding author should be prepared to collect documentation of compliance with ethical standards and send if requested during peer review or after publication.
The Editors reserve the right to reject manuscripts that do not comply with the above-mentioned guidelines. The author will be held responsible for false statements or failure to fulfill the above-mentioned guidelines.

DISCLOSURE OF POTENTIAL CONFLICTS OF INTEREST

Authors must disclose all relationships or interests that could influence or bias the work. Although an author may not feel there are conflicts, disclosure of relationships and interests affords a more transparent process, leading to an accurate and objective assessment of the work. Awareness of real or perceived conflicts of interests is a perspective to which the readers are entitled and is not meant to imply that a financial relationship with an organization that sponsored the research or compensation for consultancy work is inappropriate. Examples of potential conflicts of interests **that are directly or indirectly related to the research** may include but are not limited to the following:
Research grants from funding agencies (please give the research funder and the grant number)
Honoraria for speaking at symposia
Financial support for attending symposia
Financial support for educational programs
Employment or consultation
Support from a project sponsor
Position on advisory board or board of directors or other type of management relationships
Multiple affiliations
Financial relationships, for example equity ownership or investment interest
Intellectual property rights (e.g. patents, copyrights and royalties from such rights)
Holdings of spouse and/or children that may have financial interest in the work
In addition, interests that go beyond financial interests and compensation (non-financial interests) that may be important to readers should be disclosed. These may include but are not limited to personal relationships or competing interests directly or indirectly tied to this research, or professional interests or personal beliefs that may influence your research.
The corresponding author collects the conflict of interest disclosure forms from all authors. (**Please note that each author should complete a disclosure form.**) Examples of forms can be found here:
See below examples of disclosures:
Funding: This study was funded by X (grant number X).
Conflict of Interest: Author A has received research grants from Company A. Author B has received a speaker honorarium from Company X and owns stock in Company Y. Author C is a member of committee Z.
If no conflict exists, the authors should state:
Conflict of Interest: Author A, Author B, and Author C declare that they have no conflict of interest.

RESEARCH INVOLVING HUMAN PARTICIPANTS AND/OR ANIMALS

1) Statement of human rights

When reporting studies that involve human participants, authors should include a statement that the studies have been approved by the appropriate institutional and/or national research ethics committee and have been performed in accordance with the ethical standards as laid down in the 1964 Declaration of Helsinki and its later amendments or comparable ethical standards.
If doubt exists whether the research was conducted in accordance with the 1964 Helsinki Declaration or comparable standards, the authors must explain the reasons for their approach, and demonstrate that the independent ethics committee or institutional review board explicitly approved the doubtful aspects of the study.
The following statements should be included in the text before the References section:
Ethical approval: "All procedures performed in studies involving human participants were in accordance with the ethical standards of the institutional and/or national research committee and with the 1964 Helsinki declaration and its later amendments or comparable ethical standards."
For retrospective studies, please add the following sentence: "For this type of study formal consent is not required."

2) Statement on the welfare of animals

The welfare of animals used for research must be respected. When reporting experiments on animals, authors should indicate whether the international, national, and/or institutional guidelines for the care and use of animals have been followed, and that the studies have been approved by a research ethics committee at the institution or practice at which the studies were conducted (where such a committee exists).
For studies with animals, the following statement should be included in in the text before the References section:
Ethical approval: "All applicable international, national, and/or institutional guidelines for the care and use of animals were followed."
If applicable (where such a committee exists): "All procedures performed in studies involving animals were in accordance with the ethical standards of the institution or practice at which the studies were conducted."
If articles do not contain studies with human participants or animals by any of the authors, please select one of the following statements:
"This article does not contain any studies with human participants performed by any of the authors."

"This article does not contain any studies with animals performed by any of the authors."
"This article does not contain any studies with human participants or animals performed by any of the authors."

INFORMED CONSENT

All individuals have individual rights that are not to be infringed. Individual participants in studies have, for example, the right to decide what happens to the (identifiable) personal data gathered, to what they have said during a study or an interview, as well as to any photograph that was taken. Hence it is important that all participants gave their informed consent in writing prior to inclusion in the study. Identifying details (names, dates of birth, identity numbers and other information) of the participants that were studied should not be published in written descriptions, photographs, and genetic profiles unless the information is essential for scientific purposes and the participant (or parent or guardian if the participant is incapable) gave written informed consent for publication. Complete anonymity is difficult to achieve in some cases, and informed consent should be obtained if there is any doubt. For example, masking the eye region in photographs of participants is inadequate protection of anonymity. If identifying characteristics are altered to protect anonymity, such as in genetic profiles, authors should provide assurance that alterations do not distort scientific meaning.
The following statement should be included:
Informed consent: "Informed consent was obtained from all individual participants included in the study."
If identifying information about participants is available in the article, the following statement should be included:
"Additional informed consent was obtained from all individual participants for whom identifying information is included in this article."

RESEARCH DATA POLICY

A submission to the journal implies that materials described in the manuscript, including all relevant raw data, will be freely available to any researcher wishing to use them for non-commercial purposes, without breaching participant confidentiality.
The journal strongly encourages that all datasets on which the conclusions of the paper rely should be available to readers. We encourage authors to ensure that their datasets are either deposited in publicly available repositories (where available and appropriate) or presented in the main manuscript or additional supporting files whenever possible. Please see Springer Nature's information on recommended repositories.
List of Repositories
Research Data Policy
General repositories - for all types of research data - such as figshare and Dryad may be used where appropriate.
Datasets that are assigned digital object identifiers (DOIs) by a data repository may be cited in the reference list. Data citations should include the minimum information recommended by DataCite: authors, title, publisher (repository name), identifier.
DataCite
Where a widely established research community expectation for data archiving in public repositories exists, submission to a community-endorsed, public repository is mandatory. Persistent identifiers (such as DOIs and accession numbers) for relevant datasets must be provided in the paper
For the following types of data set, submission to a community-endorsed, public repository is mandatory:

Mandatory deposition	**Suitable repositories**
Protein sequences	Uniprot
DNA and RNA sequences	Genbank DNA DataBank of Japan (DDBJ) EMBL Nucleotide Sequence Database (ENA)
DNA and RNA sequencing data	NCBI Trace Archive NCBI Sequence Read Archive (SRA)
Genetic polymorphisms	dbSNP dbVar European Variation Archive (EVA)
Linked genotype and phenotype data	dbGAP The European Genome-phenome Archive (EGA)
Macromolecular structure	Worldwide Protein Data Bank (wwPDB) Biological Magnetic Resonance Data Bank (BMRB) Electron Microscopy Data Bank (EMDB)
Microarray data (must be MIAME compliant)	Gene Expression Omnibus (GEO) ArrayExpress

Crystallographic data for small molecules	Cambridge Structural Database

For more information: Research Data Policy Frequently Asked Questions

Data availability

The journal encourages authors to provide a statement of Data availability in their article. Data availability statements should include information on where data supporting the results reported in the article can be found, including, where applicable, hyperlinks to publicly archived datasets analysed or generated during the study. Data availability statements can also indicate whether data are available on request from the authors and where no data are available, if appropriate.
Data Availability statements can take one of the following forms (or a combination of more than one if required for multiple datasets):
1. The datasets generated during and/or analysed during the current study are available in the [NAME] repository, [PERSISTENT WEB LINK TO DATASETS]
2. The datasets generated during and/or analysed during the current study are not publicly available due [REASON WHY DATA ARE NOT PUBLIC] but are available from the corresponding author on reasonable request.
3. The datasets generated during and/or analysed during the current study are available from the corresponding author on reasonable request.
4. Data sharing not applicable to this article as no datasets were generated or analysed during the current study.
5. All data generated or analysed during this study are included in this published article [and its supplementary information files].
More examples of template data availability statements, which include examples of openly available and restricted access datasets, are available:
Data availability statements
This service provides advice on research data policy compliance and on finding research data repositories. It is independent of journal, book and conference proceedings editorial offices and does not advise on specific manuscripts.

AFTER ACCEPTANCE

Upon acceptance of your article you will receive a link to the special Author Query Application at Springer's web page where you can sign the Copyright Transfer Statement online and indicate whether you wish to order OpenChoice, offprints, or printing of figures in color.
Once the Author Query Application has been completed, your article will be processed and you will receive the proofs.

Copyright transfer

Authors will be asked to transfer copyright of the article to the Publisher (or grant the Publisher exclusive publication and dissemination rights). This will ensure the widest possible protection and dissemination of information under copyright laws.
Creative Commons Attribution-NonCommercial 4.0 International License

Offprints

Offprints can be ordered by the corresponding author.

Color illustrations

Online publication of color illustrations is free of charge. For color in the print version, authors will be expected to make a contribution towards the extra costs.

Proof reading

The purpose of the proof is to check for typesetting or conversion errors and the completeness and accuracy of the text, tables and figures. Substantial changes in content, e.g., new results, corrected values, title and authorship, are not allowed without the approval of the Editor.
After online publication, further changes can only be made in the form of an Erratum, which will be hyperlinked to the article.

Online First

The article will be published online after receipt of the corrected proofs. This is the official first publication citable with the DOI. After release of the printed version, the paper can also be cited by issue and page numbers.

OPEN CHOICE

Open Choice allows you to publish open access in more than 1850 Springer Nature journals, making your research more visible and accessible immediately on publication.
Benefits:
Increased researcher engagement: Open Choice enables access by anyone with an internet connection, immediately on publication.

Higher visibility and impact: In Springer hybrid journals, OA articles are accessed 4 times more often on average, and cited 1.7 more times on average*.
Easy compliance with funder and institutional mandates: Many funders require open access publishing, and some take compliance into account when assessing future grant applications.
It is easy to find funding to support open access – please see our funding and support pages for more information.
*) Within the first three years of publication. Springer Nature hybrid journal OA impact analysis, 2018.
Open Choice
Funding and Support pages

Copyright and license term – CC BY

Open Choice articles do not require transfer of copyright as the copyright remains with the author. In opting for open access, the author(s) agree to publish the article under the Creative Commons Attribution License.
Find more about the license agreement

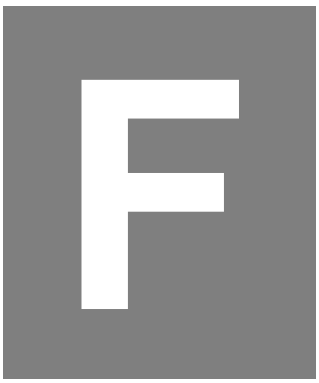
Support for Research Data Sharing

Many journals and funding agencies encourage or require data sharing in repositories. If you need help organising and sharing your research data (including code, text, raw and processed data, video and images) you should consider:
Finding a suitable data repository for your data
Uploading your data to Springer Nature Research Data Support
Contacting Springer Nature's Research Data Support Helpdesk for advice
List of recommended data repositories
Access Research Data Support
More information on Research Data Support
Contact the Research Data Helpdesk
Research Data Support is an optional Springer Nature service available to all researchers who have datasets they want to make easier to cite, share and find. The service provides a secure portal for data upload, and data and metadata are curated and improved by professional Research Data Editors. The publication of datasets is coordinated by our Research Data Editors in consultation with the researcher, and a DOI is provided to allow the dataset to be cited and shared.
Checks are carried out as part of a submission screening process to ensure that researchers who should use a specific community-endorsed repository are advised of the best option for sharing and archiving their data. Use of Research Data Support is optional and does not imply or guarantee that a manuscript will be accepted.

ENGLISH LANGUAGE EDITING

For editors and reviewers to accurately assess the work presented in your manuscript you need to ensure the English language is of sufficient quality to be understood. If you need help with writing in English you should consider:
Asking a colleague who is a native English speaker to review your manuscript for clarity.
Visiting the English language tutorial which covers the common mistakes when writing in English.
Using a professional language editing service where editors will improve the English to ensure that your meaning is clear and identify problems that require your review. Two such services are provided by our affiliates Nature Research Editing Service and American Journal Experts. Springer authors are entitled to a 10% discount on their first submission to either of these services, simply follow the links below.
English language tutorial
Nature Research Editing Service
American Journal Experts
Please note that the use of a language editing service is not a requirement for publication in this journal and does not imply or guarantee that the article will be selected for peer review or accepted.
If your manuscript is accepted it will be checked by our copyeditors for spelling and formal style before publication.

ANNEXURE



BBA — Molecular Basis of Disease author guidelines

BBA MOLECULAR BASIS OF DISEASE

One of the nine topical journals of BBA

AUTHOR INFORMATION PACK

TABLE OF CONTENTS

- **Description** p.1
- **Audience** p.1
- **Impact Factor** p.1
- **Abstracting and Indexing** p.2
- **Editorial Board** p.2
- **Guide for Authors** p.5



ISSN: 0925-4439

DESCRIPTION

BBA Molecular Basis of Disease addresses the **biochemistry** and **molecular genetics** of **disease** processes and models of human disease. This journal covers aspects of aging, cancer, metabolic-, neurological-, and immunological-based disease. Manuscripts focused on using animal models to elucidate biochemical and mechanistic insight in each of these conditions, are particularly encouraged. Manuscripts should emphasize the underlying mechanisms of disease pathways and provide novel contributions to the understanding and/or treatment of these disorders. Highly descriptive and method development submissions may be declined without full review.

Given the complex regulation of gene expression by a vast network of miRNA's, manuscripts describing the regulation of (disease-associated) genes by single miRNAs will only be considered if they provide genuine, novel insight in a disease mechanism. Further, studies restricted to a single cell line will not be considered unless they present truly novel insights.

The submission of uninvited reviews to *BBA - Molecular Basis of Disease* is strongly discouraged, and any such uninvited review should be accompanied by a coverletter outlining the compelling reasons why the review should be considered.

Benefits to authors
We also provide many author benefits, such as free PDFs, a liberal copyright policy, special discounts on Elsevier publications and much more. Please click here for more information on our author services.

Please see our Guide for Authors for information on article submission. If you require any further information or help, please visit our Support Center

AUDIENCE

Basic and clinical researchers studying molecular aspects of disease processes, Human geneticists, Biochemists, Molecular biologists, Cell biologists, Cell physiologists

IMPACT FACTOR

2017: 5.108 © Clarivate Analytics Journal Citation Reports 2018

ABSTRACTING AND INDEXING

Science Citation Index
EMBiology
Sociedad Iberoamericana de Informacion Cientifica (SIIC) Data Bases
BIOSIS
Chemical Abstracts
Current Contents/Life Sciences
EMBASE
Index Chemicus
MEDLINE®
Scopus

EDITORIAL BOARD

Executive Editors:

Jeffrey Keller, Pennington Biomedical Research Center/Louisiana State University System, Baton Rouge, Louisiana, USA
Aging, Alzheimer's disease, neurodegeneration, oxidative stress
Ronald Oude Elferink, Tytgat Institute for Liver and Intestinal Research, Amsterdam, Netherlands
Inherited liver disease, transgenic animal models, drug disposition, ABC transporters, lipid flippases
M. Paul Murphy, University of Kentucky, Lexington, Kentucky, USA

Scientific Editor (Elsevier, Cambridge, MA, USA):

Angela Schena

Editorial Board Members:

Valerie Askanas, University of Southern California, Los Angeles, California, USA
Yidong Bai, University of Texas Health Sciences Center at San Antonio, San Antonio, Texas, USA
Mitochondrial; Oxidative stress, Respiration complex, Metabolism, Mitochondrial DNA mutation
Shairaz Baksh, University of Alberta, Edmonton, Alberta, Canada
Piter Bosma, Universiteit van Amsterdam, Academisch Medisch Centrum (AMC), Amsterdam Zuidoost, Netherlands
Allan Butterfield, University of Kentucky, Lexington, Kentucky, USA
oxidative stress, Alzheimer disease and mild cogntive impairment, redox proteomics, amyloid beta-peptide
Garth J.S. Cooper
Molecular mechanisms of diabetes mellitus; experimental therapeutics of diabetes; type-2 diabetes; islet beta-cell death; islet amyloid; insulin resistance; diabetic complications; diabetic cardiomyopathy; diabetic nephropathy; diabetic neuropathy; molecular basis of dementia; molecular linkages between dementia and diabetes; Alzheimer's disease; Huntington's disease; amylin; insulin; hormonal regulation of metabolism
Angus Dalgleish, St. George's Hospital Medical School, University of London, London, UK
Tumour immunology, HIV pathogenesis, vaccines
Rafael deCabo, National Institute of Aging (NIA), Baltimore, Maryland, USA
Aging, caloric restriction, metabolism, redox pathways, sirtuins
Stuart E. Dryer, University of Houston, Houston, Texas, USA
Glomerular disease; ion channels; renal physiology; calcium signaling; electrophysiology; protein interactions; membrane transport; receptors.
Jason Dyck, University of Alberta, Edmonton, Alberta, Canada
Peter Fickert, Medical University of Graz, Weiz, Austria
Maria Figueiredo-Pereira, City University of New York (CUNY), New York, New York, USA
proteasome, neuroinflammation, neurodegeneration, prostaglandin j2, cyclooxygenase
Nikolaos G. Frangogiannis, Albert Einstein College of Medicine, New-York, New York, USA
Cardiac injury and repair
Saeid Ghavami, University of Manitoba, Winnipeg, Manitoba, Canada
Autophagy; Unfolded Protein Response; Fibrotic Disease; Apoptosis; Lung Cancer; Idiopathic Pulmonary Fibrosis; Rhabdomyosarcoma; Brian tumors
Fernando Gómez-Pinilla, University of California at Los Angeles (UCLA), Los Angeles, California, USA
Grace L. Guo, Rutgers University, Piscataway, New Jersey, USA
Elly Hol, Universitair Medisch Centrum Utrecht (UMC Utrecht), Utrecht, Netherlands
Astrocytes, Glia, Alzheimer, Stroke, Parkinson, Neurogenesis

Nancy Ip, Hong Kong University of Science and Technology, Kowloon, Hong Kong
Developmental and molecular Neurobiology, Neurothrophic factors and their receptors, neurona differentiation, neural regeneration
Takeshi Iwatsubo, University of Tokyo, Bunkyo-Ku, Japan
Sergio Lavandero, Universidad de Chile, Santiago, Chile
Cardiovascular diseases, Diabetes, Cell signaling, Cell death, autophagy, Mitochondria, Insulin, Growth factors, Intraorganelle communication
Valter D. Longo, University of Southern California, Los Angeles, California, USA
Aging, cell signaling, IGF-1, yeast models of aging
José E. Manautou, University of Connecticut, Storrs, Connecticut, USA
Hepatotoxicity Model hepatotoxicants (e.g. acetominophen, carbon tetrachloride) Hepatobiliary disposition of xenobiotics Hepatoprotection Peroxisome proliferators Transport proteins Covalent binding in hepatotoxicity Reactive intermediates in hepatotoxicity
Sara Mole, University College London (UCL), London, UK
Paula Moreira, Universidade de Coimbra, Coimbra, Portugal
Aging, Alzheimer's disease, Diabetes, Mitochondria, Neurodegeneration, Oxidative stress
Antonio Moschetta, Università di Bari, Bari, Italy
Nuclear Hormone Receptors, Liver Metabolic Disease, Gut-liver axis, Intestinal mucosa regeneration - tumorigenesis, Transcriptional regulation of Cholesterol and Lipid Metabolism
Ram Nagaraj, University of Colorado School of Medicine, Aurora, Colorado, USA
Small heat shock proteins, glycation, oxidative stress, apoptosis, cataract, diabetic retinopathy
William Orr, Southern Methodist University, Dallas, Texas, USA
Aging, redox regulation, innate immunity, circadian rhythm, caloric restriction
Athanasios Papavassiliou, University of Athens Medical School, Athens, Greece
AGE/metabolic stress signaling, Bone mechanobiology, Molecular oncology, Signaling pathways in tumorigenesis, Signal transduction to transcription factors in health and disease
Samir Kumar Patra, National Institute of Technology Rourkela (NIT), Orissa, India
Epigenetic mechanisms, DNA and Histone modifications, DNA demethylase and DNA demethylation mechanisms, regulation of gene expression, membrane lipid raft structure and signaling, Ras-MAPK and Hedgehog signaling pathways, Cancer stem cell and pluripotency.
Raghavan Raju, Augusta University, Augusta, Georgia, USA
Mitochondria, sirtuin, trauma, sepsis, oxidative stress, inflammation
Hemachandra Reddy, Texas Tech University Health Sciences Center, Lubbock, Texas, USA
Aging, Amyloid Beta, Neurodegenerative diseases, Mitochondria and Mitochondrial therapeutics.
Jun Ren, University of Wyoming, Cheyenne, Wyoming, USA
Manfredi Rizzo, Università degli Studi di Palermo, Palermo, Italy
Diabetes, atherosclerosis, cardiovascular prevention, dyslipidemia, metabolic syndrome
Luis Sobrevia, Pontificia Universidad Católica de Chile, Santiago, Chile
endothelium; trophoblast; fetus; placenta; insulin resistance; diabetes; preeclampsia; obesity in pregnancy; membrane transport; membrane receptors; adenosine; nitric oxide; L-arginine; pH; endoplasmic reticulum stress; exosomes; extracellular vesicles
Jacqueline M. Stephens, Louisiana State University, Baton Rouge, Louisiana, USA
Adipocyte, adipose tissue, obesity, insulin resistance, and STATs
Mark Sussman, SDSU Heart Institute, San Diego, California, USA
Cardiac, heart failure, stem cells, Akt kinase, Pim-1 kinase, myocardial biology
Russell H. Swerdlow, University of Kansas School of Medicine, Kansas City, Kansas, USA
Aging, Alzheimer's disease, Bioenergetics, Metabolism, Mitochondria, Neurodegeneration
Ya-Xiong Tao, Auburn University, Auburn, Alabama, USA
Holly Van Remmen, Oklahoma Medical Research Foundation, Oklahoma City, Oklahoma, USA
Arthur J. Verhoeven, Universiteit van Amsterdam, Academisch Medisch Centrum (AMC), Amsterdam Zuidoost, Netherlands
Ronald JA Wanders, Universiteit van Amsterdam, Academisch Medisch Centrum (AMC), Amsterdam Zuidoost, Netherlands
Peroxisomes, peroxisomal lipid metabolism, inherited metabolic diseases, fatty acid metabolism, amino acid metabolism
Patricia Wilson, University College London (UCL), London, UK
Kidney Genetic Disease, gene therapy, Polycystic kidney disease, Stem cells, regenerative medicine, Kidney Cancer
Silvana Zanlungo, Pontificia Universidad Católica de Chile, Santiago, Chile
cholesterol, Niemann-Pick, neurodegeneration, liver, lipids, oxidative stress
Massimo Zeviani, National Neurological Institute "Carlo Besta", Milano, Italy
Mitochondrial Disease; Oxidative Phosphorylation; mitochondrial respiratory chain; mitochondrial DNA; mtDNA mutation.

Zhuohua Zhang, Central South University, Changsha, China
ubiquitin proteasomal degradation, Parkinson disease, protein folding, connexins, epigenetics
Xiongwei Zhu, Case Western Reserve University School of Medicine, Cleveland, Ohio, USA
Neuroscience, Neurodegenerative diseases, Mitochondrial Oxidative Stress, Amyloid, Signal Transduction, Alzheimer's Disease, Parkinson's Disease

GUIDE FOR AUTHORS

Your Paper Your Way

We now differentiate between the requirements for new and revised submissions. You may choose to submit your manuscript as a single Word or PDF file to be used in the refereeing process. Only when your paper is at the revision stage, will you be requested to put your paper in to a 'correct format' for acceptance and provide the items required for the publication of your article.
To find out more, please visit the Preparation section below.

INTRODUCTION

BBA *Molecular Basis of Disease* addresses the biochemistry and molecular genetics of disease processes and their models with a specific focus on human disease.
The section covers metabolic, membrane, receptor and immunological disorders, and includes the biochemistry of differentiation disorders, tissue damage and aging. Manuscripts should emphasize the underlying mechanisms of disease pathways and provide novel contributions to the understanding and treatment of these processes. Highly descriptive and method development submissions may be declined without full review.

Types of paper

Full-length research articles, Review papers.

Reviews and mini-reviews are typically commissioned by the Editors. All Review Articles should be authoritative, state-of-the-art accounts of the selected research field, be of high interest, balanced and accurate. Beyond summaries of important scientific developments and ideas, authors are encouraged to identify and discuss how the field may be impacted or develop in the future, including insights that may be of significance to the scientific community. All BBA Review Articles undergo rigorous and full peer review, in the same way as regular research papers, and publication cannot be guaranteed. The number of co-authors of review articles is limited to five and each author is expected to make a substantial contribution to the writing of the manuscript.

Unsolicited reviews will be considered only in exceptional cases and should be preceded by a letter of enquiry from the prospective author, who should be a recognized expert in the field of the proposed article. Pre-submission enquires may be sent to the Editorial Office bbareviews@elsevier.com. Specifically, authors must provide the following in their review proposal: 1) both your own and any co-author(s) affiliation and full contact details; 2) an explanation of the current interest and significance to the broad readership of the journal, that is, compelling reasons why the review should be considered; 3) a 500-600 word summary which clearly outlines what will be discussed in the article, plus up to 20 key references that indicate the intended breadth of the proposed article (please note that references should include work published in the past 2-4 years). Only proposals that include this information will be considered. Please be sure to specify which one of the ten BBA journals you request to consider your proposal.

Reviews (full-length) should provide a comprehensive analysis on topics of broad interest to the journal's readership. Reviews should be thorough, sufficiently critical and accommodate different points of view. They should stand out from other recently published reviews on the same theme. Although Reviews are not of any fixed length, they are usually 6,000 to 10,000 words in length (excluding references and figure legends), include an abstract that is no more than 150 words, up to 100 references (should include titles), and a minimum of three figures/illustrations.

Mini-reviews are succinct, focused updates of the literature related to a question of current interest in the scientific community (typically from the last 2-3 years). Subjects covered in Mini-reviews are generally narrower, either in scope or depth, than those covered in full-length Reviews. They should highlight/analyze/discuss recent and important findings and include the author's viewpoint on how the subject relates to the current state of the field. Mini-reviews are usually 2000 to 4000 words in length (excluding references and figure legends), include an abstract that is no more than 100 words, up to 50 references (should include titles), and one to three figures/illustrations.

Contact details for submission

Papers should be submitted using the **BBA** *Molecular Basis of Disease* online submission system http://ees.elsevier.com/bbadis. For questions on the submission and reviewing process, please contact the Editorial Office at bbadis@elsevier.com.

BEFORE YOU BEGIN

Ethics in publishing

Please see our information pages on Ethics in publishing and Ethical guidelines for journal publication.

Studies in humans and animals

If the work involves the use of human subjects, the author should ensure that the work described has been carried out in accordance with The Code of Ethics of the World Medical Association (Declaration of Helsinki) for experiments involving humans. The manuscript should be in line with the Recommendations for the Conduct, Reporting, Editing and Publication of Scholarly Work in Medical Journals and aim for the inclusion of representative human populations (sex, age and ethnicity) as per those recommendations. The terms sex and gender should be used correctly.

Authors should include a statement in the manuscript that informed consent was obtained for experimentation with human subjects. The privacy rights of human subjects must always be observed.

All animal experiments should comply with the ARRIVE guidelines and should be carried out in accordance with the U.K. Animals (Scientific Procedures) Act, 1986 and associated guidelines, EU Directive 2010/63/EU for animal experiments, or the National Institutes of Health guide for the care and use of Laboratory animals (NIH Publications No. 8023, revised 1978) and the authors should clearly indicate in the manuscript that such guidelines have been followed. The sex of animals must be indicated, and where appropriate, the influence (or association) of sex on the results of the study.

Conflict of Interest

BBA Molecular Basis of Disease follows the ICMJE recommendations regarding conflict of interest disclosures. All authors are required to report the following information with each submission: (1) All third-party financial support for the work in the submitted manuscript. (2) All financial relationships with any entities that could be viewed as relevant to the general area of the submitted manuscript. (3) All sources of revenue with relevance to the submitted work who made payments to you, or to your institution on your behalf, in the 36 months prior to submission. (4) Any other interactions with the sponsor of outside of the submitted work should also be reported. (5) Any relevant patents or copyrights (planned, pending, or issued). (6) Any other relationships or affiliations that may be perceived by readers to have influenced, or give the appearance of potentially influencing, what you wrote in the submitted work. As a general guideline, it is usually better to disclose a relationship than not. This information will be acknowledged at publication in a Transparency Document link directly in the article. Additional information on the ICMJE recommendations can be found at: http://www.icmje.org/. The form for conflict of interest disclosure can be downloaded here: http://www.icmje.org/coi_disclosure.pdf (if this link does not display properly in your browser, please right-click the link and select "Save Target As..." or "Save Link as..." from the pop-up menu).

Submission declaration and verification

Submission of an article implies that the work described has not been published previously (except in the form of an abstract, a published lecture or academic thesis, see 'Multiple, redundant or concurrent publication' for more information), that it is not under consideration for publication elsewhere, that its publication is approved by all authors and tacitly or explicitly by the responsible authorities where the work was carried out, and that, if accepted, it will not be published elsewhere in the same form, in English or in any other language, including electronically without the written consent of the copyright-holder. To verify originality, your article may be checked by the originality detection service Crossref Similarity Check.

Preprints

Please note that preprints can be shared anywhere at any time, in line with Elsevier's sharing policy. Sharing your preprints e.g. on a preprint server will not count as prior publication (see 'Multiple, redundant or concurrent publication' for more information).

Use of inclusive language

Inclusive language acknowledges diversity, conveys respect to all people, is sensitive to differences, and promotes equal opportunities. Articles should make no assumptions about the beliefs or commitments of any reader, should contain nothing which might imply that one individual is superior to another on the grounds of race, sex, culture or any other characteristic, and should use inclusive language throughout. Authors should ensure that writing is free from bias, for instance by using 'he or she', 'his/her' instead of 'he' or 'his', and by making use of job titles that are free of stereotyping (e.g. 'chairperson' instead of 'chairman' and 'flight attendant' instead of 'stewardess').

Authorship

All authors should have made substantial contributions to all of the following: (1) the conception and design of the study, or acquisition of data, or analysis and interpretation of data, (2) drafting the article or revising it critically for important intellectual content, (3) final approval of the version to be submitted.

Changes to authorship

Authors are expected to consider carefully the list and order of authors **before** submitting their manuscript and provide the definitive list of authors at the time of the original submission. Any addition, deletion or rearrangement of author names in the authorship list should be made only **before** the manuscript has been accepted and only if approved by the journal Editor. To request such a change, the Editor must receive the following from the **corresponding author**: (a) the reason for the change in author list and (b) written confirmation (e-mail, letter) from all authors that they agree with the addition, removal or rearrangement. In the case of addition or removal of authors, this includes confirmation from the author being added or removed.
Only in exceptional circumstances will the Editor consider the addition, deletion or rearrangement of authors **after** the manuscript has been accepted. While the Editor considers the request, publication of the manuscript will be suspended. If the manuscript has already been published in an online issue, any requests approved by the Editor will result in a corrigendum.

Article transfer service
This journal is part of our Article Transfer Service. This means that if the Editor feels your article is more suitable in one of our other participating journals, then you may be asked to consider transferring the article to one of those. If you agree, your article will be transferred automatically on your behalf with no need to reformat. Please note that your article will be reviewed again by the new journal. More information.

Copyright

Upon acceptance of an article, authors will be asked to complete a 'Journal Publishing Agreement' (see more information on this). An e-mail will be sent to the corresponding author confirming receipt of the manuscript together with a 'Journal Publishing Agreement' form or a link to the online version of this agreement.

Subscribers may reproduce tables of contents or prepare lists of articles including abstracts for internal circulation within their institutions. Permission of the Publisher is required for resale or distribution outside the institution and for all other derivative works, including compilations and translations. If excerpts from other copyrighted works are included, the author(s) must obtain written permission from the copyright owners and credit the source(s) in the article. Elsevier has preprinted forms for use by authors in these cases.

For gold open access articles: Upon acceptance of an article, authors will be asked to complete an 'Exclusive License Agreement' (more information). Permitted third party reuse of gold open access articles is determined by the author's choice of user license.

Author rights

As an author you (or your employer or institution) have certain rights to reuse your work. More information.

Elsevier supports responsible sharing
Find out how you can share your research published in Elsevier journals.

Role of the funding source

You are requested to identify who provided financial support for the conduct of the research and/or preparation of the article and to briefly describe the role of the sponsor(s), if any, in study design; in the collection, analysis and interpretation of data; in the writing of the report; and in the decision to submit the article for publication. If the funding source(s) had no such involvement then this should be stated.

Elsevier journals comply with current NIH public access policy

Funding body agreements and policies
Elsevier has established a number of agreements with funding bodies which allow authors to comply with their funder's open access policies. Some funding bodies will reimburse the author for the gold open access publication fee. Details of existing agreements are available online.

Open access

This journal offers authors a choice in publishing their research:

Subscription

• Articles are made available to subscribers as well as developing countries and patient groups through our universal access programs.
• No open access publication fee payable by authors.
• The Author is entitled to post the accepted manuscript in their institution's repository and make this public after an embargo period (known as green Open Access). The published journal article cannot be shared publicly, for example on ResearchGate or Academia.edu, to ensure the sustainability of peer-reviewed research in journal publications. The embargo period for this journal can be found below.

Gold open access

• Articles are freely available to both subscribers and the wider public with permitted reuse.
• A gold open access publication fee is payable by authors or on their behalf, e.g. by their research funder or institution.

Regardless of how you choose to publish your article, the journal will apply the same peer review criteria and acceptance standards.

For gold open access articles, permitted third party (re)use is defined by the following Creative Commons user licenses:

Creative Commons Attribution (CC BY)
Lets others distribute and copy the article, create extracts, abstracts, and other revised versions, adaptations or derivative works of or from an article (such as a translation), include in a collective work (such as an anthology), text or data mine the article, even for commercial purposes, as long as they credit the author(s), do not represent the author as endorsing their adaptation of the article, and do not modify the article in such a way as to damage the author's honor or reputation.

Creative Commons Attribution-NonCommercial-NoDerivs (CC BY-NC-ND)
For non-commercial purposes, lets others distribute and copy the article, and to include in a collective work (such as an anthology), as long as they credit the author(s) and provided they do not alter or modify the article.

The gold open access publication fee for this journal is **USD 4050**, excluding taxes. Learn more about Elsevier's pricing policy: https://www.elsevier.com/openaccesspricing.

Green open access
Authors can share their research in a variety of different ways and Elsevier has a number of green open access options available. We recommend authors see our green open access page for further information. Authors can also self-archive their manuscripts immediately and enable public access from their institution's repository after an embargo period. This is the version that has been accepted for publication and which typically includes author-incorporated changes suggested during submission, peer review and in editor-author communications. Embargo period: For subscription articles, an appropriate amount of time is needed for journals to deliver value to subscribing customers before an article becomes freely available to the public. This is the embargo period and it begins from the date the article is formally published online in its final and fully citable form. Find out more.

This journal has an embargo period of 12 months.

Elsevier Researcher Academy
Researcher Academy is a free e-learning platform designed to support early and mid-career researchers throughout their research journey. The "Learn" environment at Researcher Academy offers several interactive modules, webinars, downloadable guides and resources to guide you through the process of writing for research and going through peer review. Feel free to use these free resources to improve your submission and navigate the publication process with ease.

Language (usage and editing services)
Please write your text in good English (American or British usage is accepted, but not a mixture of these). Authors who feel their English language manuscript may require editing to eliminate possible grammatical or spelling errors and to conform to correct scientific English may wish to use the English Language Editing service available from Elsevier's WebShop.

Submission

Our online submission system guides you stepwise through the process of entering your article details and uploading your files. The system converts your article files to a single PDF file used in the peer-review process. Editable files (e.g., Word, LaTeX) are required to typeset your article for final publication. All correspondence, including notification of the Editor's decision and requests for revision, is sent by e-mail.

Referees

Please submit the names, addresses, and e-mail addresses of 4 potential referees, as well as a brief description of their expertise relevant to your manuscript. Suggested reviewers should be individuals qualified to evaluate the work you have submitted. Editorial Board members who do not have relevant expertise on the topic of your article should not be suggested. Please note that the reviewers suggested may not be current, recent or extensive collaborators of yours, and cannot have been involved in the preparation of the manuscript.

Please note that the editor retains the sole right to decide whether or not the suggested reviewers are used. Failure to provide appropriate reviewer suggestions as noted above may result in your manuscript being returned to you without review.

Authors may request exclusion of certain referees if conflicts of interest are anticipated. However, no more than 3 such names should be given. Entire groups, institutions or countries cannot be specified for exclusion.

PREPARATION

NEW SUBMISSIONS

Submission to this journal proceeds totally online and you will be guided stepwise through the creation and uploading of your files. The system automatically converts your files to a single PDF file, which is used in the peer-review process.
As part of the Your Paper Your Way service, you may choose to submit your manuscript as a single file to be used in the refereeing process. This can be a PDF file or a Word document, in any format or lay-out that can be used by referees to evaluate your manuscript. It should contain high enough quality figures for refereeing. If you prefer to do so, you may still provide all or some of the source files at the initial submission. Please note that individual figure files larger than 10 MB must be uploaded separately.

References

There are no strict requirements on reference formatting at submission. References can be in any style or format as long as the style is consistent. Where applicable, author(s) name(s), journal title/ book title, chapter title/article title, year of publication, volume number/book chapter and the article number or pagination must be present. Use of DOI is highly encouraged. The reference style used by the journal will be applied to the accepted article by Elsevier at the proof stage. Note that missing data will be highlighted at proof stage for the author to correct.

Formatting requirements

There are no strict formatting requirements but all manuscripts must contain the essential elements needed to convey your manuscript, for example Abstract, Keywords, Introduction, Materials and Methods, Results, Conclusions, Artwork and Tables with Captions.
If your article includes any Videos and/or other Supplementary material, this should be included in your initial submission for peer review purposes.
Divide the article into clearly defined sections.

Please ensure your paper includes page numbers - this is an essential peer review requirement.

Figures and tables embedded in text

Please ensure the figures and the tables included in the single file are placed next to the relevant text in the manuscript, rather than at the bottom or the top of the file. The corresponding caption should be placed directly below the figure or table.

Peer review

This journal operates a single blind review process. All contributions will be initially assessed by the editor for suitability for the journal. Papers deemed suitable are then typically sent to a minimum of two independent expert reviewers to assess the scientific quality of the paper. The Editor is responsible for the final decision regarding acceptance or rejection of articles. The Editor's decision is final. More information on types of peer review.

REVISED SUBMISSIONS

Use of word processing software

Regardless of the file format of the original submission, at revision you must provide us with an editable file of the entire article. Keep the layout of the text as simple as possible. Most formatting codes will be removed and replaced on processing the article. The electronic text should be prepared in a way very similar to that of conventional manuscripts (see also the Guide to Publishing with Elsevier). See also the section on Electronic artwork.

To avoid unnecessary errors you are strongly advised to use the 'spell-check' and 'grammar-check' functions of your word processor.

Article structure

Subdivision - numbered sections

Divide your article into clearly defined and numbered sections. Subsections should be numbered 1.1 (then 1.1.1, 1.1.2, ...), 1.2, etc. (the abstract is not included in section numbering). Use this numbering also for internal cross-referencing: do not just refer to 'the text'. Any subsection may be given a brief heading. Each heading should appear on its own separate line.

Introduction

State the objectives of the work and provide an adequate background, avoiding a detailed literature survey or a summary of the results.

Material and methods

Provide sufficient details to allow the work to be reproduced by an independent researcher. Methods that are already published should be summarized, and indicated by a reference. If quoting directly from a previously published method, use quotation marks and also cite the source. Any modifications to existing methods should also be described.

Results

Results should be clear and concise.

Discussion

This should explore the significance of the results of the work, not repeat them. A combined Results and Discussion section is often appropriate. Avoid extensive citations and discussion of published literature.

Conclusions

The main conclusions of the study may be presented in a short Conclusions section, which may stand alone or form a subsection of a Discussion or Results and Discussion section.

Appendices

If there is more than one appendix, they should be identified as A, B, etc. Formulae and equations in appendices should be given separate numbering: Eq. (A.1), Eq. (A.2), etc.; in a subsequent appendix, Eq. (B.1) and so on. Similarly for tables and figures: Table A.1; Fig. A.1, etc.

Essential title page information

• ***Title.*** Concise and informative. Titles are often used in information-retrieval systems. Avoid abbreviations and formulae where possible.

• ***Author names and affiliations.*** Please clearly indicate the given name(s) and family name(s) of each author and check that all names are accurately spelled. You can add your name between parentheses in your own script behind the English transliteration. Present the authors' affiliation addresses (where the actual work was done) below the names. Indicate all affiliations with a lower-case superscript letter immediately after the author's name and in front of the appropriate address. Provide the full postal address of each affiliation, including the country name and, if available, the e-mail address of each author.

• ***Corresponding author.*** Clearly indicate who will handle correspondence at all stages of refereeing and publication, also post-publication. This responsibility includes answering any future queries about Methodology and Materials. **Ensure that the e-mail address is given and that contact details are kept up to date by the corresponding author.**

• ***Present/permanent address.*** If an author has moved since the work described in the article was done, or was visiting at the time, a 'Present address' (or 'Permanent address') may be indicated as a footnote to that author's name. The address at which the author actually did the work must be retained as the main, affiliation address. Superscript Arabic numerals are used for such footnotes.

Abstract

A concise and factual abstract is required. The abstract should state briefly the purpose of the research, the principal results and major conclusions. An abstract is often presented separately from the article, so it must be able to stand alone. For this reason, References should be avoided, but if essential, then cite the author(s) and year(s). Also, non-standard or uncommon abbreviations should be avoided, but if essential they must be defined at their first mention in the abstract itself.

A Regular paper should have a Summary of 100-250 words.

Graphical abstract

Although a graphical abstract is optional, its use is encouraged as it draws more attention to the online article. The graphical abstract should summarize the contents of the article in a concise, pictorial form designed to capture the attention of a wide readership. Graphical abstracts should be submitted as a separate file in the online submission system. Image size: Please provide an image with a minimum of 531 × 1328 pixels (h × w) or proportionally more. The image should be readable at a size of 5 × 13 cm using a regular screen resolution of 96 dpi. Preferred file types: TIFF, EPS, PDF or MS Office files. You can view Example Graphical Abstracts on our information site.
Authors can make use of Elsevier's Illustration Services to ensure the best presentation of their images and in accordance with all technical requirements.

Highlights

Highlights are mandatory for this journal. They consist of a short collection of bullet points that convey the core findings of the article and should be submitted in a separate editable file in the online submission system. Please use 'Highlights' in the file name and include 3 to 5 bullet points (maximum 85 characters, including spaces, per bullet point). You can view example Highlights on our information site.

Keywords

Immediately after the abstract, provide a maximum of 6 keywords, using American spelling and avoiding general and plural terms and multiple concepts (avoid, for example, 'and', 'of'). Be sparing with abbreviations: only abbreviations firmly established in the field may be eligible. These keywords will be used for indexing purposes.

Abbreviations

Define abbreviations that are not standard in this field in a footnote to be placed on the first page of the article. Such abbreviations that are unavoidable in the abstract must be defined at their first mention there, as well as in the footnote. Ensure consistency of abbreviations throughout the article.

Acknowledgements

Collate acknowledgements in a separate section at the end of the article before the references and do not, therefore, include them on the title page, as a footnote to the title or otherwise. List here those individuals who provided help during the research (e.g., providing language help, writing assistance or proof reading the article, etc.).

Formatting of funding sources

List funding sources in this standard way to facilitate compliance to funder's requirements:

Funding: This work was supported by the National Institutes of Health [grant numbers xxxx, yyyy]; the Bill & Melinda Gates Foundation, Seattle, WA [grant number zzzz]; and the United States Institutes of Peace [grant number aaaa].

It is not necessary to include detailed descriptions on the program or type of grants and awards. When funding is from a block grant or other resources available to a university, college, or other research institution, submit the name of the institute or organization that provided the funding.

If no funding has been provided for the research, please include the following sentence:

This research did not receive any specific grant from funding agencies in the public, commercial, or not-for-profit sectors.

Standards for Reporting Enzymology Data (STRENDA)
This journal follows the recommendations of the STRENDA (**St**andards for **R**eporting **En**zymology **Da**ta) Commission of the Beilstein-Institut for the reporting of kinetic and equilibrium binding data. Detailed guidelines can be found at (http://www.strenda.org/documents.html) or in this pdf file.
All reports of kinetic and binding data must include a description of the identity of the catalytic or binding entity (enzyme, protein, nucleic acid or other molecule). This information should include the origin or source of the molecule, its purity, composition, and other characteristics such as post-translational modifications, mutations, and any modifications made to facilitate expression or purification. The assay methods and exact experimental conditions of the assay must be fully described if it is a new assay or provided as a reference to previously published work, with or without modifications. The temperature, pH and pressure (if other than atmospheric) of the assay **must** always be included, even if previously published. In instances where catalytic activity or binding cannot be detected, an estimate of the limit of detection based on the sensitivity and error analysis of the assay should be provided. Ambiguous terms such as "not detectable" should be avoided. A description of the software used for data analysis should be included along with calculated errors for all parameters.
First-order and second-order rate constants: see pdf for full instructions.

Electrophoretic gels and blots
Manuscripts reporting results from blots (including Western blots) and electrophoretic gels should adhere to the following guidelines: In accordance with our policy on image manipulation, the image should not be adjusted in any way that affects the scientific interpretation displayed, e.g. by strong modification of the background or contrast. Authors should be able to provide original uncropped and unadjusted blots and gels, including molecular size markers, upon request by the editor or any of the reviewers. Similarly, in case the authors use multiple blots for protein quantitation (or draw quantitative conclusions from the blots), the authors should be able to provide upon request pictures of all full blots that have contributed to this quantitation for review purposes. Quantitation should only be performed using a minimum of 3 blots/gels, each obtained from separate experimental trials. Cropped blots in the body of the paper should retain sufficient space above and below the band (about six band widths). Any non-specific band should be labelled as such and an attempt should be made to explain its nature The image should include all relevant controls, and controls should be run on the same blot or gel as the samples. The image should also display the position of the molecular weight markers. A figure panel may not include composite images of bands originating from different blots or gels. If the figure shows non-adjacent bands from the same blot or gel, this should be clearly denoted by vertical black lines and the figure legend should provide details of how the figure was prepared. The submission of high-contrast gels and blots is discouraged, as overexposure may mask additional bands. Authors should strive for exposures with gray backgrounds. Multiple exposures should be presented in supplementary information if high contrast is unavoidable.

Math formulae
Please submit math equations as editable text and not as images. Present simple formulae in line with normal text where possible and use the solidus (/) instead of a horizontal line for small fractional terms, e.g., X/Y. In principle, variables are to be presented in italics. Powers of e are often more conveniently denoted by exp. Number consecutively any equations that have to be displayed separately from the text (if referred to explicitly in the text).

Footnotes
Footnotes should be used sparingly. Number them consecutively throughout the article. Many word processors build footnotes into the text, and this feature may be used. Should this not be the case, indicate the position of footnotes in the text and present the footnotes themselves separately at the end of the article.

Artwork

Image manipulation
While it is accepted that authors sometimes need to manipulate images for clarity, manipulation for purposes of deception or fraud will be seen as scientific ethical abuse and will be dealt with accordingly. For graphical images, this journal is applying the following policy: no specific feature within an image may be enhanced, obscured, moved, removed, or introduced. Adjustments of brightness, contrast, or color balance are acceptable as long as they are applied to the entire image and do not obscure or eliminate any information present in the original. Nonlinear adjustments (e.g. changes to gamma settings) must be disclosed in the figure legend.

Digital images in manuscripts nearing acceptance for publication may be scrutinized for any indication of improper manipulation. *BBA Molecular Basis of Disease* reserves the right to ask for original data or images and, if these are not satisfactory, we may decide not to accept the manuscript.

Electronic artwork
General points
• Make sure you use uniform lettering and sizing of your original artwork.
• Preferred fonts: Arial (or Helvetica), Times New Roman (or Times), Symbol, Courier.
• Number the illustrations according to their sequence in the text.
• Use a logical naming convention for your artwork files.
• Indicate per figure if it is a single, 1.5 or 2-column fitting image.
• For Word submissions only, you may still provide figures and their captions, and tables within a single file at the revision stage.
• Please note that individual figure files larger than 10 MB must be provided in separate source files. A detailed guide on electronic artwork is available.
You are urged to visit this site; some excerpts from the detailed information are given here.
Formats
Regardless of the application used, when your electronic artwork is finalized, please 'save as' or convert the images to one of the following formats (note the resolution requirements for line drawings, halftones, and line/halftone combinations given below):
EPS (or PDF): Vector drawings. Embed the font or save the text as 'graphics'.
TIFF (or JPG): Color or grayscale photographs (halftones): always use a minimum of 300 dpi.
TIFF (or JPG): Bitmapped line drawings: use a minimum of 1000 dpi.
TIFF (or JPG): Combinations bitmapped line/half-tone (color or grayscale): a minimum of 500 dpi is required.
Please do not:
• Supply files that are optimized for screen use (e.g., GIF, BMP, PICT, WPG); the resolution is too low.
• Supply files that are too low in resolution.
• Submit graphics that are disproportionately large for the content.

Color artwork
Please make sure that artwork files are in an acceptable format (TIFF (or JPEG), EPS (or PDF) or MS Office files) and with the correct resolution. If, together with your accepted article, you submit usable color figures then Elsevier will ensure, at no additional charge, that these figures will appear in color online (e.g., ScienceDirect and other sites) in addition to color reproduction in print. Further information on the preparation of electronic artwork.

Figure captions
Ensure that each illustration has a caption. A caption should comprise a brief title (**not** on the figure itself) and a description of the illustration. Keep text in the illustrations themselves to a minimum but explain all symbols and abbreviations used.

Tables
Please submit tables as editable text and not as images. Tables can be placed either next to the relevant text in the article, or on separate page(s) at the end. Number tables consecutively in accordance with their appearance in the text and place any table notes below the table body. Be sparing in the use of tables and ensure that the data presented in them do not duplicate results described elsewhere in the article. Please avoid using vertical rules and shading in table cells.

References
Citation in text
Please ensure that every reference cited in the text is also present in the reference list (and vice versa). Any references cited in the abstract must be given in full. Unpublished results and personal communications are not recommended in the reference list, but may be mentioned in the text. If these references are included in the reference list they should follow the standard reference style of the journal and should include a substitution of the publication date with either 'Unpublished results' or 'Personal communication'. Citation of a reference as 'in press' implies that the item has been accepted for publication and a copy of the title page of the relevant article must be submitted.

Web references
As a minimum, the full URL should be given and the date when the reference was last accessed. Any further information, if known (DOI, author names, dates, reference to a source publication, etc.), should also be given. Web references can be listed separately (e.g., after the reference list) under a different heading if desired, or can be included in the reference list.

Data references
This journal encourages you to cite underlying or relevant datasets in your manuscript by citing them in your text and including a data reference in your Reference List. Data references should include the following elements: author name(s), dataset title, data repository, version (where available), year, and global persistent identifier. Add [dataset] immediately before the reference so we can properly identify it as a data reference. The [dataset] identifier will not appear in your published article.

References in a special issue
Please ensure that the words 'this issue' are added to any references in the list (and any citations in the text) to other articles in the same Special Issue.

Reference management software
Most Elsevier journals have their reference template available in many of the most popular reference management software products. These include all products that support Citation Style Language styles, such as Mendeley and Zotero, as well as EndNote. Using the word processor plug-ins from these products, authors only need to select the appropriate journal template when preparing their article, after which citations and bibliographies will be automatically formatted in the journal's style. If no template is yet available for this journal, please follow the format of the sample references and citations as shown in this Guide. If you use reference management software, please ensure that you remove all field codes before submitting the electronic manuscript. More information on how to remove field codes.

Users of Mendeley Desktop can easily install the reference style for this journal by clicking the following link:
http://open.mendeley.com/use-citation-style/bba-molecular-basis-of-disease
When preparing your manuscript, you will then be able to select this style using the Mendeley plug-ins for Microsoft Word or LibreOffice.

Reference formatting
There are no strict requirements on reference formatting at submission. References can be in any style or format as long as the style is consistent. Where applicable, author(s) name(s), journal title/ book title, chapter title/article title, year of publication, volume number/book chapter and the article number or pagination must be present. Use of DOI is highly encouraged. The reference style used by the journal will be applied to the accepted article by Elsevier at the proof stage. Note that missing data will be highlighted at proof stage for the author to correct. If you do wish to format the references yourself they should be arranged according to the following examples:

Reference style
Text: Indicate references by number(s) in square brackets in line with the text. The actual authors can be referred to, but the reference number(s) must always be given.
Example: '..... as demonstrated [3,6]. Barnaby and Jones [8] obtained a different result ....'
List: Number the references (numbers in square brackets) in the list in the order in which they appear in the text.
Examples:
Reference to a journal publication:
[1] J. van der Geer, J.A.J. Hanraads, R.A. Lupton, The art of writing a scientific article, J. Sci. Commun. 163 (2010) 51–59. https://doi.org/10.1016/j.Sc.2010.00372.
Reference to a journal publication with an article number:
[2] Van der Geer, J., Hanraads, J.A.J., Lupton, R.A., 2018. The art of writing a scientific article. Heliyon. 19, e00205. https://doi.org/10.1016/j.heliyon.2018.e00205.
Reference to a book:
[3] W. Strunk Jr., E.B. White, The Elements of Style, fourth ed., Longman, New York, 2000.
Reference to a chapter in an edited book:
[4] G.R. Mettam, L.B. Adams, How to prepare an electronic version of your article, in: B.S. Jones, R.Z. Smith (Eds.), Introduction to the Electronic Age, E-Publishing Inc., New York, 2009, pp. 281–304.
Reference to a website:

[5] Cancer Research UK, Cancer statistics reports for the UK. http://www.cancerresearchuk.org/aboutcancer/statistics/cancerstatsreport/, 2003 (accessed 13 March 2003).
Reference to a dataset:
[dataset] [6] M. Oguro, S. Imahiro, S. Saito, T. Nakashizuka, Mortality data for Japanese oak wilt disease and surrounding forest compositions, Mendeley Data, v1, 2015. https://doi.org/10.17632/xwj98nb39r.1.

Journal abbreviations source
Journal names should be abbreviated according to the List of Title Word Abbreviations.

Video
Elsevier accepts video material and animation sequences to support and enhance your scientific research. Authors who have video or animation files that they wish to submit with their article are strongly encouraged to include links to these within the body of the article. This can be done in the same way as a figure or table by referring to the video or animation content and noting in the body text where it should be placed. All submitted files should be properly labeled so that they directly relate to the video file's content. . In order to ensure that your video or animation material is directly usable, please provide the file in one of our recommended file formats with a preferred maximum size of 150 MB per file, 1 GB in total. Video and animation files supplied will be published online in the electronic version of your article in Elsevier Web products, including ScienceDirect. Please supply 'stills' with your files: you can choose any frame from the video or animation or make a separate image. These will be used instead of standard icons and will personalize the link to your video data. For more detailed instructions please visit our video instruction pages. Note: since video and animation cannot be embedded in the print version of the journal, please provide text for both the electronic and the print version for the portions of the article that refer to this content.

Data visualization
Include interactive data visualizations in your publication and let your readers interact and engage more closely with your research. Follow the instructions here to find out about available data visualization options and how to include them with your article.

Supplementary material
Supplementary material such as applications, images and sound clips, can be published with your article to enhance it. Submitted supplementary items are published exactly as they are received (Excel or PowerPoint files will appear as such online). Please submit your material together with the article and supply a concise, descriptive caption for each supplementary file. If you wish to make changes to supplementary material during any stage of the process, please make sure to provide an updated file. Do not annotate any corrections on a previous version. Please switch off the 'Track Changes' option in Microsoft Office files as these will appear in the published version.

Research data
This journal encourages and enables you to share data that supports your research publication where appropriate, and enables you to interlink the data with your published articles. Research data refers to the results of observations or experimentation that validate research findings. To facilitate reproducibility and data reuse, this journal also encourages you to share your software, code, models, algorithms, protocols, methods and other useful materials related to the project.

Below are a number of ways in which you can associate data with your article or make a statement about the availability of your data when submitting your manuscript. If you are sharing data in one of these ways, you are encouraged to cite the data in your manuscript and reference list. Please refer to the "References" section for more information about data citation. For more information on depositing, sharing and using research data and other relevant research materials, visit the research data page.

Data linking
If you have made your research data available in a data repository, you can link your article directly to the dataset. Elsevier collaborates with a number of repositories to link articles on ScienceDirect with relevant repositories, giving readers access to underlying data that gives them a better understanding of the research described.

There are different ways to link your datasets to your article. When available, you can directly link your dataset to your article by providing the relevant information in the submission system. For more information, visit the database linking page.

For supported data repositories a repository banner will automatically appear next to your published article on ScienceDirect.

In addition, you can link to relevant data or entities through identifiers within the text of your manuscript, using the following format: Database: xxxx (e.g., TAIR: AT1G01020; CCDC: 734053; PDB: 1XFN).

Mendeley Data
This journal supports Mendeley Data, enabling you to deposit any research data (including raw and processed data, video, code, software, algorithms, protocols, and methods) associated with your manuscript in a free-to-use, open access repository. During the submission process, after uploading your manuscript, you will have the opportunity to upload your relevant datasets directly to *Mendeley Data*. The datasets will be listed and directly accessible to readers next to your published article online.

For more information, visit the Mendeley Data for journals page.

Data in Brief
You have the option of converting any or all parts of your supplementary or additional raw data into one or multiple data articles, a new kind of article that houses and describes your data. Data articles ensure that your data is actively reviewed, curated, formatted, indexed, given a DOI and publicly available to all upon publication. You are encouraged to submit your article for *Data in Brief* as an additional item directly alongside the revised version of your manuscript. If your research article is accepted, your data article will automatically be transferred over to *Data in Brief* where it will be editorially reviewed and published in the open access data journal, *Data in Brief*. Please note an open access fee of 500 USD is payable for publication in *Data in Brief*. Full details can be found on the Data in Brief website. Please use this template to write your Data in Brief.

MethodsX
You have the option of converting relevant protocols and methods into one or multiple MethodsX articles, a new kind of article that describes the details of customized research methods. Many researchers spend a significant amount of time on developing methods to fit their specific needs or setting, but often without getting credit for this part of their work. MethodsX, an open access journal, now publishes this information in order to make it searchable, peer reviewed, citable and reproducible. Authors are encouraged to submit their MethodsX article as an additional item directly alongside the revised version of their manuscript. If your research article is accepted, your methods article will automatically be transferred over to MethodsX where it will be editorially reviewed. Please note an open access fee is payable for publication in MethodsX. Full details can be found on the MethodsX website. Please use this template to prepare your MethodsX article.

Data statement
To foster transparency, we encourage you to state the availability of your data in your submission. This may be a requirement of your funding body or institution. If your data is unavailable to access or unsuitable to post, you will have the opportunity to indicate why during the submission process, for example by stating that the research data is confidential. The statement will appear with your published article on ScienceDirect. For more information, visit the Data Statement page.

Submission checklist

The following list will be useful during the final checking of an article prior to sending it to the journal for review. Please consult this Guide for Authors for further details of any item.
Ensure that the following items are present:
One author has been designated as the corresponding author with contact details:
• E-mail address
• Full postal address
• Telephone
All necessary files have been uploaded, and contain:
• Keywords
• All figure captions
• All tables (including title, description, footnotes)
Further considerations
• Manuscript has been 'spell-checked' and 'grammar-checked'
• All references mentioned in the Reference list are cited in the text, and vice versa
• Permission has been obtained for use of copyrighted material from other sources (including the Web)
For any further information please visit our customer support site at http://support.elsevier.com.

AFTER ACCEPTANCE

Online proof correction

Corresponding authors will receive an e-mail with a link to our online proofing system, allowing annotation and correction of proofs online. The environment is similar to MS Word: in addition to editing text, you can also comment on figures/tables and answer questions from the Copy Editor. Web-based proofing provides a faster and less error-prone process by allowing you to directly type your corrections, eliminating the potential introduction of errors.
If preferred, you can still choose to annotate and upload your edits on the PDF version. All instructions for proofing will be given in the e-mail we send to authors, including alternative methods to the online version and PDF.
We will do everything possible to get your article published quickly and accurately. Please use this proof only for checking the typesetting, editing, completeness and correctness of the text, tables and figures. Significant changes to the article as accepted for publication will only be considered at this stage with permission from the Editor. It is important to ensure that all corrections are sent back to us in one communication. Please check carefully before replying, as inclusion of any subsequent corrections cannot be guaranteed. Proofreading is solely your responsibility.

Offprints

The corresponding author will, at no cost, receive a customized Share Link providing 50 days free access to the final published version of the article on ScienceDirect. The Share Link can be used for sharing the article via any communication channel, including email and social media. For an extra charge, paper offprints can be ordered via the offprint order form which is sent once the article is accepted for publication. Both corresponding and co-authors may order offprints at any time via Elsevier's Webshop. Corresponding authors who have published their article gold open access do not receive a Share Link as their final published version of the article is available open access on ScienceDirect and can be shared through the article DOI link.

AUTHOR INQUIRIES

Visit the Elsevier Support Center to find the answers you need. Here you will find everything from Frequently Asked Questions to ways to get in touch.
You can also check the status of your submitted article or find out when your accepted article will be published.

© Copyright 2018 Elsevier | https://www.elsevier.com